Modelling Short and Long-term Effects of Soil Cover Depth on Tree Growth and Productivity in Reclaimed Landscapes of Northern Alberta

by

Nilusha Priyadharshani Yalingasinghe Welegedara

A thesis submitted in partial fulfillment of the requirements for the degree of

Doctor of Philosophy

in

Land Reclamation and Remediation

Department of Renewable Resources
University of Alberta

Abstract

Success in establishing productive upland forests on landforms reconstructed using mining waste mainly depends on the cover materials and depth that determine water and nutrient availability for plant growth while mitigating the potential risks or limitations of the substrate that is being reclaimed. In this study, a process based ecosystem model, *ecosys* was used to forecast short and long-term effects of soil cover depth on soil moisture and nitrogen (N) availability, salinity and thereby plant productivity in different reclamation covers on a reclaimed overburden substrate landform which has elevated salinity and sodicity. The modelled outputs were tested against measured soil moisture content (θ), rooting depth, sap flow, leaf area, salt redistribution, soil and foliar N concentrations, plant biomass production with three soil cover depths differing in thickness (35, 50, and 100 cm). The study site was a 17-year-old forest reclamation site on a slope constructed on saline sodic overburden material, capped with a cover soil, and planted with trembling aspen and white spruce in the Athabasca Oil Sands Region, Fort McMurray, Alberta, Canada. The modelled changes in soil moisture, rooting depth, tree water-use, salt redistribution, soil and foliar N concentration and aboveground tree biomass with soil cover depth followed the same trends as independent measurements. Greater θ, plant water-use, N mineralization, N uptake and consequently greater aboveground biomass were modelled in 100 cm cover *vs.* 35 cm and 50 cm covers particularly during dry and intermediate years, after the sites had reached over-story crown closure (2011 - 2015). However, a clear relationship between root zone salt concentrations, driven by upward salt migration from underlying overburden, and aboveground biomass growth was not apparent. The relative limitations on net primary productivity (NPP) from water *vs.* nutrient uptake depended on slope position in the

reclaimed landscape. Thus lower plant productivity modelled in upper slope positions was mainly controlled by θ rather than N availability and salinity.

Modelled NPP increased linearly with modelled transpiration ($R^2 > 0.9$) and N uptake ($R^2 > 0.8$) that increased with AWHC and total soil nitrogen (TN) that in turn increased linearly with cover depth. However, non-linear relationships between transpiration and AWHC and between tree N uptake and TN indicated that there is a threshold cover depth (100 cm for the current study) where further increases in AWHC and TN would have little effect on NPP, according to site conditions. After running *ecosys* with seven hypothetical covers in addition to constructed landforms (35 cm, 50 cm and 100 cm), results also indicated that there is little effect of cover depths greater than 100 cm on plant growth. The 100 cm cover achieved NPP similar to that of natural boreal mixed-wood forests of the region earlier than did the 35 cm and 50 cm covers. However the long-term (100 yrs.) modelling without any ecosystem disturbances indicated that all the reclamation covers reached a similar NPP (~400 g C m^{-2} y^{-1}) during wet years after *ca*. 25 years from start of reclamation, comparable to the NPP modelled for a similar age regenerating natural site after stand replacing fire within the region. Long-term modelling (1999 - 2099) with climate change (RCP 8.5) increased NPP in the 100 cm cover (22%) more than in the 50 cm cover (15%) and the 35 cm cover (14%) because NPP in the shallower covers declined during dry years due to lower AWHC. Also aspen *vs.* white spruce growth tended to increase with increasing cover depth and climate change due to improved water and N uptake associated with greater AWHC as well as N mineralization from increased total soil nitrogen. However, the NPP gains modelled in all the reclaimed sites under warming climate were lower than that of the regenerating natural site (45%) due to decreased soil nutrient availability, particularly phosphorus, over time.

Overall, this study demonstrates the importance of cover soil depth as a modulator of soil available moisture, nutrient availability and salt redistribution particularly during early forest development. It also demonstrated that a terrestrial ecosystem model such as *ecosys* can be a useful tool in forecasting short and long-term hydrological patterns, salt redistribution, N cycling, NPP and thereby land capability for reclamation soil covers of different depths and properties.

Preface

This thesis is an original work by Nilusha Welegedara. I was responsible for model input data collection and model runs, conducting the experiment, and analyzing and evaluation of modelled outputs against field measurements as well as manuscript composition. R.F. Grant was the supervisory author and was involved with designing of the research, model development, modelling supervision and manuscript composition. S.A. Quideau involved with concept formation, field data collection and manuscript editing. E. Lloret involved with input data collection and field experiments.

Chapter 2 of this thesis has been submitted to *Journal of Ecological Modelling* as N. P. Y. Welegedara, R. F. Grant, Sylvie A. Quideau, Simon M. Landhäusser, Morgane Merlin and E. Lloret, "Modelling hydrological characteristics and plant water-use efficiency as affected by soil cover depth in reclaimed forestlands of Northern Alberta".

Acknowledgments

First and foremost, I would like to appreciate and express my deepest gratitude to my supervisor Dr. Robert Grant who had patiently worked with me during my research. His advices, continuous encouragement and support helped me to complete this research successfully. Also would like to extend my sincere gratitude to Dr. Sylvie Quideau who had given greater guidance and advices and all the support to do laboratory studies. I also express my heartfelt thanks to Examination Committee members Dr. Scott Chang who guided and encouraged me throughout the research. I would like to give special thanks to Dr. Simon Landhäusser and Morgane Merlin for giving the guidance and data without any hesitation. I would like to thank Dr. Anne Naeth and the Land Reclamation International Graduate School (LRIGS) staff for providing a great opportunity to participate in the LRIGS program as well as the excellent advices and support given throughout the programme.

I want to thank funding organizations for providing financial support to pursue this research. Funding for the study was provided by the LRIGS at the University of Alberta, the NSERC Collaborative Research and Training Experience (CREATE) Program, and Canadian Oil Sands Network for Research and Development (CONRAD). Computational facilities for the modelling project were provided by Compute Canada and WestGrid high performance computing infrastructure, and the University of Alberta. The great support in providing field data by Syncrude Canada limited is very much appreciated and special thanks goes to Marty Yarmuch and Bonnie Drozdowski for providing support to get field data. I would like to acknowledge Jeff Kelly, Frances Leishman, Caren Jones, Cassandra McKenzie, Brittany McAdams, Jela Burkus, Luke Donnan, Kelti Eaton, Melanie Luong for field data acquisition and laboratory assistance. I extremely grateful to Dr. Zelalem Mekonnen, Dr. Symon Mezbahuddin, Dr. Sanatan Das Gupta

and Dr. Emily Lloret who helped me throughout the research. It is my humble duty to acknowledge all staff members and friends of University of Alberta who had provided their maximum co-operation, guidance and encouragement in completing my studies.

Finally, I take this opportunity to express deep gratitude to my beloved parents and my husband, Darsha and lovely son Nethmin for their love, sincere encouragement and inspiration throughout my research work.

Table of Contents

List of Tables

List of Figures

List of symbols and abbreviations

Symbol and abbreviations	Definition
AOSR	Athabasca Oil Sands Region
ASWC	Available soil water content
AWHC	Available water holding capacity
C_a	Ambient CO_2 concentration
C_b	Canopy CO_2 concentration
C_c	Aqueous CO2 concentration in canopy chloroplasts
C_i	Gaseous CO_2 concentration in canopy leaves
C_s	Solute concentration
D	Vapor pressure deficits
D_{sc}	Aqueous diffusivity-dispersivity of solute
DOC	Dissolved organic carbon
DOY	Day of year
E_c	Canopy transpiration
EC	Electrical conductivity
EPEA	Environmental Protection and Enhancement Act
ET	Evapotranspiration
f_ψ	Non-stomatal effects of plant water status on carboxylation
FC	Field capacity
FFM	Forest floor mineral mix
G	Change in heat storage
g_c	Canopy stomatal conductance
GPP	Gross primary productivity
H	Sensible heat flux
IPCC	Intergovernmental Panel on Climate Change
K	Hydraulic conductivity
K_c	Michaelis-Menten constant for carboxylation
K_{sat}	Saturated hydraulic conductivity
LAI	Leaf area index

LCCS	Land Capability Classification System for Forest Ecosystems
LE	Latent heat flux
LHS	Left hand side
MAT	Mean annual air temperature
MARE	Mean absolute relative error
M_h	Heterotrophic microbial biomass
MFT	Microbial functional type
N	Nitrogen
NEP	Net ecosystem productivity
NPP	Net primary productivity
NSSOB	Non-saline sodic overburden
NUE	Nitrogen use efficiency
θ	Soil water contents
P	Phosphorous
P	Precipitation
PET	Potential evapotranspiration
PFT	Plant functional type
PMM	Peat mineral mix
POM	Particulate organic matter
PWP	Permanent wilting point
R_a	Autotrophic respiration
r_a	Aerodynamic resistance
R_c	Oxidation of nonstructural carbon pool
r_c	Canopy stomatal resistance
r_{cmin}	Minimum canopy resistance
RCP	Representative Concentration Pathways
RF	Rainfall
R_g	Growth respiration
r_l	Leaf stomatal resistance
RLD	Root length density
R_m	Maintenance respiration

RHS	Right hand side
RMD	Root mass densities
RMSD	Root mean squares for difference
RMSE	Root-mean-squares for error
R_n	Net radiation
R_s	Respiration of remobilizable C
SR	Solar radiation
SA	Stand sap wood area to ground area ratio
SAR	Sodium adsorption ratio
SBH	South Bison Hills
σ_C	Nonstructural C product of CO_2 fixation
σ_N	Nonstructural N product of root uptake
σ_P	Nonstructural P product of root uptake
SOC	Soil organic carbon
SON	Soil organic nitrogen
SSOB	Saline sodic overburden
T_a	Air temperature
T_c	Canopy temperature
T_s	Soil temperatures
TDR	Time domain reflectometry
TN	Total nitrogen
U_c	Plant water uptake
U_{NH_4}, U_{NO_3}, and U_{PO_4}	Active uptake (+ve) or release (-ve) of N and P by microbes
U_x	Nutrient uptake by roots or mycorrhizae
V_b	CO_2-limited leaf carboxylation rate
V_c	Canopy carboxylation rates
V_g	Leaf CO_2 diffusion
WUE_P	Water-use efficiency of productivity
WUE_T	Total water-use efficiency
Ω_s	Soil hydraulic resistances

Ω_r	Root hydraulic resistances
ψ_c	Canopy water potential
$\psi_{\pi t}$	Canopy osmotic water potential
ψ_π	Soil osmotic potential
ψ_g	Gravitational potential
ψ_m	Soil matric potential
ψ_t	Canopy turgor potential
ψ_s	Soil water potential

Chapter 1

Introduction

1.1. Surface mining and reclamation approaches in the Athabasca Oil Sands Region

Northern Alberta is rich in oil sands with approximately 142,000 km^2 surface area underlain by oil sands deposits (Alberta Environment, 2014). The three major oil sands deposits in Alberta are Athabasca, Cold Lake and Peace River located within the Alberta's boreal forest region. The Athabasca Oil Sands Region (AOSR) is the largest with three percent of the total reserve (4800 km^2) deposited in near-surface soil layers that are economical to extract through open-pit mining (Fung and Macyk, 2000; Alberta Energy, 2018). Therefore, surface mining is an ongoing operation in the AOSR near Fort McMurray, and has caused large-scale land disturbance due to the removal of the vegetation, stripping off surface and subsurface soil to expose and extract the oil sands deposits. By the end of 2016, the surface mining footprint was 900 km^2, which covered 0.24% of Alberta's boreal forest and 63 km^2 has been permanently reclaimed (Environment and Parks, 2017). At the completion of oil sands mining all disturbances will be reclaimed and must meet the requirements of a functioning ecosystem and equivalent land capability according to the Alberta government regulations (Alberta Environmental Protection and Enhancement Act - EPEA).

Fine textured saline/sodic Clearwater formation (shale overburden) comprises a large portion of the geologic material (overburden) underlying most of the land surface in the Athabasca oil sands region which must be removed during the surface mining (Fung and Macyk, 2000). The overburden is predominantly placed in unmined areas and reclaimed to areas that will be mainly upland forests with small localized wetlands (Boese, 2003; Elshorbagy et al., 2005). During upland construction, overburden is generally transported to a dedicated disposal site in

another area of the mine lease to create large, out of pit landform structures with long slopes of 10 to 20% around a prominent plateau in the center (Yarmuch, M., personal communication). Following overburden contouring, a soil reclamation cover of subsoil and topsoil (soil materials salvaged prior to overburden removal) is applied (Sandoval and Gould, 1978; Fung and Macyk, 2000; Carey, 2008) over the overburden. This cover is to provide a sufficient amount of moisture and nutrients to sustain plant growth even during times of low resource availability (*e.g.,* drought) (Boese, 2003), while successfully isolating the root zone from potentially limiting conditions in the overburden material (Kessler, 2007; Meiers et al., 2011). Subsoil and topsoil placement mainly occurs during winter and early spring (*i.e.*, frozen soil conditions) which reduces the potential for soil compaction. The site is revegetated with native trees and shrub species to achieve dominantly upland forests with small, localized wetlands.

1.2. Landform substrate

Oil sands mine activities and bitumen extraction result in a number of substrates (*e.g.,* overburden, tailings sand) that will become large-scale landforms and remain in the closure reclaimed landscape. Overburden landforms currently make-up the largest extent of reclamation to date and will comprise a significant extent of the closure reclaimed landscape. Overburden physical and chemical characteristics vary depending on its geologic origin (Fung and Macyk, 2000). For some oil sands mining operations, including Syncrude's Mildred Lake mine operation, a significant proportion of the overburden consists of Clearwater Formation, which is a Cretaceous Period marine clay shale with elevated salinity and sodicity. The combination of elevated salinity and sodicity, and high clay and silt proportions of the Clearwater Formation overburden presents a unique challenge to reclamation (Fung and Macyk, 2000; Kessler, 2007).

1.3. Reclamation materials and soil cover designs

Different reclamation covers have been constructed for the range of substrates produced in oil sands mining and bitumen extraction with the intention of providing a sufficient amount of moisture and nutrients, and to mitigate potential risk(s) or limitations of a substrate (Rowland et al., 2009). Soil profiles in oil sands reclaimed areas are generally referred as soil cover designs and they are separated into three major horizons; topsoil, upper subsoil and lower subsoil (Leskiw, 1998; Yarmuch, 2003). The depth of the topsoil ranges from 0 – 20 cm, upper subsoil from 20 - 50 cm and lower subsoil from 50 - 100 cm. The soil layers correspond to LFH, A, B, BC/C horizons in natural ecosystems respectively (Leskiw, 1998). These soil cover designs are artificially built (Anthroposols) using salvaged materials from pre-disturbed areas within the mine development footprint (Yarmuch, 2003; Naeth et al., 2012). The soil cover design in oil sands reclamation is generally a two horizon design, consisting of the following:

1) Topsoil (Cover soil) - Forest floor (LFH) mineral mix (FFM) and peat mineral mix (PMM) which are mixes of LFH or peat and a portion of underlying mineral below the LFH or peat materials respectively, are the dominant topsoil in oil sands reclamation soil cover designs (Yarmuch, 2003; Quideau et al., 2017). There is no specific soil quality criteria requirement for topsoil used in reclamation; however, there are specific soil salvage requirements for cover soil outlined in mine operating approvals to ensure that the soil chemical and physical properties of salvage topsoil will be adequate for reclamation.

   The topsoil is intended to represent the organic surface litter layer of uplands soils in the region which provides beneficial properties such as good soil structure, higher water holding capacity and aeration, lower root penetration resistance, increased available nutrients and organic matter, greater microorganism population and native plant seeds and

propagules (Power et al., 1979). The FFM is most like the surface soil of upland soils, since it was salvaged from an upland forest setting. However, there is generally an insufficient volume for reclamation (Prescott et al., 2000, MacKenzie and Naeth 2010, MacKenzie, 2013), because a large portion of the pre-disturbance landscape (~50%) was originally bog and fen. Therefore, PMM is an important topsoil material to make-up the balance of the topsoil requirements for mine reclamation (Fung and Macyk, 2000; Rowland et al., 2009; Hemstock et al., 2010; Pinno and Hawkes, 2015). PMM and FFM are preferentially salvaged and directly placed in areas ready for reclamation, but if there are no areas available at the time of salvage they are stockpiled.

2) Subsoil - Subsoil is mineral soil material below surface soil layers (topsoil) and overlies the overburden layer which is unsuitable for reclamation. The subsoil physical and chemical characteristics vary depending on the parent geologic material. Subsoil ranges from coarse-textured glacio-fluvial materials to fine-textured till and lacustrine materials (Fung and Macyk, 2000). The only specific soil quality criteria for subsoil reclamation material is electrical conductivity ($\leq$ 5 dS m^{-1}), sodium adsorption ratio ($\leq$ 8) and pH ($\leq$ 8) (AER, 2015; Clause 1.1.2.vvv.1). In addition to the soil quality criteria, operating approvals for oil sands mines have specific soil salvage requirements to ensure that appropriate horizons are salvaged for subsoil.

1.4. Importance of estimating sufficient soil capping depth

Soil cover designs (*i.e.*, horizon placement configuration and capping depth) play an important role in providing sufficient moisture and nutrients for vegetation growth, while also potentially mitigating any risks or limitations of the underlying substrate (landform). The ecosystem of reclaimed overburden landforms in the AOSR is predominantly an upland forest

with small localized wetlands in depression areas that have periodically or permanently saturated soil conditions. Sufficient soil moisture storage for the upland forest is determined by the hydrological characteristics of the soil cover design and the underlying substrate. Based on the soil cover design, as well as on the soil physical and chemical properties of the soil reclamation materials and the underlying substrate, the target native ecosystem in the region for Clearwater Formation overburden landforms in Mildred Lake mine operation is the "d" ecosite (Elshorbagy and Barbour, 2007). A native "d" ecosite is an upland forest ecosystem with a mesic soil moisture regime (*e.g.*, generally moist except for short dry periods) and medium nutrient regime (Beckingham and Archibald, 1996). The mesic soil moisture regime requires an average soil profile available water holding capacity (AWHC = volumetric water content at field capacity (θ_{FC}) – volumetric water content at permanent wilting point (θ_{PWP})) of 160 mm to a maximum depth of 1 m (CEMA, 2006). The medium nutrient regime requires soil organic carbon of 35 - 70 Mg ha^{-1}, total nitrogen 1.5 - 5 Mg ha^{-1} (natural sites) or 3 - 5 Mg ha^{-1} (reclaimed sites) and C:N ratio 15-30 (CEMA, 2006; Alberta Environment, 2010).

The climate of the AOSR plays a key role in land capability, as water availability is a key driver of vegetation growth in the boreal forest. The target ecosite capability is affected by the sub-humid climate of the AOSR where potential evapotranspiration (PET) usually exceeds precipitation (*P*) (Prepas et al., 2001; Buttle et al., 2005) and by large inter-annual variability of soil water deficits (Devito et al., 2005). Hence, annual *P* and evapotranspiration (ET) are crucial factors in the forest regrowth in these regions. The soil cover design plays an important role in the annual *P* and ET balance. If *P* is to be effective in meeting demand from ET, it must first infiltrate and then be retained by the soil cover materials. The moisture retention capacity must be sufficient to sustain water uptake during extended periods when ET exceeds *P*. Therefore, a

sufficient amount of capping material (depth) is essential to overcome any water deficits particularly during the plant growing season in a low *P* environment.

One of the greatest reclamation costs for oil sands mine operations is the salvage and placement of soil reclamation materials (Elshorbagy et al., 2006; Kessler et al., 2010). Due to the large scale of an oil sands mine operation, even small increases or decreases in the placement thickness depth can have a significant effect on the reclamation costs. There may also only be a finite amount (volume) of suitable soil material available for reclamation. Therefore, oil sands mining operations strive for an optimal soil cover design (depth) that meets the intended reclamation targets, mitigates any risk(s) or limitation(s) of the landform substrate, while considering the range of climate conditions in the region. Currently, a minimum cover depth of 100 cm is mandated by the Alberta Environment to reclaim areas with saline-sodic Clearwater Formation overburden. The permit issued to Syncrude Canada Ltd. (SCL) to reclaim recent overburden areas require placement of 50 cm of suitable overburden (non-saline sodic) prior to placement of 50 cm of cover soil to achieve the mandated 100 cm total depth (Alberta Energy Regulator, 2015; Clause 6.1.34). This minimum soil cover depth requirement is based on approximately two decades of research at Syncrude's Mildred Lake mine. Research and monitoring continues on Clearwater Formation overburden reclamation to validate and potentially refine the soil reclamation cover design and strategies for Clearwater Formation overburden reclamation.

1.5. Modelling short and long-term productivity in reclaimed landforms

Following mining and reclamation, processes and functional connections of carbon, water (Elshorbagy et al., 2005) and nutrient cycling are disturbed and a period of time is required to restore ecosystem processes and connections to an acceptable level. Research and monitoring of

key soil attributes such as AWHC, salinity and available nutrients are conducted to determine whether reclaimed areas have achieved the expected ecosystem properties after reclamation. Although instrumentation and field studies can be used to measure short-term effects of soil physical, chemical and biological attributes on water and nutrient availability and salinity and hence plant productivity, they are expensive, can disturb the sites and the findings are often discontinuous and site-specific (Gower et al., 2001; Randerson et al., 2002; Huang et al., 2013). One of major limitations to assess long-term reclamation success is the stand age of most reclaimed areas have not reached an appropriate age or stage for assessment. Also assessing long-term effects with short-term data is not an easy task under variable climate conditions (Elshorbagy and Barbour, 2007). Therefore, reclamation efforts of oil sand closure landscapes need long-term forecasts of these main soil attributes and their effects on ecosystem productivity over an appropriate reclamation period.

Measured environmental attributes of a reclamation site can be used to parameterize and validate ecosystem models that can simulate key ecosystem processes that govern plant productivity during reclamation. A rigorous modeling effort based on fundamental processes governing water, energy, ionic solutes and nutrients through the soil-microbe-root-canopy-atmosphere system can provide an opportunity for both a short and a long-term forecast of plant productivity (Grant, 2001, 2014). Such forecasts might help to determine the optimum depths of cover materials and thereby improve reclamation design and strategies for future reclamation (Elshorbagy et al., 2006).

1.6. Importance of the current study

Although several modelling approaches have been conducted for water and salt dynamics of Clearwater overburden reclamation by Shurniak and Barbour (2002), Elshorbagy et al. (2005),

Elshorbagy and Barbour (2007), Keshta et al. (2010) and Huang et al. (2015a,b), more comprehensive modelling approaches with coupled transformations of water, soluble salts, nutrients, carbon and energy in soil-plant-atmosphere systems have not yet been attempted. Such an approach is important because it may contribute to an integrated understanding of these key transformations and their interactions in reclained landforms that has not been established through conceptual and empirical modelling nor through field and lab experiments. This modelling approach could enable us to determine the effects of long-term nutrient limitations or of climate change on plant productivity in reclaimed landforms which have not been addressed in any earlier study of which we are aware. Therefore in this study we have used a more comprehensive process-based terrestrial ecosystem model, *Ecosys* (Grant, 2015) to address these knowledge gaps and to assist the oil sands industry and regulators to improve cover designs and long-term reclamation strategies.

Ecosys represents multiple soil and canopy layers in soil-microbe-root-canopy–atmosphere systems at three-dimensional scales. The model simulates physical, chemical and biological processes in natural and disturbed ecosystems through coupled processes for transfers and transformations of heat, water, carbon, oxygen, nitrogen and phosphorous cycles (Grant, 2001) using site-independent algorithms (Mezbahuddin et al., 2014) to achieve realistic landscape-scale predictions of productivity under a wide range of site conditions. To date *ecosys* has not been used to model ecosystem processes in novel ecosystems undergoing reclamation. However, the model has been extensively tested against several experiments on the effects of disturbance (Grant et al., 2007b,c; 2010), drought (Grant et al., 2006a,b; Grant and Flanagan, 2007; Grant et al., 2009a,b; Sulman et al., 2012; Mezbahuddin et al., 2015), salinity (Grant, 1995), nitrogen transformations (Grant et al., 1993; Grant, 1995, 1998; Grant et al., 2010; Grant, 2013, 2014;

Mezbahuddin et al., 2017; Mekonnen et al., 2018b) and warming on ecosystem productivity (Grant et al., (2003, 2009a, 2009b, 2010, 2011); Grant, (2013, 2014); Grant et al., 2015; Mekonnen et al., (2016, 2018a,b)) over a wide range of soils, landscapes, disturbances, fertilization and climatic conditions. Therefore, *ecosys* was used to understand the processes and functional connections of water, soluble salts, nutrients (N and P) and carbon cycling in reclaimed landscapes thereby to achieve integrated assessment of key factors helping to predict the short and long-term changes in plant productivity under current climate and climate change in different cover depths constructed on hill reclaimed landform.

1.7. Overview of the studies

This study was conducted to understand and quantify the effects of soil reclamation cover depth on short and long-term plant productivity in fine textured reclaimed landforms on a slope constructed over Clearwater formation overburden in the oil sands region of Alberta. Three main soil attributes determined by cover depth that govern plant productivity in reclaimed areas (available water holding capacity, salinity and nitrogen (N) availability (CEMA, 2006; Kelln et al., 2009; Alberta Environment, 2010)) were used to evaluate the effects of cover depth on short and long-term plant productivity. A comprehensive terrestrial ecosystem model *ecosys* (Grant, 2001, 2014; Grant et al., 2012) was used to simulate effects of cover depth on soil moisture availability, salinity, N availability and thereby plant productivity. The modeling study was conducted for a 17-year-old capping research trial with three different reclamation covers (35 cm, 50 cm and 100 cm) on a saline sodic (Clearwater Formation) overburden dump referred as South Bison Hills (SBH), located on the Syncrude Canada Ltd. Mildred Lake mine site in northern Alberta (Canada). Information for weather, site management and soil properties were used to initialize and run *ecosys* for the three reclamation covers at SBH. Each reclamation cover

was represented in the model as a transect of six interconnected grid cells each of which had a dimension of 50 m x 40 m. Five grid cells represented the slopes and one grid cell represented the level area above the slope adjacent to the capping trial study area.

The sub-humid climate in the AOSR limits plant growth particularly during dry years. Thus effects of soil moisture, salinity and N on net primary productivity (NPP) and plant growth were examined during wet, intermediate and dry years after the sites reached over-story crown closure in approximately 2010 to understand the responses of cover depths under different climatic conditions. Since portions of overburden landforms have slopes of 10 to 20%, effects of different slope positions on these effects were also examined.

In Chapter 2 we explored whether the model can be used to forecast short and long-term effects of soil moisture availability in different reclamation covers on tree water-use and productivity in these constructed landforms. Then the model was used to estimate the cover depth required to provide a sufficient amount of water for plant growth in these reclaimed sites particularly during dry years. Key hypotheses that govern soil water availability, plant water uptake and thereby NPP and plant growth were modelled and tested against measured soil moisture content, rooting depth, tree water-use, leaf area and aboveground biomass production with three soil cover depths, particularly after sites reached over-story crown closure.

In Chapter 3 we described the dynamics of salinity within root zone of each cover during the 17 years after reclamation. The effects of salt concentration within root zone of each cover on plant productivity were described using a model run with saline sodic overburden, as well as a sensitivity run in the absence of saline sodic overburden. Key hypotheses that govern the solute fluxes and solute transformations and their effects on NPP were modelled and tested against field

measured electrical conductivity and aboveground biomass production with three soil cover depths.

In Chapter 4 we examined soil N dynamics and plant N uptake in the three reclaimed covers. Modelled N mineralization, N uptake, relationship between N uptake and plant productivity, foliar and litterfall N concentrations were examined in reclaimed sites particularly after the sites reached over-story crown closure to explore the effect of total nitrogen as determined by the cover depth on plant productivity. Key hypotheses that govern N mineralization, uptake and their effects on NPP and N return to soil were modelled and tested against field measured soil, foliar and surface litter N concentrations and biomass production in three soil cover depths.

In Chapter 5, projections were made with seven hypothetical cover depths together with the three constructed cover depths to estimate the threshold AWHC as determined by cover depth which achieves 95% of maximum NPP at SBH and/or similar average NPP of the target boreal mixed-wood forest. In Chapters 2, 3 and 4 we examined the short-term effects of cover depth on plant productivity in reclaimed landforms. However, the long-term effect of reclamation on the ecosystem productivity under future climate is crucial. Thus in Chapter 5, we forecasted changes in plant productivity and aboveground biomass growth to 2100 in each constructed cover with future warming under a RCP 8.5 climate change scenario. These forecastswere compared with those in a similar age natural forest in the region regenerating after a stand replacing fire to determine long-term reclamation success in constructed reclaimed sites.

Finally, the results, uncertainties in model estimates and implications of all the four study chapters were summarized in Chapter 6.

Chapter 2

Modelling hydrological characteristics and plant water-use efficiency as affected by soil cover depth in reclaimed forestlands of Northern Alberta

2.1. Introduction

Available soil water holding capacity (AWHC) is a key soil factor in any landscape as it determines infiltration, soil water retention, plant water uptake, runoff and subsurface water flows; particularly in topographically variable landscapes. Vegetation survival and growth, especially in dry climates, are governed by soil water retention as it controls plant water relations and carbon dioxide fixation (Horton and Hart, 1998). Therefore, quantifying AWHC, water movements through soil materials and plant water-use is essential for understanding how to sustain ecosystems.

Landscapes reconstructed after open-pit mining provide an opportunity to explore soil-plant-water relationships since there is a relatively detailed record of the landform and soil reclamation material characteristics and construction techniques. During reconstruction, the landforms are built with overburden materials or tailings wastes, which are generally considered unsuitable for plant growth. Often these landforms include hill structures with long and steep slopes. After the landforms are built, the overburden structures are covered with salvaged cover soil materials (subsoil and topsoil) that are suitable as a rooting medium, can support plant establishment and growth. For that the cover materials need to provide a sufficient amount of moisture and nutrients to sustain plant growth even during times of low resource availability; e.g., drought (Boese, 2003), while successfully isolating the root zone from potentially limiting conditions in the overburden material.

The properties and thicknesses of these cover materials and the underlying substrate that is being reclaimed determine resource availability. The hydrological properties of the cover materials are important drivers of water availability. These include composition (organic *vs.* mineral components) and texture as they affect water retention and hence AWHC (Keshta et al., 2010; Huang et al., 2011). Furthermore, landscape position will play a significant role since it affects water movement along slopes and thereby available soil water content (ASWC). Therefore, understanding changes in soil moisture retention in different covers is very important to understand the survival and growth of plants, particularly under long drought periods which may occur due to future climate change. Even though water retention capacity increases with cover depth, there is uncertainty on the effect of climatic variability on soil water retention and thereby on transpiration and aboveground carbon biomass production on sloping landscapes with different cover depths.

Monitoring the key soil attributes including AWHC, bulk density which determines saturated hydraulic conductivity (K_{sat}) and porosity, salinity, and available nutrients is important to understand how reclaimed areas are functioning hydrologically. Although instrumentation and field studies can be used to measure short-term effects of soil physical, chemical and biological attributes on water retention and thereby productivity, they can be expensive, destructive and findings are often discontinuous and site-specific (Gower et al., 2001; Randerson et al., 2002; Huang et al., 2013). A rigorous modeling effort based on fundamental processes governing water, energy, ionic solutes and nutrients through the soil-microbe-root-canopy-atmosphere system can provide both a short and a long-term forecast of plant productivity (Grant, 2001, 2014) and might help guide the application depths of cover materials.

Lower AWHC in shallow covers reduces the soil moisture content (θ), particularly during drier periods (Huang et al., 2015a). This reduces the soil water potential (ψ_s) and consequently canopy water potential (ψ_c), and thereby increases canopy stomatal resistance (r_c) (Grant et al., 1999). Greater r_c reduces CO_2 diffusion and carboxylation, and thereby CO_2 fixation and plant growth. These processes can be used to determine the changes in transpiration with increased AWHC in reclaimed covers that are difficult to do by field studies. All of these processes are explicitly modelled in the comprehensive terrestrial ecosystem model *ecosys* (Grant, 2001, 2014; Grant et al., 2012) which therefore does not need to be calibrated for the study site as required for most other numerical models. The ability of *ecosys* to capture effects of soil drying on ecosystem productivity have been rigorously tested against θ and energy and CO_2 fluxes measured over a wide range of climatic and site conditions: e.g. modelling of θ changes as measured by time domain reflectometry (TDR) and changes in evapotranspiration (ET) and CO_2 fluxes as measured by eddy covariance during the 2001 – 2003 drought at several boreal forests (Grant et al., 2006a), water stress effects on CO_2 and energy exchange in temperate and boreal deciduous forests (Grant et al., 2006b), effects of water deficits on energy exchange and CO_2 fixation in a semiarid grassland (Grant and Flanagan, 2007), effect of regional weather patterns on net ecosystem productivity (NEP) of Canadian forests (Grant et al., 2009a), effect of changes in temperature on NEP of boreal black spruce stands (Grant et al., 2009b), effect of hydrological variations of peatland on CO_2 fluxes (Sulman et al., 2012) and seasonal water stress in tropical peatlands (Mezbahuddin et al., 2015).

An opportunity to test model hypotheses for depth effects on hydrological functioning of reclamation covers was offered by a research project with three different reclamation covers on a large saline sodic overburden dump referred as South Bison Hills (SBH) at the Syncrude mine

site in northern Alberta (Canada). Various field and modelling studies have been conducted at this site by Shurniak and Barbour (2002), Elshorbagy et al. (2005), Elshorbagy and Barbour (2007), Kelln et al. (2007), Keshta et al. (2010) and Meiers et al. (2011). These studies focused on the effect of cover depths on soil moisture storage and soil water movements rather than on water uptake and vegetation growth, because the vegetation had not reached an appropriate level of maturity. The forest stand has now reached an acceptable age that studies have now begun to assess the overall effect of cover material depths on long-term water balance (Huang et al., 2015a) and forest growth indices (Huang et al., 2011, 2013).

To date *ecosys* has not been used to model ecosystem processes in novel ecosystems undergoing reclamation. Building on previous studies, *ecosys* was used: (1) to understand and quantify the relationship between AWHC and transpiration as determined by cover depths, (2) to understand and quantify the relationship between transpiration and growth with different reclamation cover depths, and (3) to estimate the minimum cover depth required to provide sufficient amount of water for upland plant growth while stabilizing downstream water movement.

2.2. Methods

2.2.1. General model description

Ecosys is a comprehensive mathematical model that has the ability to represent multiple soil and canopy layers in soil-microbe-canopy–atmosphere systems at three-dimensional scales. The model simulates physical, chemical and biological processes in natural and disturbed terrestrial ecosystems through the acquisition, transformation and transfer of radiation, water, carbon (C), oxygen, nitrogen and phosphorous (Grant, 2001) and includes site-independent algorithms for all the processes (Mezbahuddin et al., 2014) needed to achieve realistic landscape-

scale predictions of productivity under a wide range of site conditions without prior calibration. The key parameters and algorithms used in *ecosys* were described in Grant (2001; 2014) and Grant et al. (2012) and remain unchanged from those used in earlier studies cited above. The major algorithms that govern the lateral and vertical water movements and thereby ASWC, root growth and water uptake, transpiration and their effects on NPP in *ecosys* are given below with reference to supporting equations given in appendices A to D in the Supplement.

2.2.1.1. Energy flux, canopy water potential and gross primary productivity (GPP) as affected by soil water content

In *ecosys*, transfers of water and heat occur through a multi-layered, multi-population soil-root-canopy system driven by first order closures of energy balances at canopy, snow (if present), litter and soil surfaces. Canopy temperature (T_c) for each plant population is achieved through the first-order closure of canopy energy balance (equation (1)) (Grant et al., 1999) in which aerodynamic resistance (r_a) and r_c regulate the heat and transpiration fluxes.

$$Rn_{ci} + LE_{ci} + H_{ci} + G_{ci} = 0 \quad (1)$$

where: subscript i = species or plant functional type (PFT); Rn_{ci} = canopy net radiation (W m^{-2}), LE_{ci}= latent heat flux between canopy and atmosphere (W m^{-2}), H_{ci} = canopy sensible heat flux (W m^{-2}), G_{ci} = canopy storage heat flux (W m^{-2}).

The transpiration flux (E_{ci}) in equation (1) is coupled to total plant water uptake (U_c) which is calculated from the difference between ψ_c and ψ_s across soil and root hydraulic resistances (Ω_s and Ω_r respectively) in each rooted soil layer (equation (2)). These calculations determine the transpiration from canopy surfaces and thereby water removal from soil profiles through the roots.

$$(e_a - e_i(T_{ci}))/(r_{ai} + r_{ci}) = \Sigma_l \Sigma_r (\psi_{ci} - \psi_{sl})/(\Omega_{si,r,l} + \Omega_{ri,r,l} + \Sigma_x \Omega_{ai,r,l,x}) + X_{ci} \delta \psi_{ci}/\delta t \qquad (2)$$

where: subscripts l = soil layer, r = root or mycorrhizae, x = 1 (primary root) or 2 (secondary root or mycorrhizae); e_a = atmospheric vapor density at air temperature (T_a) and ambient humidity (g m^{-3}), $e_i(T_{ci})$ = canopy vapor density at T_{ci} (g m^{-3}), T_{ci} = canopy temperature (K), r_{ai} = aerodynamic resistance to vapor flux from canopy (s m^{-1}), r_{ci} = canopy stomatal resistance to vapor flux (s m^{-1}), ψ_{ci} = canopy water potential + canopy gravitational potential (MPa), ψ_{sl} = soil water potential (MPa), $\Omega_{si,r,l}$ = radial resistance to water transport from soil to surface of roots or mycorrhizae (MPa h m^{-1}), $\Omega_{ri,r,l}$ = radial resistance to water transport from surface to axis of roots or mycorrhizae (MPa h m^{-1}), $\Omega_{ai,r,l,x}$ = axial resistance to water transport along axes of primary or secondary roots or mycorrhizae (MPa h m^{-1}), all calculated from root lengths and surface areas, X_{ci} = canopy capacitance (m^3 m^{-2} MPa^{-1}), t = time (h).

In soil water systems, ψ_s (equation (3)) is calculated by adding soil matric potential (ψ_m) depending on θ, soil osmotic potential (ψ_π) calculated from soil salt concentrations and gravitational potentials (ψ_g) calculated from elevation (Grant, 1995).

$$\psi_s = \psi_m + \psi_\pi + \psi_g \qquad (3)$$

In *ecosys*, ψ_m is calculated by log-transforming a Campbell equation (Campbell, 1974) considering θ and θ_{FC} (soil water content at field capacity (FC)). During soil drying, lower θ decreases ψ_m, which subsequently lower ψ_s thereby U_c.

The modelled root system governs U_c through the effects of root length density (RLD) on hydraulic resistance terms in equation (2) and thereby transpiration and productivity. In *ecosys*, the root system is represented by vertical primary axes, and horizontal secondary axes emerged from primary axes in each rooted soil layer of each plant species (Grant, 1993). Root growth is

driven by transfer of nonstructural C from shoots to roots modelled from shoot-root concentration gradients determined by shoot production *vs.* root assimilation in each layer, and from root sink strength determined by distance of each root layer from canopy sources. Root growth is calculated from assimilation in primary and secondary axes according to root growth yields [C20b, C21b], controlled by root water potential (ψ_r) which determines the root turgor, by O_2 and nutrient uptake, and by soil resistance to root penetration (Grant, 1998). Hence, RLD determined by the plant CO_2 fixation as affected by AWHC.

Lower ψ_s and U_c decrease ψ_c which is the sum of osmotic (ψ_π) and turgor potentials (ψ_t) (equation (4)) where ψ_t decreases with ψ_c during soil drying according to the ψ_π (Grant et al., 1999; Grant et al., 2007c).

$$\psi_{ti} = \psi_{ci} - \psi_{\pi i} \qquad (4)$$

where: ψ_t = canopy turgor potential (MPa), ψ_π = canopy osmotic potential (MPa).

Lower ψ_t drives stomatal closure as r_c is minimum ($r_{c\min}$) when ψ_c = zero, and rises exponentially with declining ψ_t (equation (5)).

$$r_{ci} = r_{c\min i} + (r_{c\max i} - r_{c\min i}) e^{(-\beta\, \psi_{ti})} \qquad (5)$$

where: $r_{c\min}$ = minimum r_c at ψ_c = 0 MPa (s m^{-1}), $r_{c\max}$ = canopy cuticular resistance to vapor flux (=5.0 × 10^3 s m^{-1}) [Larcher, 2003], β = stomatal resistance shape parameter (= -5 MPa^{-1}) [Grant and Flanagan, 2007].

Increased r_c or decreased canopy stomatal conductance (g_c= 1/r_c) reduces CO_2 diffusion into the leaves (equation (6)), and thereby CO_2 fixation [C3, C6a].

$$V_{gi,j,k,l,m,n,o} = (C_b - C_{ii,j,k,l,m,n,o}) / r_{li,j,k,l,m,n,o} \qquad (6)$$

where: subscripts j =branch or tiller, k = node, l = canopy layer, m = leaf azimuth, n = leaf inclination, o = leaf exposure (sunlit *vs.* shaded); V_g = leaf CO_2 diffusion rate (μmol m^{-2} s^{-1}), C_b = [CO_2] in canopy air (μmol mol^{-1}), C_i = [CO_2] in canopy leaves (μmol mol^{-1}), r_l = leaf stomatal resistance (s m^{-1}).

Canopy carboxylation rates (V_c) [C3] are coupled with CO_2 diffusion rates (V_g) (equation (6)) by solving for a common value of C_i, and so are calculated from stomatal effects on diffusion and non-stomatal water stress effect (f_ψ) on CO_2 and light limited carboxylation V_b [C6a] (Grant and Flanagan, 2007). Lower GPP and thereby net primary productivity (NPP = GPP- autotrophic respiration (R_a)) are thus obtained with lower ψ_s and ψ_c.

In *ecosys*, growth of internodes, petioles and leaves is driven by R_a and consequent assimilation of non-structural carbon from V_c according to organ growth yield as well as by non-structural nitrogen, and phosphorous from root uptake. Leaf area expansion of different PFTs is controlled by leaf mass growth, leaf area:mass ratio and ψ_t [C21a].

Lower ASWC in shallow covers reduces the ψ_s during drier months due to decreasing θ from increased ET. As ψ_s decreases, soil K decreases. Lower ψ_s slow down root water uptake, ψ_c and hence ψ_t to decrease more rapidly with drying, which increases r_c and hence reduces transpiration and CO_2 fixation. This causes more plant water stress in shallow covers especially during drier months and years resulting in slower plant growth, Leaf Area Index (LAI), and thereby RLD.

2.2.1.2. Soil water transfers

In *ecosys*, precipitation (*P)* is considered as an input to the model. The difference between rates of P and infiltration influence the value of surface ponded water depth that drives runoff

(Grant et al., 2004). Precipitation in excess of ET plus infiltration, both of which increase with AWHC, will generate surface water ponding and eventually runoff. The surface runoff among the grid cells and across lateral boundaries is modelled using the Manning equation [D1a]. The velocity of surface water flow [D3] depends on the surface geometry [D5a] and slope [D5b], and surface water depth [D2] and is calculated from kinematic wave theory [D4]. Lateral snow transfer is modelled from elevational differences between snowpack surfaces in adjacent grid cells [D1b]. The rates and directions of water movements in the soil are driven by water potential gradients and governed by soil hydrological properties, and occur through micropores (saturated or unsaturated water flows) and macropores. Vertical and lateral subsurface water fluxes through soil matrices/micropores [D7] are calculated by multiplying hydraulic conductance (Green and Corey, 1971) by water potential differences using Richard's equation [D9a] and Green-Ampt equation [D9b] for unsaturated and saturated conditions respectively (Grant, 2004). Macropore water flow is also modelled in all dimensions from gravimetric water potential gradients using Poiseuille-Hagen theory based on input values for the fraction of soil volume occupied by macropores in which water is unaffected by matric forces (Dimitrov et al., 2010).

Lateral subsurface discharge is calculated as gravity-driven flow from micropores and macropores in lateral boundary cells of the landscape to an assumed external water table, the depth of which is prescribed. Subsurface discharge is thus driven by lateral hydraulic conductivities of micropores and macropores in the boundary grid cells, and by elevation differences between the boundary grid cells and the external water table [D10] as described further in Mezbahuddin et al. (2015) and Mezbahuddin et al. (2016).

The soil cover depth influences soil moisture storage and thereby runoff and interflow. At the cover and overburden interface, infiltrated water not taken up by plants accumulates because

overburden has low K. Water accumulated in excess of AWHC flows laterally (interflow) to the bottom of the landscape and is then discharged. When cover depth and hence AWHC is small, more water accumulates at the interface than in thicker covers. Therefore shallow covers have more runoff + interflow during periods when P > ET and AWHC is exceeded. More runoff and interflow during these periods leaves less water to sustain uptake during subsequent periods when P < ET and soil moisture storage declines below θ_{PWP} (soil water content at permanent wilting point (PWP)) so that vegetation may experience water stress more rapidly. Declines in ASWC with ET will be more rapid in shallow covers with smaller AWHC.

2.2.2. Site description

2.2.2.1. Climate

Modelled outputs were tested against field data from a research watershed located at SBH (56°59'44.38"N, 111°37'12.09"W) at the south edge of the Syncrude Canada Ltd. Mildred Lake mine, approximately 40 km north of Fort McMurray, in northeastern Alberta. Mean annual P (1981-2010) of the area is 418.6 mm (Environment Canada, 2014) of which approximately 70% occurs as rainfall and 30% as snowfall (Boese, 2003). Mean monthly temperature ranges between -17.4 °C (January) and 17.1 °C (July) and the mean annual temperature is 1.0 °C (Environment Canada, 2014). This climate is characterized as sub-humid continental (Koppen Classification) with short summers and long cold winters (Kelln et al., 2007).

2.2.2.2. Experimental site

The SBH site was selected for this study as it contains an instrumented trial constructed on saline sodic overburden with three different reclamation cover depths. The total height of the SBH overburden dump is 90 m, the surface of which is approximately 40 m above the pre-

disturbance elevation (Meiers, 2002). The slope of the overburden dump was designed with a 1:5 (20%) incline and final overburden placement occurred in 1996 (Boese, 2003). After construction of the SBH dump, reclamation cover materials were placed over the overburden during the 1999 winter period. Three different reclamation covers (soil caps) were used along the north facing slope of the dump, each with an area of approximately 1 ha (200 m long and 50 m wide) (Hilderman, 2011). As shown in Figure 2.1(a) each cover consisted of a layer of salvaged peat-mineral mix (PMM) underlain by a layer of subsoil material (glacial till deposits) with varying thicknesses over the overburden (cretaceous shale) (Boese, 2003) as follows:

- 35 cm - 20 cm of subsoil overlain by 15 cm of PMM
- 50 cm - 30 cm of subsoil overlain by 20 cm of PMM
- 100 cm - 80 cm subsoil overlain by 20 cm of PMM

The key physical and hydrological properties of PMM, subsoil and overburden materials are given in Table 2.1. The AWHC changes according to the reclamation materials, calculated as field measured volumetric water content at field capacity minus permanent wilting point, was highest in PMM, followed by subsoil and overburden. The estimated AWHC with Land Capability Classification System (LCCS) multipliers for the 35 cm, 50 cm and 100 cm covers were 58 mm, 82 mm and 162 mm, respectively (CEMA, 2006).

2.2.2.3. Forest reclamation program

In the spring of 1999, barley was seeded with a density of 25 kg ha^{-1} in each plot to reduce erosion and to stabilize the slope in the first year after soil placement. Fertilizer was applied prior to tree planting in the fall of 1999 at 35 kg N ha^{-1}, 46 kg P ha^{-1}, 44 kg K ha^{-1} and 14 kg S ha^{-1} (Lanoue, 2003; Garrah et al., 2013). White spruce (*Picea glauca* (Moench) Voss) and trembling aspen (*Populus tremuloides* Michx.) seedlings were then planted in alternate rows (Hilderman,

2011) in each cover with a total density of 1600 stems ha^{-1} (50:50 mix of aspen and spruce). In 2007, ingress (volunteer) aspen and willow emerged at an average density of 20000 ha^{-1} in mid and lower slopes and 10000 ha^{-1} in upper slope positions (Drozdowksi et al., 2014).

2.2.3. Field data collection

2.2.3.1. Weather

Solar radiation, maximum and minimum air temperatures, *P*, wind speed, and relative humidity were recorded daily from January1, 1999 to December 31, 2015. All the other measurements were taken from the SBH weather station on the mid-slope of the 35 cm cover, except winter *P* and solar radiation. There was uncertainty in the accuracy of the *P* data in some data collection years, hence, the winter *P* (October 1 to March 31 every year) and solar radiation until 2006 (January 1 to December 31 every year) were taken from the Fort McMurray airport weather station located approximately 40 km south from the site. Winter *P* and solar radiation from 2007 were taken from the Mildred Lake airport weather station (built in 2007) located approximately 6 km northeast of the study site. These daily data were read into *ecosys* where they were resolved into hourly values to match the hourly time step at which the model functions.

2.2.3.2. Hydrology

SBH is an instrumented watershed, and the details of the installation of all the instruments were described in Boese (2003). Both the θ and ψ_m were measured using time domain reflectometry (TDR) probes and CS 229 sensors respectively at the middle slope position of each cover along the cover profile up to an upper section of the overburden from 1999 to 2015. However, data were missing for some years due to temporary instrument failures. Values for θ in

the 50 cm cover were available only up to 2006 due to failure after re-installation of instruments in 2007 (O'Kane Consultants Inc., 2012a). These θ and ψ_m data were collected from the proprietary Syncrude watershed database and were used to derive key soil properties or to validate model outputs and thereby to test the modelled effect of cover depth on soil water storage.

2.2.3.3. Root density and depth

Root samples were collected by North Wind Land Resources Inc. in October 2013, along three transects at SBH reclamation covers to determine the effect of cover depth on rooting distribution. Six cores were collected up to a depth of 30 cm below the cover-overburden interface using a Riverside auger at each site. The collected samples were stored in a freezer at -4 ^{0}C, then thawed and washed to acquire roots. Individual roots were manually picked and oven-dried at 40 ^{0}C for 48 hrs. Then all roots were weighed on a per core basis, and root biomass density was calculated for each sampling point (Northwind Land Resources Inc., 2014; Van Rees, 2014). A full description of sampling locations and methodology, and of root extraction can be found in reports from Northwind Land Resources Inc. (2014) and Van Rees (2014). Root density data were used to test modelled root densities and thereby to understand the effect of cover depth on root growth and soil water uptake by the vegetation.

2.2.3.4. Sap flow

Sap flow data from planted trees in 35 cm and 100 cm covers were collected by the Landhäusser research group using the Heat Ratio Method (Burgess et al., 2001; Bleby et al., 2004) during the growing seasons of 2014 and 2015. Sap flow probe sets (ICT International, Armidale, NSW, Australia) were installed in randomly selected trees (Burgess et al., 2001). In summer 2014 and 2015, sap flux was measured from 18 aspen and 18 spruce trees in lower and

upper slope positions of the 35 cm cover. For the 100 cm cover, sap flux was measured from nine aspen and nine spruce trees in the lower slope position during 2014 and upper slope position during 2015. Sap flow data were recorded at 10-min. interval and these values were corrected for wounding, wood thermodiffusivity properties and for zero flow periods as described by Burgess et al. (2001) using Sap Flow Tool software (ICT International, 2017). The sap flow velocities were summarized hourly (cm h^{-1}). Then the average individual tree sap flow data were converted to sap flow per unit ground area by multiplying wound-corrected sap flow velocity by the stand sap wood area to ground area ratio (SA). The SA was calculated using the product of basal area to ground area ratio of tree stems and the fraction of basal area occupied by sapwood as described by Hogg and Hurdle (1997). These sap flow per unit ground area values were used to test modelled water uptake per unit ground area and thereby to determine the effect of cover depth on plant water relations.

2.2.3.5. Leaf Area Index

Total site LAI was measured in August 2015 at the upper and lower positions in 35 cm and 100 cm covers by the Landhäusser research group using a LAI-2200C plant canopy analyzer (LI-COR Inc., Lincoln, Nebraska, USA). These LAIs were used to test the modelled LAIs in each cover and thereby to determine the effect of cover depth on plant water relations, growth and thereby NPP.

2.2.3.6. Aboveground biomass

Aboveground carbon biomasses were estimated by Macyk et al. (2009) and Drozdowksi et al. (2011, 2014) for planted aspen and white spruce trees in 35 cm, 50 cm and 100 cm covers. The height and stem diameters at root collar and 1.3 m height of planted trees were collected annually (2007 - 2013) in 10 m x 10 m permanent sampling plots which were established in

upper, middle and lower slope positions of all the reclamation covers in 2007 (Macyk et al., 2009; Drozdowksi et al., 2011, 2014). The aboveground carbon biomass values for each species were estimated using allometric equations based on measured breast height and basal tree diameters in the sampling plots and species-specific density and expansion factors for branch and leaf/needles developed for Alberta species (Alberta Environment, 2007). These data were used to validate the modelled aboveground carbon biomass and thereby to understand the effect of cover depth on NPP.

2.2.4. Model Experiment: South Bison Hill reclamation site as represented in *ecosys* model runs

2.2.4.1. Landscape

The information for site management and soil properties collected during 1999 and 2000, were used to construct the input files used to initialize *ecosys* for SBH. These inputs represent the actual field characteristics which include site, climate, and plant and soil management data used by *ecosys* to simulate basic physical, chemical, and biological processes. Each reclamation cover was represented in the model as a transect of six interconnected grid cells each of which had a dimension of 50 m x 40 m. Five grid cells represented the slopes as shown in Figure 2.1(b) and one grid cell represented the level area above the slope corresponding to the landscape at SBH. All the input data (site, climate, soil properties, soil and plant management) were the same among reclamation covers except cover depths as described in Section 2.2.2.

2.2.4.2. Soil properties

Descriptions of soil physical and chemical conditions at the SBH site were obtained from earlier studies done by Macyk (1999), Meiers (2002) and Yarmuch (2003), while soil biological

data were taken from a study done by Lanoue (2003). The θ_{FC} and θ_{PWP} for PMM, subsoil and overburden (Table 2.1) were derived from water desorption curves developed using measured θ *vs.* ψ_m data. K_{sat} values (Table 2.1) reported by Meiers et al. (2011) were used as inputs from which the model calculated unsaturated values (Grant et al., 2004). The external water table depth at the bottom of each transect was set to 2.5 m below that of the 100 cm cover. These inputs to the model were used to drive functions for soil water movement. The three horizons of the soil profile (PMM, subsoil and upper overburden; Figure 2.1(a)) were subdivided into 15, 16 and 19 soil layers for the 35cm, 50 cm and 100 cm capping depths, respectively, to increase spatial resolution and enable comparison of θ with measured values. The overburden depth in each reclamation cover was set to a constant value (3 m) to model water movements to/from the overburden. The root studies (Karst and Landhäusser, 2014; Van Rees, 2014) that had been conducted in the study area showed that a very small fraction of roots penetrated into the overburden relative to the above soil reclamation cover, most of which were within 25 cm below the cover-overburden interface. Soil resistance equations used in the model for root growth in crops by Da Silva and Kay (1997) and Chen and Weil (2011) did not limit root penetration into overburden in the model as much as was observed. Therefore, a maximum rooting depth of 25 cm below the subsoil-overburden interface was chosen for each soil cover treatment.

2.2.4.3. Land management

Barley was seeded (spring 1999) and fertilizer application was modelled as practiced in the field (fall 1999) which was described under the forest reclamation program in Section 2.2.3. Aspen and white spruce PFTs were planted at the densities described in the Section 2.2.3. Grass and clover PFTs were seeded in each grid cell as ground cover species. In 2007, ingress plants

were planted at as the density described under Section 2.2.3. The model was run for 17 years (1999 - 2015) using the daily weather data described in Section 2.3.1.

2.2.4.4. Model validation

To test the accuracy with which *ecosys* simulated water infiltration from precipitation and water removal from evaporation, transpiration (Eqn. 2), runoff [D1a] and subsurface discharge [D10] in the different capping treatments, modelled θ from the depths corresponding to those of TDR probe measurements were regressed on θ measured daily by TDR probes in 35 cm and 100 cm covers from 2011 to 2015. Both modelled and measured total soil moisture storage in each cover were estimated by adding the products of θ and layer thickness for each soil layer down to the cover-overburden interface. The modelled total water storage in 35 cm and 100 cm covers was regressed on total water storage estimated from measured θ. Modelled water removal through uptake was directly tested by regressing hourly averages of aspen and spruce sap flow against the modelled hourly water uptake (Eqn. 2) from the 35 cm cover at upper and lower slope positions (2014 and 2015), and from the 100 cm cover at lower slope (2014) and upper slope (2015) positions. Accuracy of the simulations were evaluated from the mean absolute relative error (MARE) calculated using equation (7), and from regression intercepts ($a \rightarrow 0$), slopes ($b \rightarrow 1$), coefficients of determination ($R^2 \rightarrow 1$), root mean squares for difference (RMSD$\rightarrow$0) from regressions of modelled on measured θ, modelled on estimated total water storage, and measured sap flow on modelled water uptake. RMSDs from sap flow regressions were compared with root-mean-squares for error (RMSE) of aspen (n = 9) and spruce (n = 9) sap flow measurements.

$$\text{MARE} = \frac{\sum\left|\frac{Ei-Si}{Ei}\right|}{n} \quad (7)$$

where: *Ei* is the estimated total soil moisture using TDR data at every time step, *Si* is the simulated value, and *n* is the total number of data points (Elshorbagy et al., 2007).

A non-linear regression model with an asymptotic distribution was used to quantify the relationship between AWHC and transpiration and a linear regression model was used to quantify the relationship between transpiration and NPP with different reclamation cover depths.

2.3. Results

The current study was mainly focused on the 2011 - 2015 period to understand the soil cover depth effect on water balance components and aboveground biomass production after the reclamation covers had reached over-story crown closure and sites were at nearly steady-state for transpiration (Garrah et al., 2013). One drier year (2011), two wet years (2012 and 2013) and two intermediate years (2014 and 2015) with annual *P* of 238 mm, 507 mm, 462 mm, 385 mm and 340 mm, respectively were experienced during this period.

2.3.1. Modelled *vs.* measured soil water contents in different reclamation covers

The modelled θ in the PMM, subsoil and overburden layers of middle slope positions in 35 cm and 100 cm covers followed the same pattern as TDR measurements (Figure 2.2) during the non-frozen period (April 1 to October 31). The θ in 50 cm cover was not included since a re-installation of TDR probes in 2007 resulted in an abrupt change in monitoring trends. Small deviations were observed in the modelled θ compared to the measured values (Figure 2.2). The average RMSD for PMM and subsoil materials in the 35 cm cover were *ca*. 0.07 m^3 m^{-3} and 0.03 m^3 m^{-3} respectively whereas the RMSD for PMM and subsoil in 100 cm cover were 0.04 m^3 m^{-3} and 0.02 m^3 m^{-3} respectively (Table 2.2). The use of common θ_{FC} and θ_{PWP} for each material in all

reclamation covers (Table 2.1) may have contributed to RMSD because measured values varied among the reclamation covers as described in Section 2.4.2.

The coefficients of determination for measured and modelled θ (R^2) were lower for the lower layers of subsoil and overburden layers (Table 2.2) due to lower variation of θ. The magnitude and variation of θ were greater in upper PMM layers, indicating more rapid infiltration and uptake, and decreased with depth in subsoil and overburden layers due to lower AWHC and K, and hence slower infiltration and uptake (Table 2.1). Greater θ variation was observed in upper PMM layers (0 - 10 cm) of the 35 cm cover (Figure 2.2) compared to the 100 cm cover because lower AWHC in the 35 cm cover caused PWP to be reached earlier during dry periods and saturation earlier during wet periods as water percolation to the overburden was slow. The TDR probe readings at 42 cm depth in the 35 cm cover showed lower θ compared to other overburden layers in the three reclamtion covers. Huang et al. (2015a) suggested these lower θ may be due to coarser materials around the sensor. The difference between modelled and measured θ in overburden may be due to the lower reliability of TDR readings under saturated conditions as mentioned by Elshorbagy et al. (2005).

The total soil moisture in the reclamation covers modelled at the middle slope of each cover showed a similar pattern to that estimated from the measured θ (Figure 2.3). The total soil moisture in the 100 cm cover was estimated only for the 2014 and 2015 due to failure of TDR probe at 20 cm during 2011 - 2013 as well as TDR probes at 55 cm and 90 cm during 2013. The coefficients of determination (R^2) for the regressions of modelled total water storage on estimated total water storage as described in Section 2.4.4 were 0.5 and 0.7 for 35 cm and 100 cm covers, respectively. The RMSD for 100 cm and 35 cm covers were 18 mm and 16 mm whereas MARE were 6% and 12%, respectively. The ASWC (Figure 2.3) was high (θ remained

well above PWP) in each cover during wet years (2012 and 2013) and so was able to provide required amount of moisture for plant growth. However, ASWC was low for the 35 cm and 50 cm covers during the drier (2011) and intermediate year (2015), and soil moisture storage reached PWP earlier than for the 100 cm cover (Figure 2.3). Total soil moisture content in 35 cm and 50 cm covers declined close to the PWP even during a shorter dry period in wet and intermediate years due to lower AWHC.

Higher total soil moisture storage was modelled for lower slope positions compared to middle and upper slope positions in each cover (Figure 2.4) especially during spring snow melting and intensive rainfall periods. The modelled θ in lower slope position remained higher throughout the year compared to middle and upper slope positions which showed greater water decline during drier periods (Figure 2.4). The differences of modelled θ among the slope positions were more prominent in the 100 cm cover than in the 35 cm and 50 cm covers (Figure 2.4) due to higher AWHC.

2.3.2. Modelled *vs.* measured root growth in different covers

Declines in θ modelled in Figures 2.2–2.4 were driven by root water uptake calculated from RLD (Eqn. 2) modelled from root mass densities (RMD). The modelled RMD (Figure 2.5) lay within the standard deviations of measured values except at 50 cm soil depth and in the lowest layer of 50 cm cover (25 cm below the cover-overburden interface). However, the observed RMD in different covers were not significantly different ($P > 0.1$) due to large uncertainties in measured values indicated by the large standard deviations. The percentage of modelled tree root lengths within the upper 30 cm of the 35 cm, 50 cm, and 100 cm covers were 93%, 92%, and 90%, respectively, and the total modelled root density in the 35 cm and 50 cm covers were 15% and 10% higher than the 100 cm cover. The percentages of modelled root

lengths in overburden were 1.9%, 1.7% and 1.3% for the 35 cm, 50 cm, and 100 cm covers, respectively. Slightly higher modelled root percentages were observed in overburdens of the 35 cm and 50 cm covers in which root penetration was limited to 60 cm and 75 cm, respectively. Overall, exponential declines in both modelled and measured RMD with depth were apparent in each cover and deeper modelled root distributions in the 100 cm cover were corroborated by deeper measurements of RMD.

2.3.3. Modelled root water uptake *vs.* measured sap flow

Root water uptake in *ecosys* was driven by RLD and limited by ψ_s (Eqn. 2) from ASWC. The lower ASWC in the 35 cm profile (Figure 2.3) indicated greater limitation to plant water uptake than in the 100 cm profile. This limitation was tested by comparing modelled plant water uptake (RHS of Eqn. 2) with measured sap flow (Figures 2.6 and 2.7) at upper and lower slope positions in the 35 cm and 100 cm covers during dry (day of year (DOY) 172-178) and wet (DOY 208-214) periods in 2015 (Figure 2.3). The modelled uptake was always within the standard deviation of the average measured sap flow (Figures 2.6 and 2.7) except during the last two days of the dry period in the upper slope of the 35 cm cover. The modelled uptake rates followed the same diurnal and seasonal patterns as the average sap flow of planted trees with $R^2 > 0.5$ ($p < 0.001$) and RMSDs < 0.02 mm h^{-1} (Table 2.3). The higher RMSE (n=9) compared to RMSD indicate limited opportunity to improve agreement between modelled uptake and measured sap flow rates in each cover without further reducing uncertainty in measured rates.

Differences in modelled water uptake and measured sap flow per unit ground area between aspen and spruce in different reclamation covers were partly determined by the differences in LAI driven by differences in growth (Section 2.1.1). Different LAIs were modelled for the aspen and spruce in each cover (Table 2.4). In 2015, modelled maximum LAI of aspen across all slope

positions in the 35 cm and 100 cm covers were 1.4 and 2.0 whereas those of white spruce were 1.4 and 1.1, respectively. The differences in seasonal transpiration/sap flow per unit ground area among different covers were closely related to the LAIs of aspen and spruce, and more similar transpiration/sap flow values for aspen and spruce were observed for the 35 cm cover (Table 2.4). However, lower seasonal sap flow of spruce in 100 cm *vs.* 35 cm cover in 2014 as well as lower spruce *vs.* aspen transpiration/sap flow in 100 cm cover than in 35 cm cover in both years (Table 2.4), indicated smaller spruce LAI relative to aspen in the 100 cm cover. In the 2015 wet period (indicated in Figure 2.3), the maximum hourly transpiration of aspen and white spruce in the 35 cm cover was approximately 0.07 mm hr^{-1} (Figures 2.6(b) and 2.6(d)). However, in the 100 cm cover, aspen had higher transpiration (~0.12 mm hr^{-1}) and spruce had similar values to those in the 35 cm cover (Figures 2.6(c) and 2.6(e)). The cumulative tree (aspen + spruce) transpiration was greater for the 100 cm cover than the 35 cm cover, with greater contributions from aspen than from spruce, during the study period (Table 2.4). The comparison did not include the 50 cm cover, for which sap flow data were not collected.

More rapid transpiration was modelled for both aspen (except 2014) and spruce plants in the lower slope position (Table 2.4 and Figure 2.7) due to greater ASWC (Figure 2.4). The cumulative modelled uptake differences between slope positions in all the covers were smaller with greater *P* during 2014 but were greater with less *P* during 2015 (Table 2.4). These modeled values at different slope positions could only be compared to the measured sap flows for the 35 cm cover (Table 2.4 and Figure 2.7) due to field data availability. A clear slope position effect on tree water relations during the dry period was indicated by the lower uptake and sap flow of aspen and spruce in upper slope (Figures 2.7(b) and 2.7(d)) compared to lower slope positions (Figures 2.7(c) and 2.7(e)) in the 35 cm cover. Also, the cumulative sap flow in spruce was

higher at the lower than at the upper slope position (Table 2.4). Even though aspen sap flow at the lower slope position was higher than at the upper slope position during the dry period (Figures 2.7(c) and 2.7(b)), cumulative aspen sap flow in the 35 cm cover over the entire growing season was similar at both slope positions (Table 2.4).

2.3.4. Effects of soil moisture on water relations of trees

Modelled water uptake was strongly controlled by plant water relations (ψ_c and g_c). Stomatal conductance (g_c) is determined by ψ_t (Eqn. 5), which is in turn determined by ψ_c (Eqn. 4). In the model, g_c directly affected transpiration, which was in close equilibrium with water uptake (Eqn. 2), and CO_2 fixation (Eqn. 6). The effect of AWHC on ψ_c, g_c and CO_2 exchange modelled in the 35 cm cover was compared with that in the 100 cm cover during the wet and dry periods for aspen (Figure 2.8) and spruce (Figure 2.9). The modelled ψ_c, g_c and CO_2 exchange remained high in both the 35 cm and 100 cm covers during the wet period for both aspen and spruce (Figure 2.8(b1-b3) and Figure 2.9(b1-b3)). However in the dry period, lower ψ_c from reduced U_c (Figures 2.6 and 2.7) forced lower g_c and hence CO_2 flux for both aspen and spruce in the 35 cm

cover (Figure 2.8(a1-a3) and Figure 2.9(a1-a3)). In spruce, water uptake (Figure 2.6), g_c and CO_2 flux (Figure 2.9(a1-a3)) in the 35 cm cover nearly stopped during the drying period, reducing plant growth. In the 100 cm cover, modelled water uptake (Figure 2.6), ψ_c, g_c, and CO_2 flux (Figure 2.8(a1-a3) and Figure 2.9(a1-a3)) during the drying period did not decline as much as in the 35 cm cover (Figure 2.6), this was driven by greater soil moisture storage (AWHC; Figure 2.3) and more water uptake from a deeper root system (Figure 2.5). However, a slightly greater soil drying effect on tree water status was modelled and observed for spruce than for aspen (Figures 2.6, 2.8 and 2.9). The modelled CO_2 flux per unit ground area (Figure 2.8(b3) *vs.* Figure

2.9(b3)) was also affected by greater aspen *vs.* spruce LAI in the 100 cm cover than in the 35 cm cover (Table 2.4).

The water relations of aspen (Figure 2.10) and spruce (Figure 2.11) in different covers under different climates were further elaborated during mid-July in a drier (2011) and wetter (2012) year. These results follow the same pattern as observed during the wet and dry periods of 2015 (Figures 2.8 and 2.9). Soil cover depth had a minimal effect on ψ_c, g_c and CO_2 flux of aspen and spruce during the wetter year (Figure 2.10(b2-b4) and Figure 2.11(b2-b4)). However, substantial declines were modelled in the 35 cm and 50 cm covers during the drier year indicating greater water stress and reduced productivity (Figure 2.10(a2-a4) and Figure 2.11(a2-a4)).

2.3.5. Net primary productivity and aboveground biomass with different reclamation covers

The modelled CO_2 fluxes in trees in the 35 cm and 50 cm covers were lower compared to the 100 cm cover during drier months and years (e.g. Figures 2.10 and 2.11) resulting in lower GPP and NPP. Modelled annual NPPs of aspen, spruce and total vegetation for drier, intermediate and wetter years are given in Table 2.5. Modelled NPP was smallest during the driest year (2011) for all the covers, but particularly in upper slope positions in the 35 cm and 50 cm covers, and was greatest during the wettest year (2013). Then NPP remained stable during subsequent years with intermediate *P* (2014 and 2015). The decline in NPP of the 35 cm and 50 cm covers *vs.* the 100 cm cover was greatest during drier years and greater NPP gains with *P* were modelled for the 35 cm cover as water became less limiting for growth (Table 2.5). Thus, NPP of the upper slope position in the 35 cm cover during the driest and wettest years was 48% and 75% respectively of those in the 100 cm cover. The NPP followed the same slope position

pattern as for the θ, uptake and transpiration with higher NPP modelled in the lower slope position in 2015 (Table 2.5). The slope position effect on NPP was greatest during the driest year as indicated by reductions in total NPP of greater than 60% at upper slopes *vs.* lower slopes of the 35 cm and 50 cm covers, and disappeared during wetter years (2013 and 2014) (Table 2.5).

Lower NPP in drier periods lowered the biomass production in 35 cm and 50 cm covers over the reclamation period (Figure 2.12). The average modelled aboveground carbon biomass of aspen, spruce and total (aspen + spruce) along the slope in each reclamation cover followed the same trend as the estimated biomass from field measurements (Figure 2.12). Comparatively higher grass and clover aboveground carbon biomasses (*ca.* 300 g C m^{-2}) (data not shown) and a very low tree aboveground carbon biomass (< 50 g C m^{-2}) were modelled in each cover until 2005 (Figure 2.12). In 2006 (after six years of reclamation), trees started to dominate the grasses and grew exponentially (Figure 2.12) thereafter with greater irradiance interception from more elevated leaf area. Trees in the 100 cm cover grew more rapidly than those in the 50 cm and 35 cm covers and showed a greater aspen growth relative to spruce (Figure 2.12(a-c)). The average measured and modelled aspen:spruce biomass ratios (2007 - 2013) declined from 4.9 and 6.0 in the 100 cm cover to 1.5 and 2.7 in the 50 cm cover, and 1.1 and 2.2 in the 35 cm cover (Figure 2.12), respectively. These modelled ratios were driven by differences in the modelled CO_2 fluxes for aspen and spruce in Figures 2.8, 2.9, 2.10 and 2.11 where CO_2 fluxes were higher for aspen in the 100 cm cover than the 35 cm and 50 cm covers, but were lower for spruce.

2.3.6. Relationship between AWHC and transpiration and, plant water-use as determined by cover depth

Differences in modelled transpiration with different cover depths (Figures 2.6 and 2.7) should cause differences in total water-use efficiency (WUE_T) which was estimated from annual

modelled ET and NPP of planted trees, runoff and subsurface discharge of water to downstream ecosystems. The non-linear regression model indicated that annual modelled transpiration increased at a decreasing rate with AWHC (R^2 = 0.99) and 99% of maximum or asymptote transpiration for the site during wet, intermediate and dry years was achieved when AWHC reached 162 mm (Figure 2.13(a)). Also a greater effect of AWHC on transpiration was modelled during dry *vs.* intermediate and wet years (Figure 2.13(a)).

A positive linear relationship was derived between modelled transpiration and NPP (slope of the line represents planted tree water-use efficiency of productivity (WUE_P)). Even though the WUE_P differences were not significant among covers ($p > 0.05$), a higher WUE_P was estimated in the 100 cm cover (2.59 g C kg^{-1} H_2O) than in the 50 cm (2.47 g C kg^{-1} H_2O) and 35 cm (2.40 g C kg^{-1} H_2O) covers (Figure 2.13(b)). The average annual modelled ET derived from modelled energy balances (Eqn. 1) was > 100% of measured *P* in drier years, ~85% during intermediate years and ~60% in wet years for all the covers. The average annual (2011 - 2015) modelled ET ratios were 78%, 81% and 83% of measured *P* for the 35 cm, 50 cm and 100 cm covers respectively. However, annual modelled transpiration:evaporation increased with increasing cover LAI during the study period (Table 2.6). Thus, WUE_T estimated from annual modelled ET and NPP of planted trees, increased non-linearly with increasing cover depth and a greater WUE_T was estimated in the 100 cm cover than in the 35 cm and 50 cm covers (data not shown).

Modelled ET was subtracted from *P* to understand changes of other water balance components in each cover under different climatic conditions (Table 2.6). The *P*-ET in each cover was equal to the sum of modelled runoff, subsurface discharge and change in θ. Negative *P*-ET was modelled for all the covers in the driest year (2011), during which water was extracted from deeper soil layers (Figure 2.2) to maintain transpiration and thereby productivity. The *P*-ET

was greatest in the wettest year 2012 (Table 2.6) during which ASWC rose even in the 35 cm cover (Figure 2.3). The average of annual modelled runoff in all the covers during 2011 - 2015 was approximately 47 mm. However, the 35 cm cover had slightly higher modelled runoff than the other two covers during heavy rainfalls in the second consecutive wettest year (2013) due to lower AWHC (Table 2.6) and hence infiltration. The modelled subsurface discharge was not much different among the three covers during the drier years, but that from the 100 cm cover was lower during the wetter years 2012 and 2013 and higher during the subsequent intermediate years 2014 and 2015. The average annual and inter-annual range of modelled water release (runoff + subsurface discharge) from 35 cm, 50 cm and 100 cm covers to downstream wetlands were 101 mm (54–173 mm), 99 mm (57–172 mm), and 95 mm (59–157 mm), respectively. Most subsurface discharge and runoff occurred during snow melting (Table 2.6) except in the wettest year 2013 when summer subsurface discharge exceeded 50%, and runoff from the three covers exceeded 1 mm. Even though small fluctuations of subsurface discharge were observed between drier and wetter years, the overall subsurface discharge:precipitation ratio declined in each cover over the reclamation period (1999 - 2015) as ET increased with tree growth.

2.4. Discussion

2.4.1. Greater cover depth will increase water storage and ASWC

The modelled and measured θ and thereby total soil water storage showed that the ASWC increased with increasing cover depth. Thus, the 100 cm cover was able to maintain an ASWC greater than the PWP facilitating water uptake during dry periods compared to 35 cm and 50 cm covers. This ability was apparent in the model by the more rapid declines of modelled ASWC relative to AWHC in upper PMM layers of the 35 cm and 50 cm covers that caused earlier depletion of ASWC to PWP than in those of the 100 cm cover (Figures 2.2 and 2.3). Greater

water uptake from upper layers was forced by less water uptake from lower layers in the shallow covers due to a shallow root system. These modelled soil water storage results were similar to the findings from earlier research by Shurniak (2003), Elshorbagy et al. (2007), Kelln (2008), and Huang et al. (2015a) who modelled soil water storage in different covers at the SBH site using numerical models. However, these earlier modelling studies were conducted using hydrological models, which had to be calibrated for the study site e.g. Hydrus-1D and System dynamics watershed model (SDWM), and all root growth was assumed to occur only within the cover layers.

2.4.2. Greater soil water storage will increase transpiration in reclaimed areas

In *ecosys*, ψ_m was calculated from θ using modified Campbell and Green-Ampt methods and thus modelled ψ_m and thereby ψ_s (Eqn. 3) changed considerably during wet and dry periods according to changes in θ. During wet periods, higher θ (Figure 2.3) raised ψ_s and lowered Ω_s, hastening U_c and thereby maintaining high ψ_c (Eqn. 2) and g_c in all covers. Consequently, the transpiration rates of PFTs in different slopes (Figure 2.7) were not limited by θ during wet periods due to adequate vertical recharge through P. During dry periods, lower θ in the 35 cm and 50 cm covers than in the 100 cm cover (Figure 2.3) reduced transpiration to an extent that was consistent with measured sap flow rates (Figure 2.6). This decline was modelled from the effects of lower θ, ψ_m and thereby ψ_s (Eqn. 3) during dry periods, which increased Ω_s and consequently lowered U_c (Eqn. 2). This lower U_c led to lower ψ_c, ψ_t and hence lower g_c through the equilibration of plant water uptake (RHS in Eqn. 2) with transpiration (LHS Eqn. 2). Also, less root growth modelled deeper in the 35 cm and 50 cm covers (Figure 2.5) increased Ω_r and so

further reduced U_c, and hence transpiration relative to those in the 100 cm cover (Figure 2.6). In addition, the reduced LAI modelled prognostically from reduced NPP with 35 cm and 50 cm covers (Table 2.4) further reduced transpiration. The modelled g_c and LAI in the 100 cm cover were consistent with observations of Strilesky et al. (2017) for SBH plateau which had similar reclamation cover depth and composition, and reached over-story canopy closure as 100 cm cover.

A greater plant water uptake in the 100 cm cover (Figure 2.6(c) and Figure 2.6(e)) than in the 35 cm cover (Figure 2.6(b) and Figure 2.6(d)) was possible with lower Ω_s due to higher ASWC (Figure 2.3) and $\psi_{s,}$ as well as by larger aspen LAI, which increased R_n in the canopy energy balance (Eqn. 1) relative to spruce (Table 2.4). Transpiration by deciduous trees such as aspen tends to be greater than that by conifers (i.e. spruce), so that greater transpiration in the 100 cm cover may be partially caused by a proportionally greater aspen leaf area *vs.* spruce leaf area compared to the other covers. The maximum uptake/sap flow rate of aspen in the 100 cm cover in a mixed stand with LAI of 1.9 in this study (Figure 2.6; Table 2.4), was close to the range (0.12–0.16 mm hr^{-1}) for different aspen clones at a mature parkland site with LAI of 1.4 during a warm year, but lower than that in a pure stand of aspen with larger LAI (2.3) at mature boreal site (~0.4 mm hr^{-1}) estimated from sap flow measurements by Hogg and Hurdle (1997). However, the aspen spacing was larger in the current study as it was in a mixed stand, so that slower uptake would be expected on an area basis.

Greater stomatal response to soil drying was observed for spruce compared to aspen. Spruce species have a long leaf lifespan with lower g_c and thereby lower transpiration (Angstmann et al., 2013), lower leaf N and hence lower $V_{c\max}$ [C6b], and greater root axial resistivity (Larcher, 2003) as modelled in Grant (2004) and Grant et al. (2005). However, in

mixed species stands spruce trees may have much more leaf area than aspen trees. In the model, the larger root axial resistivity used for white spruce compared to aspen delayed overnight rehydration and thereby forced greater ψ_c sensitivity to root water uptake. Mencuccini and Grace (1996) and Gao et al. (2002) also attributed the greater sensitivity of conifer transpiration to lower xylem conductance compared to broadleaf trees.

The modelled and measured results for θ, U_c, ψ_c, and transpiration indicated that greater covers depths stored more water and thereby maintained greater water uptake and transpiration. These results were also supported by the previous field and modelling studies conducted by Kelln (2008), Kelln et al. (2009), Huang et al. (2015a) indicating increased transpiration with greater cover depths. However, the relationship between AWHC and transpiration increased at a decreasing rate with increasing cover depth (Figure 2.13(a)). This relationship indicated that transpiration will increase little with AWHC above a threshold value (0.95 of the asymptote) depending on the site conditions which for the current study was 162 mm. This threshold will be further evaluated in Chapter 5 using a wider range of hypothetical covers.

2.4.3. Increased plant water uptake from greater soil water storage will increase CO_2 fixation and hence NPP

Modelled plant water uptake and measured sap flow, modelled transpiration and modelled and measured aboveground biomass indicated that CO_2 fixation and thereby NPP increased linearly with plant water uptake from greater reclamation cover depths. Water uptake and hence NPP of 35 cm and 50 cm covers in the model declined particularly during dry periods due to lower AWHC (Table 2.5). The lower g_c from lower θ (described in Section 4.1) in 35 and 50 cm covers forced partial or full stomatal closure and thereby slower CO_2 diffusion and lower C_i. The

slower diffusion and lower C_i reduced CO_2 fixation (Eqn. 6) reducing annual NPP particularly with 35 cm and 50 cm covers during dry years.

Root growth is an important variable for modelling cover soil depth effects on NPP, as root growth and rooting space are greatly influenced by soil cover properties and govern water and nutrient uptake. Like LAI, root growth in *ecosys* is fully prognostic, driven by soil water and nutrient status and by root-shoot C and nutrient exchange. The importance of root growth to NPP was examined in previous modelling studies by Grant (1991), Grant (2014) and Mezbahuddin et al. (2015). Modelled and measured root biomass densities of all the covers showed the highest densities near the surface and exponential decline caused by declining root sink strength with soil depth (Figure 2.5) as found in the undisturbed boreal forest (Strong and La Roi, 1983; Yuan and Chen, 2010). The greater water uptake and higher θ variation in upper soil layers *vs.* lower layers (Figure 2.2) was caused by the greater root densities near surface soil layers. Through a comprehensive literature synthesis, Jackson et al. (1996) stated that boreal forests have a shallow rooting profile where 80-90% of roots are within the upper 30 cm of soil. The modelled root density in the 100 cm cover showed a similar pattern. Modelled root lengths in the overburden of each cover were within the range (1.3% to 2.2%) found by Lazorko and Van Rees (2012) in overburden materials at different reclamation sites. These lower percentages indicated a limited water uptake from overburden. However, slightly higher modelled total root length in overburden of the 35 cm cover compared to other covers (Figure 2.5) indicated more water uptake from overburden layers with shallow covers during drier periods (Figure 2.2). This may partially offset the reduced uptake from the PMM and subsoil material in shallow covers.

2.4.4. Growth of different PFTs with different AWHC in reclaimed covers

In the model, competition among PFTs for irradiance, water and nutrients was governed by vertical profiles of canopy leaf area and root lengths driven by plant growth so that different phenology, irradiance interception, CO_2 fixation rates and water uptake rates in each PFT determined its growth in the competitive environment (Mekonnen et al., 2018b). Early colonizing ruderal herbaceous species were dominant on the SBH site (Shurniak, 2003; Kessler, 2007), competing for above and belowground resources with the newly planted trees (Bockstette et al., 2017). Modelled herbaceous species showed similar growth patterns as those observed in the field during 1999-2006 (data not shown). Early in succession planted tree growth was suppressed by the herbaceous competition for water and nutrient uptake with these ground cover species as their root length densities were greater compared to those of the planted tree seedlings. Later in succession grass and clover densities gradually declined (data not shown) as tree root growth increased the competition for water and nutrients and the increasing tree canopy cover reduced light availability in the understory.

In the model, deciduous PFTs were modelled with greater specific leaf area (SLA) and less clumping, allowing greater light interception, and with greater leaf N content and hence leaf CO_2 fixation capacity and g_c (Grant, 2015; Mekonnen et al. 2018b), particularly during early stand development, and with more rapid nutrient uptake and loss from greater leaf turnover. Therefore, aspen growth was modelled to be more rapid than white spruce growth in young reclaimed sites due to more rapid water uptake and greater photosynthetic capacity from greater leaf nutrient contents. Faster growth of aspen relative to spruce was modelled in the 100 cm cover due to more favorable soil nutrient and water status that favored the more open and rapid nutrient cycling of deciduous PFTs. The modelled aspen:spruce biomass ratios therefore increased with

cover depth which was consistent with measured values (Figure 2.12) and with observations of Kelln (2008) that there is a tendency for greater aspen growth and less white spruce growth with increased cover depth. These changes in PFTs affected the WUE_P in different covers that were derived from the relationship between transpiration and NPP (Figure 2.13(b)). Thus, the greater aspen growth increased the WUE_P in the 100 cm cover to become more similar to the average WUE_P of woody trees in the temperate climate zone (Larcher, 2003) compared to the other two covers.

2.4.5. Greater cover depth caused greater WUE_T and less interannual variability in subsurface discharge

Greater LAI (Table 2.4) and hence less ground surface exposure in the 100 cm *vs.* the 35 cm and 50 cm covers increased transpiration (Figures 2.6 and 2.7) but reduced evaporation (Table 2.6), partially offsetting effects of cover depth on ET. However, evaporation (Table 2.6) represents an unproductive water loss from the reclaimed areas whereas transpiration (Table 2.6 and Figures 2.6 and 2.7) is correlated with CO_2 fixation (Figures 2.8 and 2.9). Thus, greater transpiration *vs.* evaporation increased WUE_T in the 100 cm cover compared to the 35 cm and 50 cm covers (data not shown).

The sub-humid climate reduced the modelled lateral water flow (runoff + subsurface discharge) in summer relative to ET (Table 2.6). No runoff (Table 2.6) was modelled during summer except in 2013 as K of PMM (Table 2.1) was enough to infiltrate most of the precipitation (Elshorbagy et al., 2007; Kelln, 2008). The modelled runoff mainly occurred during snow melting which was similar in all the covers for most of the years and the average annual runoff (~ 47 mm) was in the upper limit of the range of measured average annual (2003 - 2012) runoff (18.5 - 47 mm) from four weirs which were installed at different locations in the SBH

(O'Kane Consultants Inc, 2012b). The 100 cm cover had the highest AWHC (Figure 2.3) and thereby could store more infiltrated water that was not taken up by plants during rewetting, reducing modelled subsurface discharge (e.g. 2012 and 2013 in Table 2.6). However, greater ASWC following rewetting could increase subsequent subsurface discharge modelled from the 100 cm cover (i.e. 2014 and 2015 in Table 2.6). Therefore modelled subsurface discharge in 100 cm cover showed less inter-annual variability with changes of P (Table 2.6) relative to 35 cm and 50 cm covers. This low variability might improve hydrological stability in downstream ecosystems, which is an important element of closure landscape reclamation.

2.4.6. Effect of slope position on plant productivity in reclaimed landscapes

Reclaimed sites may experience drier upper slopes than would natural or pre-mining sites as they have greater slopes, lower upslope inflow, and an overburden layer with low K (Table 2.1) (Tani, 1997; Buttle et al., 2005; Kessler, 2007; Redding and Devito, 2008). In *ecosys*, the effects of slope position on ASWC were modelled from gravity-driven downward water movements through runoff [D1a], subsurface flow [D7] and downslope snow redistribution [D1b]. Even though a clear slope position effect on θ was not modelled during early reclamation period (1999 - 2006) in the SBH site (data not shown), modelled ASWC showed a clear slope position effect after the planted trees starts exponential plant growth (after seven years from start of reclamation) as water demand increased with vegetation growth. In addition, several drier years during the early reclamation period (1999 - 2006) as indicated in the weather data might have limited downward water movement giving little ASWC variation along the slope. However, the current modelling study clearly identified lower slope positions as having increased ASWC (Figure 2.4), root water uptake (Figure 2.7 and Table 2.3) and hence NPP (Table 2.5) after the stand reached canopy closure. The modelled soil water redistribution along the slope was

consistent with the findings from Kelln et al. (2008) who found wetter lower slopes in the SBH site after eight years from reclamation, and Ketcheson and Price (2016), who found wetter lower slopes in reclaimed area after seven years of reclamation. Overall, both modelled and measured results (Figures 2.4 and 2.7 and Tables 2.4 and 2.5) indicate the importance of slope position in determining plant productivity that needs to be considered when evaluating the productivity of reclaimed landscapes with large slopes.

2.4.7. Summary

In summary, increasing cover depth from 35 cm and 50 cm to 100 cm improved plant water relations and hence increased ecosystem transpiration, CO_2 fixation, and tree growth. Considering the modelled results, we suggest that on this site the 100 cm cover provided sufficient amount of water for maintaining tree growth during both the wet and dry periods while stabilizing downstream water movement. Since transpiration increased non-linearly with AWHC, cover depth that determines the AWHC will have little effect on transpiration after it reached the threshold AWHC according to the site conditions. It indicates the importance of optimizing transpiration to achieve target NPP for the reclaimed sites according to the ecological aspects since transpiration is linearly related to NPP. Therefore, reclamation success in recovering target NPP according to the end land-use or ecosite requires:

(1) Sufficient cover depth to achieve threshold AWHC (162 mm for the current study to achieve “d” ecosite) to avoid water stress during dry years

(2) Consideration of how cover depth influences the growth of different plant species

(3) Consideration of how water movement down artificial slopes affects NPP.

In *ecosys*, the effect of cover depth on water availability and movement, plant water relations and biomass production were modelled from basic soil-plant-atmosphere hydrological

processes, the parameters of which were derived from basic research conducted independently from the current study and so remained unchanged from those used in earlier studies as stated in the supplement. Model findings should therefore be robust. Collectively, results of this study also demonstrate the ability of *ecosys* to predict the cover depth required to achieve target NPP in reclaimed upland areas according to the ecological aspects without calibrating to a specific site so that *ecosys* model would be useful for further studies in reclaimed areas with a wide range of reclamation materials, compositions, PFTs, and weather conditions.

Table 2.1. Key soil properties used to model the three reclamation covers.

Property	**PMM**	**Subsoil (Till)**	**Overburden**
Bulk density (Mg m^{-3})[a]	0.90	1.65	1.85
Sand content (g kg^{-1})[b]	374	329	130
Silt content (g kg^{-1})[b]	271	320	421
Clay content (g kg^{-1})[b]	355	351	449
Saturated hydraulic conductivity (mm h^{-1})[c]	28.80	7.20	0.10
Volumetric water content at FC -0.01 MPa (m^3 m^{-3})[d]	0.40	0.30	0.27
Volumetric water content at PWP -1.5 MPa (m^3 m^{-3})[d]	0.25	0.25	0.25
Total organic carbon (g C kg^{-1})[e]	171	10	7
Organic nitrogen (g N kg^{-1})[e]	5.87	0.50	0.35
Organic phosphorous (g P kg^{-1})	0.39[f]	0.05*	0.035*

[a]From Boese (2003) and Elshorbagy et al. (2005)
[b]From Yarmuch (2003)
[c]From Meiers (2011)
[d]Derived from soil water desorption curves developed using field measured θ *vs.* ψ_m data from Syncrude Canada Ltd. research database.
[e]From Macyk (1999) and Yarmuch (2003)
[f]From Lanoue (2003)
*estimated as 0.1 x organic nitrogen

Table 2.2. Summary statistics of regressions of daily soil moisture content (θ) modelled at the depths corresponding to those at which the time domain reflectometry (TDR) probes were installed in the 35 cm and 100 cm covers on daily θ measured by TDR probes (2011-2015)[a].

Cover type	**Material type**	**Soil depth (cm)**	***n***	***a***	***b***	R^2	**RMSD** ($m^3\ m^{-3}$)
35 cm	Peat -Mineral	5	1289	0.16	0.70	0.41	0.08
	Mix	10	1548	-0.01	1.06	0.50	0.07
	Subsoil	20	1548	0.12	0.66	0.40	0.03
		25	1548	0.09	0.66	0.30	0.03
		32	1548	0.12	0.58	0.33	0.04
	Overburden	42	1548	0.22	0.22	0.30	0.02
100 cm	Peat-Mineral	5	1368	0.06	0.91	0.41	0.06
	Mix	20	479	0.05	0.81	0.61	0.03
	Subsoil	30	1368	0.06	0.82	0.40	0.02
		55	1368	-0.03	1.08	0.51	0.02
		90	1368	0.00	1.03	0.23	0.03
	Overburden	125	1368	0.19	0.40	0.11	0.02

[a]Intercept (*a),* slopes *(b*) from simple linear regressions of modelled on measured ($p < 0.001$). R^2 = coefficient of determination and RMSD = root mean square for difference from simple linear regressions of modelled on measured. RMSE (root mean square for error) values were not calculated as there was only one TDR probe installed at each sampling depth. Measured TDR values from Syncrude watershed research database.

Table 2.3. Summary statistics from regressions of average sap flow rates on modelled root water uptake during the vegetation growing period (June-August) of 2014 and 2015 in 35 cm and 100 cm covers[a].

Plant Species	**Year**	**Cover type**	***n***	***a*** (mm h^{-1})	***b***	R^2	**RMSD** (mm h^{-1})	**RMSE** (mm h^{-1})
Aspen	2014	35cm Upper slope	2207	0.017	0.79	0.65	0.01	0.08
		35cm Lower slope	2207	0.016	0.74	0.67	0.01	0.09
		100 cm Lower slope	2207	0.022	1.07	0.76	0.02	0.08
	2015	35cm Upper slope	2190	0.01	0.7	0.53	0.01	0.06
		35cm Lower slope	2207	0.007	0.79	0.67	0.01	0.07
		100 cm Upper slope	2207	0.014	0.76	0.60	0.02	0.09
White Spruce	2014	35cm Upper slope	2207	0.006	0.94	0.58	0.01	0.07
		35cm Lower slope	2207	0.007	1.50	0.63	0.02	0.09
		100 cm Lower slope	2207	0.002	1.20	0.68	0.01	0.07
	2015	35cm Upper slope	2207	0.0007	0.90	0.57	0.01	0.05
		35cm Lower slope	2207	0.0001	1.32	0.50	0.02	0.07
		100 cm Upper slope	2207	0.005	1.33	0.60	0.01	0.08

[a]Intercept (*a),* slopes *(b*) from simple linear regressions of measured on modelled values ($p < 0.001$). R^2 = coefficient of determination and RMSD = root mean square for differences. RMSE = root mean square for error (n = 9) of sap flow/unit ground area calculated using stand sap wood area to ground area ratio (SA) as described by Hogg and Hurdle (1997).

Table 2.4. Cumulative modelled transpiration (mm) and measured sap flow (mm) during growing periods (June-August), and modelled and measured LAI (m^2 m^{-2}) in August in 2014 - 2015 at upper and lower slope positions of 35 cm, 50 cm and 100 cm reclamation covers.

Year	Plant Species	Slope position	35 cm				50 cm			100 cm			
			Transpiration /Sap flow		LAI		Transpiration		LAI	Transpiration /Sap flow		LAI	
			Mod	Mea (±SD)	Mod	Mea (±SD)¶	Mod	Mea (±SD)¶	Mod	Mod	Mea (±SD)	Mod	Mea (±SD)¶
2014	Aspen	Upper	56	69 (38)	1.38	N/A	64	N/A	1.58	88	N/A	1.99	N/A
		Lower	56	68 (40)	1.42	N/A	67	N/A	1.67	85	117 (41)	2.00	N/A
	Spruce	Upper	40	47 (30)	1.14	N/A	42	N/A	1.19	35	N/A	0.96	N/A
		Lower	47	70 (43)	1.42	N/A	47	N/A	1.35	37	42 (31)	1.08	N/A
2015	Aspen	Upper	46	49 (16)	1.13	N/A	51	N/A	1.31	80	76 (40)	1.89	N/A
		Lower	59	48 (21)	1.47	N/A	71	N/A	1.69	88	N/A	2.03	N/A
	Spruce	Upper	40	28 (13)	1.22	N/A	38	N/A	1.22	33	45 (31)	1.02	N/A
		Lower	53	38 (19)	1.52	N/A	53	N/A	1.46	43	N/A	1.21	N/A
	Total Tree	Upper	N/A	N/A	2.35	2.40 (0.88)	N/A	N/A	2.53	N/A	N/A	2.91	3.46 (0.68)
		Lower	N/A	N/A	2.99	2.34 (0.81)	N/A	N/A	3.15	N/A	N/A	3.24	3.21 (1.04)

¶SD = Standard deviation (mm) for measured sap flow (n=9), Mod = modelled, Mea = measured.

Table 2.5. Net primary productivity (NPP) modelled from 2010 to 2015 in three cover depths (35 cm, 50 cm and 100 cm) under different climatic conditions.

Year	**Precipitation** (mm)	**Mean Annual Temperature** (^{0}C)	**Slope Position**	**Net primary productivity** (g C m^{-2} y^{-1})								
				35 cm cover			**50 cm cover**			**100 cm cover**		
				Aspen	**Spruce**	**Total¶**	**Aspen**	**Spruce**	**Total¶**	**Aspen**	**Spruce**	**Total¶**
2010	405	2.81	Upper	109	42	**228**	155	48	**270**	255	33	**340**
			Lower	293	81	**381**	404	80	**492**	470	50	**523**
2011	238	2.31	Upper	73	36	**136**	123	46	**186**	227	37	**281**
			Lower	302	88	**403**	395	88	**495**	450	58	**520**
2012	507	1.96	Upper	180	77	**276**	248	88	**347**	335	58	**404**
			Lower	304	106	**425**	359	94	**468**	423	65	**502**
2013	462	1.13	Upper	243	114	**366**	304	120	**434**	402	76	**485**
			Lower	259	115	**387**	306	104	**422**	388	75	**477**
2014	385	0.64	Upper	230	124	**365**	269	124	**406**	370	84	**467**
			Lower	221	126	**359**	270	115	**396**	347	84	**444**
2015	340	3.12	Upper	185	128	**330**	217	124	**357**	352	95	**464**
			Lower	242	151	**406**	290	142	**444**	375	109	**497**

¶Total NPP is the summation of aspen, spruce and other species NPP.

Table 2.6. Modelled water balance components in three cover depths (35 cm, 50 cm and 100 cm) after planted trees reached over-story crown closure.

Year	**P-ET** (mm)			**Transpiration** (mm)			**Evaporation** (mm)			**Subsurface discharge** (mm) **[Summer subsurface discharge]**			**Runoff** (mm) **[Summer runoff]**		
	35 cm	**50 cm**	**100 cm**	**35 cm**	**50 cm**	**100 cm**	**35 cm**	**50 cm**	**100 cm**	**35 cm**	**50 cm**	**100 cm**	**35 cm**	**50 cm**	**100 cm**
2011	-7	-24	-38	132	157	172	113	105	104	11 [<1]	14 [2]	13 [2]	43 [0]	43 [0]	46 [0]
2012	217	206	200	183	201	208	106	99	98	64 [11]	53 [8]	39 [5]	33 [0]	22 [0]	26 [0]
2013	168	160	152	203	219	227	91	83	83	120 [69]	122 [66]	109 [51]	53 [10]	50 [6]	48 [2]
2014	101	93	87	204	216	223	80	75	75	58 [11]	57 [11]	65 [13]	47 [0]	51 [0]	52 [0]
2015	35	27	17	222	232	245	82	80	77	21 [<1]	20 [2]	27 [6]	59 [0]	60 [0]	64 [0]

¶Annual measured precipitation – modelled evapotranspiration.

(a)

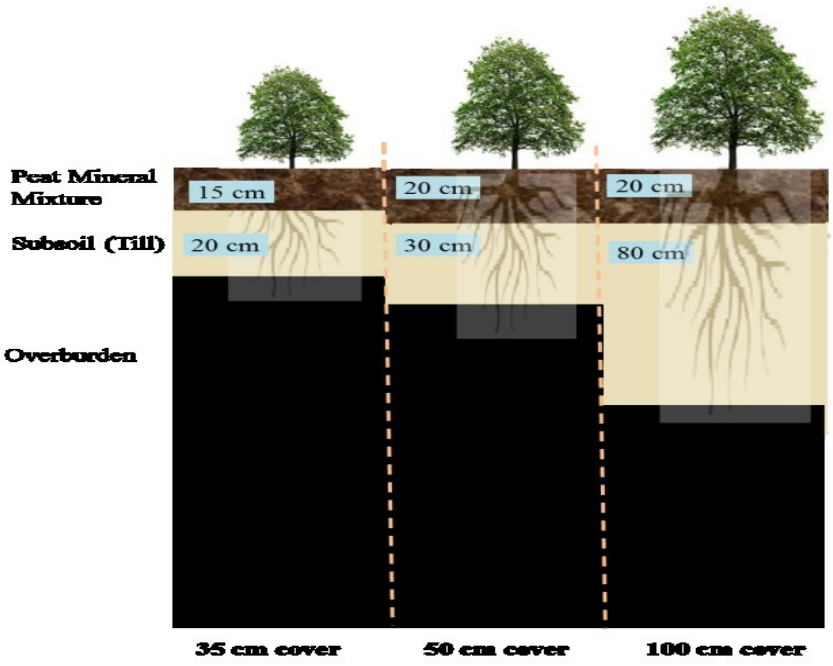

(b)

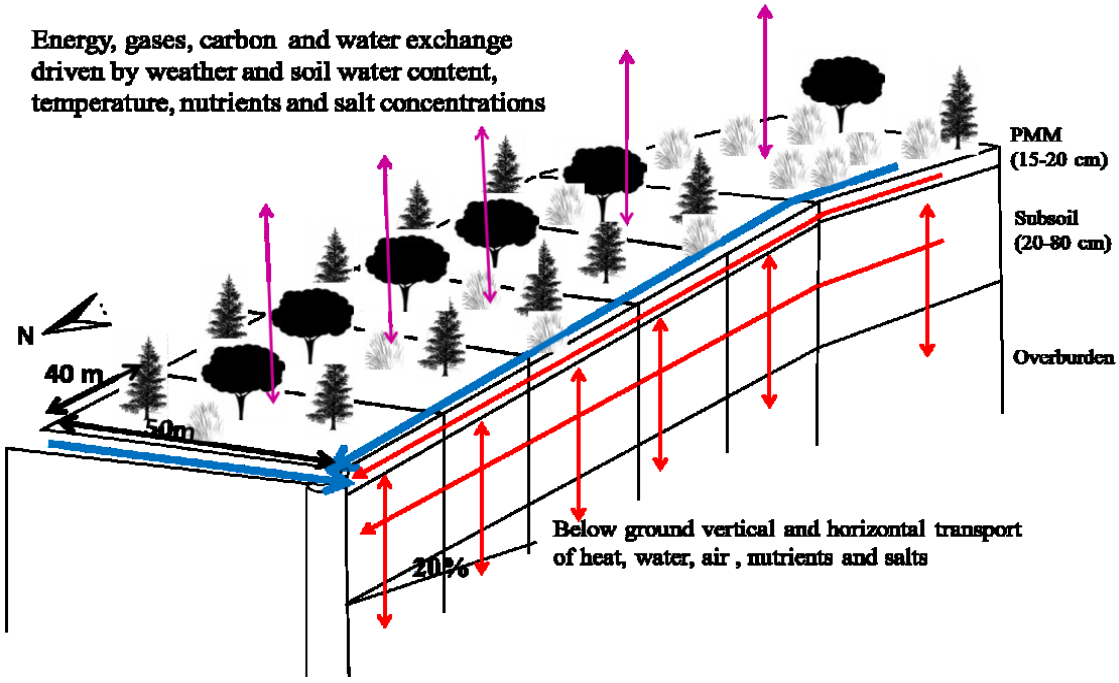

Figure 2.1. (a) Design of South Bison Hill (SBH) reclamation covers (b) SBH reclamation site as represented in model, *ecosys* considering fully coupled carbon, energy, water, and nutrient cycles. Belowground vertical and horizontal transport of heat, water, air, nutrients and salts are represented by red arrows; aboveground energy, gases, carbon, and water exchange represented by purple arrows. The blue arrows represent the runoff in the site. Each reclamation cover was represented in the model as a transect of six interconnected grid cells (50 m x 40 m).

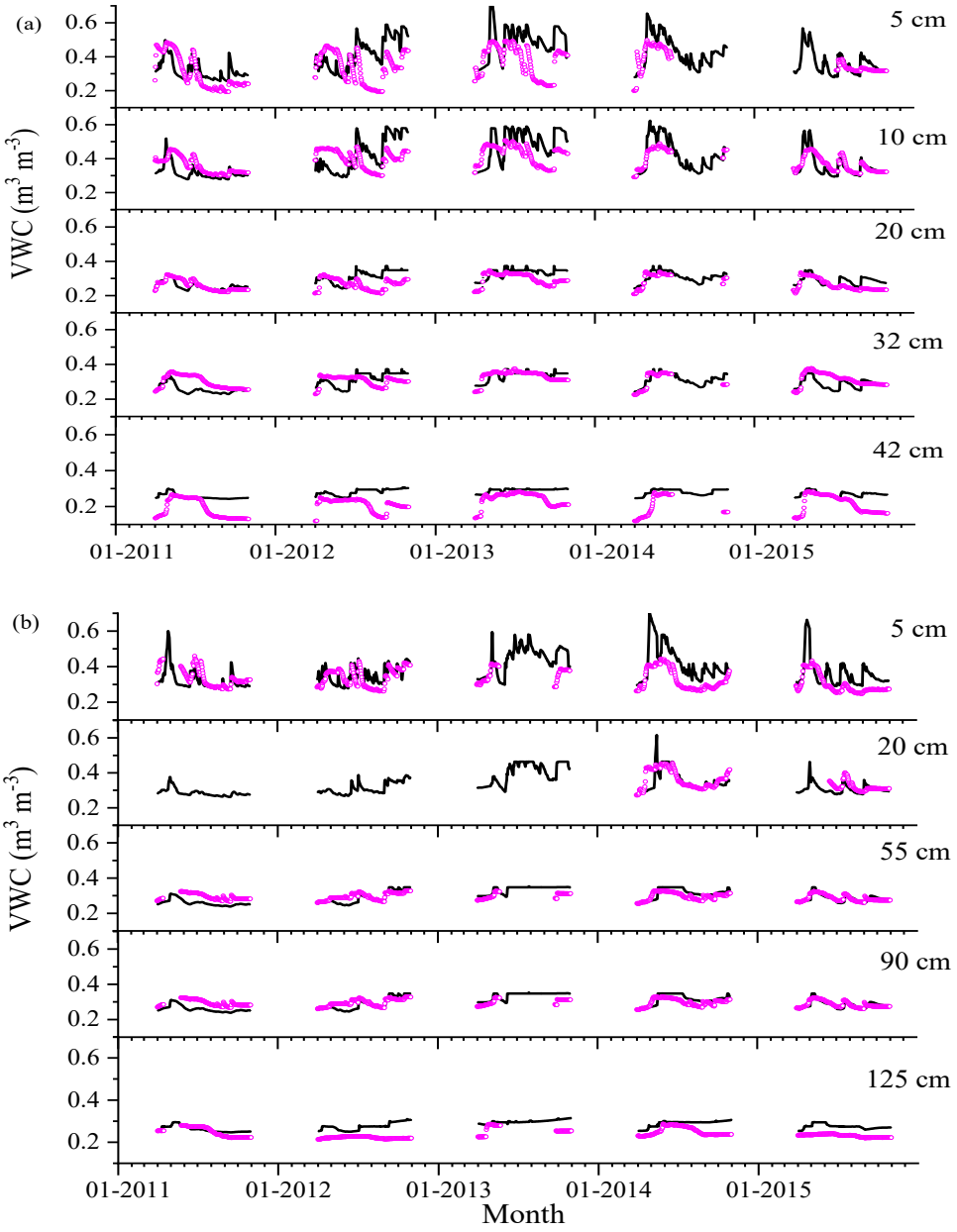

Figure 2.2. Modelled (black lines) and measured (purple dots) volumetric water contents (VWC) at different depths at middle slope position in (a) 35 cm and (b) 100 cm reclamation covers during non-frozen period (01st April to 31st October) after planted trees reached over-story crown closure. Measured time domain reflectometry (TDR) values from Syncrude watershed research database.

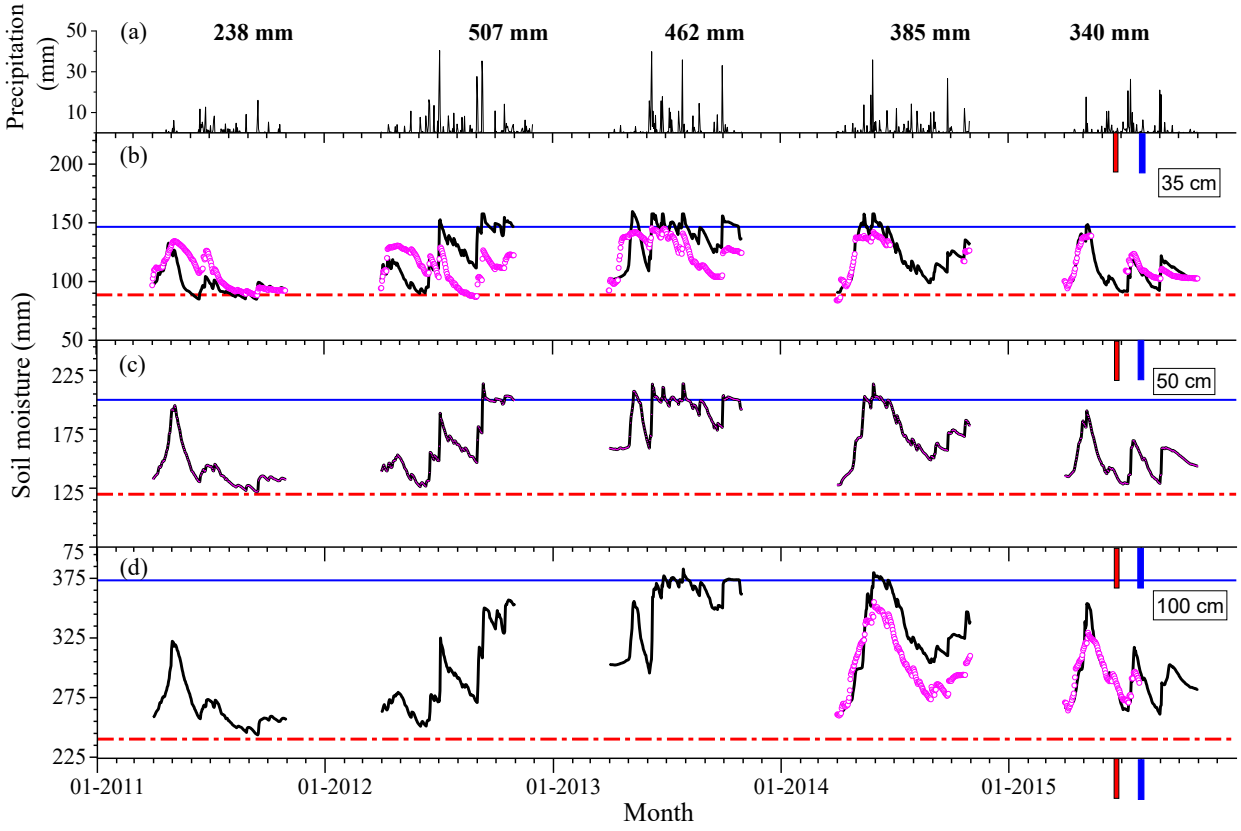

Figure 2.3. (a) Precipitation, and the estimated total soil moisture from measured θ (purple dots) and modelled (black lines) total soil moisture at middle slope in the (b) 35 cm, (c) 50 cm and (d) 100 cm reclamation covers during non-frozen periods (01st April to 31st October) after planted trees reached over-story crown closure. The measured θ in 50 cm cover was not included since a re-installation of TDR probes in 2007 resulted in an abrupt change in monitoring trends. Dashed red and solid blue lines indicate the estimated water content at permanent wilting point (PWP) and field capacity (FC) respectively. The available soil water holding capacity (AWHC) is apparent from the vertical distance between these lines. The strips indicate the dry (red) and wet (blue) periods in 2015, which were used to examine modelled water relations (Figures 2.6-2.9) below.

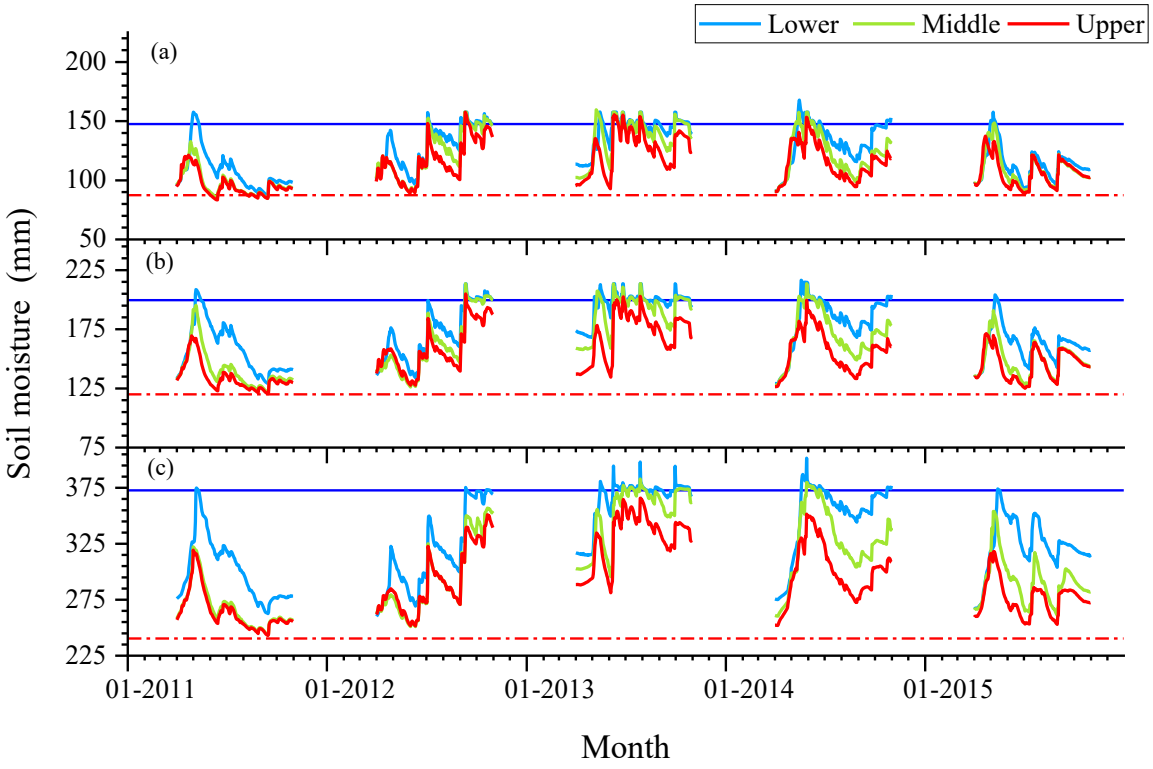

Figure 2.4. Modelled total soil moisture in lower (blue lines), middle (green lines) and upper (red lines) slope positions in (a) 35 cm cover (b) 50 cm cover (c) 100 cm cover during non-frozen period (01st April to 31st October) after planted trees reached over-story crown closure. Dashed red and solid blue lines indicate the estimated water content at permanent wilting point (PWP) and field capacity (FC) respectively. The available soil water holding capacity (AWHC) is apparent from the vertical distance between these lines.

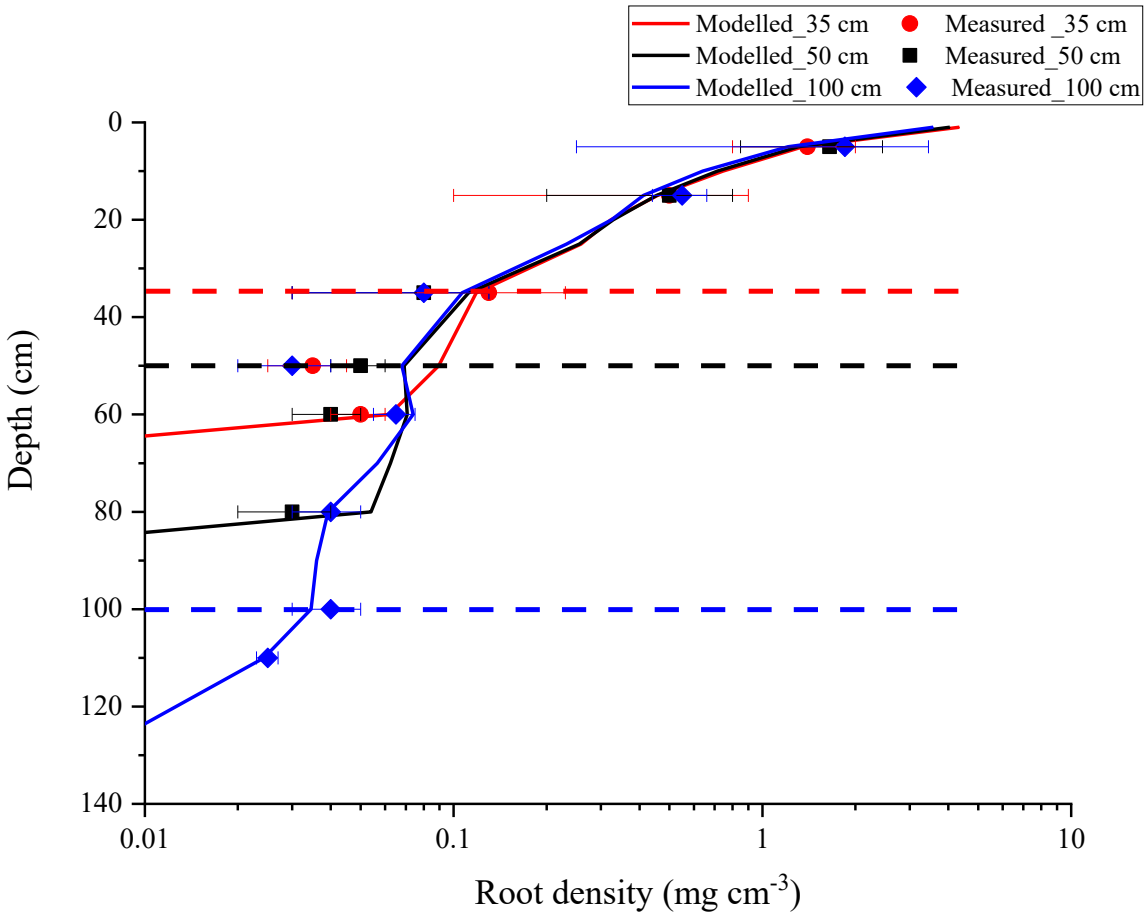

Figure 2.5. Average measured (symbols) (Northwind Land Resources Inc., 2014 and Van Rees, 2014) and modelled (lines) dry root biomass densities with soil depth along the slope in 35 cm (red), 50 cm (black) and 100 cm (blue) covers in October 2013. The dashed lines indicate the top of overburden layer in each cover.

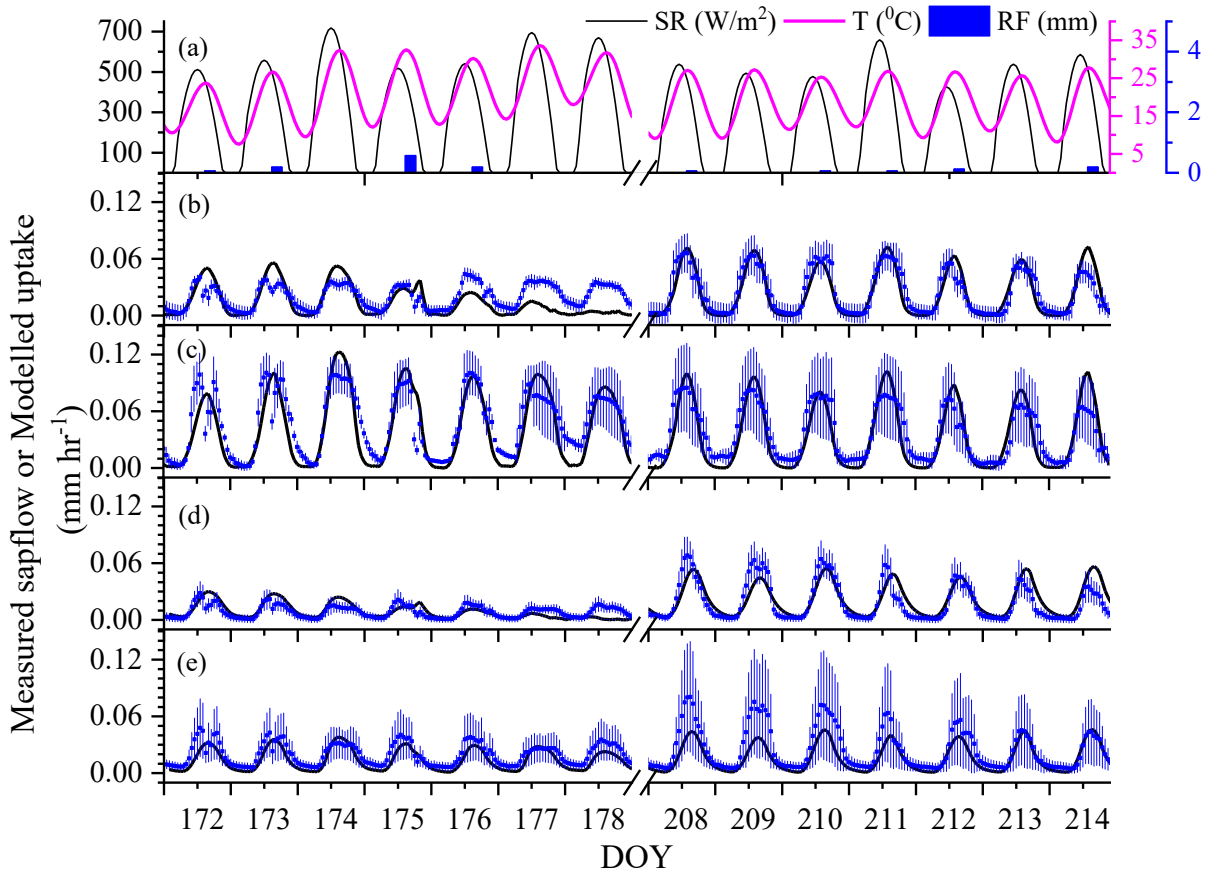

Figure 2.6. (a) Hourly solar radiation (SR), temperature and precipitation resolved by *ecosys* from measured daily data, and (b-e) hourly modelled (black lines) uptake and average measured sap flow rate (blue dots) of aspen in (b) 35 cm and (c) 100 cm cover upper slopes, and of white spruce in (d) 35 cm and (e) 100 cm cover upper slopes during dry (day of year (DOY) 172-178) *vs.* wet (DOY 208-214) periods in 2015.

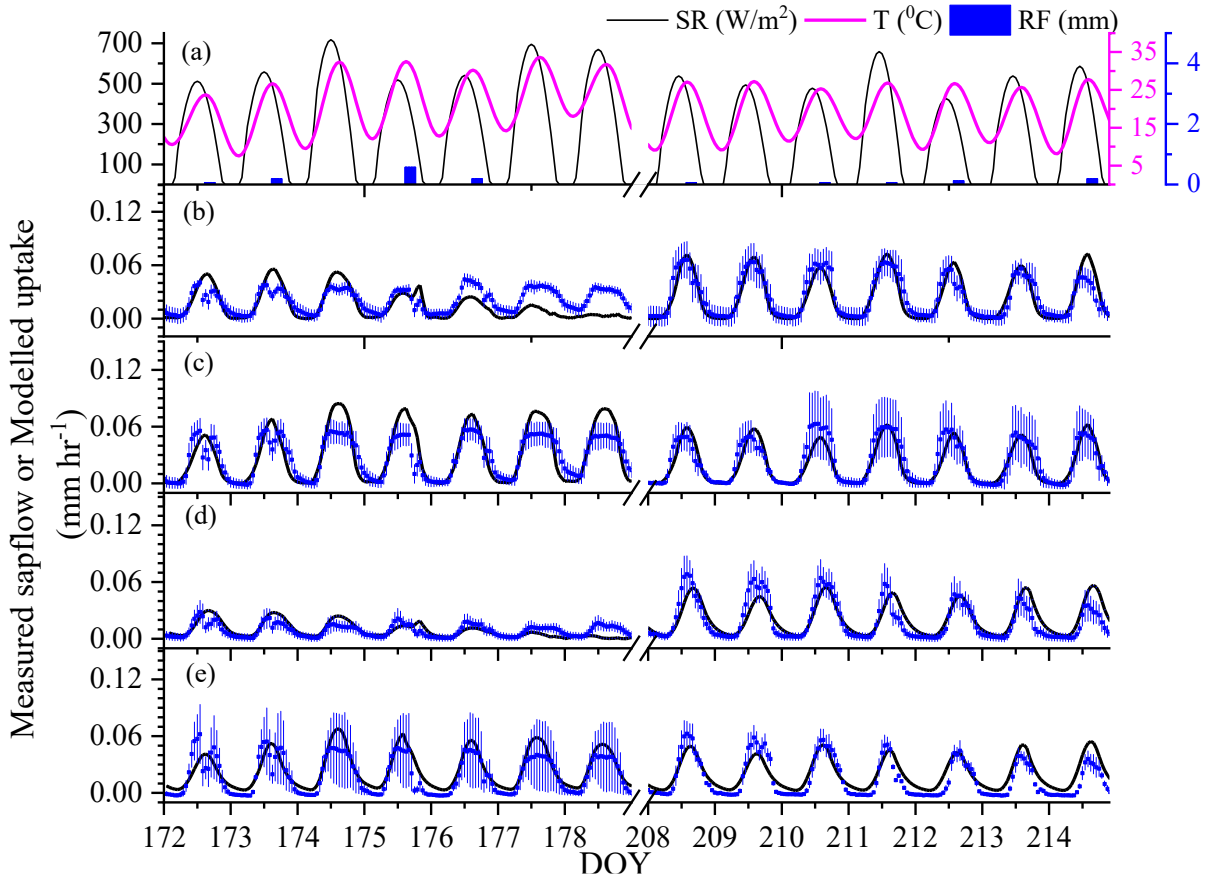

Figure 2.7. (a) Hourly solar radiation (SR), temperature and precipitation resolved by *ecosys* from measured daily data and (b-e) hourly modelled (black lines) uptake and average measured sap flow (blue dots) of aspen at the (b) upper slope and (c) lower slope positions, and of white spruce at the (d) upper slope and (e) lower slope positions in 35 cm cover during dry (day of year (DOY) 172-178) *vs.* wet (DOY 208-214) periods in 2015.

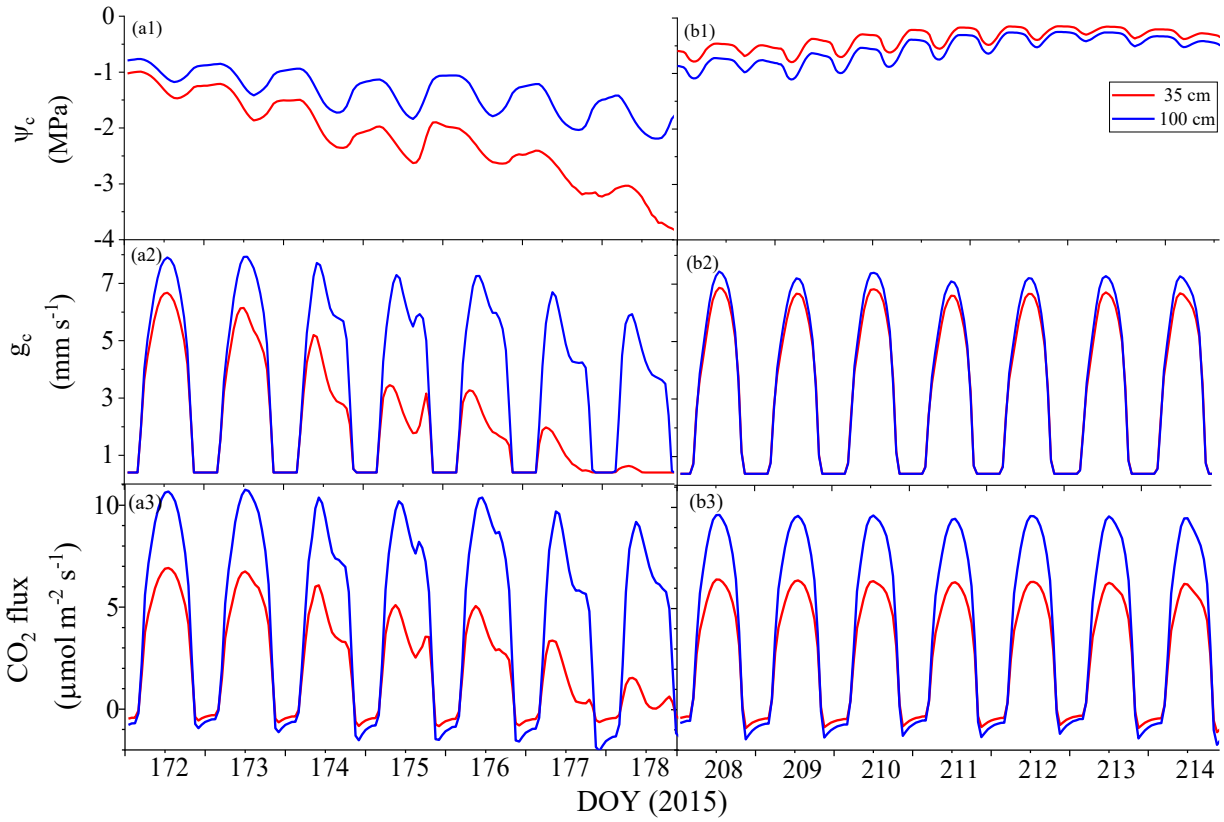

Figure 2.8. Modelled (a1, b1) canopy water potential (ψ_c), (a2, b2) canopy stomatal resistance (g_c) and (a3, b3) net canopy CO_2 fixation (CO_2 flux) of aspen in 35 cm cover upper slope (red lines) and the 100 cm cover upper slope (blue lines) during dry (day of year (DOY) 172-178) *vs.* wet (DOY 208-214) period in 2015.

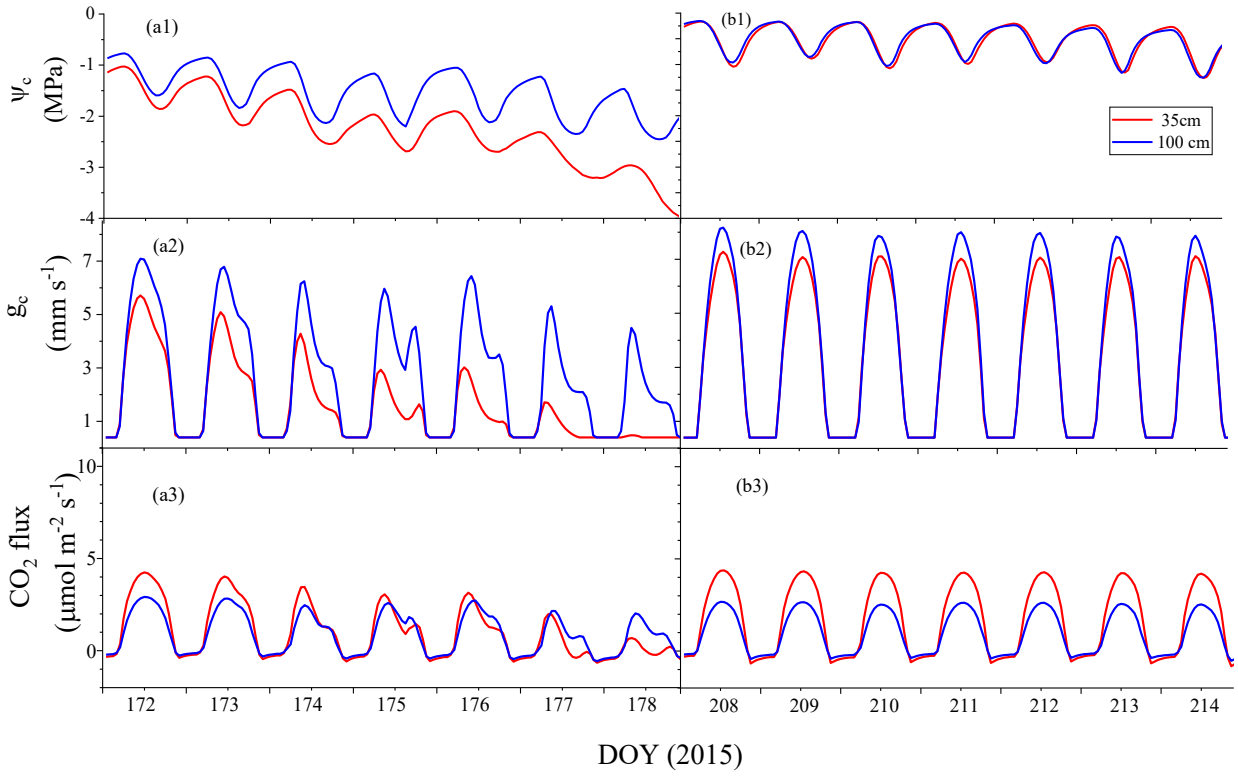

Figure 2.9. Modelled (a1, b1) canopy water potential (ψ_c), (a2, b2) canopy stomatal resistance (g_c) and (a3, b3) net canopy CO_2 fixation (CO_2 flux) of white spruce in 35 cm cover upper slope (red lines) and 100 cm cover upper slope (blue lines) during dry (day of year (DOY) 172-178) *vs.* wet (DOY 208-214) period in 2015.

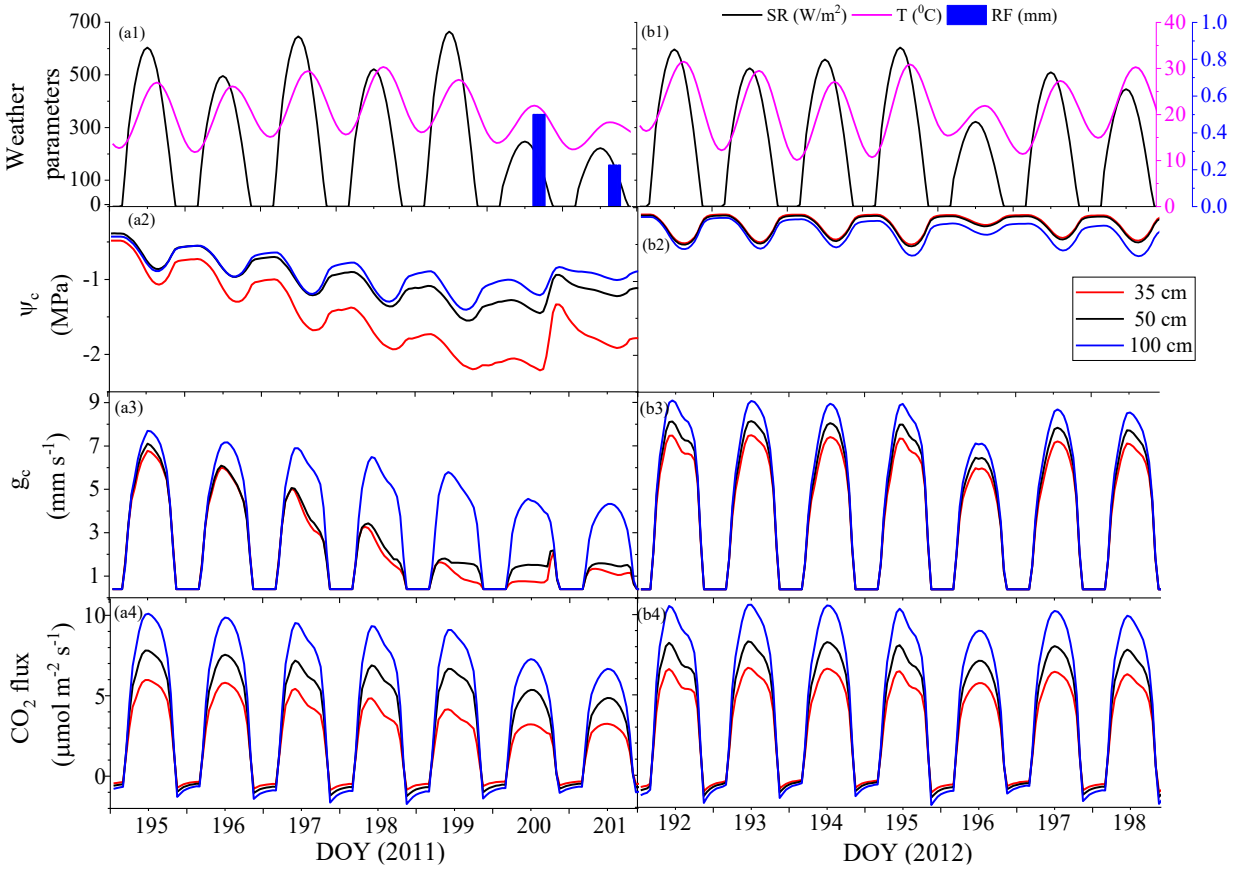

Figure 2.10. (a1, b1) Hourly solar radiation (SR), temperature and precipitation resolved by *ecosys* from measured daily data and modelled average (a2, b2) canopy water potential (ψ_c), (a3, b3) canopy stomatal resistance (g_c) and (a4, b4) net canopy CO_2 fixation (CO_2 flux) of aspen along the slope in 35 cm (red lines), 50 cm (black lines) and 100 cm (blue lines) reclamation covers during drier year 2011 (day of year (DOY) 195-201) *vs.* wetter year 2012 (DOY 192-198).

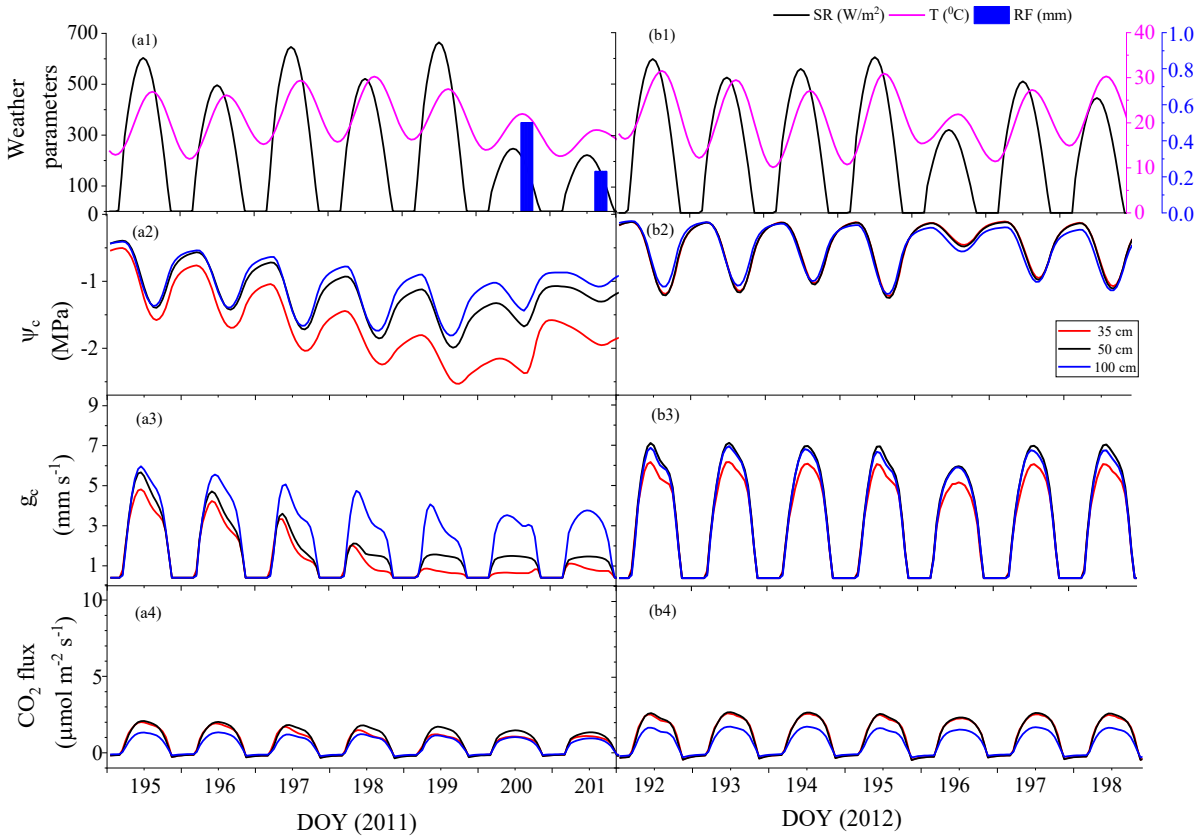

Figure 2.11. (a1, b1) Hourly solar radiation (SR), temperature and precipitation resolved by *ecosys* from measured daily data and modelled average (a2, b2) canopy water potential (ψ_c), (a3, b3) canopy stomatal resistance (g_c) and (a4, b4) net canopy CO_2 fixation (CO_2 flux) of white spruce along the slope in 35 cm (red lines), 50 cm (black lines) and 100 cm (blue lines) reclamation covers during drier year 2011 (day of year (DOY) 195-201) *vs.* wetter year 2012 (DOY 192-198).

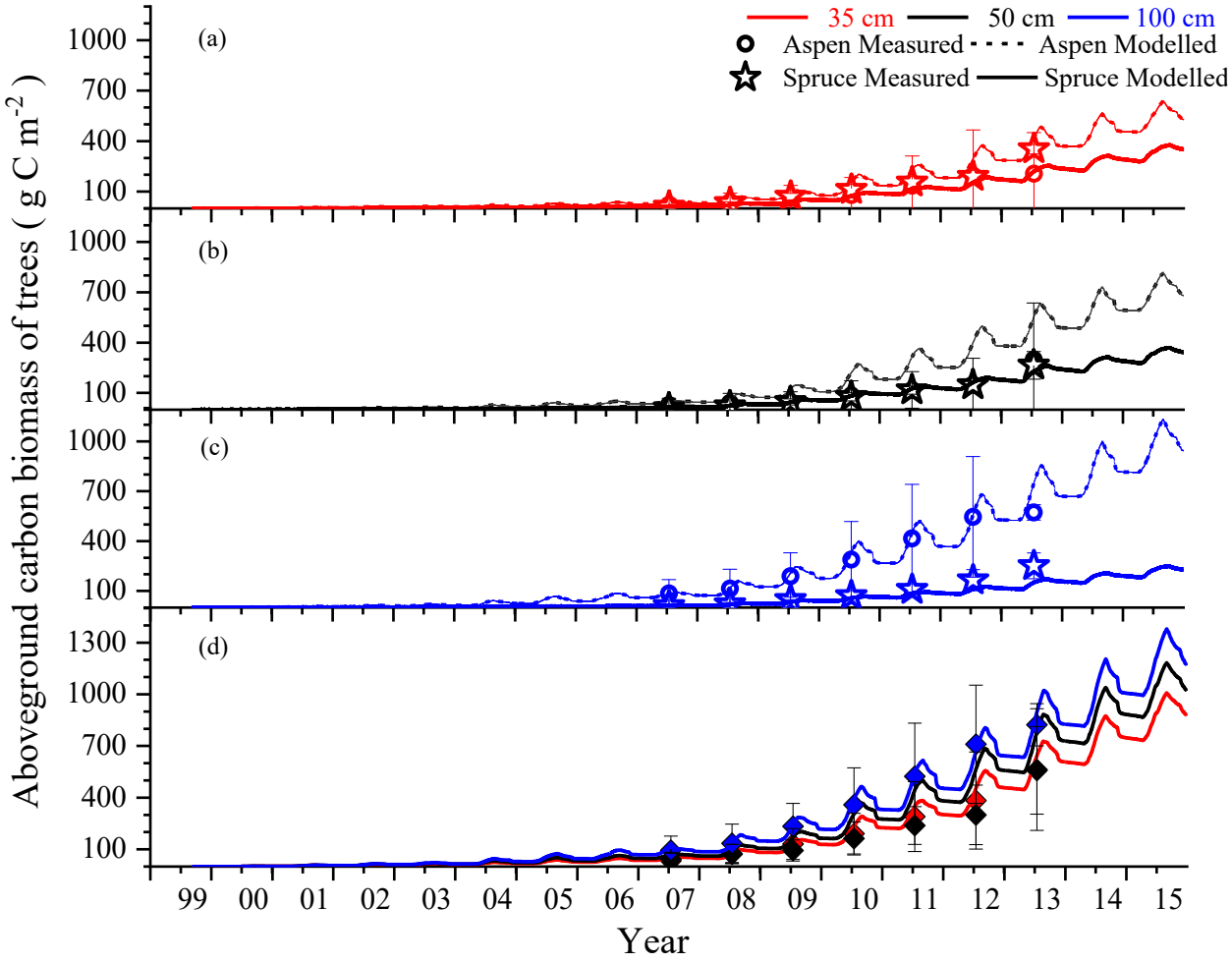

Figure 2.12. Modelled (lines) and measured (open symbols) aspen and white spruce aboveground carbon biomass along the slope positions in (a) 35 cm cover (b) 50 cm cover and (c) 100 cm covers, and (d) total tree carbon biomass modelled (lines) and measured (closed symbols) in 35 cm (red), 50 cm (black) and 100 cm (blue) reclamation covers since site construction. Open stars represent the measured white spruce and open circles represent the measured aspen. Measured aboveground carbon biomass values from Macyk et al. (2009) and Drozdowksi et al. (2011, 2014).

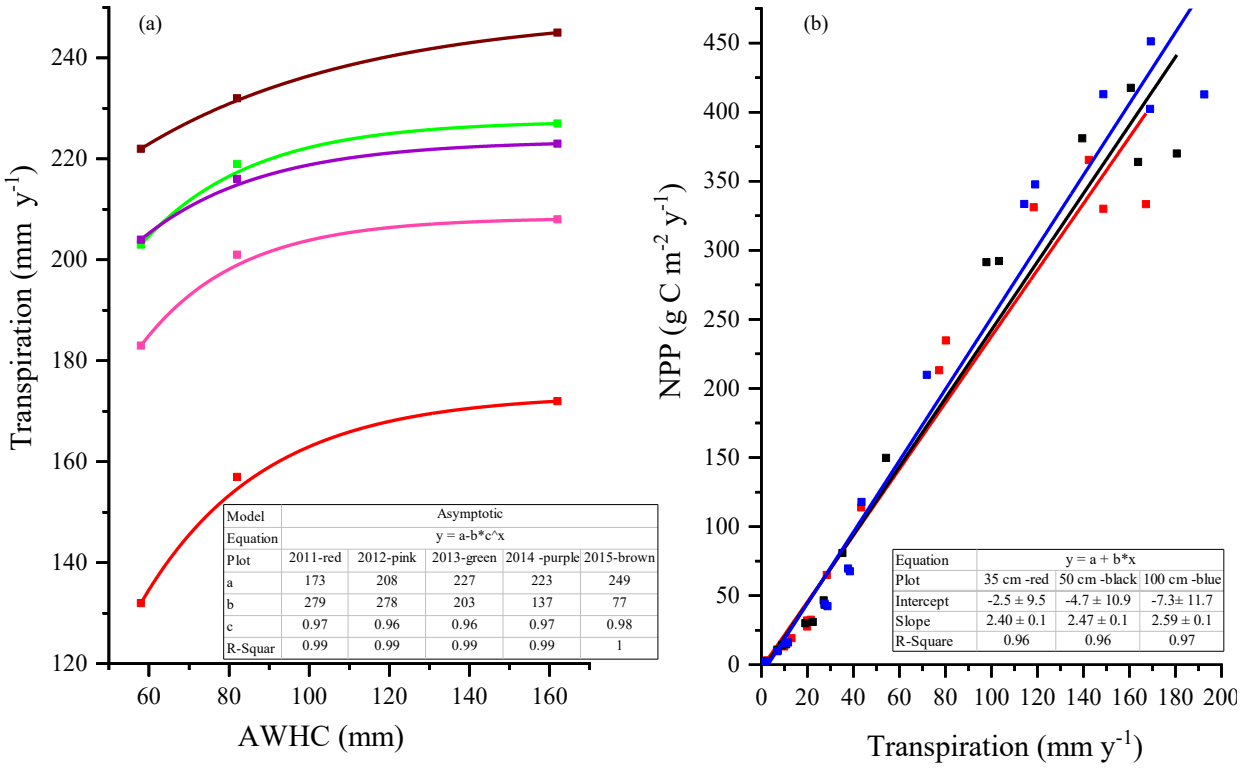

Figure 2.13. (a) Relationship between estimated available water holding capacity (AWHC) (dots represent the AWHC as determined by cover depth for each plotted line) and modelled transpiration during 2011 - 2015 (after planted trees reached over-story crown closure) and (b) relationship between modelled transpiration and net primary productivity (NPP) of planted trees in reclamation covers since site construction (slope of the lines represent the planted tree water-use efficiency of productivity (WUE_P)) in 35 cm (red line), 50 cm (black line) and 100 cm (blue line) reclamation covers.

Chapter 3

Modelling salt redistribution as affected by cover depths and topography in reclaimed saline-sodic overburden upland forests of Northern Alberta

3.1. Introduction

Achieving equivalent land capability according to the Environmental Protection and Enhancement Act (EPEA) is the ultimate goal of restoration in disturbed oil sand landscapes within the Athabasca oil sand region (AOSR). The main target of northern Alberta upland forest restoration is to achieve boreal mixedwood forests mainly comprised of white spruce (*Picea glauca* (Moench) Voss) and trembling aspen (*Populus tremuloides* Michx.) (Lilles et al., 2012). During surface mining in AOSR, overburden (mostly saline sodic) waste stripped prior to the access of oil sands is produced in large volumes (Fung and Macyk, 2000; Chaikowsky, 2003; Amos et al., 2015). This excavated overburden is used to backfill open pits or placed in unmined areas to construct uplands while covering with non-saline reclamation materials to give better growth media for plants (Sandoval and Gould, 1978; Kessler et al., 2010). Large, out of pit landform structures of overburden are created, consisting of side slopes of approximately 10 to 20% and a relatively flat plateau in the center. For some oil sand mine operations the overburden is comprised mainly of Clearwater shale which is marine in origin and contains a large amount of gypsum and pyrite (Wall, 2005; Hilderman, 2011; Appels et al., 2017). Oxidation of this pyrite during excavation and placement generates sulfuric acid, which accelerates weathering of the overburden, leading to a generation of more soluble salts (Hilderman, 2011; Appels et al., 2017). Therefore, one of the major challenges related to reclamation of these disturbed lands in AOSR is elevated salinity from saline-sodic shale overburden waste (mean electrical conductivity ~10

dS m^{-1} [maximum ~17] and mean SAR ~17 [maximum ~35]) (Kessler, 2007) that may inhibit plant growth and degrade soil structure (Purdy et al., 2005; Barbour et al., 2007; Kelln, 2008; Lilles et al., 2012). Therefore, a sufficient amount of cover materials must be placed that will provide a suitable depth for plant root development that considers upward migration of salts and sodium in the reclamation cover (Carey, 2008).

Restoration with inadequate cover material could create unproductive lands due to greater salt concentration within the root zone. Greater soluble salt accumulation decreases the osmotic water potential and hence the soil water potential in the root zone that reduces plant water uptake (Grant, 1995). In addition to osmotic stress, accumulation of salts in the root zone reduces plant growth by accumulating salts in plant tissues and interfering with nutrient uptake and translocation within the plant (NRC, 1993). Furthermore, greater Sodium content adversely affects soil structure (Chaikowsky, 2003) and thereby reduces water infiltration. Plant growth and microbial activities are also considerably reduced with increased salinity in the soil (Smith and Doran, 1996). Soils are usually decribed as saline when the electrical conductivity (EC) in saturated paste exceeds 4 dS m^{-1} (Richards, 1954). However, the salt tolerance level and EC threshold or reduced plant growth are species specific (Smith and Doran, 1996; Howat, 2000). Some plants experience suppressed growth when EC reaches 2 dS m^{-1} (Edwards 1985; Howat, 2000). In forest ecosystems within the oil sands regions, 0 - 2 dS m^{-1} of EC is considered as the optimum and 2 - 4 dS m^{-1} level is considered as marginally acceptable (Leskiw, 1998; CEMA, 2006; Kessler, 2007).

Declines in growth and productivity of boreal species with increased salinity (aspen and white spruce) was reported by previous greenhouse (McKenzie et al., 1993; Maynard et al., 1996; Howat, 2000; Khasa et al., 2002) and field (Lilles et al., 2012) studies. However, Purdy et

al. (2005) suggested that upland forest landscapes can be achieved in saline areas as long as saline soils remain below the root zone and have an adequate supply of freshwater for plant growth. Therefore, having sufficient cover material depth is important to provide a sufficient cover for the root zone to buffer any salt migration from overburden to the cover material. Topography also can be a very important factor in salt redistribution. Salt movement from upper to lower slopes can increase salt concentration in lower slope areas. The water perched above the cover-overburden interface creates downslope lateral subsurface flow (interflow) in sloping landscapes (Kelln, 2008). This gravity driven flow can move salts from upper to lower slope positions in reclaimed areas and also to lower surrounding areas. This could lead to salinization of these areas.

Long term monitoring is important to determine changes in salt redistribution within the root zone of reclaimed covers and thereby effects on the target ecosystem restoration. However, the effects of long term salinity on growth and productivity of boreal tree species in reclaimed ecosystems are not well understood. Also knowing salt redistribution along the soil profile over time helps to determine the cover material depth required to maintain a reasonable salt concentration in the root zone. Oil sand mine operations continually strive for an optimal soil cover depth(s) that will achieve equivalent land capability due to the reclamation costs associated with soil salvage and placement, as well as the limited soil resources available for reclamation (Kessler et al., 2010). Therefore confirming the appropriate soil reclamation cover depth is important for the oil sands mine industry. Field research studies are expensive and findings may have limited applicability (*e.g.*, site-specific) as they are dependent on weather, soil chemical, physical and hydrological properties (Gower et al., 2001; Randerson et al., 2002; Huang et al., 2013). Also long term sampling can adversely affect reclamation success due to continuous

disturbances. A rigorous modeling effort based on fundamental processes governing water, energy, ionic solutes and nutrient interactions among the soil-microbe-root-canopy-atmosphere system can provide both short and long-term land capability restoration forecasts to the reclamation community. If ecosystem models can accurately model salt generation in saline sodic overburden and movement into reclamation covers and surrounding areas, they could be used to predict the suitable cover depth for future reclamation to minimize long term root zone osmotic stress under a different climate regime.

Previous field and modelling studies of salinity were conducted on three reclamation covers at South Bison Hills (SBH) by Wall (2005), Nichol et al. (2006), Kessler (2007), Kessler et al. (2010), Hilderman (2011), Klohn Crippen Berger Ltd. (2013), Huang et al. (2015b) and Appels et al. (2017). These studies were mainly focused on salt production in saline sodic overburden and salts movements to the cover soil and along the slopes rather than on vegetation growth and salinization of surrounding areas with different cover depths. They observed higher soluble salt concentration and EC values in cover material just above the cover overburden interface predominantly due to upward salt diffusion.

Modelling salinity effects on plant productivity requires that key processes, which these effects are known to occur, be explicitly represented in mathematical models. Greater salt concentration within the root zone reduces osmotic water potential, soil water potential and consequently plant water uptake. Lower plant water uptake from these root zones reduces the canopy water potential, and thereby increases canopy stomatal resistance (r_c) (Grant et al., 1999) causing declines in CO_2 diffusion and carboxylation, and thereby in CO_2 fixation. These processes are explicitly modelled in the comprehensive terrestrial ecosystem model *ecosys* (Grant (2001, 2014); Grant et al., 2012). *Ecosys* has been rigorously tested against field

experiments under a wide range of environmental conditions. *Ecosys* has been used to model the effect of salinity on crop growth and plant water use under different salinity levels in different sites by Grant (1995). Although *ecosys* has not yet been used to model these processes in reclaimed lands, in the current study *ecosys* was used to model salt redistribution, soil osmotic potential (ψ_π), soil water potential (ψ_s) and thereby the influence of salinity on plant water uptake and productivity. The current study was conducted (1) to understand long term salinity changes in reclaimed areas with different cover depth (2) to understand the effect of salinity on vegetation growth, particularly during drier periods, and thereby determine suitable cover depth for reclamation, and (3) to understand long term topographical effects on salt discharge from reclaimed sites.

3.2. Materials and Methodology

3.2.1 General model description

Ecosys is a comprehensive mathematical model that has the ability to represent multiple soil and canopy layers in soil-microbe-canopy–atmosphere systems at three-dimensional scales. The model simulates physical, chemical and biological processes in natural and disturbed terrestrial ecosystems through the acquisition, transformation and transfer of radiation, water, carbon, oxygen, nitrogen and phosphorous (Grant, 2001) and includes site-independent algorithms for all the processes, so as to achieve realistic landscape-scale predictions of productivity under a wide range of site conditions. The key parameters and algorithms used in *ecosys* were described in Grant (2001; 2014) and Grant et al. (2012) and remain unchanged from those used in earlier studies cited above. The major algorithms that govern the lateral and vertical solute fluxes and solute transformations, osmotic potential and thereby soil water potential, plant water uptake and their effects on net primary productivity (NPP) in *ecosys* are given below with

reference to supporting equations given in appendices B to E in the Supplement as listed in Table 2.1.

3.2.1.1. Salt redistribution and effect of salinity on soil water potential

In *ecosys*, solute fluxes are initialized with solute concentrations (C_s) of NH_4^+, H^+, Na^+, K^+, Ca^{2+}, Mg^{2+}, Fe^{2+}, Al^{3+}, Cl^-, OH^-, NO_3^-, HCO_3^-, CO_3^{2-}, PO_4^{3-}, and SO_4^{2-} in each soil layer according to results from saturated paste extracts. All of these solutes are subjected to convective-dispersive transfer vertically and laterally (Bresler, 1973) among different soil layers (equation (1)). Convective transfer is controlled by water flow and solute concentrations whereas dispersive transfer is controlled by aqueous solute concentration gradient and dispersivity in soil calculated as functions of water flux and water filled porosity [D20] and water flow length [D21] (Grant, 1995, 2001). Also the diffusive component of dispersivity has a tortuosity term calculated from θ^2 [D20] so that it declines with soil drying.

$$Q_s = Q_w [C_s] + 2 D_{sc} ([C_s]_x - [C_s]_{x+1})/(L_x + L_{x+1}) \qquad (1)$$

where: Q_s = aqueous flux of solute (g m^{-2} h^{-1}), Q_w = subsurface water flow (m^3 m^{-2} h^{-1}) [D7], C_s = aqueous concentration of solute in soil (mol m^{-3}), D_{sc} = aqueous diffusivity-dispersivity of solute (m^2 h^{-1}), L_x = length of landscape element in vertical or horizontal dimensions (m).

Solute concentrations $[C_s]$ are controlled by precipitation-dissolution [E1 – E9] and ion pairing reactions [E22 – E55] according to solubility products, and by adsorption- desorption through cation [E10 – E15] and anion [E16 – E20] exchange reactions according to selectivity coefficients (Grant, 2001). In reclaimed landscapes, saline sodic overburden contains higher C_s than do reclamation covers so that these solutes may move up into the reclamation covers through vertical convective-dispersive transfers across the cover-overburden layer resulting

saline root zones. In addition, overburden contains large amounts of gypsum, the dissolution of which increases the salinity in root zone through upwards diffusion of SO_4^{2-} and Ca^{2+}. Further, water accumulates at cover-overburden interface due to lower saturated hydraulic conductivity (*K)* of overburden which enhances the upwards salt movements. Salt migration into the root zone is greater in shallow covers due to shorter distance for salts to diffuse from the cover- overburden interface into the root zone.

Salinity is commonly measured in soils as electrical conductivity (EC). In *ecosys*, EC of the soil solution is calculated by the summation of each ion's EC calculated from C_s, valence and an ion-specific coefficient (equation (2)) (Grant, 1995, 2001). These calculated EC values were used for model validation against EC measurements.

$$EC = \sum_{S=1}^{S} aC_s.V \qquad (2)$$

where: EC = soil electrical conductivity (dS m^{-1}), V= valence of the ion, a = ion specific coefficient, S = number of ion species represented in the model.

The calculation of aqueous ion concentrations in *ecosys* is described in Grant (1995) and solution concentrations of all ions and ion pairs are used to calculate ψ_π (equation (3)).

$$\psi_\pi = -RT\sum_{S=1}^{S} C_s.10^{-6} \qquad (3)$$

where: ψ_π = soil osmotic potential (MPa), R = gas constant (J mol^{-1} K^{-1}), T = soil temperature (K).

In soil water systems, ψ_s (equation (4)) is calculated by adding ψ_m depending on θ, soil osmotic potential (ψ_π) depending on soil C_s and gravitational potentials (ψ_g) depending on elevation (Grant, 1995). Higher C_s in the cover and overburden (within the root zone) decrease the ψ_π (equation (3)) and subsequently ψ_s (equation (4)) (Grant, 1995).

$$\psi_s = \psi_m + \psi_\pi + \psi_g \qquad (4)$$

3.2.1.2. Canopy water potential and gross primary productivity as affected by changes in soil water potentials due to salt movement

In *ecosys*, surface energy exchanges (equation (5)) derived from incoming shortwave and longwave radiation, air temperature, humidity, and wind speed are used to determine efflux of ET from canopy layers [B1b and B1c] regulated by aerodynamic resistance (r_a) and canopy stomatal resistances (r_c), and of evaporation (E) from canopy, snow, surface litter [D6a] and soils surfaces [D6b] regulated by r_a (Grant et al., 1999).

$$Rn_{ci} + LE_{ci} + H_{ci} + G_{ci} = 0 \qquad (5)$$

where: subscript i = species or plant functional type (PFT); Rn_{ci} = canopy net radiation (W m^{-2}), LE_{ci} = latent heat flux between canopy and atmosphere (W m^{-2}), H_{ci} = canopy sensible heat flux (W m^{-2}), G_{ci} = canopy storage heat flux (W m^{-2}).

The transpiration flux (E_{ci}) in equation (5) is coupled to total water uptake (U_c) which is calculated from the difference between ψ_c and ψ_s across soil and root hydraulic resistances (Ω_s) and (Ω_r) in each rooted soil layer (equation (6)). These calculations determine the transpiration from canopy surfaces and thereby water removal from soil profiles through the roots.

$$(e_a - e_i(T_{ci}))/(r_{ai} + r_{ci}) = \Sigma_l \Sigma_r (\psi_{ci} - \psi_{sl})/(\Omega_{si,r,l} + \Omega_{ri,r,l} + \Sigma_x \Omega_{ai,r,l,x}) + X_{ci}\delta \psi_{ci}/\delta t \qquad (6)$$

where: subscripts l = soil layer, r = root or mycorrhizae, x =1, 2 (1= primary root, 2 = secondary root; e_a = atmospheric vapor density at air temperature (T_a) and ambient humidity (g m^{-3}), $e_i(T_{ci})$ = canopy vapor density at T_{ci} (g m^{-3}), T_c = canopy temperature (K), r_{ai} =aerodynamic resistance to vapor flux from canopy (s m^{-1}), r_{ci} = canopy stomatal resistance to vapor flux (s m^{-1}), ψ_{ci} = canopy water potential (MPa), ψ_s = soil water potential (MPa) , $\Omega_{si,r,l}$ = radial resistance to water transport from soil to surface of roots or mycorrhizae (MPa h m^{-1}), $\Omega_{ri,r,l}$ = radial resistance

to water transport from surface to axis of roots or mycorrhizae (MPa h m^{-1}), $\Omega_{ai,r,l,x}$ = axial resistance to water transport along axes of primary or secondary roots or mycorrhizae (MPa h m^{-1}), all calculated from root lengths and surface areas, X_{ci} = canopy capacitance (m^3 m^{-2} MPa^{-1}), t = time (h).

Greater C_s in root zone decreases ψ_π (equation (3)) and which subsequently lowers ψ_s (equation (4)). During soil drying, lower θ lowers ψ_m and increases C_s and hence lowers ψ_π so that further decreases ψ_s.

Lower ψ_s and hence U_c decrease ψ_c which decreases canopy turgor potential (ψ_t) (equation (7)) (Grant et al., 1999).

$$\psi_{ti} = \psi_{ci} - \psi_{\pi i} \qquad (7)$$

where: ψ_t = canopy turgor potential (MPa), ψ_c = canopy water potential (MPa), ψ_π = canopy osmotic potential (MPa) calculated from canopy solute concentrations.

Lower ψ_t controls stomatal closure as r_c is minimum (r_{cmin}) at zero ψ_c and rises exponentially with declining ψ_t (equation (8)) causing full stomata closure when ψ_t reaches zero MPa.

$$r_{ci} = r_{cmini} + (r_{cmaxi} - r_{cmini})\, e^{(-\beta\, \psi_{ti})} \qquad (8)$$

where: r_{ci} = canopy stomatal resistance to vapor flux (s m^{-1}) r_{cmin} = minimum r_c at ψ_c = 0 MPa (s m^{-1}) calculated from carboxylation rates [C5], r_{cmax} = canopy cuticular resistance to vapor flux (= 5.0×10^3 s m^{-1}) [Larcher, 2003], β = stomatal resistance shape parameter (= -5 MPa^{-1}) [Grant and Flanagan, 2007], ψ_t = canopy turgor potential (MPa).

Increased r_c or decreased canopy stomatal conductance ($g_c = 1/r_c$) reduces CO_2 diffusion into the leaves (equation (9)) thereby CO_2 fixation [C3].

$$V_{gi,j,k,l,m,n,o} = (C_b - C_{ii,j,k,l,m,n,o}) / r_{li,j,k,l,m,n,o} \qquad (9)$$

where: subscripts i = species or plant functional type (PFT), j = branch or tiller, k = node, l = canopy layer, m = leaf azimuth, n = leaf inclination, o =leaf exposure (sunlit vs. shaded); V_g = leaf CO_2 diffusion rate (μmol m^{-2} s^{-1}), C_b = [CO_2] in canopy air (μmol mol^{-1}), C_i = [CO_2] in canopy leaves (μmol mol^{-1}), r_l = leaf stomatal resistance (s m^{-1}).

Canopy carboxylation rates (V_c) are coupled with CO_2 diffusion rates by solving for a common value of C_i, and so are calculated from stomatal and nonstomatal effects on CO_2 and light limited carboxylation (Grant and Flanagan, 2007). Lower GPP and thereby NPP (GPP – autotrophic respiration (R_a)) are thus obtained with lower ψ_s and ψ_c as affected by ψ_π from C_s determined by salt movement (Section 3.2.1.1). Lower r_c from higher C_s reduces the CO_2 fixation and thereby growth of plants in shallow covers compared to those in the deeper cover.

Steep slopes created during upland reclamation increase downslope salt movement through lateral subsurface flow of water which accumulates at the cover-overburden interface. This movement causes salt discharge to lower surrounding areas through water discharge from the toe of the hillslope in the reclaimed sites. This salt movement causes salinization in the lower slope positions and downslope areas. As reclamation progresses root zone C_s and thereby EC in lower slopes reach the threshold level for plant productivity (4 dS m^{-1}), particularly in shallow covers. Thus, lower plant growth will be observed in lower slope positions particularly with shallow covers.

3.2.2. Site description

South Bison Hills (SBH) watershed is located within the Syncrude Canada Ltd. Mildred Lake mine operation, Alberta, Canada. The mean annual temperature and the mean annual precipitation (1981 -2010) of the SBH area are 1.0 °C and 418.6 mm respectively (Environment Canada, 2014) and the area is classified as sub-humid climate (Kelln et al., 2007). The SBH capping trial research watershed began in 1998, constructed on ~100 x 10^6 m^3 of saline-sodic (Clearwater Formation) overburden with overlying soil covers and extends over a 2 km^2 area with a plateau (Huang et al., 2015b). The slope of the overburden dump was designed with a 1:5 (20%) incline (Boese, 2003). Three adjacent covers with depth of 35 cm, 50 cm and 100 cm constructed along the north facing slope (5 horizontal:1 vertical) of SBH were used as the experimental sites for the study. Each cover was approximately 200 m in length and 50 m in width (approximately 1 ha) and consisted of peat mineral mix (PMM) and subsoil materials which overlaid saline sodic overburden as in Figure 2.1 (a). In the spring of 1999, barley was seeded to a density of 25 kg ha^{-1} in each plot to reduce erosion and to stabilize the slope. Fertilizer was applied prior to tree planting at the rate of 35 kg N ha^{-1}, 46 kg P ha^{-1}, 44 kg K ha^{-1} and 14 kg S ha^{-1} (Lanoue, 2003; Garrah et al., 2013). In the fall of 1999, white spruce (*Picea glauca* (Moench) voss) and aspen (*Populus tremuloides* Michx.) seedlings were planted in alternate rows (Hilderman, 2011) in each cover with a total density of 1,600 stems ha^{-1} (50:50 mix of aspen and white spruce) to revegetate to a mixed-wood boreal forest. Further details of site description and reclamation methods can be found in Sections 2.2.2.1 and 2.2.2.2.

3.2.3. Field data collection

3.2.3.1. Weather

Solar radiation, maximum and minimum air temperatures, precipitation (*P)*, wind speed, and relative humidity were recorded daily from January 1, 1999 to December 31, 2015. Except for winter *P* and solar radiation, all the other measurements were taken from the SBH weather station which was built on the middle slope of the 35 cm cover. There was uncertainty in the accuracy of the P data in some data collection years, hence, the winter *P* (October 1 to March 31 every year) and solar radiation until 2006 (January 1 to December 31 every year) were taken from the Fort McMurray airport weather station located approximately 40 km south from the site. Winter *P* and solar radiation from 2007 were taken from the Mildred Lake airport weather station (built in 2007) located approximately 6 km northeast of the study site. These daily data were read into *ecosys* where they were resolved into hourly values to match the hourly time step at which the model functions.

3.2.3.2. Hydrology

SBH is an instrumented watershed, and the details of the installation of all the instruments were described in Boese (2003). Both the θ and ψ_m were measured using time domain reflectometry (TDR) probes and CS 229 sensors respectively at the middle slope position of each cover from 1999 to 2015. However, data were missing for some years due to temporary instrumentation failures. Values of θ in the 50 cm cover were only used to 2006; instruments were replaced in 2007 which resulted in a shift of measured readings pre- and post-instrument replacement (O'Kane Consultants Inc., 2012a). These θ and ψ_m data were downloaded from the proprietary Syncrude watershed database and were used to derive key soil properties or to validate model outputs and thereby to determine the effect of cover depth on soil water storage.

3.2.3.3. Aboveground biomass

Aboveground biomass carbon was estimated by Macyk et al. (2009) and Drozdowksi et al. (2011, 2014) for planted aspen and white spruce trees in 35 cm, 50 cm and 100 cm covers. The height, base and breast diameters of planted trees were collected annually (2007 - 2013) from 10 m x 10 m permanent sampling plots which were established in upper, middle and lower slope positions of all the reclamation covers in 2007 (Macyk et al., 2009; Drozdowksi et al., 2009, 2014). The aboveground biomass carbon values for each species were estimated using allometric equations relating to measured breast height and basal tree diameters in the sampling plots and species specific density and expansion factors for branch and leaf/needles developed for Alberta species (Alberta Environment, 2007). These data were used to validate the modelled aboveground carbon biomass and thereby to understand the effect of cover depth on net primary productivity.

3.2.3.4. Salinity measurements

In July 2013, pits were dug up to 30 cm in top, middle and bottom slope positions of each reclamation cover. Soil cores were used to take soil samples at 7.5 cm intervals in 35 cm cover and 10 cm intervals in 50 cm and 100 cm covers for each pit, and subsamples were taken to increase the accuracy of measured values. The EC and pH in saturated paste extracts (McKeague, 1978) were measured using an Accumet XL200 pH/conductivity meter. The EC values measured in June 2002, October 2005, August 2007, August 2008, and September 2012 were taken from the experiments done by Kessler (2007), Hilderman (2011) and Northwind Land Resources Inc. (2014). The same saturated paste extraction procedure was followed to measure EC in all the experiments. These data were used to validate the modelled EC values.

3.2.4. Model experiment: South Bison Hill reclamation site as represented in *ecosys* model runs

3.2.4.1. Landscape

The information for site management and soil properties collected during 1999 and 2000, were used to construct the input files used to initialize *ecosys* for SBH. These inputs represent the actual field characteristics which include site, weather, and plant and soil management data used by *ecosys* to simulate site conditions during the experiment. Each reclamation cover was represented in the model as a transect of six interconnected grid cells each of which had a dimension of 50 m x 40 m. Five grid cells represented the slopes as shown in Figure 2.1 (b) and one grid cell represented the level area above the slope corresponding to the landscape at SBH. All the input data (site, weather, soil properties, soil and plant management) were the same among reclamation covers except cover depths as described in Section. 2.2.2.1.

3.2.4.2. Soil properties

Soil physical and chemical properties were taken from the studies done by Macyk (1999), Meiers (2002) and Yarmuch (2003) and soil biological properties were taken from the study done by Lanoue (2003) in the SBH site. The θ_{FC} and θ_{PWP} for PMM, subsoil and overburden (Table 2.2) were derived from water desorption curves developed using measured θ vs. ψ_m data. Although measured TDR values had indicated slightly different θ_{FC} and θ_{PWP} at different depths in the three covers, average values were used for each material in each reclamation treatment so that modelled differences in soil and plant water status and in plant growth could be attributed to those in capping depth. Saturated hydraulic conductivity values (Table 2.2) reported by Meiers et al. (2011) were used as inputs from which the model calculated unsaturated values (Grant et al., 2004). The key soil chemical properties used to model salt redistribution in PMM, subsoil and

overburden are given in Table 3.1. The pH and soluble ion concentrations were measured from saturated paste extracts and further details of analytical methods can be found in Macyk (1999), Yarmuch (2003) and Wall (2005). Although the measured soluble ion concentrations in saturated extracts showed variation for each material in the slope positions in the three covers, average values were used for each material in each reclamation treatment so that modelled differences in salt redistribution and osmotic stress and in plant growth could be attributed to those in capping depth. A trace amount of gypsum (100 g Ca Mg^{-1}) was included in the lowest subsoil layer in each cover as observed by Wall (2005). These data were used as inputs in the model to drive soil functions for salt movement. The three horizons of the soil profile (PMM, subsoil (till) and upper overburden (Figure 2.1 (a))) were subdivided into 15, 16 and 19 soil layers for the 35 cm, 50 cm and 100 cm capping depths respectively to increase spatial resolution and enable comparison of water and salt movements with measured values. The overburden depth in each reclamation cover was set to a constant value (3 m) to model water and salt movements to/from the overburden. The root studies (Karst and Landhäusser, 2014; Van Rees, 2014) that had been conducted in the study area showed that only a very small fraction of roots penetrated into the overburden, most of which were within 25 cm below the cover-overburden interface. Soil resistance equations used in the model for root growth in crops by Da Silva and Kay (1997) and Chen and Weil (2011) did not limit root penetration into overburden in the model as much as was observed. Maximum rooting depth in the model was therefore restricted to 25 cm below the interface for each cover.

3.2.4.3. Land management

At the beginning of simulation runs (1999) the modelled landscapes were initialized with the soil properties described in Section 3.2.3.1 and seeded with barley and fertilized in spring

1999 as described in Section 3.2.2.1. Aspen and white spruce plant functional types (PFTs) and grass and clover PFTs were seeded in each grid cell in summer 1999 at the densities described under the reclamation method in Section 2.2.2.2. In 2007, ingress plants were seeded as described under Section 2.2.2.2. The model was run for 17 years (1999 - 2015) using the daily weather data described in Section 2.2.3.1.

3.2.4.4. Model runs with hypothetical non-saline sodic overburden

A parallel modelling was performed for the three reclamation covers substituting the larger overburden salt concentrations (Ca^{2+}, Mg^{2+}, Na^{+}, K^{+}, SO_4^{2-}, and Cl^{-}) with smaller subsoil mineral soil concentrations and with trace gypsum amount in overburden (10 g Ca $Mg^{-1)}$ with everything else unchanged. The outputs from these parallel modelling were used to compare the effect of the saline-sodic overburden (SSOB) used to represent site conditions with those of a hypothetical non-saline-sodic overburden (NSSOB) to estimate overburden salt effects on ψ_π, ψ_s, ψ_c and thereby NPP.

3.2.4.5. Model validation

Model results for θ, water uptake and aboveground carbon biomass were validated with field measured values at different slope positions for the three cover depths as described in the Section 2.3. Modelled EC in each reclamation cover was compared with field measured values to validate modelled salt movement at different slope positions over the reclamation period.

3.3. Results

3.3.1. Modelled *vs.* measured salt redistribution in different reclamation covers

Modelled salt redistribution patterns indicated by EC calculated from C_s (Eqn 2) in each cover were consistent with the field observed redistribution patterns over the reclamation period

(Figures 3.1 and 3.2), with most of the modelled EC (Figures 3.1 and Figure 3.2) lying within the standard deviations of measured values. However, the observed EC in different covers were not significantly different ($P > 0.1$) due to large uncertainties in measured values indicated by the standard deviations (Figure 3.1). Different cover depths showed similar trends in which EC increased with soil depth to largest values in the overburden. Modelled salinity levels in upper subsoil soil layers (20 - 50 cm) increased during 5-6 years from start of reclamation. Greater modelled EC in cover material was observed within the 10 - 15 cm zone above the cover-overburden interface (interface) particularly in 35 cm and 50 cm covers (Figures 3.1 and 3.2). Thus, EC in soil more than 25 cm (Figure 3.2b) and 40 cm (Figure 3.2h) below the surface in the 35 cm and 50 cm covers respectively approached 4 dS m^{-1} (threshold level for adverse effects on productivity) while that in the 100 cm cover approached this threshold at 90 cm (Figure 3.2n).

After 2008, a gradual levelling off and subsequent decline of simulated EC was modelled at 10 cm above the interface in the 35 cm (Figure 3.2b) and 50 cm (Figure 3.2h) covers. This decline was due to balancing salt movement into the root zone by diffusion with salt removal from the root zone by lateral water flow and subsurface discharge caused by greater precipitation after 2008 (Figure 3.2). However, modelled EC values at 90 cm in the 100 cm cover did not show any decline during the same period (Figure 3.2 n). In addition, a greater decline of EC was modelled and measured in the overburden layer below the interface in the 35 cm (Figure 3.1b-d and Figure 3.2c) and 50 cm (Figure 3.1f-h and Figure 3.2i) covers *vs.* 100 cm cover (Figure 3.1j-l and Figure 3.2o). These values indicated more rapid early salt movement from the overburden into the root zone in the shallow covers.

Steep slopes created during reclamation caused downslope water flow through lateral subsurface and surface runoff (Section 2.3.6). This flow drove downslope salt movement through

lateral convective-dispersive transfer (Eqn 1) causing slight EC differences modelled with slope positions in each cover that were comparable with measured differences (Figure 3.1). Even though slightly higher EC was measured and modelled in the root zone at lower or middle slope positions in all the covers (Figure 3.1), a clear consistent topographical pattern was not identified during 2002, 2008, 2012 (Figure 3.1) and 2015 (data not shown), indicating a limited effect of topography on salt movement within the reclamation period.

The modelled EC in the NSSOB runs was always less than 1 dS m^{-1} in the root zones of all the reclamation covers (data not shown), indicating that increases in EC modelled in the root zones of the covers (Figures 3.1 and 3.2) could be attributed to salinity that originated in the overburden.

3.3.2. Effect of cover depth on osmotic water potential within the root zone

The increased C_s modelled with SSOB reduced the ψ_π (Eqn 3) along the soil profile in each cover from that modelled with NSSOB (Figure 3.3). As expected, C_s and ψ_π modelled with SSOB (Figure 3.3) followed a profile similar to that of EC calculated from C_s (Eqn (2)) (Figure 3.1) for all the covers. Therefore, greatest C_s was modelled in the lowest overburden layer (Figure 3.3 a-c) and gradually declined towards the cover-overburden interface due to upwards salt movements. However, modelled C_s with NSSOB was very low for all the covers (Figure 3.3) so that modelled ψ_π (Eqn 3) remained high. These differences in C_s and ψ_π between SSOB and NSSOB in the root zones in Figure 3.3 can be attributed to the salinity originating in the overburden.

3.3.3. Effect of saline sodic overburden on NPP and aboveground biomass

The effect of modelled C_s and ψ_π in SSOB vs. NSSOB covers on water relations (ψ_c and g_c) and CO_2 exchange were likely to be more apparent with drier soil and so were compared during the dry year 2011 (Figure 3.2) for aspen (Figure 3.4) and spruce (Figure 3.5). A clear decrease in modelled ψ_c and g_c and thereby a slight decline in CO_2 flux were modelled in the 35 cm cover with SSOB vs NSSOB for both aspen and spruce (Figures 3.4 (a1-a3) and 3.5 (a1-a3)) indicating that salts originating in the overburden below the shallow cover reduced ψ_π, ψ_s, ψ_c and thereby CO_2 fixation. A slight decrease in ψ_c, g_c and CO_2 flux in aspen and a slight increase in ψ_c, g_c and CO_2 flux in spruce (Figures 3.4 (b1-b3) and 3.5 (b1-b3)) were modelled in the 50 cm cover with SSOB vs. NSSOB during the same dry period. A slight increase in ψ_c, g_c and CO_2 flux in both aspen and spruce were modelled in the 100 cm cover with SSOB vs. NSSOB. Greater adsorbed NH_4^+ in soil profile and slightly higher plant N stress were modelled in all the covers with NSSOB than with SSOB (data not shown). The soil volume above the overburden was greater for 100 cm cover than the other two covers thereby more NH_4^+ was adsorbed to the soil particles with NSSOB. This adsorption effect might become more apparent with the less salt effect on ψ_s with NSSOB in the 100 cm cover. Therefore, the decline of ψ_c, g_c and CO_2 flux in PFTs in 100 cm cover with NSSOB was attributed to less desorption of adsorbed NH_4^+ from cation exchange sites by smaller cation (Ca^{2+}, Mg^{2+}, K^+ and Na^+) concentrations modelled in root zones above NSSOB, thereby reducing plant nitrogen uptake particularly in dry year due to lower θ.

No reductions in $\psi_\pi, \psi_s, g_c, \psi_c$ and CO_2 fixation were modelled with SSOB vs. NSSOB during wetter years (data not shown). This was attributed to increasing ψ_s and ψ_π from salt dilution with greater θ in the root zone during wetter years.

Reductions in CO_2 fixation modelled with SSOB relative to NSSOB in shallow covers during drier years (Figure 3.4a3) did not much affect long-term tree NPP and growth. The average planted tree NPP modelled with SSOB was similar to that with NSSOB across slope positions in all the covers after crown closure (data not shown). However, slightly smaller aspen biomass and consequently slightly greater spruce biomass was modelled with SSOB vs. NSSOB for 35 cm and 50 cm covers (Figure 3.6 a,b). However similar biomass was modelled with SSOB and NSSOB for both aspen and spruce in the 100 cm cover (Figure 3.6c). The modelled total planted tree biomasses were similar with NSSOB and SSOB for all the covers (3.6d) due to offsetting changes in aspen and spruce growth. Model results indicated that salts originating in the saline overburden did not adversely affect tree growth under the conditions at SBH.

3.3.4. Salt discharge to surrounding areas from reclaimed landscapes

Lower total salt discharge rates were modelled for all the reclamation covers until 2008 and higher rates were modelled thereafter (Figure 3.7), varying with subsurface discharge rates in Table 2.6 in Chapter 2. The subsurface water discharge rates were low before 2008 because of lower precipitation vs. evapotranspiration (data not shown). After 2008, a slightly higher steady salt discharge rate (~1.5 mol m^{-2} y^{-1}) was modelled in 35 cm and 50 cm covers except for the driest (2011) and wettest (2013) years which showed temporary fluctuations (Figure 3.7). In the early reclamation period before 2008, slightly higher salt discharge rates were modelled in 35 cm and 50 cm covers than in the 100 cm cover from which greater discharge rates were modelled in wet years after 2012 (Figure 3.7). Lower salt discharges in 2011 were consistent with the lower precipitation (Figure 3.7) and hence lower downslope water flow and subsurface discharge (Table 2.6 in Chapter 2). However, greater θ in a subsequent wet year (2013) increased salt discharge particularly in the 100 cm cover. Even though the water discharge was low (Table 2.6

in Chapter 2), greater EC and C_s in lower root zone of the 100 cm cover (Figure 3.2n and Figure 3.3c) contributed to the increased salt discharge. The modelled salt discharge rates were consistent with the modelled EC in lower subsoil (Figure 3.2b,h,n) and upper overburden (Figure 3.2c,i,o) layers which showed a stable value after 2008 (Figures 3.1 and 3.2) particularly in 35 cm and 50 cm covers. This stable EC indicates that upward salt diffusion from the overburden into the root zone had equilibrated with lateral transport and discharge from the root zone.

3.4. Discussion

3.4.1. Influence of cover depth on root zone salt concentrations

The similar EC gradients modelled and measured in the three covers during the reclamation period indicated the ability of *ecosys* to simulate salt movement from the saline overburden into the covers. In *ecosys*, upward salt diffusion from overburden into cover material was modelled from convective-dispersive transfer driven by vertical solute concentration gradients between the overburden and the cover (Eqn 1) (Figure 3.1 and 3.3). The measured and modelled θ in the overburden changed little (Figure 2.2), because of low K (Table 2.1), indicating limited water exchange and hence limited contribution of convection to salt movement between the overburden and the cover. Studies conducted by Kessler (2007), Hilderman (2011) and Klohn Crippen Berger Ltd. (2013) found a similar salt distribution pattern in three different cover depths in SBH and stated that diffusion was the major upwards salt transport mechanism in these covers.

Salt diffusion modeled from the overburden was also affected by soil water-filled porosity in the covers. In *ecosys*, greater distance of salt movement modelled in the 100 cm cover *ca*. 60 cm above the interface (indicated by slightly increased EC in Figure 3.2m and Figure 3.1j,l), consistent with observations in Klohn Crippen Berger Ltd. (2013), was modelled through greater

aqueous dispersivity in soil as a function of greater water filled porosity [D 20] (Figure 2.3 in Chapter 2). This indicated that the distance of upward salt transport from the overburden into the covers during land reclamation were also affected by cover θ. Smaller salt movement distances were modelled with lower θ in shallower covers because lower θ reduced D_{sc} in Eqn 1.

Stabilization of modelled C_s in the cover occurred when upward diffusion equilibrated with lateral flow and discharge of the diffused salts. Early C_s stabilization following slight declines in the 35 cm and 50 cm covers vs. 100 cm cover (Figure 3.2), indicated the influence of cover depth on the C_s stabilization. The 35 cm and 50 cm covers in our study were closer to the overburden and had lower soil volume (Figure 2.1a). Therefore C_s above the overburden increased during the early reclamation period before 2008, apparent as rising root zone EC, but decreased gradually thereafter (Figures 3.1 and 3.2) due to increased salt discharge with lateral flow (Figure 3.7). These results were consistent with Nichol et al. (2006) (as cited in Klohn Crippen Berger Ltd. (2013)) who predicted that salinity levels would decrease over the reclamation period after reaching a maximum level due to salt discharge from the reclamation covers at SBH, using a modelling study. They further suggested that this maximum salinity could be reached 5-100 years after the start of land reclamation according to downslope lateral flow and net water percolation rates in these covers.

Salt concentration gradients driving diffusion were maintained by salt generation within the overburden. The increased salinity level during 1-3 years from the start of reclamation (Figure 3.2) indicated the diffusive movement of salts already present in the overburden (Table 3.1). Dissolution of both pyrite (FeS_2) and gypsum ($CaSO_4$) generated additional soluble salts in the marine origin shale overburden as described in a sequence of reactions by the Kessler (2007). Pyrite was not modelled in *ecosys* therefore continued generation of soluble salts, particularly

SO_4^{-2}, from shale overburden in the model was limited to those from gypsum dissolution governed by a solubility product [E4]. Rates of dissolution were controlled by those of product (Ca^{2+} and SO_4^{2-}) removal through convective-dispersive transport into the covers according to set aqueous diffusivity values. These rates eventually equilibrated with rates of discharge through downslope flow. If the steady salt discharge rate (~1.5 mol m^{-2} y^{-1}) was similar to diffusion driven by the gypsum dissolution rate plus diffusion of other salts, the average daily SO_4^{2-} production for all the covers was *ca.* 0.33 g SO_4^{2-}-S m^{-2} day^{-1} for the non-frozen period, assumed to be 150 days in this calculation, because little or no salt generation and diffusion occurs in winter (Kelln, 2008; Appels et al., 2017) due to lower temperature and θ. This estimated salt production rate was within the ranges that were calculated by Hilderman (2011) (0.04 - 0.77 g SO_4^{2-}-S m^{-2} day^{-1}), by Huang et al. (2015b) (0.12 - 3.32 g SO_4^{2-}-S m^{-2} day^{-1}) and by Appels et al. (2017) which were 0.23-2.77 g SO_4^{2-}-S m^{-2} day^{-1} during the non-frozen period at SBH. But the value was lower than the estimated value by Wall (2005) of 0.43 g m^{-2} day^{-1} SO_4^{2-}-S. These rates contributed to declines in overburden EC modelled in Figure 3.2c-e,i-j and o.

The modelled and measured results demonstrated that C_s within the root zones in 35 cm and 50 cm covers (starting from 25 cm and 40 cm below soil surface respectively) *vs.* 100 cm cover reached the threshold level for affecting plant productivity (4 dS m^{-1}) during the early reclamation period (before 2008) due to upwards salt movements through dispersive transfers.

3.4.2. Root zone salt concentration effects on water relations

In *ecosys*, the effect of greater root zone C_s on plant growth was modelled through a sequence of processes representing basic theories in salinity and its effects on soil-plant-atmosphere water relations (e.g. Larcher, 2003), avoiding site specific parameters. Therefore salt effects on the modelled water relations depended on the inputs of soil properties, weather, and

soil and plant management without site-specific calibration of model parameters (Grant, 1995). In *ecosys*, greater C_s in the root zone reduced ψ_π (Eqn 3), ψ_s (Eqn 4), U_c and thereby ψ_c (Eqn 6). Lower ψ_c reduced ψ_t and g_c and hence CO_2 fixation and plant growth. However, effects of ion toxicities or other ion deficiencies were not included in *ecosys* so that the salinity effect was entirely attributed to osmotic stress (Grant, 1995).

Average salinity within root zones was greater than 4 dS m^{-1} in the 35 and 50 cm covers but not in the 100 cm cover above SSOB. The reductions of ψ_c, g_c and CO_2 fixation in 35 cm and 50 cm covers with SSOB vs NSSOB (Figure 3.4 and 3.5) indicated that salts originating in the SSOB adversely affected the water relations and CO_2 fixation in thinner covers particularly in dry periods. The effect of salinity on CO_2 fixation (Figures 3.4 and 3.5) under limited water content modelled in the 35 cm cover (Figure 2.3 in Chapter 2) was consistent with the suggestion by Lilles et al. (2010) that fine-textured saline reclaimed sites need to have an adequate amount of water storage to avoid adverse effects of salinity on plant growth. However, under the current climate represented by weather data from 1999 to 2015, the dry conditions under which these adverse effects of salinity occurred were sufficiently infrequent that long-term tree growth was minimally affected.

In addition to decreased ψ_π, modelled salt generation in the overburden also increased NH_4^+ availability by forcing greater desorption of adsorbed NH_4^+. The effect of decreased ψ_π was greater for shallower covers due to lower θ and ψ_π. However, the effect of increased NH_4^+ availability was greater in thicker covers due to greater θ and ψ_π. Lower ψ_c, g_c and thereby slightly higher CO_2 fixation in both aspen and spruce in 100 cm cover with SSOB vs. NSSOB, indicated (Figures 3.4 and 3.5) the positive effect of greater cation concentrations within the root zone, particularly Ca^{2+} which was generated through gypsum dissolution. The effect of cover

depth on NH_4^+ availability and uptake will be examined in more detail in Chapter 4. The increased NH_4^+ availability and plant uptake modelled here with the presence of Ca^{2+} was demonstrated by Koenig and Pan (1996) using laboratory, greenhouse and field experiments. They attributed increased soil solution NH_4^+ concentration with greater Ca^{2+} to preferential adsorption of Ca^{2+} and the consequent displacement of NH_4^+ from soil exchange sites. However, further work is needed to elaborate the effect of gypsum particularly Ca^{2+} in overburden on nutrient availability in reclaimed landscapes.

The limited effect of salinity on tree water relations and growth modelled in this study was consistent with earlier observations on reclaimed and natural saline landforms in the AOSR. Purdy et al. (2005) stated that boreal mixed-wood species could exist in sites with salinity greater than 10 dS m^{-1} as long as salts remain below the root zone and sufficient freshwater (from surface flow or precipitation) available for plant growth. Lilles et al. (2010) also found that typical boreal forest species grew in the areas with a forest floor plus 20 cm of low saline soil (< 4 ds m^{-1}) as in the 50 cm or 100 cm covers in Figure 3.2. However, all of the sites in these studies were wet for most of the growing season and did not have any moisture or nutrient limitation.

The adverse effects of salinity modelled during dry periods in this study were more apparent in modelled CO_2 fixation and growth of aspen (Figure 3.4) than of spruce (Figure 3.5). This model result was consistent with observations on naturally saline sites in the northern Alberta boreal forest region where aspen growth was reduced when topsoil EC was less than 4 dS m^{-1} and subsoil EC was 4-23 dS m^{-1} (McKenzie et al., 1993; Lilles et al., 2012) but spruce growth was not (Lilles et al., 2012). Greater spruce growth modelled in the current study with SSOB vs. NSSOB was enabled by reduced competition for light and nutrients with reduced

aspen growth. Renault et al. (1999) also found slightly higher survival rate of white spruce than of aspen grown in consolidated tailing with added NaCl plus Na_2SO_4. More rapid water uptake by aspen (Peterson and Peterson, 1995) than by spruce (Figures 2.6, 2.7) reduced θ particularly in shallow covers during dry periods. Lower θ in a saline soil further reduced water uptake by aspen giving a greater response to salinity by aspen than by white spruce.

3.4.3. Effect of slope position on root zone salt concentrations and salt discharge to downslope areas

In *ecosys*, downslope salt movement in the cover mainly occurred through convective transfer (Eqn 1) because of greater K and smaller lateral salt concentration gradients. Thus changes in salt discharge followed those in water discharge driven by excess precipitation (Figure 3.7). Even though wetter lower slope positions were modelled during the study (Figure 2.4), a clear consistent topographical pattern for salt redistribution in the cover was not modelled in this study (Figure 3.1). These model results were consistent with the findings from field studies by Kessler (2007) and Klohn Crippen Berger Ltd. (2013) who could not establish a clear topographical effect of salinity at SBH. However, clear modelled EC increase from upper to lower and lower to middle slope positions in the 35 cm overburden (Figure 3.1d), indicated that there might be a long-term topographic effect on C_s redistribution which is not evident during this time period of this study. In SBH, water was drained to the ditches at the bottom of the constructed reclamation slopes. Therefore, salt movement into lower slope positions modelled from downslope water flow was offset by modelled salt discharge driven by modelled water discharge to the ditches (Table 2.6 in Chapter 2). Thus measured and modelled EC in the root zone of lower slope position was not increased in the current study. The salt discharge was not reduced with deeper cover, in fact it was increased due to greater diffusion with greater θ in the

100 cm cover as discussed in Section 3.4.1.1. However, if the salts discharged from steep reclaimed sites with SSOB are not properly managed, there is a greater potential for salinization in ecosystems receiving this discharge.

3.4.4. Summary

In summary, some plant growth reduction was modelled with salinity in shallow covers during dry years but a relationship between root zone salt concentration and biomass growth was not apparent. Shallow covers reached equilibration between salt discharge and salt generation earlier than did the thicker covers. Therefore upland reclamation with SSOB should consider:

(1) Long term salinity evaluation to understand the effect of salts on forestland productivity.

(2) Adequate cover depth to lower EC within the root zone as plant growth in shallow covers affected by greater salt concentration particularly during drier years.

(3) More frequent droughts could reduce long-term plant growth and adversely affect establishment of commercial forest due to osmotic stress in covers with lower ψ_s determined by the cover depth.

(4) Downslope discharge of salts transported from overburden to covers in reclaimed watersheds will increase the risk of salinization in down slope areas.

Collectively, the findings showed that ecosystem models such as *ecosys* are well adapted for predicting short and long-term salinity effects in reclaimed landscapes and forest productivity with different reclamation depths, materials under different weather and management conditions.

Table 3.1. Key soil chemical properties used to model salt redistribution in three reclamation covers.

Chemical Properties		Peat Mineral Mix	Subsoil/Till	Overburden
pH[a]		5.8	7.8	7.5
Cation exchange capacity	($cmol^{+}\ kg^{-1}$)[b]	86.3	15.6	20.6
Aluminum	(g Al Mg^{-1})	0.4	0	0
Iron	(g Fe Mg^{-1})	0.4	0	0
Calcium [a]	(g Ca Mg^{-1})	79	117	409
Magnesium [a]	(g Mg Mg^{-1})	24	28	263
Sodium [a]	(g Na Mg^{-1})	35	102	2339
Potassium [a]	(g K Mg^{-1})	6	6	92
Sulfate [a]	(g S Mg^{-1})	20	42	748
Chloride[a]	(g Cl Mg^{-1})	15	22	105
Gypsum[c]	(g Ca Mg^{-1})	0	0	3000

[a] from Macyk (1999)
[b] from Yarmuch (2003)
[c] from Wall (2005) and Hilderman (2011)

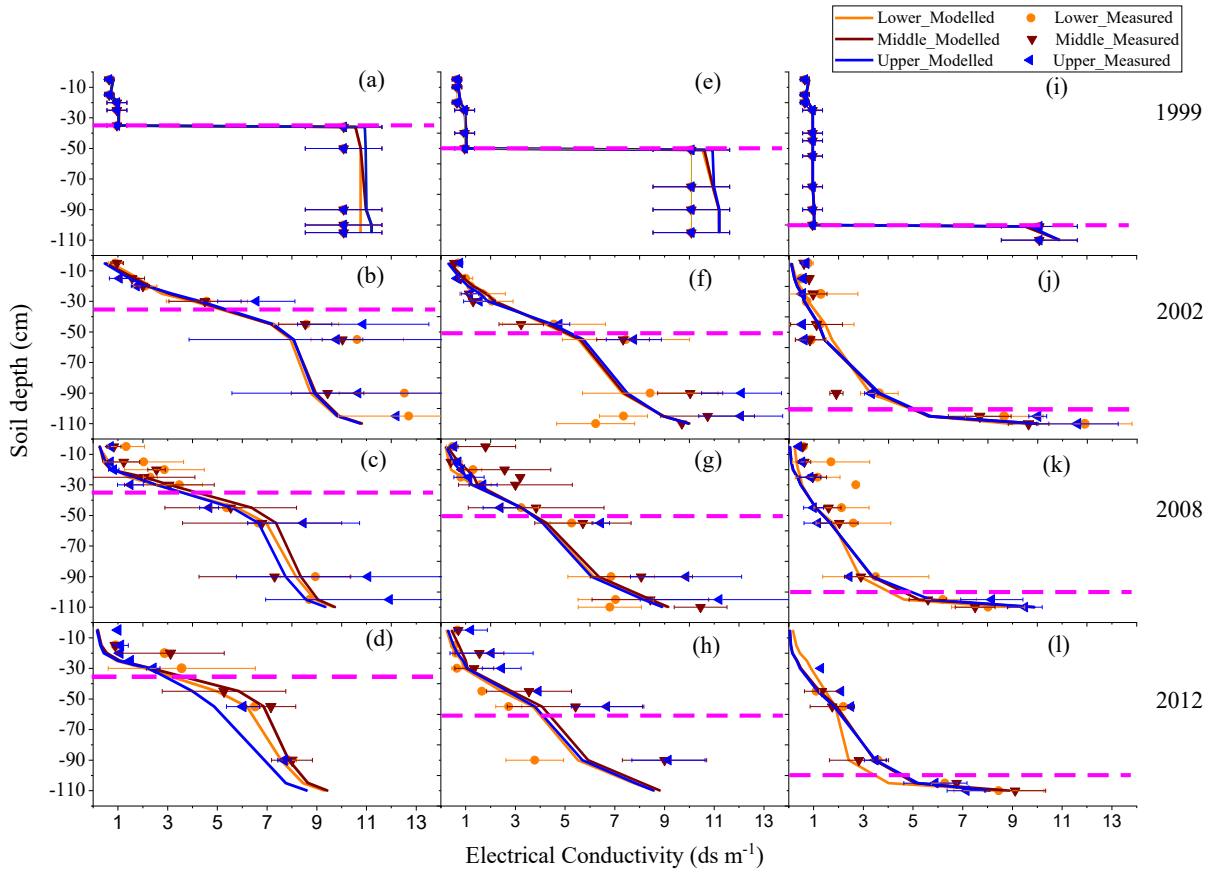

Figure 3.1. Mean modelled (solid line) and measured (symbols) electrical conductivity profiles at lower (orange), middle (brown) and upper (blue) slope positions in (a-d) 35 cm, (e-h) 50 cm and (i-l) 100 cm covers during 1999 (June), 2002 (June), 2008 (August), and 2012 (September). Vertical bars represent standard deviation of replications within each slope. Measured data from Macyk (1999), Hilderman (2011) and Klohn Crippen Berger Ltd. (2013). The pink dash lines indicate the top of overburden layer in each cover.

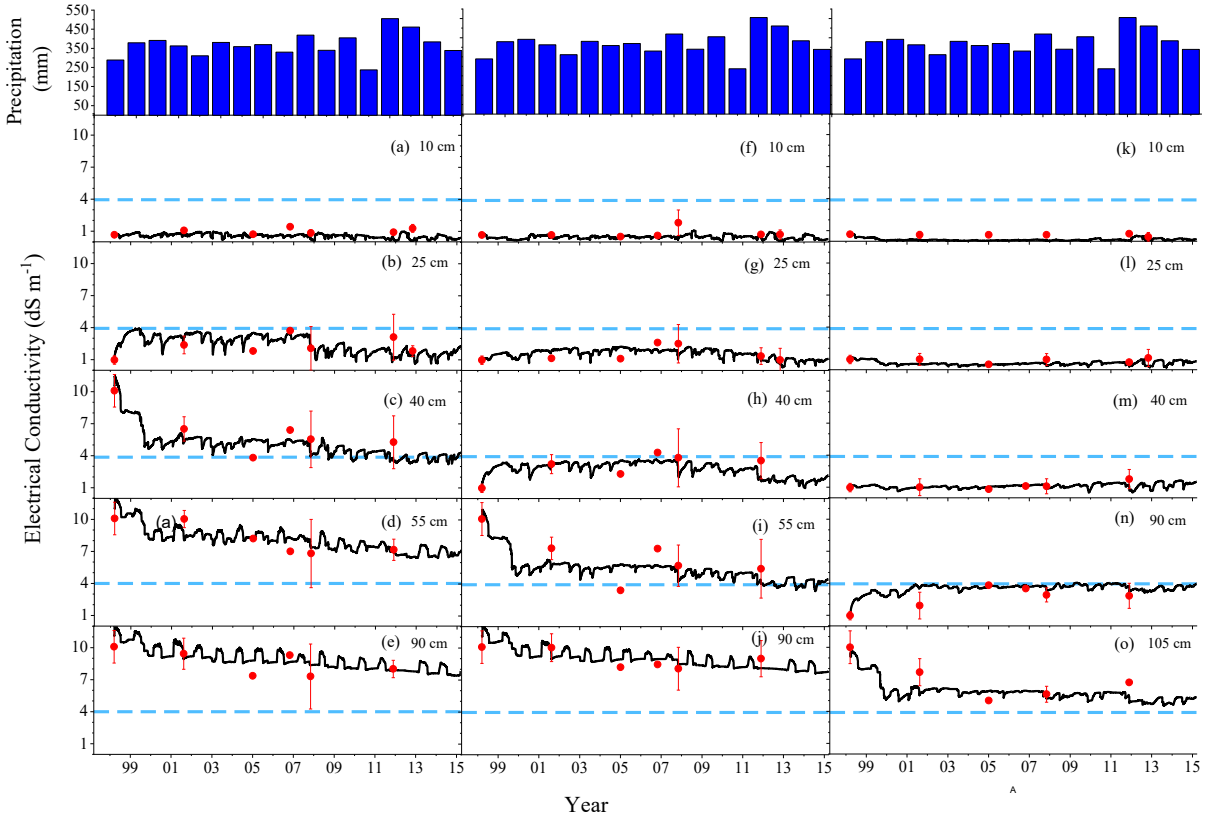

Figure 3.2. Measured annual precipitation (blue bars) and daily modelled (black solid line) and measured (red dots) electrical conductivity at 10 cm, 20 cm, 40 cm, 55 cm, 90 cm and 105 cm soil depths at middle slope position in (a - e) 35 cm, (f-j) 50 cm and (k-o) 100 cm covers during the reclamation period. So b, h and n show EC at 10 cm above the overburden, and c, i and o show EC at 5 cm below the overburden in the 35, 50 and 100 cm covers. Vertical bars represent standard deviation of replications within each slope. Measured data from Macyk (1999), Hilderman (2011) and Klohn Crippen Berger Ltd. (2013). The light blue dash lines indicate the threshold EC value (4 dS m^{-1}).

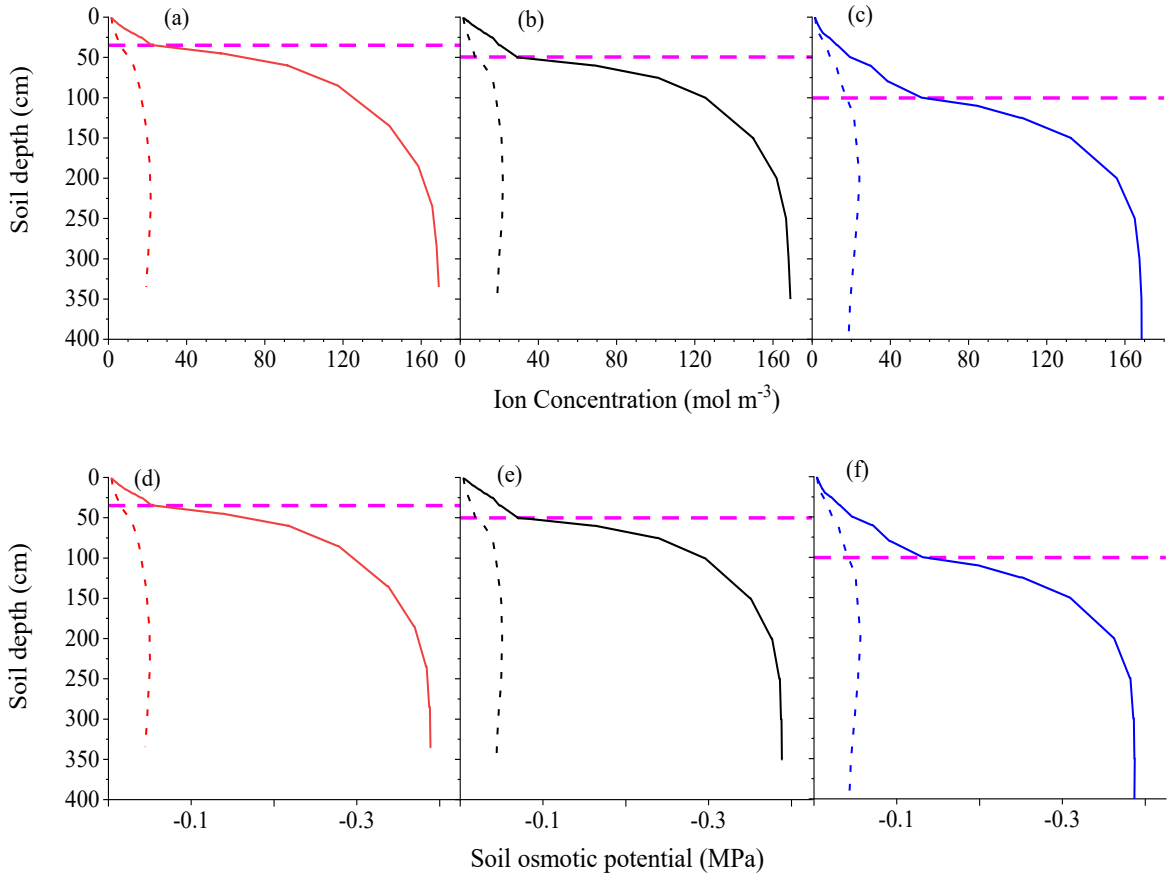

Figure 3.3. Modelled ion concentrations (a-c) and soil osmotic potential (d-f) in 35 cm (red), 50 cm (black), and 100 cm (blue) covers during the drier year 2011 (195-201) with saline sodic overburden and non-saline overburden. The solid lines represent the values modelled with saline sodic overburden and dash lines represent the modelled values with non-saline overburden.

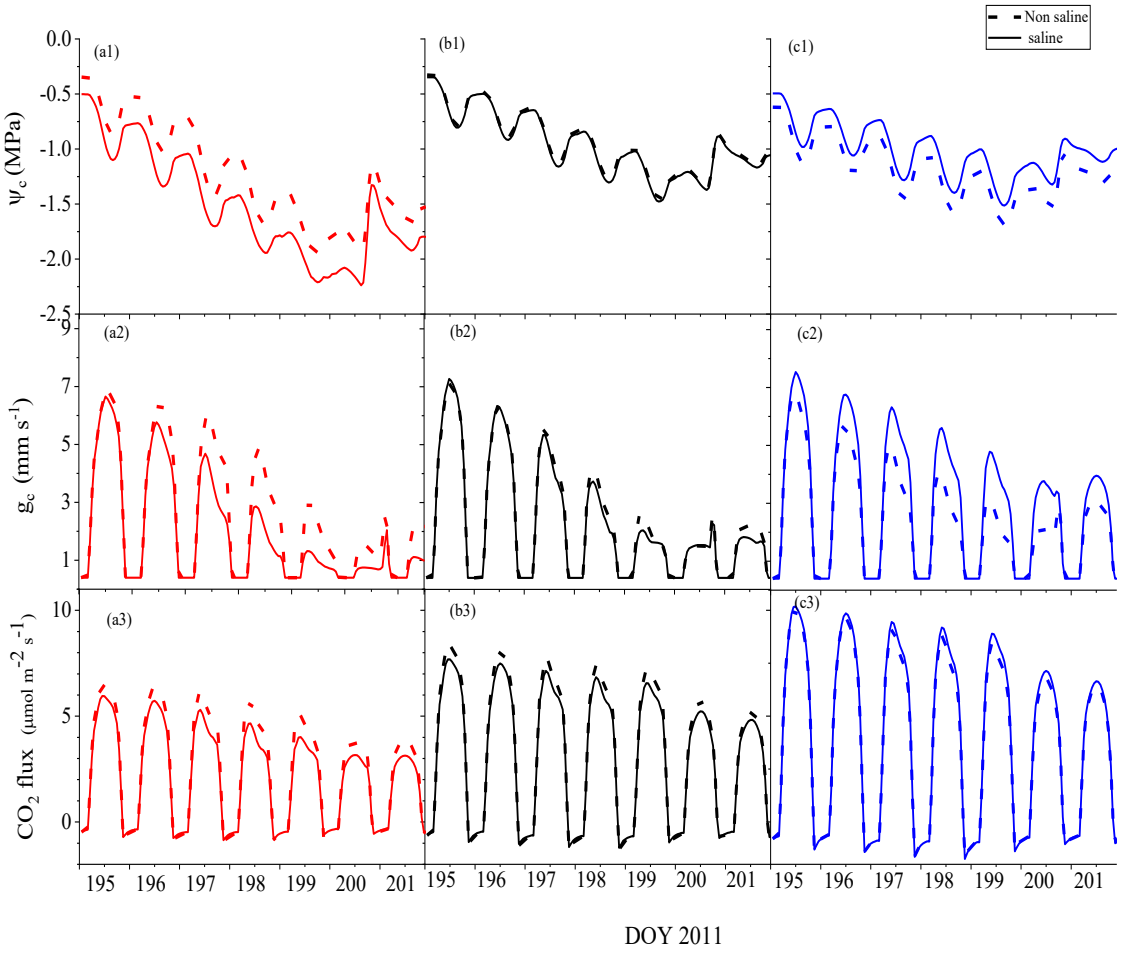

Figure 3.4. Modelled average (a1-c1) canopy water potential, (a2-c2) canopy stomatal resistance and (a3-c3) net canopy CO_2 fixation of aspen along the slopes in 35 cm (red lines) 50 cm (black lines) and 100 cm covers (blue lines) during drier year 2011 (195-201) with saline sodic (solid lines) vs. non-saline sodic (dash lines) overburden.

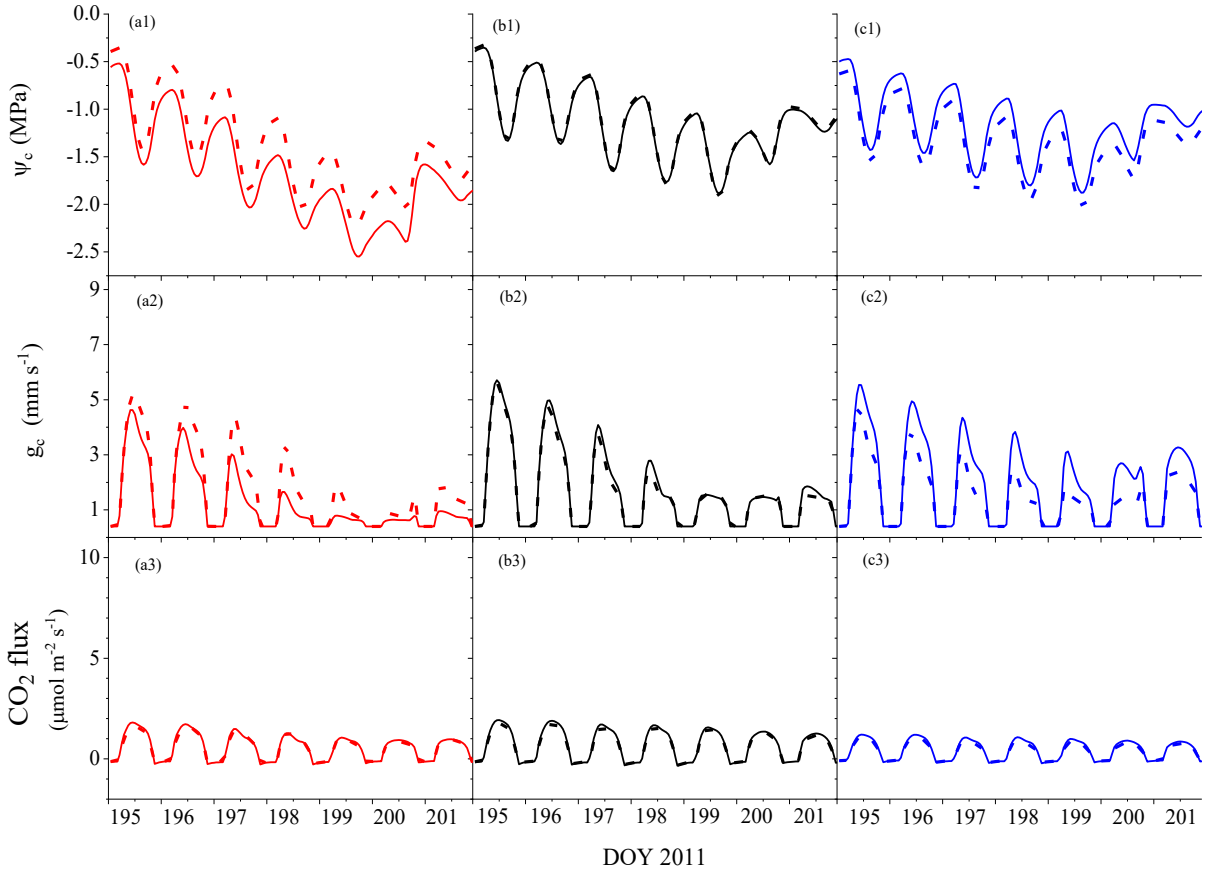

Figure 3.5. Modelled average (a1-c1) canopy water potential, (a2-c2) canopy stomatal resistance and (a3-c3) net canopy CO_2 fixation of white spruce along the slopes in 35 cm (red lines) 50 cm (black lines) and 100 cm covers (blue lines) during drier year 2011 (195-201) with saline sodic (solid lines) vs. non-saline sodic (dash lines) overburden.

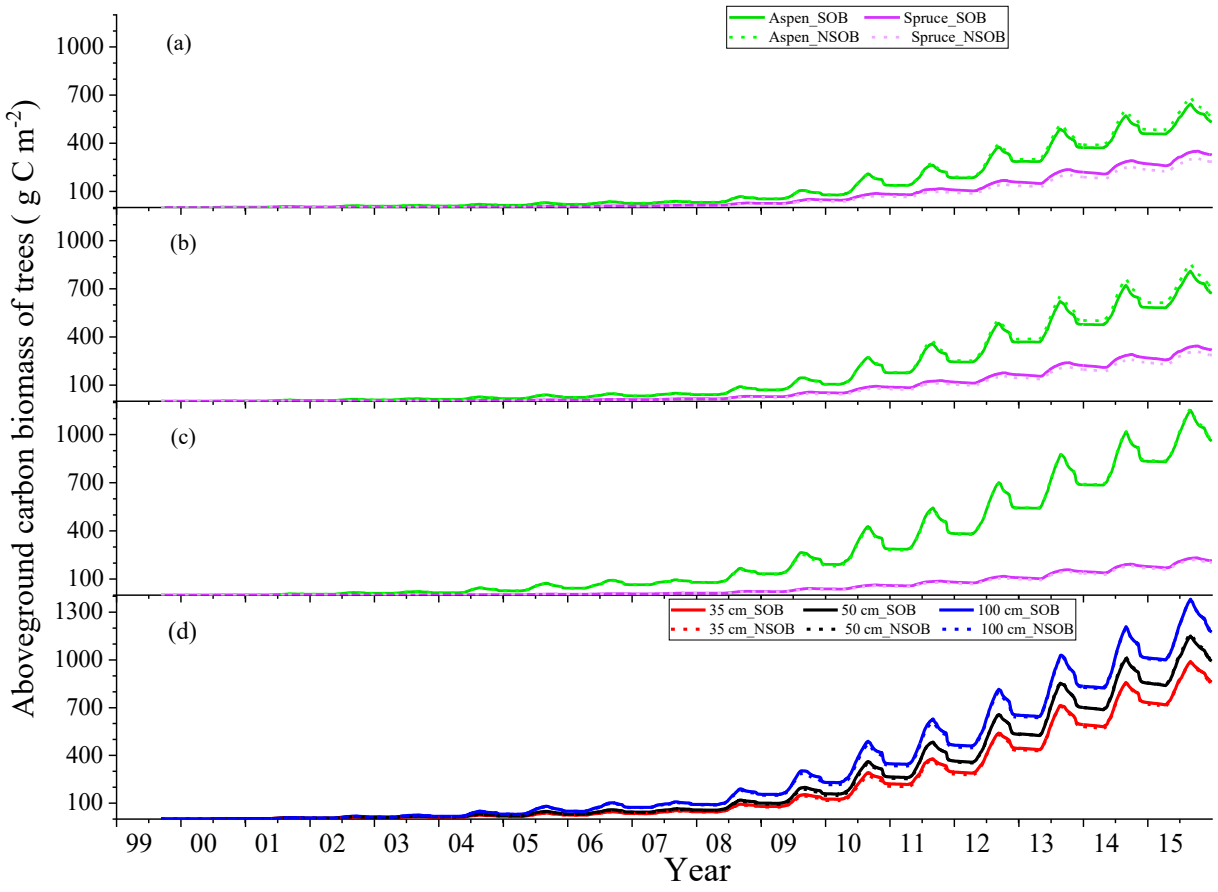

Figure 3.6. Modelled aspen and white spruce aboveground carbon biomass along the slopes in (a) 35 cm cover (b) 50 cm cover (c) 100 cm covers, and (d) total modelled planted tree carbon biomass in 35 cm (red), 50 cm (black) and 100 cm (blue) reclamation covers since site construction. Solid lines represent the carbon biomasses with saline sodic overburden and dash lines represent the carbon biomasses with non- saline sodic overburden.

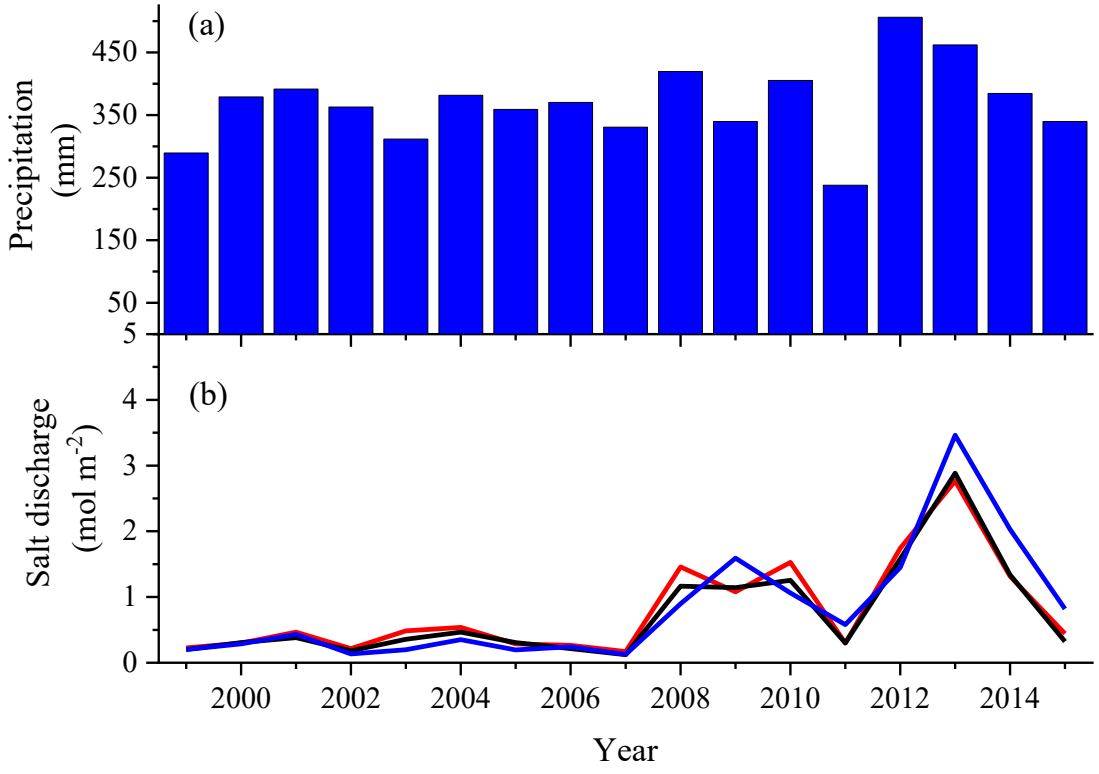

Figure 3.7. (a) annual measured precipitation and (b) modelled salt discharge from 35 cm (red), 50 cm (black) and 100 cm (blue) reclamation covers to downslope watershed since site construction.

Chapter 4

Modelling nitrogen mineralization and plant nitrogen uptake as affected by soil cover depth in reclaimed upland forestlands of Northern Alberta

4.1. Introduction

Nutrient availability particularly nitrogen (N) greatly influences aboveground and belowground productivity and carbon sequestration in terrestrial ecosystems (Nadelhoffer et al., 1985; De Vries et al., 2009). Also N is considered as the most important nutrient often limiting aboveground productivity in boreal forests (Mahendrappa and Salonius 1982; Van Cleve et al. 1983; Kaye and Hart 1997). Therefore, understanding N availability and uptake is important to determine plant growth and thereby early forest development in boreal forest ecosystems after any land disturbances.

Re-establishing equivalent land capability after open-pit mining considerably depends on nutrient availability in capping materials, considering that mining by-products used in reclamation have lower nutrient content particularly N and lower microbial activity than does native soil (Fung and Macyk, 2000; Sobek et al., 2000; Naeth et al., 2013; Macdonald et al., 2015). Upland forest floor (LFH) and peat mineral mix (PMM), which is a mix of peat and a portion of underlying mineral below the peat, are mainly used as the capping materials in reclaimed areas (Rowland et al., 2009; Alberta Environment and Water, 2012). However, PMM has been used as the main nutrient source in most reclaimed areas due to its abundance since a large proportion of the mining footprint consists with bogs and fens (Fung and Macyk, 2000; Rowland et al., 2009; Hemstock et al., 2010; Pinno and Hawkes, 2015). In reclaimed areas particularly where PMM is used as the main amendment, available N for plant uptake is low due to slow decomposition and mineralization because of low microbial activities and large C:N ratio

(McMillan et al., 2007; Hemstock et al., 2010; Duan et al., 2015). Therefore a thin PMM layer itself may not be able to provide an adequate amount of available N to support early plant growth. Duan and Chang (2015) and Duan et al. (2015) stated the importance of sufficient cover depth above tailings sand or overburden substrate to enhance soil nutrient availability in reclaimed areas while speeding up nutrient cycles.

Monitoring and understanding short term and long-term changes in N mineralization, N transport, N uptake and its effect on plant growth in different reclaimed covers are important to evaluate N limitation for early forest regeneration in reclaimed landscapes. Field and greenhouse experiments can be conducted to understand short term changes in N availability and its effect on productivity. However these experiments are expensive, destructive, time consuming and findings are often discontinuous and site-specific (Gower et al., 2001; Randerson et al., 2002; Huang et al., 2013) and so have low prediction capacity with different reclamation materials, site characteristics and weather. However, a rigorous modeling effort based on fundamental processes governing water, energy, salt and nutrient interactions throughout the soil-microbe-root-canopy-atmosphere system can provide both short and long-term forecasts of land capability restoration to the reclamation community. If ecosystem models can accurately simulate N mineralization, N transport and uptake in reclaimed soils as affected by composition and depth of cover material, they could be used to predict the suitable cover material depth required to reduce nutrient limitation during reclamation with different cover material.

Plant N uptake in reclaimed covers is determined by $[NH_4^+]$ and $[NO_3^-]$ in the soil solution maintained by decomposition and mineralization of soil organic matter, and by movement of N from soil solution to the root system through active uptake by roots. Root system characteristics including density, surface area, length and N uptake kinetics, as well as soil moisture content (θ)

and plant growth determine active nutrient uptake by the plant (Anghinoni and Barber, 1980; Grant and Robertson, 1997; Grant, 2013). Shallow covers have lower organic matter content and shallower root systems than do thicker covers (Section 2.3.2 in Chapter 2). This reduces decomposition and net N mineralization through the cover and thereby N availability and plant N uptake. Lower N uptake reduces leaf N content in plants causing declines in CO_2 fixation and gross primary productivity (GPP).

All of these processes are explicitly modelled in the comprehensive terrestrial ecosystem model *ecosys* (Grant (2001, 2014); Grant et al., 2012; Grant, 2013). The ability of *ecosys* to capture the effects of soil N status on N transformations, uptake and thereby plant productivity has been rigorously tested against soil and plant N stocks measured over a wide range of climate and site conditions: e.g. simulation of N dynamics, N uptake and its effect on GPP in agricultural (Grant et al., 1993; Grant, 1995, 1998), forest (Grant et al., 2010) and peatland (Mezbahuddin et al., 2017) ecosystems; effect of elevated atmospheric CO_2 and soil warming on N mineralization and cycling and thereby on forest productivity (Grant, 2013, 2014) and warming effects on N cycling and shrub expansion in Arctic tundra (Mekonnen et al., 2018b).

Even though several laboratory, greenhouse and field studies have addressed N availability in reclaimed sites in the Athabasca Oil Sands Region (McMillan et al., 2007; Hemstock et al., 2010; MacKenzie and Quideau (2010, 2012); Duan and Chang, 2015; Duan et al., 2015), no study has been conducted to determine the effect of cover depth on N availability, plant N uptake and thereby plant growth in upland reclaimed sites. These previous studies were mainly focused on the N availability and mineralization of different reclamation materials; i.e., Forest floor – mineral mix (FFM) and PMM and effect of fertilizer applications. They found that PMM has slower mineralization and thereby lower available N than does FFM, and N fertilization can be

used to improve plant growth particularly of white spruce in reclaimed areas constructed over overburden materials.

To date *ecosys* has not been used to study nutrient availability and uptake processes in novel ecosystems undergoing reclamation. Therefore, in the current study *ecosys* was used (1) to understand and quantify the relationship between total soil N (TN), soil N mineralization and tree N uptake as determined by cover depths, (2) to understand and quantify the relationship between tree N uptake and NPP, and (3) to understand the effect of NPP on N in litterfall and thereby N cycling. An opportunity to test modelled effects of soil cover depth on profile net N mineralization, N uptake and NPP was offered by a research project with three different reclamation covers on a large saline sodic overburden dump referred as South Bison Hills (SBH) at the Syncrude Canada Ltd. Mildred Lake mine site in northern Alberta (Canada).

4.2. Methods

4.2.1. General model description

Ecosys is a comprehensive mathematical model that has the ability to represent multiple soil and canopy layers in soil-microbe-canopy–atmosphere systems at three-dimensional scales. The model simulates physical, chemical and biological processes in natural and disturbed terrestrial ecosystems through the acquisition, transformation and transfer of radiation, water, carbon, oxygen, nitrogen and phosphorous (Grant, 2001) using site-independent algorithms (Mezbahuddin et al., 2014), to achieve realistic landscape-scale predictions of productivity under a wide range of site conditions. The key parameters and algorithms used in *ecosys* were described in Grant (2001; 2014) and Grant et al. (2012) and remain unchanged from those used in earlier studies cited above. The major algorithms that govern the nutrient availability and

transformations, nutrient uptake and translocation, and their effects on NPP in *ecosys* are given below with reference to supporting equations given in appendices A to H in the Supplement.

4.2.1.1. Decomposition and nutrient mineralization as affected by cover depth

In *ecosys*, decomposition occurs concurrently in five organic matter-microbe complexes (coarse woody litter, leaf and fine non-woody litter, animal manure (if present), particulate organic matter (POM), and humus). The woody and non-woody plant litter and animal manure originate from outside the soil profile and POM and humus derive from products of litter decomposition (POM from lignin and associated products) and microbial decomposition (humus). Microbial growth from litter and manure decomposition primes that from POM and humus decomposition. Each complex comprises C, N and P in five organic states: solid organic; dissolved organic (DOC, DON and DOP); sorbed organic, microbial biomass and microbial residue (Grant, 2001, 2013). Microbial biomass is an active agent of transformation in *ecosys*, and the rate of decomposition of each component in each substrate is a first-order function of the decomposer biomass (M_h) of heterotrophic microbial functional types (MFT) including obligate aerobes (bacteria and fungi), facultative anaerobes (denitrifiers), obligate anaerobes (fermenters), heterotrophic (acetotrophic) and autotrophic (hydrogenotrophic) methanogens, and aerobic and anaerobic heterotrophic diazotrophs (non-symbiotic N_2 fixers) [A1, A2] (Grant, 2001, 2013). The rate of decomposition also depends on the substrate concentration [A3, A5], soil temperature (T_s) (Arrhenius function) [A6] and θ [A4] (Grant et al., 2007a; Grant, 2014). The rate of decomposition determines the transfer of substrate C, N and P into DOC, DON and DOP (Grant, 2014). The N and P concentrations in each complex are derived from those in the originating litterfall, and control the release of N and P through decomposition. Greater soil volume above the overburden will provide greater organic matter substrate and available soil water holding

capacity (AWHC) in thicker covers *vs.* shallower covers, causing greater decomposition and mineralization.

The C, N and P availability in the soil is governed by the MFTs. All MFTs maintain as much as possible a set minimum ratio of C:N and C:P during decomposition through mineralization (equation (1a)) or immobilization of NH_4^+ (equation (1b)), immobilization of NO_3^- [A26c], and mineralization or immobilization of $H_2PO_4^-$ [A26d,e], thereby controlling $[NH_4^+]$, $[NO_3^-]$ and $[H_2PO_4^-]$ in soil solution of different covers.

$$U_{NH4i,n,j,l} = (M_{i,n,j,l,C}\, C_{Nj} - M_{i,n,j,l,N}) \qquad U_{NH_4} < 0 \qquad \text{(Mineralization)} \qquad (1a)$$

$$U_{NH4i,n,j,l} = \min \{(M_{i,n,j,l,C}\, C_{Nj} - M_{i,n,j,l,N}), \qquad U_{NH_4} > 0 \qquad \text{(Immobilization)}$$

$$U'_{NH_4}\, a_{i,n,j,l}\, ([NH_4^+{}_{i,n,j,l}] - [NH_4^+{}_{mn}]) / ([NH_4^+{}_{i,n,j,l}] - [NH_4^+{}_{mn}] + K_{NH4})\} \qquad (1b)$$

where: subscripts i = substrate-microbe complex, n = MFT, j = kinetic component, l = soil or litter layer; U_{NH_4} = NH_4^+ uptake (+ve) or release (-ve) by microbes (g N m^{-2} h^{-1}), $M_{i,n,j,l,C}$ = microbial C (g C m^{-2}), $M_{i,n,j,l,N}$ = microbial N (g N m^{-2}), $C_{N,j}$ = maximum ratio of $M_{i,n,j,N}$ to $M_{i,n,j,C}$ maintained by $M_{i,n,j,C}$ (= 0.22 and 0.13 for j = labile and resistant components respectively), U'_{NH_4} = maximum U_{NH_4} at 25 ºC and non-limiting NH_4^+ (g N m^{-2} h^{-1}) (= 5.0 x 10^{-3}), a = microbial surface area (m^2 m^{-2}), $[NH_4^+{}_{i,n,j,l}]$ = concentration of NH_4^+ at microbial surfaces (g N m^{-3}), $[NH_4^+{}_{mn}]$ = concentration of NH_4^+ at microbial surfaces below which U_{NH_4} = 0 (g N m^{-3}) (= 0.0125), K_{NH_4} = M-M constant for NH_4^+uptake at microbial surfaces (g N m^{-3}) (= 0.4) (Grant et al., 1993a,b; 2010).

DOC, DON and DOP are also adsorbed or desorbed according to the soluble concentrations [A8 - A10]. The lower DOC, DON and DOP content from lower decomposition

and mineralization rates per unit area in shallow covers cause lower NH_4^+, NO_3^- and $H_2PO_4^-$ contents in the soil solution.

4.2.1.2. Nitrogen uptake as affected by cover depth

Decomposition and microbial turnover rates in different reclamation covers control the $[NH_4^+]$, $[NO_3^-]$ and $[H_2PO_4^-]$ in the soil solution. The NH_4^+, NO_3^- and $H_2PO_4^-$ ion concentrations (g m^{-3}) could be similar among different cover depths, but the content (g m^{-2}) will vary with the volume of the soil in which these concentrations occur. These ion contents are also controlled by N and P uptake by roots and mycorrhizae from mass flow and diffusion coupled with active uptake (equation (2)) (Grant, 1998), and by microbes through mineralization/immobilization (equation (1b)).

$$U_{Xi,r,l} = \{U_{wi,r,l}[X_l] + 2\pi L_{i,r,l} D_{exl} ([X_l] - [X_{i,r,l}]) / \ln(d_{i,r,l} / r_{ri,r,l})\}$$

$$= U'_X (U_{O2i,r,l} / U'_{O2i,r,l}) A_{i,r,l} ([X_{i,r,l}] - [X_{mn}])/([X_{i,r,l}] - [X_{mn}] + K_X) f_{tl} f_{iXi,r,l} \quad (2)$$

where: subscripts i= plant functional type (PFT), l = soil layer, r = root or mycorrhizae; $U_{Xi,r,l}$ = nutrient uptake by roots or mycorrhizae (g m^{-2} h^{-1}), $U_{wi,r,l}$ = root water uptake (m^3 m^{-2} h^{-1}), $[X_l]$ = nutrient concentration (g m^{-3}) in soil, L = root length (m m^{-2}), D_{eXl} = effective dispersivity-diffusivity of X during root uptake (m^2 h^{-1}), $[X_{i,r,l}]$ = concentration of X at root or mycorrhizal surfaces (g m^{-3}), $d_{i,r,l}$ = half distance between adjacent roots assumed equal to uptake path length (m), U'_X = maximum U_X at 25 ºC and non-limiting X (g m^{-2} h^{-1}) (=5.0 x 10^{-3}) [Barber and Silberbush, 1984], $U_{O2i,r,l}$ = O_2 uptake by roots and mycorrhizae under ambient O_2 (g O m^{-2} h^{-1}), $U'_{O2i,l,r}$ = O_2 uptake by roots and mycorrhizae under non limiting O_2 (g O m^{-2} h^{-1}), A = root or mycorrhizal surface area (m^2 m^{-2}), $[X_{mn}]$ = concentration of X at root or mycorrhizal surfaces

below which U_X = 0 (g m^{-3}) (= 0.0125), K_X = M-M constant for X uptake at root or mycorrhizal surfaces (g m^{-3}) (= 0.4), f_{ti} = temperature effect, $f_{iX\boldsymbol{i,r,}}$= product inhibition on root X uptake.

The modelled root system governs U_X through the effects of root length density on diffusion path lengths ($d_{i,r,l}$) and surface area ($A_{i,r,l}$) in equation (2). In *ecosys*, the root system is represented by vertical primary axes, and horizontal secondary axes emerged from primary axes in each rooted soil layer of each PFT (Grant, 1993). Root growth is modelled from the assimilation of non-structural C (σ_C) which is the product of canopy CO_2 fixation [C20b, C21b] transferred to roots along concentration gradients, coupled with assimilation of the non-structural N (σ_N) and P (σ_P) which are the products of root and mycorrhizal N and P uptake into primary and secondary axes (equation 2) according to root growth yields. Root length extension is driven by root mass growth [C21b,c].

Root growth and hence assimilation is controlled by root water potential which determines root turgor, by soil resistance (Da Silva and Kay, 1997) which determines root penetration (Grant, 1998), and by root nutrient status represented by σ_C:σ_N:σ_P ratios. The decline of root densities with increased soil depth is modelled from declining sink strength for non-structural C transfers with increasing distance from canopy sources. Root growth is also controlled by O_2 uptake driven by aqueous concentration of O_2 in the soil [C14] and by nutrient uptake which raises σ_N or σ_P. Soil O_2 concentration is maintained by vertical transport that largely depends on air-filled porosity [D17a,b,c] and so declines with increasing soil depth and soil bulk density (Grant, 1998). Therefore root growth is restricted in soil by larger bulk density, soil and root hydraulic resistances (Ω_s and Ω_r respectively), by smaller O_2 concentration and lower [NH_4^+] and [NO_3^-] and thereby less U_x and σ_N. Total root growth increases with cover depth. Thus

greater plant N uptake in thicker *vs.* shallow covers is facilitated by the deeper root system with greater root length and surface area.

4.2.1.3. Gross primary productivity as affected by N uptake

In *ecosys*, amounts of σ_C, σ_N and σ_P in each organ are governed by translocation along branch-root-mycorrhizal concentration gradients [C50 - C53] created by σ_C which is the product of branch CO_2 fixation [C1, C12], and of σ_N and σ_P from root and mycorrhizal uptake *vs.* consumption of σ_C, σ_N and σ_P from growth respiration and organ growth [C20] (Grant, 1998). Nutrient concentrations and turgor potentials control the production and consumption of σ_C, σ_N and σ_P in different plant organs and so control concentration gradients and hence translocation in different organs. Lower amounts of soil N and P and shallower root systems in shallow covers will reduce root N and P uptake and thereby reduce root σ_N and σ_P stocks. The lower root σ_N and σ_P reduce the root–branch concentration gradient and hence reduce the translocation of these stocks to the shoots [C50, C51]. This lower amount of σ_N and σ_P in shoots reduces foliar σ_N:σ_C and σ_P:σ_C ratios [C11] which have two effects on GPP:

(1) They reduce activities of rubisco [C6a] and chlorophyll [C7a] through product inhibition [C11], thereby simulating the suppression of CO_2 fixation by leaf σ_C accumulation.

(2) They reduce the structural N:C and P:C ratios at which leaves are formed because σ_C, σ_N and σ_P are the substrates for leaf growth. Lower structural ratios cause a proportional reduction in areal concentrations of rubisco [C6b] and chlorophyll [C7b], reducing leaf CO_2 fixation.

Lower GPP and thereby net primary productivity (NPP = GPP – autotrophic respiration (R_a)) are thus obtained with lower N uptake with shallower covers. In *ecosys*, growth of

internodes, petioles and leaves is driven by R_a which is driven by σ_C from canopy carboxylation rates according to organ growth yield as well as by σ_N and σ_P from root uptake. Leaf area expansion of different PFTs, controlled by leaf mass growth, leaf area:mass ratio and canopy turgor potential (ψ_t) [C21a], will also decline with shallower covers.

In contrast, greater N uptake in thicker covers increases the foliar N concentration and thereby foliar production and leaf area. This increases the areal concentration of rubisco and chlorophyll driving CO_2 fixation. Greater σ_C production through CO_2 fixation drives increases in root growth, N uptake and thereby NPP and leaf area in thicker covers.

4.2.1.4. Autotrophic respiration and litterfall

In *ecosys*, R_a in each tree branch and root axis is derived from two components:

(1) First-order respiration of σ_C [R_c in C14] which is first used for maintenance respiration (R_m). The excess (R_c-R_m) is used for growth respiration (R_g) which drives organ growth [C20] according to organ water [C17] and nutrient status.

(2) Respiration of remobilizable C (R_s) in leaves and supporting structures to meet R_m when it exceeds R_c [C15].

Environmental constraints such as water, heat and nutrient stress lower σ_C and hence R_c [C14] with respect to R_m [C16] and so increase R_s [C15], hastening litterfall of associated non-remobilizable C [C18]. R_s also drives the withdrawal of remobilizable N and P from leaves and supporting structures into σ_N and σ_P pool and litterfall of associated non-remobilizable N and P. Thus in *ecosys,* R_s determines the loss of non-remobilizable C, N and P (mostly structural) as litterfall from leaves and twigs or roots and mycorrhizae [C18a,b,c], and the internal recycling of

remobilizable C, N and P (mostly nonstructural protein) into nonstructural pools $\sigma_{C,}$ σ_N and σ_P, depending on ratios of σ_N:σ_C or σ_P:σ_C [C19a,b,c] (Grant et al., 2007c; Grant, 2013).

Smaller plant biomass in shallow *vs.* thicker covers reduce the quantity and quality [C19b] of litterfall and forest floor development due to lower foliar production and lower σ_N:σ_C or σ_P:σ_C ratios particularly for aspen. Thus, shallow covers will experience slower decomposition due to decreased leaf and fine non-woody litter and so reduce long term N cycling.

4.2.2. Site description

4.2.2.1. Reclaimed site

The effect of reclamation cover depth on N mineralization and N uptake was evaluated at the SBH watershed located in lease no. 17 within the Syncrude Canada Ltd. Mildred Lake operation, Alberta, Canada. The mean annual temperature and precipitation (1981 - 2010) of the SBH area are 1.0 °C and 418.6 mm respectively (Environment Canada, 2014) and the climate is classified as sub-humid continental (Koppen Classification) with short summers and long cold winters (Kelln et al., 2007). The SBH watershed was constructed in 1996 using ~100 x 10^6 m^3 of saline - sodic overburden with overlying soil covers and extends over a 2 km^2 area with a plateau (Huang et al., 2015b). The slope of the overburden dump was designed with a 1:5 (20%) incline (Boese, 2003). Three adjacent covers with soil depths of 35 cm, 50 cm and 100 cm constructed along the north facing slope of SBH were used as the experimental sites for the study. Each cover was approximately 200 m in length and 50 m in width (approximately 1 ha) and consisted of peat mineral mix (PMM) and subsoil materials (glacial till deposits) which overlaid saline sodic overburden as in Figure 2.1 (a). In the spring of 1999, barley was seeded with a density of 25 kg ha^{-1} in each plot to reduce erosion and to stabilize the slope. Fertilizer was applied prior to tree planting at the rate of 35 kg N ha^{-1}, 46 kg P ha^{-1}, 44 kg K ha^{-1} and 14 kg S ha^{-1} (Lanoue,

2003; Garrah et al., 2013). In fall 1999, white spruce (*Picea glauca* (Moench) Voss) and trembling aspen (*Populus tremuloides* Michx.) seedlings were planted in alternate rows (Hilderman, 2011) in each cover with a total density of 1,600 stems ha^{-1} (50:50 mix of aspen and white spruce) to achieve a mixed-wood boreal forest. Further details of site description and reclamation methods can be found in Sections 2.2.2.1 and 2.2.2.2.

The target ecosystem of the SBH reclaimed site is the "d" ecosite upland forest (Elshorbagy and Barbour, 2007) characterized by lower moisture or nutrient limitation on plant growth (medium nutrient regime), which includes organic carbon 35 - 70 Mg ha^{-1}, total nitrogen 1.5 - 5 Mg ha^{-1} (natural sites) or 3 - 5 Mg ha^{-1} (reclaimed sites) and C:N ratio 15-30 (CEMA, 2006; Alberta Environment, 2010).

4.2.2.2. Natural forest site

Plant and soil N stocks from reclamation covers were compared with those in a natural landscape approximately 14 km north (57°7'11.69"N, 111°36'23.90"W) from SBH near the Beaver river on the western side of the Athabasca river. The site was selected using fire, vegetation and ecosite maps and is 4 years younger than the SBH. This site is a typical "*d"* ecosite, containing silty loam to sandy loam soil with an aspen dominant stand (nearly 99%), recovering from fire that had occurred during 2003 (Das Gupta, 2015).

4.2.3. Field data collection for reclaimed site

4.2.3.1. Weather

Solar radiation, maximum and minimum air temperatures, precipitation (*P)*, wind speed, and relative humidity were recorded daily from January 1, 1999 to December 31, 2015. All the other measurements were taken from the SBH weather station on the middle slope of the 35 cm

cover, except for winter *P* and solar radiation. There was uncertainty in the accuracy of the *P* data in some data collection years, hence the winter *P* (from 1st October to 31st March every year) and solar radiation until 2006 (from 1st January to 31st December every year) were taken from the Fort McMurray airport weather station (approximately 40 km south from the study sites) and winter *P* and solar radiation from 2007 were taken from the Mildred Lake airport weather station (built in 2007), located approximately 6 km northeast of the site. These daily data were read into *ecosys* where they were resolved into hourly values to match the hourly time step at which the model functions.

4.2.3.2. Hydrology

The SBH is an instrumented watershed, and the details of the installation of all the instruments were described in Boese (2003). Both the θ and soil matric potential (ψ_m) were measured using time domain reflectometry (TDR) probes and CS 229 sensors respectively at the middle slope position of each cover along the cover profile up to an upper section of the overburden from 1999 to 2015. These θ and ψ_m data were downloaded from the proprietary Syncrude watershed database and were used to derive soil water content at permanent wilting point (θ_{PWP}) and field capacity (θ_{FC}) from which soil water contents were modelled that determined the effects of soil moisture on decomposition and nutrient uptake. Further details of hydrology measurements in reclaimed sites can be found in Sections 2.2.3.2.

4.2.3.3. Aboveground biomass

Aboveground carbon biomasses were estimated by Macyk et al. (2009) and Drozdowksi et al. (2011, 2014) for planted aspen and white spruce trees in 35 cm, 50 cm and 100 cm covers. The height and stem diameters at root collar and 1.3 m height of planted trees were collected

annually (2007 - 2013) in 10 m x 10 m permanent sampling plots which were established in upper, middle and lower slope positions of all the reclamation covers in 2007 (Macyk et al., 2009; Drozdowksi et al., 2011, 2014). The aboveground carbon biomass values for each species were estimated using allometric equations relating to measured breast height and basal tree diameters in the sampling plots and species specific density and expansion factors for branch and leaf/needles developed for Alberta species (Alberta Environment, 2007). These data were used to validate modelled aboveground carbon biomass and thereby to understand the effect of cover depth on NPP.

4.2.3.4. Leaf Area Index (LAI)

Total site LAIs were measured in August 2015 at upper and lower positions in the 35 cm and 100 cm covers using a LAI-2200C plant canopy analyzer (LI-COR Inc., Lincoln, Nebraska, USA). These LAIs were used to test the modelled LAIs in each cover and thereby to determine the effect of cover depth on N uptake, foliar production and thereby NPP.

4.2.3.5. Soil nutrient measurements

The reclamation covers were sampled in July 2013, when pits were dug up to 30 cm in top, middle and bottom slope positions of each reclamation cover. Soil cores were used to take soil samples at 7.5 cm intervals in 35 cm cover and 10 cm intervals in 50 cm and 100 cm covers for each pit, and subsamples were taken to increase the accuracy of measured values. The collected samples were shipped and stored in a freezer at -4 ^{0}C, then thawed and analysed to determine total C, TN, NO_3^- and NH_4^+. The mineral N ($NH_4^+$and NO_3^-) was extracted using 2M KCL extracts of moist soil and was analyzed colorimetrically on a SmartChem Discrete Wet Chemistry Analyser (Westco Scientific Instruments, USA). Subsoil samples dried to a consistent weight and ground using Ball Mill MM200 (Brinkmann Retsch) were used to determine total C

and N using dry combustion analysis (Nelson and Sommers, 1996) on an elemental analyzer (Costech Model 4010, Florence, Italy). The average values were used to determine the effect of cover depth on soil nutrient contents.

4.2.3.6. Foliar nutrient measurements

In July 2012, 2013 and 2015, spruce, aspen and understory plant samples were collected to determine foliar chemistry. For aspen and spruce, three healthy trees at upper, mid and bottom slope positions in each reclamation cover were selected and healthy new leaves were sampled for each sampling site with three sub samples. For the understory, a quadrant was used to collect samples for each sampling site with three replicates. In 2015, surface litter depths developed on PMM were measured and surface litter samples were collected at each slope position in each cover with three replicates. All of these samples were placed in paper bags, and shipped to the laboratory. Then they were dried to a consistent weight at 65^0C and grounded using Ball Mill MM200 (Brinkmann Retsch). Foliar and litterfall total carbon and nitrogen were measured using dry combustion method on an elemental analyzer (Costech Model 4010, Florence, Italy). These values were used to validate the modelled foliar and surface litter N concentrations and thereby to understand the effect of cover depth on N deficiency in soil and tree PFTs.

4.2.4. Field data collection in natural forest site

4.2.4.1. Soil nutrient measurements

In August 2012, samples were collected randomly from forest floor and mineral soil around the site using a bulk density core. These collected samples were shipped to the laboratory and stored at 4 ^{0}C until laboratory analysis. A full description of sampling locations and methodology can be found in Das Gupta (2015). In August 2014, six sampling points were

selected randomly around the same site and soil pits were made up to 1 m. Soil samples were taken using soil cores at every 10 cm interval along the wall of the soil pits. Collected samples were shipped and stored at 4 ^{0}C until laboratory analysis. Soil nutrients (total C, TN, NO_3^- and NH_4^+) in the samples collected in both years were analysed using the same procedure as described in Section 4.2.2.2.5.

4.2.4.2. Foliar nutrient measurement

In August 2012 and 2014, aspen leaves were collected at each sampling point with three replicates for foliar nutrient analysis. These samples were collected and analysed using the same protocols as those at the SBH site as described in Section 4.2.2.2.6.

4.2.5. Model experiment: South Bison Hill reclamation site as represented in ecosys model runs

4.2.5.1. Landscape:

The information for site management and soil properties collected during 1999 and 2000, were used to construct the input files used to initialize *ecosys* for SBH. These inputs represent the actual field characteristics including site, weather, and plant and soil management data used by *ecosys* to simulate site conditions during the experiment. Each reclamation cover was represented in the model as a transect of six interconnected grid cells each of which had a dimension of 50 m x 40 m. Five grid cells represented the slopes as shown in Figure 2.1 (b) and one grid cell represented the level area above the slope corresponding to the landscape at SBH. All the input data (site, weather, soil properties, soil and plant management) were the same among reclamation covers except cover depths as described in Section 2.2.2.1.

4.2.5.2. Soil properties

Soil physical and chemical properties were taken from the studies done by Macyk (1999), Meiers (2002) and Yarmuch (2003) and soil biological properties were taken from the study done by Lanoue (2003) in the SBH site. The θ_{FC} and θ_{PWP} respectively for PMM, subsoil and overburden (Table 2.2) were derived from water desorption curves developed using measured θ *vs.* ψ_m data. Although measured TDR values (described in Section 4.2.2.2.2) had indicated slightly different θ_{FC} and θ_{PWP} for PMM, subsoil and overburden among the three covers, average values were used for each material in each reclamation treatment so that modelled differences in soil and plant water status and in plant growth could be attributed to those in capping depth. Saturated hydraulic conductivity values (Table 2.2) reported by Meiers et al. (2011) were used as inputs from which the model calculated unsaturated values (Grant et al., 2004). The key soil nutrients used to simulate nutrient status in PMM, subsoil and overburden are given in Table 4.1. Further details of soil properties used in modelling can be found in Section 2.2.4.2.

4.2.5.3. Land management

At the beginning of simulation runs (1999) the modelled landscapes were initialized with the soil properties described in Section 4.2.3.1 and seeded with barley in spring 1999 as described in Section 4.2.2.1. Aspen and white spruce PFTs and grass and clover PFTs were seeded in each grid cell in summer 1999 at the densities described under the reclamation method in Section 2.2.2.2. In 2007, ingress plants were seeded as described in Section 2.2.2.2. The model was run for 17 years (1999 - 2015) using the daily weather data described in Section 2.2.3.1.

4.2.5.4. Nitrogen inputs used in model runs

Nitrogen fertilizer application was modelled prior to tree planting in the fall of 1999 as described in Section 4.2.2.1.1. Ammonium and nitrate concentrations in precipitation were set to 0.8 mg N L^{-1} and 0.3 mg N L^{-1} respectively to give wet N deposition rates, and atmospheric ammonium concentration was set to 2.03 nmol mol^{-1} to give dry N deposition rates reported in Alberta Environment and Parks (2014). The clover PFT simulated symbiotic N_2 fixation [F12] and heterotrophic diazotroph MFTs simulated non-symbiotic N_2 fixation [A27] during the model runs.

4.2.5.5. Model validation

Model results for θ, water uptake and aboveground carbon biomass were validated with field measured values at different slope positions for the three cover depths as described in Section 2.3. Two-way ANOVA was used to determine if significant differences existed among measured soil and foliar N at different slope positions in reclamation covers and the natural site. Also modelled foliar and surface litter N concentrations in each reclamation cover were compared with field measured values to validate modelled foliar N status over the reclamation period. Statistical analyses were performed using version 9.2 of SAS (SAS Institute Inc., Cary, NC). Modelled annual profile net N mineralization in each cover was taken from annual sums of hourly modelled net N mineralization ($U_{NH4i,n,j,l}$ in Eqn. 1(a)) by all kinetic components j of all MFTs n in all substrate-microbe complexes i, in all soil layers l within the soil profiles.

A non-linear regression model with an asymptotic form was used to quantify the relationship between estimated TN and modelled annual net N mineralization. Linear regression models were used to quantify the relationship between modelled annual net N mineralization and annual tree N uptake, and between modelled annual tree N uptake and modelled NPP of aspen,

white spruce and total tree NPP averaged over transects in different reclamation cover depths. Nitrogen use efficiency was estimated from annual modelled N uptake and modelled NPP of aspen and white spruce (NUE =NPP/N_{uptake}), where NPP and N_{uptake} were in g C m^{-2} y^{-1} and g N m^{-2} y^{-1} respectively.

4.3. Results

4.3.1. Soil C and N contents in different reclamation covers and in natural site

At the beginning of reclamation (1999), model runs were initialized with measured SOC and TN (Table 4.2) so that both SOC and TN content within the soil profile increased directly with increasing depth of PMM and subsoil materials. Modelled SOC and TN in all the covers increased slightly during the next 13 years (1999 - 2012). In the model, C gains were modelled from NPP – (heterotrophic respiration + losses from runoff and subsurface discharge) and N gains were modelled from sum of all N inputs from deposition and fixation less any N losses from runoff, subsurface discharge and gaseous emissions. The measured and modelled soil C:N ratios (*ca.* 27:1) in the reclamation covers (data not shown) were similar ($p > 0.05$) after 13 years from reclamation. The TOC concentration in PMM in each reclamation cover (Table 4.1) was significantly lower ($p < 0.05$) than in the LFH in the regenerating natural site (240 ± 80 g C kg^{-1}) as PMM has less soil organic C than peat and LFH due to its mineral component. However, the TOC content within the soil profile in all the reclamation covers (Table 4.2) was greater than the measured TOC content in natural site (178±19 Mg C ha^{-1}) root zone (100 cm) due to greater thickness (15 or 20 cm) and bulk density (0.9 Mg m^{-3}) of the PMM layers at SBH than of the thickness (*ca.* 7.5 cm) and bulk density (0.2 Mg m^{-3}) of LFH layer in the natural site. Also the TN in each reclamation cover (Table 4.2) was greater than the measured TN within the natural site root zone (5.6 ±1 Mg N ha^{-1}). The mineral N (NH_4^+ + NO_3^-) concentration in reclaimed

covers (<10 μg g^{-1}) was lower than in the natural LFH (30 μg g^{-1}) and did not show a significant difference ($p = 0.1$) among the covers (data not shown).

4.3.2. Modelled profile net N mineralization rates and N uptake in different reclamation covers

Different SOC and TN contents in reclamation covers determined the net N mineralization rates and nutrient availability in the soil profile. Modelled annual profile net N mineralization averaged over slope positions in each cover increased until over-story crown closure in 2010 and declined gradually thereafter (Figure 4.1). In 2003, lower growing season precipitation particularly from May to August (*ca.* 65 mm) reduced the net N mineralization in all the covers.

The greater modelled profile net N mineralization in the 100 cm cover *vs.* the 35 cm and 50 cm covers (Figure 4.1) enabled greater annual N uptake (Table 4.3 and Figure 4.2). In *ecosys*, greater N uptake in the 100 cm cover *vs*. the other two covers was driven by greater mineral N content from more rapid mineralization (Figure 4.1), greater θ and a deeper root system (Figure 2.5) (Eqn. 2). Tree N uptake during early succession of the SBH site (1999 - 2006) was suppressed by the pioneer grass and clover PFTs (Figure 4.2(b)). However, tree N uptake gradually increased relative to that by pioneer PFTs in each cover along the slope positions during exponential tree growth (2006 - 2010) and then declined gradually thereafter (Figure 4.2). Clear reductions of tree N uptake in 35 cm and 50 cm covers *vs.* 100 cm cover were modelled after 2003 (Figure 4.2(e)) due to lower net N mineralization (Figure 4.1), with lower θ (Figure 2.3) from lower AWHC. Greater N uptake was modelled in the upper *vs.* lower slope positions during wet years and less during dry and intermediate years particularly in 35 cm and 50 cm covers (data not shown).

A greater proportion of modelled total tree N uptake in each cover (Figure 4.2(e)) was from the modelled aspen (Figure 4.2(d)) *vs.* white spruce (Figure 4.2(c)). However, greater aspen:spruce N uptake ratio was modelled in 100 cm cover followed by 50 cm and 35 cm covers due to greater aspen:spruce growth ratios with deeper covers as described in Section 2.3.5 and Figure 2.12 in Chapter 2.

4.3.3. Effect of total nitrogen on net N mineralization and N uptake

The net N mineralization rate increased with increasing TN as determined by cover depth during dry (2011) and intermediate years (2014 and 2015), after the sites reached the over-story crown closure (Figure 4.3(a)). However, increases in net N mineralization rates were not proportional to those in TN in Table 4.2 (i.e. net N mineralization declined relative to TN in g N g N^{-1} y^{-1}). The differences of net N mineralization rate between covers were smaller during wet years (2012 and 2013) due to sufficient water supply for microbial growth (Figure 4.3(a)) particularly in 35 cm and 50 cm covers.

The non-linear regression model indicated that annual modelled N uptake increased at a decreasing rate with TN in reclamation covers during dry (R^2 = 1), intermediate (R^2 = 0.5) and wet (R^2 = 0.9) years, and that 90%, 98%, and 85% of maximum N uptake for the site during dry (2011), intermediate (2014 and 2015) and wet (2012 and 2013) years respectively, were achieved with 17 Mg N ha^{-1} of TN (Figure 4.3(b)). Also, the relationship indicated by slope in Figure 4.3(b) was strong during dry and intermediate years but was weak during wet years. Asymptotes gradually declined (Figure 4.3(b)) with the downwards trend in net N mineralization modelled after 2010.

A strong positive linear relationship (slope = 0.9 ±0.1, R^2 = 0.8) was derived between modelled net N mineralization and modelled tree N uptake (Figure 4.3(c)). The reduced uptake

with water stress in dry year (2011) left more mineral N for uptake in wet years (2012 and 2013), as indicated by the greater N uptake (Figure 4.3(b)) *vs.* net N mineralization (Figure 4.3(a)) modelled during 2012 and 2013. Minimal N losses as emissions to the atmosphere and through water discharge to downslope areas (data not shown) modelled in each cover after planted trees reached crown closure indicated that almost all the N mineralized through decomposition was taken up by the trees.

4.3.4. Effect of N uptake on NPP in different reclamation covers

Greater N uptake enhanced plant growth through increased plant σ_N pool as described in Section 4.2.1.3. The lower NPP averaged along the slope positions in the 35 cm and 50 cm covers *vs.* the 100 cm cover during dry and intermediate years (Table 4.3) was caused by greater water limitation (Section 2.4.2.1 in Chapter 2) and salinity (Section 3.3.3 in Chapter 3). However, the effects of water limitation and salinity on NPP in three covers were minimal during the wet years (Table 4.3). The modelled aspen, white spruce and total NPP showed a positive linear relationship with N uptake (Figure 4.4) and hence NPP in reclamation covers increased with increasing cover depth due to greater tree N uptake. Thus reduced NPP during wet years (Table 4.3) was linked to decreased N uptake from 35 cm and 50 cm covers *vs.* 100 cm cover. The NUE of white spruce (91 g C g N^{-1}) was greater than that of the aspen (87 g C g N^{-1}) as indicated by the slopes in Figures 4.4(a,b). However, greater N uptake of aspen *vs.* white spruce increased the aspen NPP in all the reclamation covers (Figure 4.4(b)). The greater NPP modelled in the 100 cm cover (Table 4.3) from increased N uptake raised foliar production (Section 4.2.1.3) from that in the other two covers as indicated by the greater modelled and measured LAI (Table 4.3).

4.3.5. Modelled *vs.* measured N concentrations in foliage and litterfall

Both modelled and measured aspen and white spruce foliar N concentrations at different slope positions (data not shown) in three reclamation covers (Figure 4.5) followed a similar pattern and did not show significant difference among slope positions or covers over the study period ($p = 0.4$). The measured aspen foliar N concentration in natural site was similar ($p = 0.5$) to the values modelled and measured in reclaimed covers (Figure 4.5 (a)). Measured foliar N concentration in ground cover PFTs (clover and grass) were also similar ($p = 0.1$) among different reclamation covers (data not shown).

Greater foliar production contributed to a greater litterfall (Table 4.4) and thereby greater surface litter stock in 100 cm cover *vs.* 35 cm and 50 cm covers (Figure 4.6). Both the modelled (*ca.* 21 mg N g C^{-1}) and measured (*ca.* 23 mg N g C^{-1}) N concentrations of surface litter that developed on PMM were similar ($p > 0.05$) among three reclamation covers (Figure 4.6(a)). However, the modelled surface litter N concentrations were similar to white spruce foliage, but were lower than that of the aspen foliage (Figures 4.5 and 4.6), indicating N remobilization during senescence (Section 4.2.1.4.). In 2015, significantly greater ($p < 0.05$) surface litter depth was measured in the 100 cm (2.28 cm) cover compared to the 35 cm (1.5 cm) and 50 cm (1.7 cm) covers (Figure 4.6(b)). The surface litter depth that derived from modelled surface litter carbon accumulation along the slope positions in each cover was similar to that of the measured values and increased ($p < 0.05$) with the increasing cover depth (Figure 4.6(b)). These greater modelled and measured surface litter depths were driven by greater surface litterfall C (Table 4.4) in the 100 cm cover *vs.* 35 cm and 50 cm covers after sites reached the over-story crown closure. In addition, a greater surface litter depth on PMM was measured in the lower slope position in each cover compared to upper slope position ($p < 0.05$) due to greater plant growth

(data not shown). However, modelled surface litter depth did not show significant differences among the slope positions ($p > 0.05$). The greater modelled aspen: white spruce litter N ratio in the 100 cm cover (10:1) *vs.* 50 cm (5:1) and 35 cm (4:1) covers increased the annual N return to the soil. This increased ratio was caused by the greater aspen LAI modelled in 100 cm cover (Table 4.3) *vs.* other two covers. Also, greater aspen leaf turn over (1 y^{-1}) *vs.* white spruce (*ca.* 0.25 y^{-1}) increased the aspen litterfall in each cover compared to white spruce. This litterfall provides N for subsequent mineralization in reclamation covers as described in Section 4.3.2.

4.4. Discussion

4.4.1. Changes in profile net N mineralization with time after reclamation

The initial modelled and estimated (from field measurements) total SOC and TN contents in all the reclamation covers, and the modelled SOC and TN after 13 years of reclamation (Table 4.2) were much greater than in the regenerating natural site. They were also greater than the target amounts to achieve medium nutrient regime in a 'd' ecosite which includes organic carbon 35 - 70 Mg ha^{-1} and TN 3.0 - 5.0 Mg ha^{-1} (CEMA, 2006; Alberta Environment, 2010), although the reclamation soil profile C:N ratio was at the upper limit of the recommended ratio (15 - 30) in CEMA (2006).

Modelled net N mineralization rates driven by SOC and TN in reclamation covers changed markedly with time since reclamation (Figure 4.1). Lower N mineralization rates modelled during the early reclamation period (Figure 4.1) were attributed to the lower microbial biomass N (data not shown) and lower labile N content in PMM as described by Hemstock et al. (2010) and Kwak et al. (2015). However, C and N cycling rose gradually with continuing C fixation by grass and clover and with continuing N_2 fixation during early reclamation period until 2006. The increase in modelled net N mineralization during 2008 - 2010 was mainly driven by the

decomposition of clover and grass plants from gradual dieback caused by tree crown closure during exponential tree growth after 2006 as indicated by increased tree N uptake and decreased understory N uptake (Figure 4.2). The large N content from symbiotic N_2 fixation in clover primed N mineralization in all the covers during this period. Also greater soil water content with increased precipitation (Figure 4.1(a)) further facilitated N mineralization during this period. The greater net N mineralization modelled during 2008 - 2010 in Figure 4.1 is specific to the use of a leguminous pioneer PFT such as clover in the current study and might change with different pioneer PFTs. However, priming N mineralization by clover indicated that legumes could be used to enhance soil N availability in reclaimed landforms (Macdonald et al., 2015). The greater tree litterfall after 2010 (Table 4.4) caused increased C:N ratios in litterfall that may have contributed to decline of net N mineralization by increasing immobilization (Devito et al., 1999; Grant, 2013) relative to mineralization (Eqn. 1(a,b)).

The modelled net N mineralization rates during growing seasons (May-September) in the three covers after the sites reached over-story canopy closure in 2010 (*ca.* 80% of annual profile net N mineralization in Figures 4.1 and 4.3(a)) were within the upper limit of the ranges measured by McMillan et al. (2007) from buried bag incubation in the surface 7 cm of the PMM during the growing season (May-September) in reclaimed and natural areas (0.3 - 3 g N m^{-2}), and measured by Carmosini et al. (2003) from buried bag incubation in the upper 20 cm of the soil profile for mature (2.1 ±1 g N m^{-2}) and logged (1.3 ±5 g N m^{-2}) aspen dominant forest soil in Boreal Plain, Western Canada. Also the N mineralization rate modelled during May-September (*ca.* 2.8 g N m^{-2}) in 100 cm cover was similar to the value (*ca.* 2.72 g N m^{-2}) measured by Hemstock (2008) from resin-core incubation in the same site. Thus the modelled values were

consistent with the field measurements. However, the greater SOC and TN in reclamation covers did not cause the net N mineralization rates to be greater than those of natural forest sites.

4.4.2. Greater profile net N mineralization with greater soil cover depth

The greater modelled net N mineralization in 100 cm *vs.* 35 cm and 50 cm covers particularly in dry and intermediate years (Figures 4.1 and 4.3(a)) was enabled by the greater substrate (SOC and TN) for decomposition (Table 4.2) as described in the Section 4.2.1.1 and by greater θ [A4] and thereby greater microbial activities (Eqn1). A positive correlation between net N mineralization rate and θ as determined by precipitation is apparent in several studies in boreal forest (Stottlemyer and Toczydlowski, 1999; Carmosini et al., 2003) and in reclaimed sites similar to SBH (McMillan et al., 2007; Hemstock et al., 2010), and hence greater N mineralization was modelled in 35 cm and 50 cm covers during wet years (Figure 4.3(a)). The relationship between TN as determined by cover depth and net N mineralization in Figure 4.3(a) is specific to the PMM and mineral subsoil materials used in this study, and would change with different capping material e.g. LFH.

However, modelled net N mineralization rate rose non-linearly with TN (Fig. 4.3(a)) so that specific net N mineralization (net N mineralization/ total nitrogen) declined from 0.003 g N mineralized g^{-1} TN y^{-1} in the 35 cm cover to 0.0025 g N mineralized g^{-1} TN y^{-1} in the 50 cm cover and 0.002 g N mineralized g^{-1} TN y^{-1} in the 100 cm cover. The modelled rate in the 35 cm cover was similar to one of 0.003 g N mineralized g^{-1} TN measured by McMillan et al. (2007) from buried bag incubation in the surface 7 cm of the PMM in oil sands reclaimed areas during growing season, and was within the lower limit of the range of 0.003 – 0.048 g N mineralized g^{-1} TN y^{-1} measured by Hemstock et al. (2010) from resin-core incubation in the upper 7 cm of the PMM amendments in oil sands reclaimed areas in Athabasca Oil Sands Region, Fort McMurray,

which had similar PMM composition to SBH. However, the modelled specific net N mineralization rates in all the covers were lower than that of 0.007 g N mineralized g^{-1} TN y^{-1} measured by Devito et al. (1999) from buried bag incubation in the upper 10 cm of the soil profile in natural peatland and of 0.03 g N mineralized g^{-1} TN y^{-1} measured in the upper 20 cm of the soil profile in mature conifer-mixed forests in Canadian shield catchments which had similar C:N ratio to SBH site. The use of TN within the entire soil profile to estimate the modelled specific net N mineralization rather than within the surface 7 - 10 cm soil to estimate measured rates contributed to lower modelled rates in the current study. Also lower N mineralization rates in the mineral soil layers than in the PMM layers (Persson and Wiren, 1995; Devito et al., 1999) caused lower modelled rates in the current study.

The decline of specific net N mineralization rate from 35 cm and 50 cm to 100 cm cover indicated limited N mineralization in lower layers of deeper covers. Exponential decline of net N mineralization below 10 cm in mineral soil under natural forest was attributed by Boone (1992), Persson and Wiren (1995) and Devito et al. (1999) to decreasing C and N concentrations deeper in the soil profile. However, in reclaimed sites subsoil has the same C and N concentrations with depth in the soil profile so that net N mineralization would not decline with depth. Thus decline in specific N mineralization modelled in lower subsoil layers in deeper covers could be explained by:

(1) Declining soil temperature with depth in the soil profile as modelled (data not shown) and measured (O'Kane Consultants Inc., 2013, 2014) in thicker covers which slowed N mineralization modelled in lower soil layers [A13]. These declines were greater with increasing tree LAI after over-story canopy closure (Table 4.3) that reduced the net radiation at the ground surface particularly in the 100 cm cover.

(2) Declines in soil temperature with depth were caused by slower warming in spring as modelled [D12, D13] (data not shown) and measured (O'Kane Consultants Inc., 2013, 2014) in the SBH site, so that deeper soil mineralizes more slowly than does shallower soil even with the same composition.

(3) Modelled aqueous O_2 concentration in lower soil layers in the 100 cm cover declined to values that limited N mineralization (< 5 g O_2 m^{-3}) [H3, H5] during wet years [D15, D17] particularly in lower slope positions.

(4) The contribution of net N mineralization from decomposition of recent litterfall from NPP particularly after exponential plant growth did not increase proportionately with TN.

Thus lower soil temperature [A6] and O_2 availability [A14, A16] limited the microbial activities and hence N mineralization in lower soil layers (Struecker and Joergensen, 2015; Jones et al., 2018) resulting lower specific net N mineralization in deeper covers.

4.4.3. Greater N uptake with greater N mineralization in thick covers

Greater modelled mineralization in the 100 cm cover *vs.* the 35 cm and 50 cm covers drove more rapid tree N uptake (Figures 4.2 and 4.3(c)) by raising NH_4^+ and NO_3^- production (Eqn. 2). Greater N uptake in all the covers during 2009 - 2013 was facilitated by the decomposition and mineralization of clover plant residues as indicated by increased mineralization (Figure 4.1(b); 2008 - 2010). However, after the mineralized N from clover decomposition was over, tree N uptake returned to a lower steady rate. Also greater mineralization during precipitation (Figures 4.1 and 4.3(a)) facilitated N uptake. The relationship between net N mineralization and N uptake (Figure 4.3(c)) was similar to that derived by Todd et al. (2000) in 7 - 27 years old reclaimed Bauxite mine sites in Jarrahdale, Australia which had a similar C:N ratio (22-39), N mineralization rates (3.4 - 10 g N m^{-2} y^{-1}) and N uptake rates (3 – 9 g N m^{-2} y^{-1}) in the upper 10

cm soil. This relationship (Figure 4.3) indicated that N uptake was limited by net N mineralization (*b* near 1 in Figure 4.3(c)) except with water stress in the 35 cm cover during 2011, even with greater TN in deeper covers.

The modelled annual N uptakes (Figure 4.2) in three covers were greater than the estimated average N uptake in boreal coniferous forests (0.51 ± 0.2 g N m^{-2} y^{-1}), but closer to the boreal deciduous mature forests in Alaska (2.5 g N m^{-2} y^{-1}) (Cole and Rapp, 1981). However, the modelled N uptakes were within the ranges of uptake (0.1 - 5 g N m^{-2} y^{-1}) estimated by Shenoy et al. (2013) in regenerating fire disturbed forest sites (16 year old stands) in Alaska.

Achieving rapid root growth and thereby deeper root systems in planted trees is important to avoid nutrient stress (Grossnickle, 2005) and to enable rapid N uptake sufficient for plant growth especially in a harsh environment like that of the reclaimed site initially without a forest floor to facilitate nutrient cycling (Pinno et al., 2012). Thus the deeper root system in the 100 cm cover facilitated N uptake (Eqn. 2) as described in Section 4.2.1.2., and increased plant growth by reducing nutrient stress during the early reclamation period. The N uptake in 35 cm and 50 cm covers was controlled by θ (Figure 2.3 in Chapter 2) and mineralized N (Figure 4.3(a)) during dry and intermediate years *vs.* wet years. Consequently lower foliar production was modelled in these covers (Table 4.3) from lower AWHC and N uptake that reduced σ_C from CO_2 fixation, reducing shoot to root σ_C concentration gradient [C50] and translocation of σ_C from shoot to root, and thereby reducing root growth and N uptake [C23g].

4.4.3.1. Greater N uptake from deciduous *vs.* coniferous trees in thicker covers

Total tree N uptake and cycling depends on the species composition of the forest stand because faster N cycling has been observed in deciduous stands *vs.* conifers (Pastor, 1987; Jerabkova et al., 2006; Shenoy et al., 2013). In the model, faster growing deciduous species such

as aspen drove greater N uptake rates *vs.* conifers such as white spruce (Figure 4.2d *vs.* c) in all the reclamation covers, consistent with observations by Lambers and Poorter (1992), Kronzucker et al. (1997), Min et al. (2000) and Nitschke et al. (2017) in different boreal forests. The N uptake of a 16 year old severely burned boreal forest site (stem density = 8 m^{-2}) in Alaska also showed similar N uptake by aspen and white spruce (Shenoy et al., 2013) to that modelled after 16 years in the current study. The modelled N uptakes of aspen and spruce in the 100 cm cover (Figure 4.2(c,d)) which had the similar aspen:white spruce ratio to the recovering burned site, were within the ranges of estimated N uptake by aspen (3.5 - 4.2 g N m^{-2}) and by white spruce (0.8 - 0.9 g N m^{-2}) for 120 growing days (Shenoy et al., 2013).

4.4.4. Greater plant N uptake increased CO_2 fixation, NPP and carbon biomass production in thicker covers

The greater N mineralization and thereby uptake (Eqn. 2) in the 100 cm cover raised the root and mycorrhizal σ_N in the model driving more rapid transfer of σ_N from mycorrhizae to roots [C53], and from root to branches [C51]. These transfers raised canopy and foliar σ_N:σ_C hastening CO_2 fixation [C6b, C8b] and hence NPP. Thus NPP increased linearly with increasing tree N uptake as determined by cover depth (Figure 4.4). Greater root–shoot transfers of σ_N [C51] and greater shoot production of σ_C in the model [C6, C8] drove more rapid shoot growth [C20a]. This raised the modelled foliar production in 100 cm *vs.* 35 cm and 50 cm covers as indicated by the greater LAI (Table 4.3). The measured and modelled foliar N concentrations were not significantly different among the reclamation covers (Figure 4.5). However, the greater LAI in 100 cm cover indicated greater N uptake to maintain increased areal densities of rubisco [C6b] and chlorophyll [C7b], and thereby CO_2 fixation, NPP and subsequently increased biomass growth (Figure 2.12 in Chapter 2). Similar structural N concentration in foliage of all

the covers may be due to greater CO_2 fixation enabled by greater N uptake in 100 cm cover which increased both the σ_C and σ_N commensurately, maintaining stable N concentration although C and N uptake amounts increased with the leaf mass. In contrast, reduced N uptake in 35 cm and 50 cm covers reduced the foliar σ_N:σ_C and thereby reduced the CO_2 fixation [C6b, C8b] through product inhibition [C11]. This caused lower shoot growth, foliar production and thereby lower LAI in 35 cm and 50 cm covers and consequently lower NPP and biomass growth, particularly during wet years (Table 4.3) when there was no water limitation or salt effect. The modelled lower NPP *vs.* N uptake in drier year (2011) than in wetter years (2012 and 2013) (Table 4.3 and Figure 4.4) indicated that NPP in shallow covers was more controlled by θ and salinity during dry years, and more by N uptake during wet years. Similar modelled NPP in different slope positions during wet years and greater modelled NPP in lower *vs.* upper slope positions in drier years (Table 2.6), indicated that NPP of upper slope positions was more controlled by θ than by N availability during drier years.

The aspen and white spruce NUE derived from modelled N uptake and NPP (Figure 4.4(a,b)) followed a similar pattern to that described by Nitschke et al. (2017) who measured NUE along disturbance and nutrient availability gradient in boreal forests in southwest Yukon. Modelled NPP of aspen and white spruce (Figure 4.4) in the current study included both the above and belowground NPP. Thus the average NUE for aspen (*ca.* 60 g C g^{-1} N) and white spruce (*ca.* 80 g C g^{-1} N) estimated by Nitschke et al. (2017) using aboveground vegetation were lower than the NUE in the current study. However, the NUE in reclamation covers (slope of Figure 4.4(c)) was within the range (65 - 160 g C g^{-1} N) estimated by Finzi et al. (2007) in temperate forests.

The average asymptote N uptake was 4.6 g N m^{-2} y^{-1} for the reclamation covers after the sites reached over-story canopy closure (Figure 4.3(b)). According to Figure 4.4(c), an average of 4.4 g N m^{-2} y^{-1} (±0.3 g N m^{-2} y^{-1}) is required to achieve average NPP for boreal mixed-wood forest (*ca.* 400 g C m^{-2} y^{-1}) as estimated by Gower et al. (2001), Kimball et al. (2006) and Stinson et al. (2011). This average NPP was achieved at SBH with a TN of 17 Mg N ha^{-1} in the 100 cm cover for the current study, from which N uptake was within the standard error of 95% of asymptote N uptake. However, the target NPP depends on end land use and the average NPP for Canada's managed boreal forests (302 g C m^{-2}), as estimated by Kurz et al. (2013) could be achieved at SBH with TN of 12.9 Mg N ha^{-1} (that of the 50 cm cover) for the current study. Although all sites at SBH have an adequate TOC and TN content (Table 4.2) required to achieve a rich nutrient regime (CEMA, 2006) with no N limitation, tree N uptake was lower in the 35 cm cover due to lower decomposition and mineralization of organic nitrogen due to water limitation and lower microbial activities in PMM as observed by McMillan et al. (2007) and Hemstock et al. (2010). These quantified threshold values could vary with the quality of reclamation material and hence they pertain to the PMM and subsoil materials used in the current study.

4.4.5. Foliar N concentrations indicated N deficiency in reclaimed covers

Foliar nutrient concentrations are frequently used to diagnose nutrient deficiencies in forestry as they are significantly correlated with forest growth and productivity (Ballard and Carter, 1986; Wang and Klinka, 1997). Even though the modelled and measured aspen foliar N concentrations (Figure 4.5(a)) were below the optimum concentration of 69 mg N g C^{-1} for *Populus* spp. (Hansen, 1994), it was higher in each cover and in a regenerating natural site than the critical level for vascular plant growth (31 mg N g C^{-1}) (Kirkby, 2012). Foliar N concentration of 31 - 52 mg N g C^{-1} indicates optimal white spruce growth (Nienstaedt and

Zasada, 1990). The modelled and measured white spruce foliar N concentration (Figure 4.5(b)) showed a moderate-severe N deficiency (22 - 27 mg N g C^{-1}) in all the reclamation sites according to the criteria of Ballard and Carter (1986) and Nienstaedt and Zasada (1990). However, the modelled and measured white spruce foliar N concentration in the current study was greater than the mean foliar N concentration (22 mg N g C^{-1}) measured by Chang et al. (2010) in six natural white spruce stands in the AOSR and were within the range (16 - 29 mg N g C^{-1}) measured by Wang and Klinka (1997) in 102 white spruce stands in the Sub-boreal spruce zone of British Colombia. Through an *in situ* study, Duan and Chang (2015) also found that white spruce growth in reclaimed sites with PMM overlying overburden was limited by the low N availability. This lower spruce foliar N concentration may be attributed to the lower N availability in constructed sites and thereby lower uptake by the spruce (Figure 4.2(c)) *vs.* aspen.

Although the foliar N concentrations were similar among the reclamation covers, tree N uptakes were different. Aspen growth was positively correlated (correlation coefficient = 0.9) with soil TN as found by Chen et al. (1998), but increase in growth was not proportional to that of TN in the soil profiles. Thus greater N availability in the 100 cm cover may also have contributed to the greater aspen N uptake and growth under the competitive environment in reclaimed landscapes. In *ecosys*, deciduous PFTs were modelled with greater N requirements from greater leaf N content and more rapid leaf turnover and hence more rapid nutrient loss than were coniferous PFTs, but with faster growth from more rapid CO_2 fixation with greater leaf N concentration. Thus, faster growth of aspen relative to spruce was measured and modelled with more favourable soil N and water status in thicker covers (Figure 2.12 in Chapter 2). The lower N uptake, foliar N content turnover, but greater NUE in white spruce *vs.* aspen indicated that

white spruce is an efficient N conserver and hence enable to maintain NPP in areas with lower N availability (Nitschke et al., 2017) such as 35 cm cover in this study (Figure 4.4(a)).

4.4.6. Greater NPP increased litterfall in thicker covers ensuring greater long-term N cycling

Success in restoration of reclaimed boreal forests depends on establishing natural nutrient cycles particularly N since boreal forest productivity is limited by lower N availability in the soil (Mahendrappa and Salonius, 1982; Kaye and Hart, 1997; Carey, 2008). Even though early plant growth in all the reclamation sites was mainly governed by organic matter (Table 4.2) and the residual N in the soil from fertilizer application, litterfall mineralization contributed increasingly to plant N uptake later in the reclamation period (Table 4.4). The greater foliar production particularly by aspen indicated by greater LAI in the 100 cm cover, increased litterfall (Table 4.4) and thereby surface litter depth developed on the reclamation cover (Figure 4.6(b)). Deciduous forests i.e aspen have shown higher N uptake, N requirement and fast turnover and thereby greater N return to soil due to greater quantity and better quality of litter (Van Cleve et al. 1983; Shenoy et al., 2013). In contrast, coniferous stands showed lower N cycling due to lower annual litterfall with lower N and lower quality from higher lignin content (Van Cleve et al., 1983; Jerabkova et al., 2006). Thus greater modelled N return from greater aspen:spruce litter N ratio in the 100 cm cover *vs.* the 35 cm and 50 cm covers hastened aspen N uptake and growth in the 100 cm cover, further hastening N cycling from that in the 35 cm and 50 cm covers. Greater soil water storage and lower salinity facilitated mineralization and microbial growth in the 100 cm cover further hastening N cycling**.** Thus long term plant growth in the 100 cm cover will be less limited by N availability relative to that in the 35 cm cover with a tendency to long term N limitation for plant growth.

4.4.7. Summary

In summary, greater profile net N mineralization and N uptake were modelled in the 100 cm cover *vs.* the 35 cm and 50 cm covers particularly during dry and intermediate years. The θ influenced the net N mineralization in each cover over the reclamation period. However, modelled net N mineralization rate relative to TN decreased with increasing cover depth due to reduced microbial activities from lower temperature and O_2 concentrations in lower soil layers. Even though the foliar N concentration did not vary with cover depth, lower N uptake caused lower NPP in shallow covers particularly during wet years that did not show any water stress or salinity effects. However, N deficiency in all the covers for white spruce and aspen growth was evident by the modelled and measured foliar N concentration. The 100 cm cover showed greater foliar production and thereby greater litterfall and N return to soil than in the 35 cm and 50 cm covers ensuring establishment of early N cycle in 100 cm cover similar to natural sites recovering after severe fire disturbances.

Even though NPP increased linearly with N uptake (Figure 4.4(c)), a non-linear relationship between TN and modelled N mineralization that drove tree N uptake (Figure 4.3(b)) indicated that cover depth that determines the TN will have little effect on NPP beyond a threshold TN depending on site conditions. The average boreal mixed-wood forest NPP and 95% of estimated asymptote N uptake were achieved with TN of 17 Mg N ha^{-1} (100 cm cover) using the PMM and subsoil for the current study. However the N uptake requirement varies according to the target NPP or end land use of reclaimed sites. Also the relationships between TN and N mineralization as well as TN and N uptake are site specific and vary with the composition of reclamation materials, C:N ratios and environmental conditions. Thus these relationships need to be developed for different sites to find the required TN that does not limit the plant growth.

Therefore, reclamation success in recovering target NPP for the reclaimed sites according to the end land use requires:

(1) Sufficient cover depth to provide enough organic matter and soil moisture to facilitate N mineralization and N cycling thereby to avoid N limitation for plant growth

(2) Consideration of how cover depth and N availability influences the growth of different plant functional types.

Collectively, results of this study also demonstrate the ability of *ecosys* to predict the effect of cover depth on profile net N mineralization, N uptake, the relationship between N uptake and NPP and N return to the soil in reclaimed upland areas with a wide range of reclamation materials, compositions, PFTs, and weather conditions without calibrating to a specific site.

Table 4.1. Key soil nutrient properties used to model nutrient cycling in three reclamation covers.

Nutrient availability		**Peat Mineral Mix**	**Subsoil/Till**	**Overburden**
TOC[a]	(g C Mg^{-1})	171000	10000	7000
Organic N[a]	(g N Mg^{-1})	5867	500	350
Organic P	(g P Mg^{-1})	390 [c]	50*	35*
$NH4^{+}$ [b]	(g N Mg^{-1})	4	0.8	12
$NO3^{-}$ [b]	(g N Mg^{-1})	1.2	0.2	1.2
Exchangeable P [b]	(g P Mg^{-1})	5	0.1	0.1

[a] from Macyk (1999) and Yarmuch (2003)
[b] from Macyk (1999)
[c] Lanoue (2003)
*estimated as 0.1 x organic nitrogen

Table 4.2. Modelled total soil organic carbon (SOC) and total nitrogen (TN) in three reclamation covers at the beginning (1999) and after 13 years (2012) of reclamation.

Cover type	**Total SOC** (Mg C ha^{-1})		**Total nitrogen** (Mg N ha^{-1})	
	1999	2012	1999	2012
35 cm	265 (±27)	267	9.5 (±3)	9.7
50 cm	359 (±36)	361	12.9 (±4)	13.2
100 cm	443 (±42)	445	17.0 (±9)	17.3

Values are averages with standard error of the mean indicated in parentheses. In 1999, modelled values were initialized from measured values.

Table 4.3. Modelled nitrogen uptake, net primary productivity (NPP) and leaf area index (LAI) averaged over slope positions in three cover depths (35 cm, 50 cm and 100 cm) after planted trees (aspen + white spruce) reached over-story crown closure.

Year	**Precipitation (mm)**	**N uptake** (g N m^{-2} y^{-1})			**NPP** (g C m^{-2} y^{-1})			**LAI** (m^2 m^{-2})		
		35 cm	**50 cm**	**100 cm**	**35 cm**	**50 cm**	**100 cm**	**35 cm**	**50 cm**	**100 cm**
2011	238	2.99	3.83	4.33	224	309	368	1.84	2.26	2.43
2012	507	3.81	4.33	4.62	347	404	444	2.13	2.41	2.44
2013	462	3.71	3.97	4.37	383	440	484	2.53	2.85	2.95
2014	385	2.97	3.19	3.65	356	397	445	2.69	2.92	3.00
2015	340	2.73	2.79	3.39	362	403	472	2.74 (2.4±0.1) ¶	2.95	3.10 (3.3±0.1) ¶

¶ Measured average Leaf Area Index ±standard error of the mean.

Table 4.4. Modelled (Mod) and measured (Mea) annual surface litterfall (in fall) carbon and modelled litterfall nitrogen averaged over slope positions in three reclamation covers[a]

Year	**Litterfall carbon** (g C m^{-2} y^{-1})						**Litterfall nitrogen** (g N m^{-2} y^{-1})		
	35 cm		50 cm		100 cm		35 cm	50 cm	100 cm
	Mod	Mea[a]	Mod	Mea[a]	Mod	Mea[a]	Mod	Mod	Mod
2011	43	33	49	43	64	56	0.80	0.93	1.02
2012	26	26	34	36	61	58	0.80	0.88	0.97
2013	35	33	43	41	67	65	0.85	0.92	1.02
2014	45		55		70		0.76	0.85	1.01
2015	50		62		83		0.58	0.67	0.85

[a] Measured values from Drozdowksi et al. (2014).

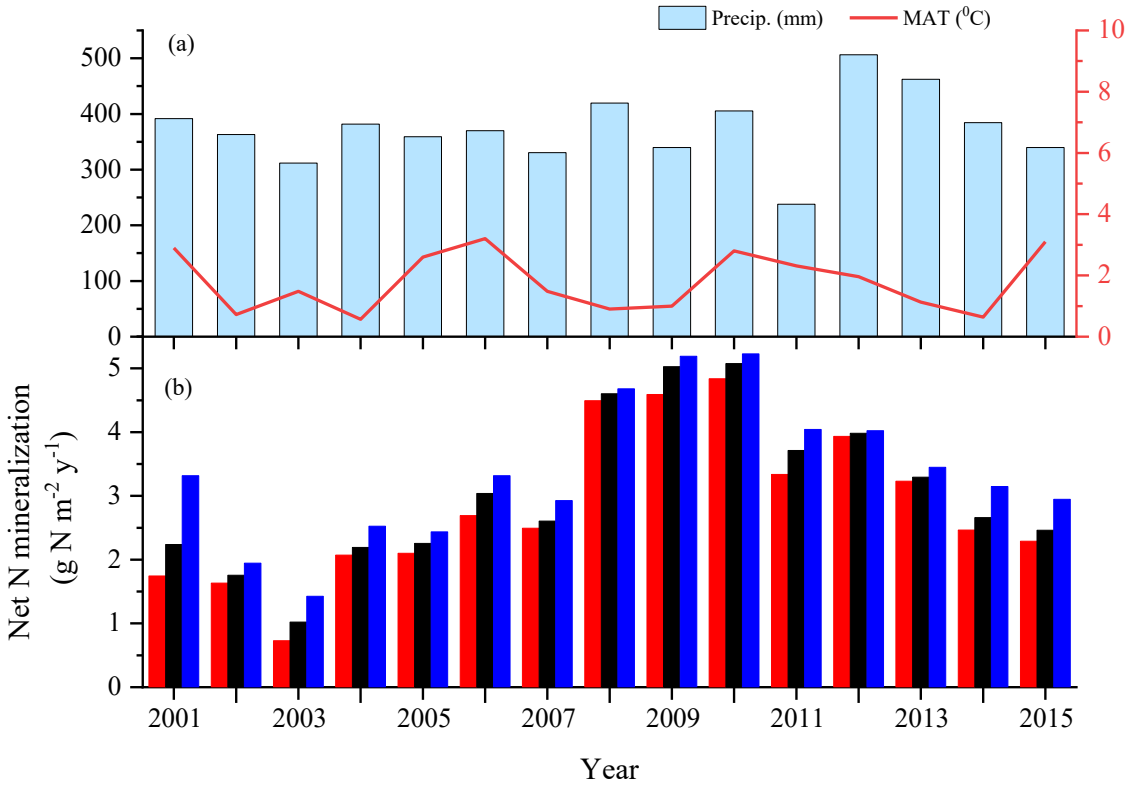

Figure 4.1. (a) Measured annual precipitation and mean annual air temperature (MAT) (b) modelled annual net N mineralization in soil profile averaged over slope positions in 35 cm (red), 50 cm (black) and 100 cm (blue) covers. Modelled annual profile net N mineralization in each cover was taken from annual sums of hourly modelled net N mineralization ($U_{NH4i,n,j,l}$ in Eqn. 1(a)) by all kinetic components j of all MFTs n in all substrate-microbe complexes i, in all soil layers l within the soil profiles. Lower growing season precipitation in 2003 caused lower mineralization in each cover.

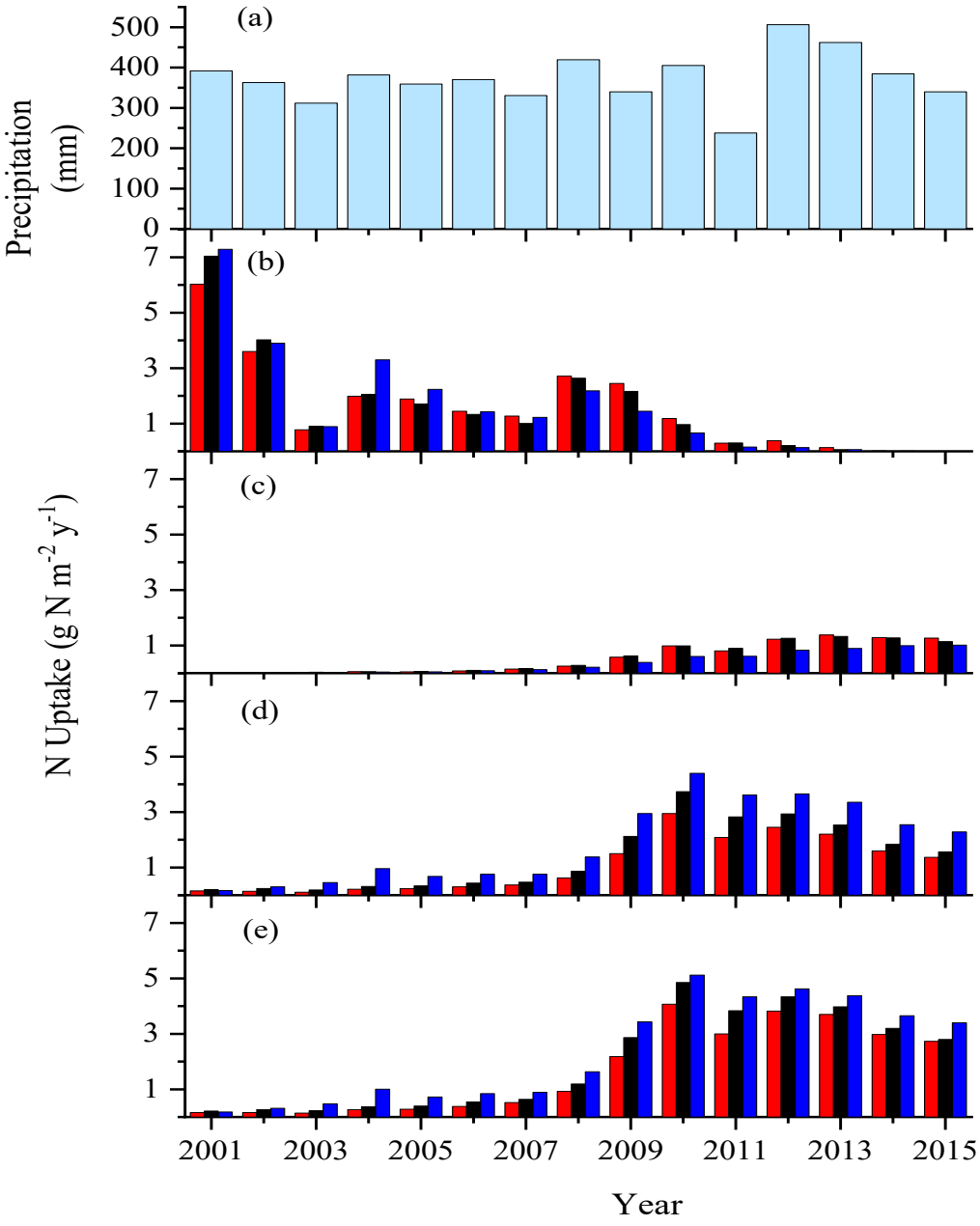

Figure 4.2. (a) Measured annual precipitation and modelled annual (b) understory (clover + grass) (c) white spruce (d) aspen and (e) total tree N uptake averaged over slope positions in 35 cm (red), 50 cm (black) and 100 cm (blue) covers from 2001.

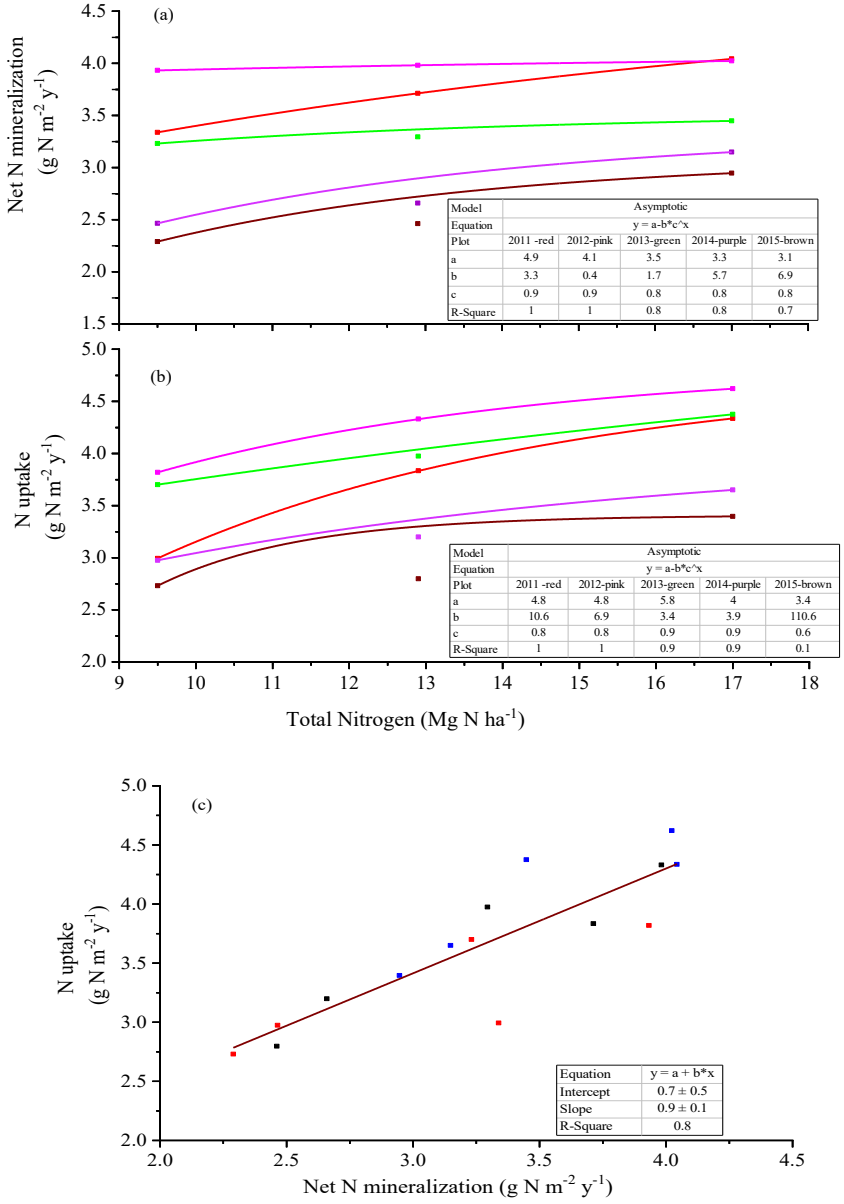

Figure 4.3. (a) Relationship between estimated total nitrogen (TN) in the reclaimed soil profile and modelled net N mineralization, (b) relationship between estimated TN and modelled total tree N uptake (aspen + white spruce) and (c) relationship between modelled net N mineralization and modelled total tree N uptake during 2011 - 2015 (after planted trees reached over-story crown closure in 2010). One drier year (2011), two wet years (2012 and 2013) and two intermediate years (2014 and 2015) were experienced during this period. The red, black and blue dots in (c) represent the 35 cm, 50 cm and 100 cm reclamation covers respectively. The reduced N uptake with water stress in the 35 cm cover (TN = 9.5 Mg N ha^{-1}) in dry year (2011) left more mineral N for uptake in wet years (2012 and 2013), as indicated by the greater N uptake (Figure 4.3(b)) *vs.* net N mineralization (Figure 4.3(a)) modelled during 2012 and 2013.

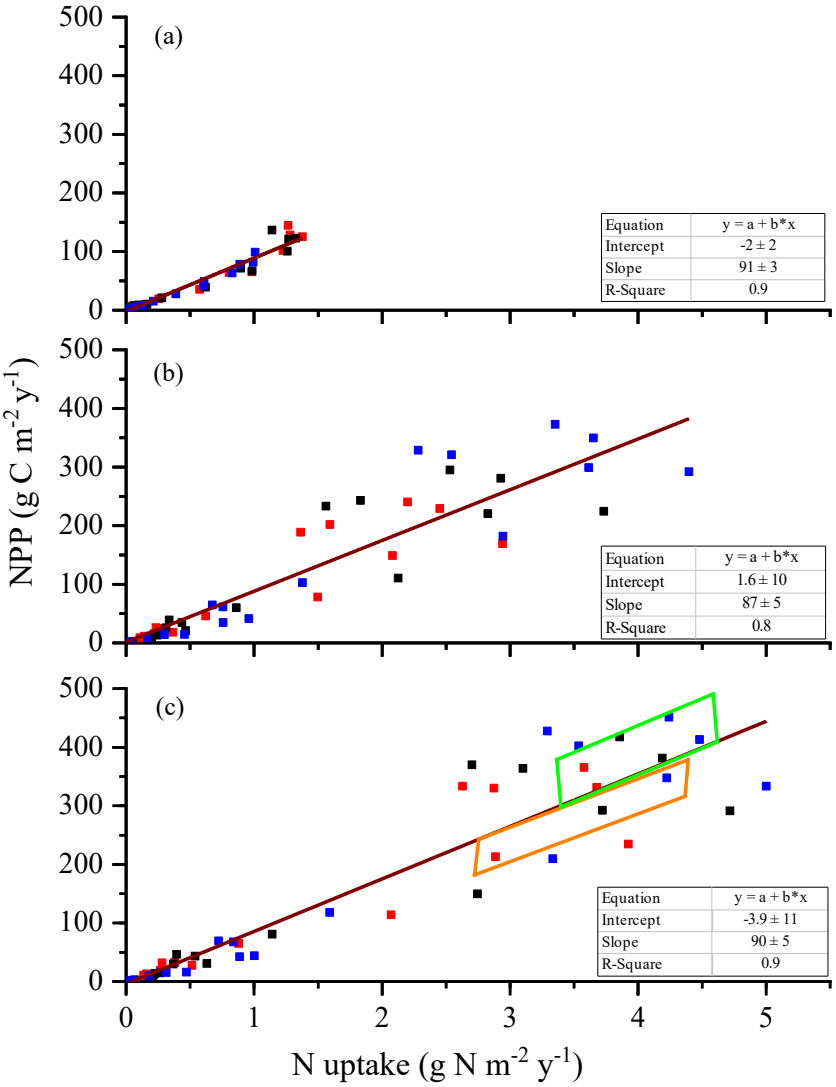

Figure 4.4. Relationship between modelled N uptake and modelled net primary productivity in (a) white spruce, (b) aspen and (c) total tree in reclaimed covers. Slope of the lines in graphs represent the nutrient-use efficiency (NPP/N_{uptake}). The red, black and blue dots represent the 35 cm, 50 cm and 100 cm reclamation covers respectively. The modelled lower total NPP *vs.* N uptake in drier year (2011, covered by orange rectangle) than in wetter years (2012 and 2013, covered by green rectangle) indicated that NPP in shallow covers was more controlled by θ and salinity during dry years, and more by N uptake during wet years.

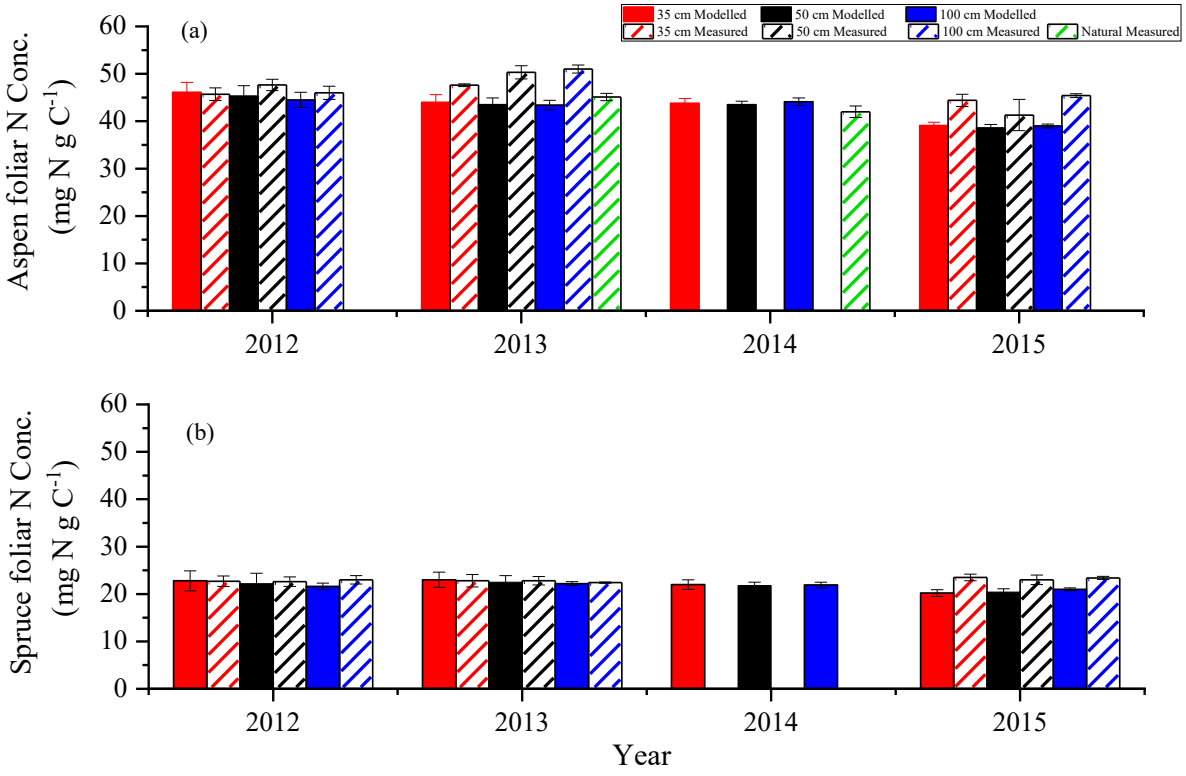

Figure 4.5. Modelled (filled bars) and measured (striped bars) foliar N concentrations of (a) aspen (b) white spruce along the slope positions in 35 cm (red), 50 cm (black) and 100 cm (blue) covers, and natural site (green stripped bar) during July in 2012, 2013, 2014, and 2015. Vertical bars represent standard error of the mean in each site, measured (n=9) and modelled from slope positions (n=5).

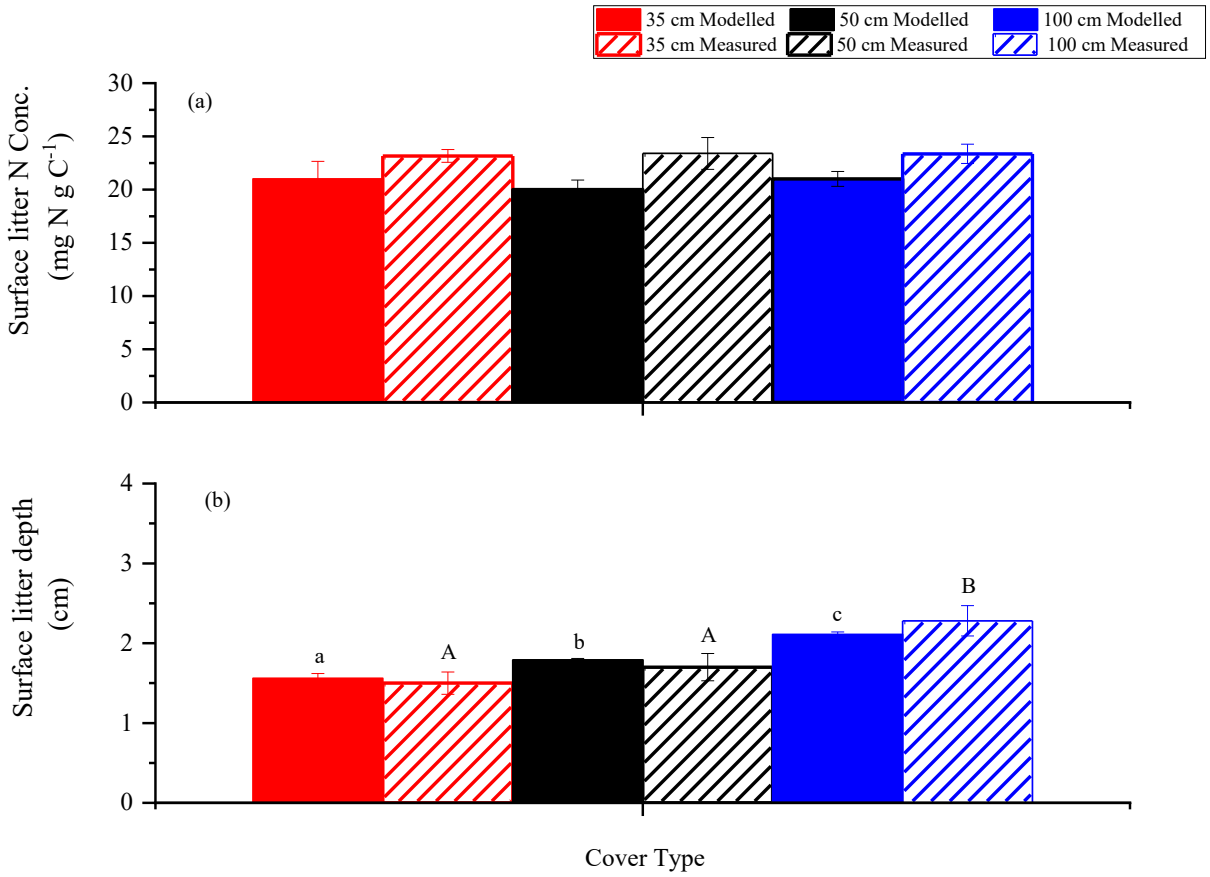

Figure 4.6. Modelled (filled bars) and measured (striped bars) (a) N concentrations in surface litter developed on PMM and (b) surface litter depth developed on PMM in 35 cm (red), 50 cm (black) and 100 cm (blue) covers in July 2015. Vertical bars represent standard error of the mean, modelled from slope positions (n=5) and measured site (n=9). Capital letters indicate significant differences of measured values and lower letters indicate significant differences of modelled values among cover types (α= 0.05).

Chapter 5

Modelling long-term effects of reclamation cover depth on forest regeneration in reclaimed landscapes in Northern Alberta under current and future climates

5.1. Introduction

The growth and thereby productivity of planted trees in landforms constructed after open pit mining have been adversely affected by various undesirable soil characteristics such as low available water holding capacity (AWHC), compaction, salinity, topography and low nutrient availability (Fung and Macyk, 2000; Kessler, 2007; Kelln, 2008; Duan and Chang, 2015; Macdonald et al., 2015). Therefore different covers have been constructed across open pit mining sites to overcome these effects depending on availability of cover materials, parent materials in the region and construction strategies (Rowland et al., 2009). In addition, various laboratory, greenhouse, field and modelling studies have been conducted to determine the short and long-term effects of these adverse conditions on growth of planted trees in reclaimed landforms. Some of these previous studies found that severity of the adverse conditions in reclaimed landforms declined with increasing cover depth (Elshorbagy et al., 2007; Kelln et al., 2007; Kessler, 2007; Keshta et al., 2010; Meiers et al., 2011; Huang et al., 2015; Macdonald et al., 2015). Results of the current modelling study (Chapters 2-4) also indicated that increases of AWHC and nutrient availability, as well as declines of negative effects of salinity, raised gross and net primary productivity (GPP and NPP) with increasing cover depth. However these results also demonstrated that increased cover depth had little effect on productivity once a threshold capping depth was exceeded, depending on site conditions. The cost of reclamation is

considerably increased with cover depth (Bradshaw, 1997; Boese, 2003; Elshorbagy et al., 2006) so that addition of more cover materials than required will further increase the cost without much benefit in NPP. Therefore sufficient and economical cover depth application is required to achieve productivity in reclaimed landforms according to target land use.

However long-term forest growth in reclaimed landforms will occur under a climate that is different from that under which the study was conducted. Thus restoration of reclaimed landforms in Northern Alberta is also affected directly and indirectly by future warming, particularly with amplified warming effects in higher latitudes (IPCC 2013; Mekonnen et al., 2018a). Warming directly affects GPP in boreal climates by improving kinetics of carboxylation and thereby rates of CO_2 fixation (Bernacchi et al., 2001; Mekonnen et al., 2016), and indirectly affects GPP in water-limiting areas particularly with lower AWHC due to increased evapotranspiration, soil drying and hence more frequent water stress (Grant et al., 2008; Mekonnen et al., 2016). Warming may further increase the adverse effects of salinity on plant productivity in water limiting areas by decreasing osmotic (ψ_π) and thereby soil water potential (ψ_s) more than under current climate. Warming also hastens decomposition and nitrogen (N) mineralization, N uptake and hence CO_2 fixation (Ineson et al., 1998; Hart, 2006), so that productivity in both reclaimed and natural areas will increase under warming. Therefore identifying cover depth required to ensure re-establishment of reclaimed landforms under different climatic conditions is essential to achieve equivalent land capabilities under warming. Warming may also affect GPP through changes in plant species composition, as demonstrated by previous warming studies (Shaver et al., 2000; Hudson and Henry, 2009; Pieper et al., 2011; Mekonnen et al., 2018b). Thus, understanding changes in planted species composition in reclaimed areas under warming is important to establish target ecosystems.

The effects of warming on GPP, NPP and biomass production in reclaimed lands are uncertain. A rigorous modeling effort based on fundamental processes governing water, energy, ionic solutes and nutrient interactions through the soil-microbe-root-canopy-atmosphere system can provide both short and long-term forecasts of land capability restoration for reclamation landforms under different climatic conditions. The ability of *ecosys* to capture the effects of warming on CO_2 fixation, NPP and thereby net ecosystem productivity have been rigorously tested against measured fluxes across different ecosystems: e.g. in diverse temperate and boreal forests (Grant et al., 2009a, 2009b, 2010; Grant, 2013, 2014), and Arctic tundra (Grant et al., 2003, 2011, 2015, 2017) in higher latitudes and different regions of North America (Mekonnen et al., 2016, 2018a,b). To date modelling studies have not been conducted to study warming effects in novel ecosystems undergoing reclamation. Therefore, in this study the comprehensive terrestrial ecosystem model *ecosys* (Grant (2001, 2014); Grant et al., 2012) was used to identify the threshold AWHC required to reach target NPP for the reclaimed site by adding seven hypothetical cover depths (60 cm -150 cm) to the three cover depths (35 cm, 50 cm and 100 cm) examined in these studies, and to determine the relationship between constructed cover depths and long-term plant productivity under current and warming climates. The main objectives of this study were (1) to understand and quantify the AWHC required to achive 95% of maximum NPP (threshold) after the site had reached over-story crown closure under current climate and (2) to understand whether this threshold AWHC determined by cover depth is sufficient to meet water demand in reclaimed landforms under a future climate change scenario

5.2. Methods

5.2.1. General model description

Ecosys is a comprehensive mathematical model that has the ability to represent multiple soil and canopy layers in soil-microbe-canopy–atmosphere systems at three-dimensional scales. The model simulates physical, chemical and biological processes in natural and disturbed terrestrial ecosystems through the acquisition, transformation and transfer of radiation, water, carbon, oxygen, nitrogen and phosphorous (Grant, 2001) using site-independent algorithms (Mezbahuddin et al., 2014) to achieve realistic landscape-scale predictions of productivity under a wide range of site conditions. The key parameters and algorithms used in *ecosys* were described in Grant (2001; 2014) and Grant et al. (2012) and remain unchanged from those used in earlier studies. The major algorithms that govern the water relations (Chapter 2), salinity (Chapter 3) and N availability (Chapter 4) and their effects on NPP in *ecosys* were desribed in previous chapters with reference to supporting equations given in the Supplement. The processes that govern the direct and indirect effects of warming on carbon fixation and thereby NPP and forest biomass production, as described below, have been explicitly modelled in the *ecosys* (Grant et. al., 1999, 2007; Grant, 2014). The general description and parameters that are most relevant to modelling impacts of warming and concurrent raise in CO_2 on GPP and NPP are given below with reference to supporting equations given in the Supplement.

5.2.1.1. Direct effects of warming on CO_2 fixation and GPP in the constructed and natural landscapes

Direct effects of warming on productivity are mainly determined by the air temperature (T_a). In *ecosys*, all canopy biological processes are driven by canopy temperature (T_c) and thereby GPP is determined by T_c solved from first-order closure of the canopy energy balance

[B1a] as affected by T_a. Effects of rising T_c on carboxylation [C6b and C10a], oxygenation [C6d and C10b], and Michaelis–Menten constant for carboxylation (K_c) [C6e, C10d and C10e] are modeled with Arrhenius functions for light and dark reactions (Grant et al., 2007a) using parameters from Bernacchi et al. (2001, 2003). Thus, CO_2 fixation and GPP are directly affected by increased T_a. Canopy carboxylation rates [C6a] are coupled with CO_2 diffusion rates [C2] by solving for a set ratio for intercellular to canopy gaseous CO_2 concentration (C_i:C_b) maintained under ambient CO_2 concentration (C_a), irradiance, T_c, leaf nutrient content and canopy water potential (ψ_c) (Grant et al., 2007a). The increase of C_i assumed to be raised proportionately with elevated C_a increases the mesophyll aqueous CO_2 concentration and thereby canopy carboxylation and GPP under climate change (Grant, 2013). Raising T_c improves kinetics of carboxylation more in cooler climates (Bernacchi et al., 2001) due to larger temperature sensitivity of biological processes (Q_{10}) at lower temperatures. Raising T_c also increases K_c (Bernacchi et al., 2001, 2003) while reducing aqueous CO_2 concentration in canopy chloroplasts (C_c) to C_i (Farquhar et al., 1980). In cooler climates such as that in this study, the positive effect of warming on carboxylation kinetics is greater than the negative effects of warming on K_c and C_c so that warming increases CO_2 fixation (Shaver et al., 2000).

5.2.1.2. Indirect effects of warming on GPP and NPP in the constructed and natural landscapes

5.2.1.2.1. Water relations: Indirect effects of warming on plant productivity depend on the changes in the environment from changing T_a (Shaver et al., 2000). Rising T_a affects GPP indirectly by increasing vapor pressure deficits (D) (assuming relative humidity does not change) and hence potential evapotranspiration, which may not be offset by increased moisture availability in soil profiles, causing soil drying (Grant et al., 2008). The effect of D on

evapotranspiration in *ecosys* is solved through the first-order closure of the energy balance [B1a]. Greater transpiration lowers ψ_c [B14] and raises canopy stomatal resistance (r_c) [B2b] reducing CO_2 diffusion and fixation [C2, C3] (Grant et al., 2008). Thus, GPP in reclaimed landforms with lower *vs.* higher AWHC is greatly affected by warming due to decreasing soil water content (θ) from increasing evapotranspiration. Also autotrophic respiration (R_a) continuously increases with T_c [C13] even though CO_2 fixation does not. However, concurrent increase in C_a reduces the transpiration by raising C_a - C_i and hence r_c [B2], thereby slowing soil drying (Grant et al., 2006a, 2012). Therefore the increase in growth from increased CO_2 fixation under elevated C_a offsets the reduction in growth from greater D under rising T_a (Grant et al., 2006a).

Thus, CO_2 fixation and GPP will increase with T_a in all reclaimed landforms within the study site and regenerating natural sites as they are located within the cooler regions. However, the productivity in shallow covers may decrease particularly in drier years, if the effect of increased T_a on ET is greater than that of elevated C_a.

5.2.1.2.2. Nitrogen availability and uptake: Warming hastens soil N mineralization [A26] and root active N uptake [C23] modelled by an Arrhenius function of soil temperature (T_s) [A6]. Thus, N uptake and plant productivity increase with soil warming (Grant, 2014). However, lower AWHC in shallow *vs.* deeper covers limits the N uptake from reduced N demand for growth under warming particularly during dry years.

Further description of the major algorithms that govern the direct (CO_2 fixation) and indirect effects (water relations and nutrient uptake) of warming on GPP and growth of different PFTs in *ecosys* can be found in Grant et al. (2006a), Grant (2014), and Mekonnen et al. (2016, 2018a,b).

5.2.2. Model Experiment: South Bison Hill reclamation site as represented in *ecosys* model runs

5.2.2.1. Landscape

The information for site management and soil properties collected during 1999 and 2000, were used to construct the input files used to initialize *ecosys* for SBH. These inputs represent the actual field characteristics which include site, climate, and plant and soil management data used by *ecosys* to simulate basic physical, chemical, and biological processes. Each reclamation cover was represented in the model as a transect of six interconnected grid cells each of which had a dimension of 50 m x 40 m. Five grid cells represented the slopes as shown in Figure 2.1 (b) and one grid cell represented the level area above the slope corresponding to the landscape at SBH. All the input data (site, climate, soil properties, soil and plant management) were the same among reclamation covers except cover depth as described in Section 2.2.2.1.

5.2.2.2. Soil properties

Soil physical and chemical data were taken from the studies done by Macyk (1999), Meiers (2002) and Yarmuch (2003) and soil biological data were taken from the study done by Lanoue (2003) in the SBH site. The soil water content at field capacity and permanent wilting point (θ_{FC} and θ_{PWP} respectively) for PMM, subsoil material and overburden (Table 2.2 in Chapter 2) were derived from water desorption curves developed using measured θ *vs.* soil matric potential (ψ_m) data. Although measured time domain reflectometry (TDR) values had indicated slightly different θ_{FC} and θ_{PWP} for the PMM, subsoil and overburden materials in each of the three covers, average values were used for each material in all reclamation treatments so that modelled differences in soil and plant water status and in plant growth could be attributed to those in

capping depth. Further details of soil properties used in modelling can be found in Section 2.2.4.2.

5.2.2.3. Land management

Fertilizer application was modelled as practiced in the field at the beginning of simulation runs (1999). Aspen and white spruce PFTs and grass and clover PFTs were seeded in each grid cell at the densities described under the reclamation method in Section 2.2.2.3. In 2007, ingress plants were seeded at as the density described under Section 2.2.2.3. The model was run for 17 years (1999 - 2015) using the daily weather data described in Section 2.2.3.1.

5.2.2.4. Simulation runs with hypothetical cover depths

Projections were made with seven hypothetical covers with cover depth of 60 cm, 70 cm, 80 cm, 90 cm, 120 cm, 140 cm and 150 cm covers together with the three constructed cover depths (35 cm, 50 cm and 100 cm) (Figure 5.1) to determine the threshold AWHC for the site which achieves 95% of maximum NPP under site conditions and/or similar average NPP of the target boreal mixed-wood forest. The thickness of peat-mineral mix (PMM) layer was set to 20 cm for all the covers except 35 cm cover which remained 15 cm, so that subsoil depths were changed to get hypothetical cover depths. Except cover depth all the other factors were kept constant to model plant growth as described in Sections 2.2.4, 5.2.2.2 and 5.2.2.3 in the hypothetical covers. The AWHC in each cover was calculated using field measured FC and PWP values in each horizon of the soil profile on the basis of soil texture (CEMA, 2006) and SOC and TN were calculated using measured TOC and TN percentages in each reclamation material (Table 5.1). The model was run for 17 years (1999 - 2015) using the daily weather data described in Section 2.2.3.1. The modelled NPP at different slope positions were averaged to get NPP in each reclamation cover.

5.2.2.5. Long-term simulation runs under current and warming climates

Long-term projections of cover depth effects on forest productivity under current climatic conditions were conducted by running the model for 100 years (1999 - 2099) with repeating sequences of 1999 - 2016 weather data. Future warming was driven by gradual changes in T_a and P from those in the current climate derived from RCP 8.5 climate change scenario ensemble projections (Table 5.2), downscaled and averaged across 15 CMIP5 models (Wang et al., 2016), extracted from the model grid cell within which the SBH site is located. Atmospheric carbon dioxide concentration (C_a) changes (CO_2 concentrations for the RCP) derived from Meinshausen et al. (2011) were used to model concurrent gradual rise in CO_2 with warming. The modelled GPP and NPP at different slope positions were averaged to get GPP and NPP in each reclamation cover.

5.2.3. Natural forest site following fire

Long-term GPP and NPP modelled from reclamation covers were compared with those modelled in a regenerating severely burned natural forest landscape approximately 14 km north (57°7'11.69"N, 111°36'23.90"W) from SBH near the Beaver river on the western side of the Athabasca river. The site was selected using fire, vegetation and ecosite maps and was 4 years younger than the SBH. This site was a typical "*d"* ecosite which was the target ecosite of the reclaimed landforms, with sandy loam to silty loam soil developed from till and glaciofluvial sediments (Crown and Twardy, 1970; Das Gupta, 2015). The site was a trembling aspen dominant stand (nearly 99%), with a few sporadic white spruce (*Picea glauca* (Moench) Voss.), recovering from fire that had occurred during 2003 (Das Gupta, 2015). The estimated AWHC within the root zone calculated using field measured FC and PWP values in each horizon of the soil profile on the basis of soil texture (CEMA, 2006) was > 200 mm for the natural site.

5.2.3.1. Natural forest site as represented in *ecosys*

The natural forest site was a plain landform represented in the model as a grid cell with a dimension of 50 m x 20 m. The model run with weather data (1948 - 1998) from the North American Regional Reanalysis (NARR) and Fort McMurray airport station and SBH weather data (1999 -2003) was used to form a 56-year (1948 to 2003) spin-up for the site. This spin-up allowed the model to generate a stable, mature forest prior to the fire disturbance. Then a stand replacing fire was introduced in May 2003 after which aspen was seeded with the density of 1600 stems ha^{-1} and white spruce with density of 50 stems ha^{-1} in June 2003. The model was run to 2015 using the same weather files as those at SBH. Several properties in the LFH (*ca.* 7.5 cm) and mineral soil layers (0 - 100 cm); i.e: bulk density, texture, pH, TOC, TN and mineral N were collected from the site (2012 - 2014), and other soil physical, chemical and biological properties were taken from soil data for the site in the Unified North America Soil Map (UNASM) dataset (Liu et al., 2013) as described in Mekonnen et al. (2016) and used as inputs to the model runs. Long-term forest productivity in the natural site after severe burning was simulated by running the model for 97 years (2003-2099), with repeating sequences of 1999 - 2016 weather files the same as those used for SBH runs as described in Section 5.2.2.5. Future warming and concurrent raise in CO_2 were driven by an RCP 8.5 climate change scenario ensemble projections (Table 5.2), as for the constructed landforms in SBH.

5.3. Results

5.3.1. Changes in NPP and aboveground carbon biomass with increased AWHC in reclaimed landforms

Modelled NPP under current climate increased non-linearly with increasing AWHC among the hypothetical reclamation covers as determined by cover depth (Figure 5.2). These differences were greater during dry (i.e. 2011; P = 238 mm) *vs.* wet years (i.e. 2012, 2013; P = 485 mm) after the site had reached over-story crown closure in 2010. In wet years, greater NPP was modelled in all the covers (asymptote at 478 g C m^{-2} y^{-1}) compared to dry years (asymptote at 386 g C m^{-2} y^{-1}). In dry years, a greater NPP increase (162 g C m^{-2} y^{-1}) was modelled with the highest *vs.* lowest AWHC as determined by cover depth whereas smaller NPP increases were modelled during intermediate (125 g C m^{-2} y^{-1}) and wet (123 g C m^{-2} y^{-1}) years (Figure 5.2). The 95% of maximum NPP was reached at 162 mm (similar to that of the 100 cm cover in the current study). Consequently tree growth increased little with AWHC greater than 162 mm (Figure 5.3).

5.3.2. Long-term changes in GPP and NPP in reclaimed landforms *vs.* regenerating natural forest under current and warming climates

Long-term modelling can help to forecast reclamation trajectories in constructed landforms with different cover depths. Modelled GPP and NPP under current climate increased exponentially in each cover during the first 15 years from start of reclamation (Figure 5.4b,c) and then approached a steady rate. After canopy closure, GPP and NPP variations followed the precipitation and temperature patterns particularly in 35 cm and 50 cm covers. Greater productivity differences were modelled among the three covers during the first 25 years, but later all the covers reached a similar average NPP during wet years. However during dry years, NPP in the 35 cm and 50 cm covers was nearly 100 g C m^{-2} y^{-1} lower than the NPP in 100 cm cover

after reaching the steady rate (Figure 5.4b). In 2021, 2038, 2055, 2072 and 2089 (same weather as in 2003), NPP declined to half of the average in each cover due to lower growing season precipitation particularly from May to August (*ca.* 65 mm). Modelled GPP and NPP in the natural site rose gradually during first 25 years and followed the same pattern as reclamation covers during later years (Figure 5.4a,b). However, slightly higher plant productivity in natural site *vs.* reclaimed sites was modelled in wet years following dry years. The average modelled NPP (2015 - 2099) in 35 cm, 50 cm and 100 cm covers compared to that of regenerating natural site under current climate were 90%, 95% and 98% respectively.

Long-term GPP and NPP patterns in these landscapes may change under future warming and concurrent rise in CO_2. Warming was accompanied by the increased precipitation (Figure 5.5a). The effect of 100 years of gradual rise in T_a and precipitation according to the RCP 8.5 climate change scenario (Table 5.2) on modelled GPP and NPP varied according to the reclamation cover depth. A clear warming effect on GPP and NPP started to become apparent after 50 years from start of reclamation (Figure 5.5b,c). The average NPP modelled after 100 years of gradual warming increased by 60 g C m^{-2} y^{-1} (14%), 66 g C m^{-2} y^{-1} (15%) and 100 g C m^{-2} y^{-1} (22%) in 35 cm, 50 cm and 100 cm covers, respectively compared to that modelled under current climate (Figure 5.5b). Smaller increases were modelled with shallower covers because during dry years under warming, NPP in the 35 cm and 50 cm covers declined by 5 % and 1% from NPP modelled under current climate respectively compared to the 100 cm cover, which increased NPP by 3% from NPP modelled under current climate.

Aspen productivity in the regenerating natural site responded strongly to warming (Figure 5.5b,c) and modelled average NPP increased by 240 g C m^{-2} y^{-1} (45%), a much greater increase than those in the reclamation landforms. In the natural site, greater increases in GPP and NPP

under warming *vs.* current climate were modelled in intermediate years (2047, 2064, 2081, 2098) following dry years (Figure 5.5b,c) due to increases in N uptake (data not shown). These increases were caused by reduced N uptake relative to mineralization in drier years that left more mineral N for uptake in following intermediate and wet years as described in Section 4.3.3 in Chapter 4.

The much greater increases in GPP and NPP modelled in the natural site than in the reclaimed sites were mainly attributed to nutrient availability. Low N mineralization and uptake rates and hence lower foliar N concentrations modelled (as described in Section 4.2.1.3 in Chapter 4) over 100 years under current climate (Table 5.3) indicated that long-term plant productivity in reclaimed covers was limited by the availability of soil N. Reductions in foliar N and P concentrations modelled over 100 years under warming *vs.* current climate (Table 5.3) indicated that both available N and P limited the GPP and NPP gains with warming in the reclaimed site. In contrast, greater increases in N mineralization and N uptake were modelled in the regenerating natural site under warming (Table 5.3). This greater N mineralization and uptake increased the rubisco activities and hence productivity of aspen in the natural site (as described in Section 4.2.1.3 in Chapter 4). Also greater modelled aspen and spruce foliar P concentrations indicated that plant productivity in the natural site was not limited by soil P availability. Lower modelled foliar P concentrations modelled in aspen and spruce in the reclaimed sites were mainly attributed to the greater average N:P ratio in PMM (15:1) compared to LFH (10:1) in the natural site (Lanoue, 2003).

Greater N mineralization and uptake modelled in the natural site (Table 5.3) was partly attributed to increases in T_s modelled in the LFH and upper 20 cm of the mineral soil at the natural site of 2 - 4 ^{0}C over those at similar depths in the PMM and subsoil at the reclaimed sites

(data not shown), particularly under warming due to aspect, slope and PFTs. Also greater C and N concentrations in LFH *vs.* PMM in reclaimed sites (as described in Section 4.3.1 in Chapter 4) facilitated the N mineralization in the natural site.

5.3.3. Changes of tree aboveground carbon biomass under current climate and climate warming

Under current climate, differences in tree aboveground carbon biomass among reclamation covers (Figure 5.6a) were mainly determined by the early tree growth as indicated by greater NPP differences among the covers during first 15 years (Figure 5.4b). After 50 years from start of reclamation, the 50 cm cover reached a similar aboveground carbon biomass as in the 100 cm cover (Figure 5.6a) due to greater NPP in later wet years. However, the differences during early regeneration in the 35 cm *vs.* 100 cm covers were maintained during the rest of the run. After 100 years from reclamation, modelled aboveground biomass in reclamation covers under current climate was ~ 85% of that in the regenerating natural site due to increased GPP and NPP in natural site *vs*. reclaimed sites during wet years following dry years (Figure 5.4).

Even though modelled GPP and NPP increased gradually with warming (Figure 5.5), the modelled carbon biomass in 35 cm and 50 cm covers under warming climate decreased compared to modelled values under current climate (Figure 5.6) whereas 100 cm cover had similar aboveground carbon biomass under warming climate to that modelled under current climate after 100 years. Modelled aboveground biomass in the natural site increased by ~46 % after 100 years under gradual warming (Figure 5.6) compared to the biomass modelled after 100 years under current climate. Therefore long-term modelled aboveground biomass in reclamation covers after 100 years of gradual warming was only 56% of that in the regenerating natural site. The lower biomass gains in reclaimed sites *vs.* natural site under warming climate were

attributed to the reduced GPP and NPP gains due to nutrient limitation particularly P in reclaimed sites as described in Section 5.3.2.

5.3.4. Long term effects of cover depth and warming on PFT changes

Changes of modelled aboveground carbon biomass under warming *vs.* current climate (Figure 5.6) were derived from changes in aspen and white spruce NPP. In the 35 cm cover, a small decline of white spruce NPP and hence biomass offset a small gain of aspen NPP and biomass under warming *vs.* current climate (Figures 5.7(a,b) and 5.8(a,b)). However, a greater decline in white spruce NPP and hence biomass and a greater gain in aspen NPP and biomass were modelled in the 50 cm cover under warming *vs.* current climate (Figures 5.7(c,d) and 5.8(c,d)). There was a small decline in modelled white spruce that was more than offset by a greater increase in modelled aspen in the 100 cm cover (Figures 5.7(e,f) and 5.8(e,f)) under warming *vs.* current climate. Overall, these results indicated a greater aspen *vs.* white spruce growth with increased cover depth and warming (Figures 5.7 and 5.8).

5.4. Discussion

5.4.1. Forest productivity in reclaimed sites under warming climate limited by the nutrient availability

Increases of average GPP and NPP in all the sites in response to warming in the current study were consistent with free air CO_2 enrichment (FACE) experiments (King et al., 2005; Norby et al., 2005; Stoy et al., 2008) which found productivity increase with CO_2 enrichment, as well as remote sensing (Ciais et al., 1995; Myneni et al., 1997) studies and modelling studies conducted by Grant et al. (2001, 2006a), Hickler et al. (2008), Grant (2014) and Mekonnen et al. (2016, 2018a), who found productivity increases in higher latitudes and in boreal forests under

warming. Productivity in boreal forests is constrained by temperature and length of growing season (D'Orangeville et al., 2016). Thus productivity increases with warming in the model were mainly attributed to greater length of growing season (Myneni et al., 1997; Mekonnen et al., 2018a) and hence duration of CO_2 fixation (Grant et al., 2011; Mekonnen et al., 2018b), and to more rapid carboxylation kinetics from greater Q_{10} in cooler climates (Bernacchi et al., 2001, 2003). These more rapid kinetics were sustained by increased plant N uptake under warming due to more rapid N mineralization from soil warming (Grant et al., 2006a). Thus, modelled GPP and NPP in reclaimed sites and natural forest site rose with warming according to the direct and indirect processes described in Sections 5.2.1.1 and 5.2.1.2.

The average increase of 240 g C m^{-2} y^{-1} in NPP modelled in natural site after 97 years of gradual warming was consistent with the average annual NPP increase (~ 200 g C m^{-2} y^{-1}) of temperate forests in New England, USA, modelled using HADGE global circulation model (GCM) and RCP 8.5 climate change scenario by Duveneck and Thompson (2017) over 90 years as well as greater NEP increase (200 g C m^{-2} y^{-1}) measured using eddy covariance by Stoy et al. (2008) in late successional (80 -100 years old) hardwood forest at Duke under ~7.5 ^{0}C increase of MAT. Also the percentage of modelled NPP increase (*ca.* 45 %) in natural site after 97 years of gradual warming and rising C_a was consistent with the percentage of NPP increase (*ca.* 32 %) estimated by Chen et al. (2000) in Canada's forests from 1895 to 1996 under increased T_a (~ 2 ^{0}C) and CO_2 fertilization (370 *vs.* 290 μmol mol^{-1}), and NPP increase (~40%) of fire disturbed boreal forest in Prince Albert, Canada over 100 years estimated by Peng and Apps (1999) with GISS GCM 2x CO2 climate change scenario plus increased atmospheric CO_2 (doubling over 100 years). Moreover, the percentage of aspen biomass increase (*ca.* 46 %) in natural site after 100 years of gradual warming and rising C_a compared to that under current climate was consistent

with the percentage increase in aspen biomass (*ca.* 40 %) measured after 7 years under elevated CO_2 in FACE experiment in Rhinelander conducted without N limitation (King et al., 2005). The use of high-emission representative concentration pathway (RCP 8.5) for climate change scenario (Table 5.2) may also contributed to the greater NPP modelled in natural site after 97 years of warming.

However the poor responses of GPP and NPP to warming modelled at the SBH reclamation covers *vs.* those at the regenerating natural site under warming indicated the limitations for plant growth in reclaimed landforms with increased T_a and precipitation. These limitations were;

(1) Lower nutrient availability: The modelled foliar N and P concentrations (as described in Section 4.2.1.3. in Chapter 4) in aspen and white spruce at SBH (Table 5.3) indicated severe long-term N and P limitations for plant growth in reclaimed sites particularly under warming. The modelled aspen foliar N and P concentrations in all the reclaimed sites (Table 5.3) particularly under warming climate were much lower than the optimum foliar concentration of 69 mg N g C^{-1} (Hansen, 1994) and 5 mg P g C^{-1} for aspen (Van den Driessche 2000). Theses lower and gradual declining foliar N and P concentrations indicated the gradual increase of nutrient limitation for plant growth in reclaimed sites. In addition, modelled N and P foliar concentrations in white spruce (Table 5.3) showed long-term severe N deficiency (< 21 mg N g C^{-1}) and severe P deficiency (< 2 mg P g C^{-1}) in all the reclamation sites particularly under warming (Ballard and Carter, 1986). The N mineralization rates in reclaimed sites as shown in Figure 4.1 in Chapter 4 remained steady with time after 2015 (Table 5.3) due to N accumulation in wood, roots and soil over time, leaving less N for mineralization and

uptake (Table 5.3). This caused gradual decline in foliar N concentration and lower productivity gains in reclaimed sites under warming. These modelled results were consistent with the FACE experiment (Norby et al., 2010) conducted in a deciduous sweet gum forest stand over 11 years in Tennessee with limited N availability which showed a greater decline of foliar N concentration (*ca.* 14 mg N g^{-1} C) and lower NPP gain (9%) under elevated CO_2 (550 μmol mol^{-1}) compared to current ambient CO_2 concentration. The gradual decline of foliar P concentration in aspen and white spruce under warming (Table 5.3) indicated that P limitation became more severe in reclaimed sites under warming. However, the modelled aspen foliar N concentration in natural site under current and warming climates was within the range (40 – 60 mg N g C^{-1}) measured by Chang et al. (2010) in eight natural aspen stands in the AOSR. Also modelled aspen foliar P concentration in natural site was greater than the optimum P concentration (> 5 mg P g C^{-1}) and hence indicated sufficient N and P availability for plant growth.

(2) Topographical effects: Reclaimed sites were constructed with 20% north facing slope. In the current study, lower NPP was modelled in the upper slope positions compared to lower slope positions as described in Section 2.4.6 in Chapter 2, particularly in the 35 cm and 50 cm covers. Hence the GPP and NPP gains averaged over slope positions in reclaimed sites were lower compared to the flat regenerating natural site. Also the north facing slope at SBH caused smaller increases in soil temperature particularly under warming due to the lower incoming solar radiation (Bonan, 2015). However the effect of aspect on plant productivity in the flat natural site was minimal and soil temperature increased more than at the reclaimed sites particularly under warming due to increased

solar radiation at the ground surface. The greater solar radiation at ground surface in natural site may also be attributed to the greater aspen dominance which has greater leaf turnover causing greater soil exposure in spring and fall.

(3) Limited root growth in lower soil layers: Compaction and salinity of mining waste under soil covers at SBH limited root growth and thereby plant growth (described in Section 2.3.2 in Chapter 2). Also limiting root growth to 25 cm below the overburden surface in the current study contributed to lower N and P uptake causing smaller GPP and NPP gains with warming climate.

(4) Competition among plant species: The natural site was aspen-dominant and reclaimed sites were mixed-wood forests. Thus competition among PFTs for light, water and nutrients might be also attributed to the lower productivity gains in reclaimed sites with warming climate. Also greater aspen leaf turn over (1 y^{-1}) increased the aspen litterfall in natural site compared to mixed-wood forests in reclaimed landforms. This more labile litterfall provided N for subsequent mineralization in modelled natural sites as described in Section 4.3.2 in Chapter 4.

5.4.1.1. Lower nutrient availability in reclaimed landforms *vs.* regenerating natural site determined by soil materials

Increased soil temperature through warming and greater organic C, N and P concentrations in LFH at the natural site increased the microbial activities and hence mineralization, non-symbiotic N_2 fixation, and nutrient uptake (Section 5.2.1.2.2). Thus aspen in natural sites fully benefits from the flush of N and P from decomposing LFH under warming. However, the modelled lower N mineralization, N uptake and hence lower foliar nutrient concentrations in aspen and white spruce indicated that GPP and NPP gains in reclaimed areas *vs.* natural site were

mainly limited by the nutrient availability particularly by P under climate change. Lower P availability in reclaimed sites at SBH *vs.* regenerating natural site was consistent with the field observations of Howell et al. (2017) and Dietrich (2018) who found lower P availability in reclaimed landforms with PMM *vs.* recovering natural sites from fire in AOSR, and greenhouse experiment of Pinno et al. (2012) who found a lower foliar P concentration in aspen grown on PMM (1.5 mg P g C^{-1}) compared to aspen grown on FFM (2.7 mg P g C^{-1}). Also in a laboratory incubation, Quideau et al. (2017) found a lower N and P release from PMM *vs.* FFM used for land reclamation due to wider C:P and N:P ratios in PMM than in the FFM. Severe N limitation in reclaimed sites under warming climate may be offset by (1) increased wet N deposition (Section 4.2.5.4 in Chapter 4) through increasing precipitation occurred concurrently with warming (Figure 5.5.a) and (2) increased non-symbiotic N_2 fixation under warming due to increased N demand, increased microbial biomass (*ca.* 20% over 100-year warming) and activities. However P limitation will not be offset by any environmental input. Thus P fertilization may be needed to achieve a productivity gain in reclaimed areas similar to natural sites under climate change.

5.4.1.2. Greater cover depth caused greater NPP under warming climate

The greater positive effect of warming and elevated C_a observed in the 100 cm cover *vs.* 35 cm and 50 cm covers, was driven by the greater AWHC and total N content in the 100 cm cover (Table 5.1). The productivity decline in 35 cm cover through soil drying from increased T_a was offset by the increased precipitation and reduced transpiration from elevated C_a that accompanied warming. Thus reduced transpiration with rising C_a may reduce the adverse effect of low AWHC in shallow covers during drier years. The NPP increase in 100 cm cover (*ca.* 22%) after 100 years of gradual warming was consistent with the percentage of NPP increase

(*ca.* 23%) measured by Norby et al. (2005) in FACE experiment using four different forest plantations under elevated CO_2 (550 μmol mol^{-1}) *vs.* atmospheric CO_2 concentration (376 μmol mol^{-1}) without N addition. However, a lower NPP enhancement (*ca.* 15%) was projected by Hickler et al. (2008) for boreal forest under climate change using LPJ-GUESS dynamic vegetation model. Thus modelled NPP after 100 years of gradual warming (Figures 5.4b and 5.5b) indicated that AWHC of 162 mm (similar to that in the 100 cm cover) was sufficient to reach these estimated increase of NPP of mature boreal mixed-wood forests (15% - 23%) under warming climate. However NPP gains in all of these reclaimed sites were limited by the soil nutrients compared to a regenerating natural site as described in the Section 5.4.1.

In this study, we assumed that ecosystem disturbances did not occur in the study sites over 100 years. However, the frequency and intensity of fires (Kasischke et al., 1995), insect outbreak (Kurz et al., 1995, 2008; Logan et al., 2003) and diseases are predicted to increase in boreal forest under warming. Therefore these uncertainties related to disturbances with warming need also to be considered when forecasting long term productivity.

5.4.2. Greater aspen *vs.* white spruce growth under warming

The aboveground carbon biomass gain over the 100 years modelled from white spruce growth was greater than that of aspen in 35 cm and 50 cm covers under current climate, because white spruce accumulates and retains more leaf area over time as described by Cannell (1982) due to lower leaf turnover (*ca.* 0.25 y^{-1}). Thus lower white spruce *vs.* aspen growth reduced the total aboveground biomass gain over 100 years under warming *vs.* current climate in 35 cm and 50 cm covers (Figures 5.7 and 5.8).

In the model, competition among PFTs for irradiance, water and nutrients was governed by vertical profiles of canopy leaf areas [C21a] and root lengths [C21b,c] driven by plant growth so

that different rates of C, nutrient and water uptake, transfer and release by each PFT determined its growth in the competitive environment (Mekonnen et al., 2018b). Deciduous PFTs were modelled with greater specific leaf area (SLA) and less clumping, allowing greater light interception, and with greater leaf N content and hence leaf CO_2 fixation capacity and g_c. Deciduous PFTs were also modelled with lower axial resistivity which, with greater g_c increased water uptake rates relative to conifer PFTs (Grant, 2015; Mekonnen et al., 2018b). Thus a greater water uptake rate was modelled and measured in aspen *vs.* spruce in the reclaimed sites as described in Section 2.3.3 in Chapter 2. Deciduous PFTs were also modelled with greater N requirements from greater leaf N content and more rapid leaf turnover and hence nutrient loss. Thus, faster growth of aspen relative to spruce was modelled with more favourable soil nutrient and water status that allowed more rapid N and water uptake in deeper covers and under warming. Warming in spring caused earlier leaf out and leaf expansion and later leaf fall (Mekonnen et al., 2018b) in aspen, hence more carbon uptake and growth that improved competion for resources. However, warming would also cause earlier dehardening and later hardening and hence more C uptake in conifers (Mekonnen et al., 2018a). The increased aspen *vs.* white spruce growth under warming in this study (Figures 5.7 and 5.8) was consistent with the modelling study of Cortini et al. (2012), who found a greater aspen growth than white spruce in mixed-wood forests under warming. In that study they suggested that increased aspen *vs.* spruce growth with increased mean annual temperature (MAT) may be due to either "aspen moderating effect on white spruce growth, limiting response of spruce to temperature increases due to light limitations or to more aggressive competition of aspen with white spruce for water and light under warming".

Rapid aspen *vs.* white spruce growth modelled in the reclaimed sites during the early reclamation period (< 20 years) particularly under warming (Figures 5.7 and 5.8) was consistent with observations by Chen and Popadiouk (2002) and Macpherson (2000) of rapid aspen *vs.* white spruce growth during the first 40 years of stand recovery after stand-replacing disturbances in boreal mixedwood forests. Even though white spruce growth measured in the field was very slow during early development, high productivity could be achieved in later in stand development as described by Man and Lieffers (1999) using natural unmanaged forest inventory. Thus early aspen dominent stands can be changed into white spruce dominent or co-dominent mixedwood forest (Macpherson, 2000) over the reclamation trajectory as modelled in the 35 cm and 50 cm reclamation covers (Figures 5.7 and 5.8). These observations corroborated model performances on dominant forest development in reclaimed sites under current and warming climates. In the current study, the 35 cm cover showed a greater tendency to develop spruce dominant forests under both current and warming climate. However, the 50 cm cover showed a greater tendency to develop white spruce dominant forest under current climate and mixed-wood forest under warming. The 100 cm cover showed a greater tendency to develop mixed-wood forest under current climate and aspen dominant forests under warming. These indicated that greater water uptake (as described in Section 2.3.3 in Chapter 2) and N uptake (as described in Section 4.4.3.1 in Chapter 4) of aspen *vs.* white spruce affected aspen competition with spruce and thereby determined the end stand type on these reclaimed sites. Modelling spruce dominant forest in 35 cm cover under current and warming climates indicated that greater nitrogen use efficiency in white spruce *vs*. aspen (as described in Section 4.4.4 in Chapter 4) enabled long term NPP and biomass growth in 35 cm cover with lower N mineralization and N availability (Table 5.3).

5.4.3. Estimating threshold AWHC for reclaimed landforms with saline sodic overburden under current climate

Previous modelling studies (described in Chapters 2, 3 and 4) indicated that AWHC was the main factor that controls the NPP in reclaimed sites since increased AWHC increased water uptake and transpiration (Chapter 2), reduced salinity effects (Chapter 3), and increased N mineralization and N uptake (Chapter 4). Therefore the relationship between AWHC and NPP could be used to derive the threshold cover depth for target NPP in reclaimed areas.

The modelled and measured results for θ, plant water uptake (U_c), ψ_c, and transpiration described in Chapter 2, indicated that thicker cover depth store more water and thereby maintain greater transpiration related to shallow cover depths particularly during dry years due to greater AWHC. The increased transpiration in thicker *vs.* shallow cover depths during dry and wet years (Table 2.4 in Chapter 2) increased CO_2 fixation and thereby GPP and NPP (Table 2.5 in Chapter 2 and Figure 5.2). Some plant growth reduction was modelled with salinity in shallow covers during dry years (Figures 3.4 - 3.6 in Chapter 3) but not during wet years, due to reduced osmotic water potential within the root zone. Also plant N status improved from increased mineralization (Figure 4.1 in Chapter 4 and Table 5.3) due to greater total nitrogen and AWHC as described in Chapter 4, increased CO_2 fixation in thicker covers (Table 4.3 and Figure 4.4(c) in Chapter 4). These processes caused smaller NPP differences to be modelled during wet years and greater NPP differences during dry years among hypothetical reclamation covers (Figure 5.2).

The strong non-linear relationship between AWHC as determined by the cover depth and modelled NPP (Figure 5.2) was derived from the non-linear relationship between AWHC and modelled transpiration (Figure 2.13(a)) and a positive linear relationship between modelled

transpiration and modelled NPP (Figure 2.13 (b)). The non-linear relationship between AWHC and transpiration was attributed to the potential transpiration (~ 250 mm) according to site conditions. After water uptake approached potential transpiration i.e. transpiration approaches atmospheric demand from *D*, increase of transpiration with further increase in AWHC was minimal. The linear relationship between transpiration and NPP (i.e. WUE) was attributed to the concurrent stomatal regulation of transpiration and CO_2 uptake [B2a] and hence carboxylation [C3].

The relationship between estimated AWHC and modelled NPP in hypothetical covers (Figure 5.2) indicated that the threshold AWHC for 95% of asymptotic NPP in the reclaimed sites of this study was 162 mm which was close to that estimated for the 100 cm cover. However the relationship between AWHC and cover depth is specific to the cover material; e.g. the PMM and subsoil material used in the current study. These modelling results were consistent with the findings from Huang et al. (2015) who found a strong non-linear relationship between cover depth and transpiration and little incremental increase of transpiration after cover depth exceeded 100 cm for the SBH site using HYDRUS-1D model. Also other previous field and modelling studies conducted on the three reclamation covers at SBH by Shurniak and Barbour (2002), Elshorbagy et al., (2007), Kelln et al. (2007), Keshta et al. (2010) and Meiers et al. (2011) have found that 100 cm reclamation cover depth was sufficient to provide soil moisture for plant growth during warm and dry summers inherent to this sub-humid climatic region. This depth was further corroborated by the modelled aboveground carbon biomass in hypothetical covers (Figure 5.3) which showed minimal biomass gain with AWHC greater than 162 mm. The minimal biomass gain after AWHC reached 162 mm was attributed to the non-linear relationship between AWHC and transpiration and linear relationship between transpiration and NPP.

The NPP in all the reclamation landforms and natural forest site modelled for 100 years under current climate levelled off at about 20-30 years after disturbances as described by Amiro et al. (2000) for regenerating forests in Boreal Plains of Alberta following fire, using a data set, satellite images and modelling. These modelled trajectories also followed the dynamics of stand-level NPP described by Kurz et al. (2013) in fire disturbed boreal forests, with NPP levelling off after ~30 years from a fire disturbance and remaining steady thereafter. The 100 cm cover enabled a long-term average NPP of ~ 400 g C m^{-2} y^{-1} to be modelled, similar to that of mature boreal mixed-wood forests (Gower et al., 2001; Kimball et al., 2006; Stinson et al., 2011) and to the upper limit of NPP in Alberta Boreal plains of *ca.* 366 ± 88 g C m^{-2} y^{-1} estimated by Amiro et al. (2000). This modelled NPP was attained earlier in the 100 cm cover than in the 35 cm and 50 cm covers. However after 25 years, all the covers reached similar NPP during wetter years. Reaching full productivity earlier with the 100 cm cover than with the other two covers will be important for commercial forestry, which is the most common end land use of reclaimed landforms in AOSR (Alberta Environment, 2010).

5.4.4. Summary

The non-linear relationship between AWHC as determined by cover depth and modelled NPP indicated that effect of AWHC on NPP was minimal after reaching a threshold AWHC under SBH site conditions (162 mm for the current study). The plant productivity at the SBH site showed negative effects of 35 cm cover depth on plant growth (AWHC = 58 mm for the current study), but less negative effects with greater than 50 cm cover depth (AWHC = 82 mm for the current study), and minimal effect with greater than 100 cm depth (AWHC = 162 mm for the current study). However, the suitable cover depth for reclamation is site-specific and mainly depends on the target land use and other factors such as mining waste, reclamation materials,

climatic conditions, topography, and PFTs. Even though 100 cm cover reached the most productive stage earlier than the other two covers, long term modelling under current climate projected that all the reclamation covers have ability to achieve productive forests similar to regenerating natural forest, after 25 years of reclamation. However, modelled foliar N and P concentrations and lower plant productivity gain in reclaimed sites *vs.* natural site under warming indicated long term N and particularly P limitations in reclaimed landforms constructed with PMM. This model finding indicated the requirement of proper P management at SBH to enable forest growth to respond to increasing C_a and warming climate. The modelled results also showed that aspen became increasingly dominant with increasing cover depth and warming. These projections could be changed with ecosystem disturbances such as fire, insect and disease outbreaks that have been predicted to increase under warming in boreal forests.

Collectively, results of this study demonstrate the ability of *ecosys* to predict the short and long-term forest productivity in reclaimed landforms with different cover depths without calibrating to a specific site so that *ecosys* model would be useful for further long-term studies in reclaimed areas with a wide range of reclamation materials, compositions, PFTs, and weather conditions.

Table 5.1. Average estimated available soil water holding capacity (AWHC), soil organic carbon (SOC), total N (TN) at the beginning of reclamation and modelled net primary productivity (NPP) of planted trees in hypothetical covers after the sites reached over-story crown closure (2011 - 2015).

Cover type	**AWHC** (mm)	**SOC** (Mg C ha^{-1})	**TN** (Mg N ha^{-1})	**NPP** (g C m^{-2})
35 cm	58	265	9.5	334
50 cm	82	359	12.9	391
60 cm	98	375	13.7	407
70 cm	114	392	14.6	424
80 cm	130	409	15.4	427
90 cm	146	425	16.2	430
100 cm	162	443	17.0	444
120 cm	194	475	18.7	449
140 cm	226	509	20.3	460
150 cm	242	525	21.2	468

[1] The AWHC was calculated using field measured FC and PWP values in each horizon of the soil profile on the basis of reclamation matterial (CEMA, 2006). SOC organic carbon (TOC) and total nitrogen (TN) were calculated using measured TOC and TN percentages in reclamation material of each layer respectively.

Table 5.2. Changes in seasonal maximum and minimum air temperatures, and precipitation predicted from climate normal (1981 - 2010) *vs.* (2070 - 2100) under RCP 8.5 climate change scenario ensemble projections downscaled and averaged across 15 CMIP5 models (Wang et al., 2016), and extracted from a corresponding grid cell within which the SBH site is located. Atmospheric carbon dioxide concentration (C_a) changes were derived from Meinshausen et al. (2011).

Season	**Changes from current value** (^{0}C)		**Ratio to current value** (Multiplier)	**Ratio to current value** (Multiplier)
	Max. Temp	**Min. Temp**	**Precipitation**	**Atmospheric CO_2 concentration**
Winter	4.5	6.8	1.4	1.9
Spring	4.9	5.3	1.3	1.9
Summer	5.3	5.4	1	1.9
Autumn/Fall	5.2	5.6	1.2	1.9

Table 5.3. Modelled nitrogen (N) mineralization, tree N uptake and foliar total N and phosphorous concentrations of aspen and white spruce in reclaimed covers (35 cm, 50 cm and 100 cm) and a regenerating natural site with a 17-year recurring sequence of weather data (i.e. same weather as in 2013) under current (B= benchmark) and warming climate (CC) over 100 years.

Year	Cover type							
	35 cm B	35 cm CC	50 cm B	50 cm CC	100 cm B	100 cm CC	Natural B	Natural CC
N mineralization ($g\ N\ m^{-2}\ y^{-1}$)								
2013	3.2	3.2	3.3	3.3	3.5	3.5	4.4	4.7
2031	2.0	2.1	2.2	2.4	2.3	2.4	5.7	6.3
2048	2.0	2.3	2.3	2.7	2.4	2.7	5.8	6.7
2065	2.1	2.4	2.3	2.9	2.5	3.0	6.4	7.6
2082	2.2	2.5	2.5	3.2	2.7	3.3	6.1	8.6
2099	2.4	2.8	2.6	3.5	2.7	3.6	6.3	9.7
N uptake ($g\ N\ m^{-2}\ y^{-1}$)								
2013	3.7	3.8	3.9	3.9	4.3	4.3	1.2	1.4
2031	1.9	2.1	2.1	2.4	2.3	2.8	4.7	5.3
2048	1.8	2.2	2.1	2.2	2.3	3.0	5.1	5.8
2065	1.8	2.3	2.1	2.9	2.4	3.0	5.6	6.8
2082	1.9	2.5	2.1	3.1	2.4	3.2	5.6	7.9
2099	1.9	2.6	2.2	3.4	2.5	3.7	5.8	9.1
Aspen foliar total (structural + non-structural) N concentration ($mg\ N\ g\ C^{-1}$)*								
2013	40	38	40	38	40	38	33	32
2031	30	27	28	26	28	26	45	42
2048	32	29	32	27	28	26	45	41
2065	31	28	32	26	28	25	45	39
2082	31	28	31	26	28	25	43	40
2099	31	29	31	25	28	24	43	35
Aspen foliar total (structural + non-structural) P concentration ($mg\ P\ g\ C^{-1}$)*								
2013	4.9	4.8	4.8	4.5	4.7	4.4	7.8	7.9
2031	3.8	3.2	3.8	3.3	3.7	3.2	8.9	8.5
2048	3.9	3.2	4.1	3.0	3.5	2.8	9.4	8.0
2065	3.9	3.0	4.3	3.0	3.5	2.7	9.9	7.8
2082	3.9	3.0	4.4	3.0	3.6	2.7	8.9	8.8
2099	4.1	3.2	4.4	2.9	3.9	2.6	8.4	10
White spruce foliar (structural + non-structural) N concentration ($mg\ N\ g\ C^{-1}$)*								
2013	25	23	24	23	24	23	13	13
2031	16	15	17	17	18	17	24	21
2048	16	15	16	16	18	16	29	26
2065	16	15	16	15	17	16	29	25
2082	16	14	16	15	17	15	28	25
2099	15	14	16	14	17	14	28	24
White spruce foliar (structural + non-structural) P concentration ($mg\ P\ g\ C^{-1}$)*								
2013	3.1	3.0	3.0	2.8	2.7	2.6	2.9	3.0
2031	1.7	1.6	1.9	1.9	2.0	1.8	5.7	5.5
2048	1.7	1.6	1.8	1.8	2.0	1.7	6.7	5.6
2065	1.7	1.6	1.8	1.7	2.0	1.7	7.4	5.0
2082	1.7	1.5	1.9	1.7	2.0	1.6	6.4	5.7
2099	1.8	1.5	1.9	1.6	2.0	1.6	5.6	6.6

* Modelled foliar N or P concentrations in July of each year.

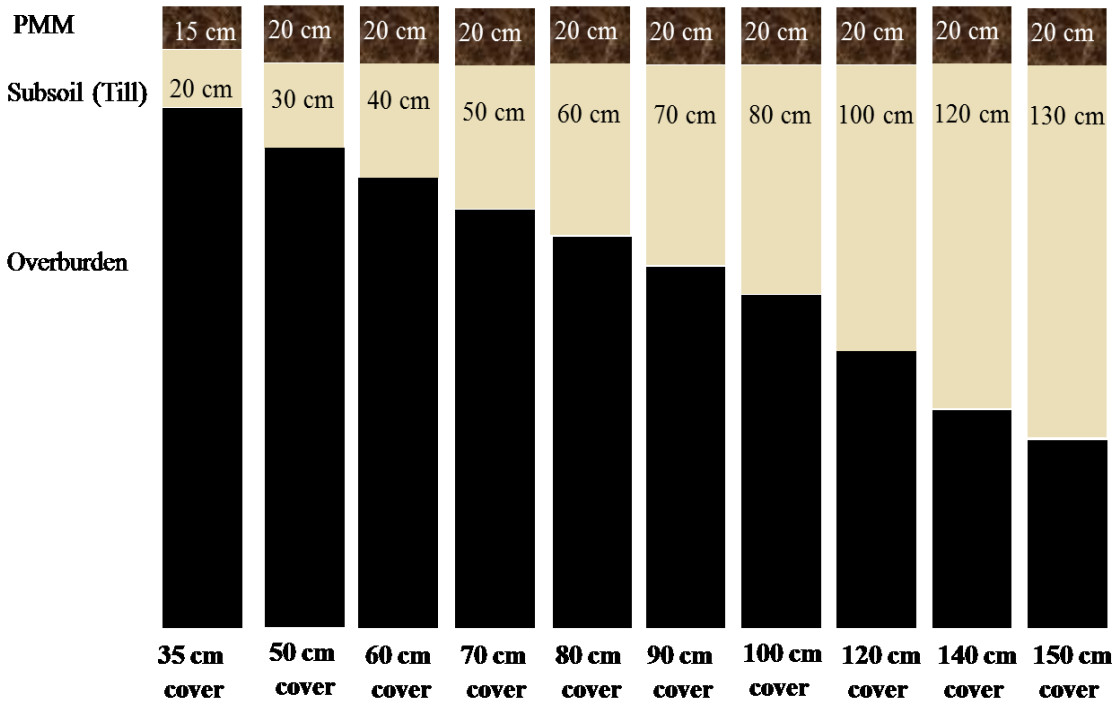

Figure 5.1. Schematic diagram of hypothetical soil covers. The thickness of PMM layer was set to 20 cm for all the covers except 35 cm cover and subsoil depths were changed to get different hypothetical cover depths.

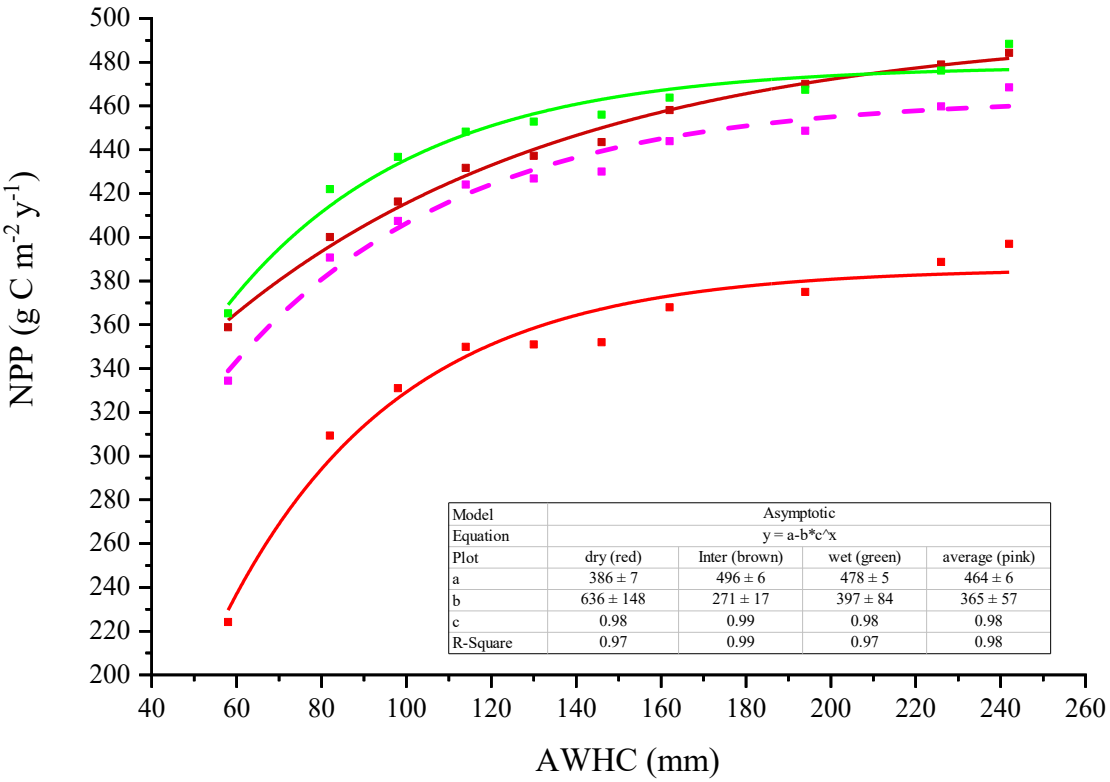

Model	Asymptotic			
Equation	y = a-b*c^x			
Plot	dry (red)	Inter (brown)	wet (green)	average (pink)
a	386 ± 7	496 ± 6	478 ± 5	464 ± 6
b	636 ± 148	271 ± 17	397 ± 84	365 ± 57
c	0.98	0.99	0.98	0.98
R-Square	0.97	0.99	0.97	0.98

Figure 5.2. The relationship between available soil water holding capacity (AWHC) and modelled net primary productivity (NPP) of planted trees in dry (2011, red), wet (2012 and 2013, green) and intermediate years (2014 and 2015, brown) in different hypothetical covers after planted trees had reached the over-story crown closure under current climate. Dash pink line represents the average modelled NPP changes with estimated AWHC for the 2011- 2015 period.

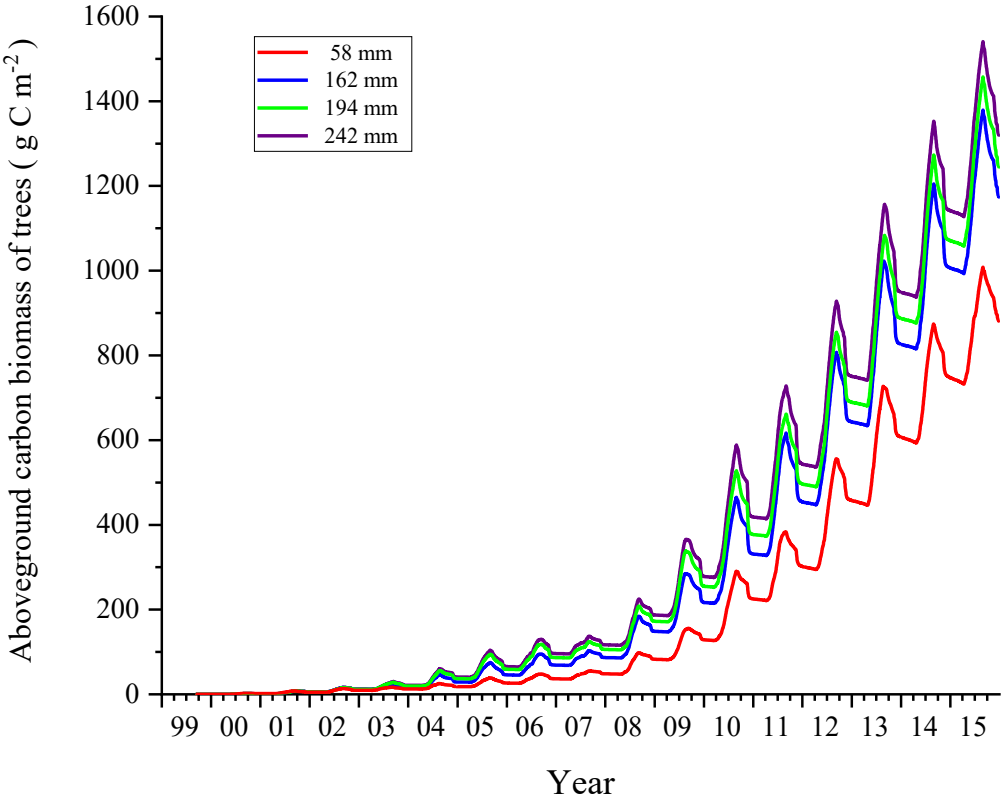

Figure 5.3. Modelled total tree aboveground carbon biomass since site construction averaged over slope positions in 58 mm (red), 162 mm (blue), 194 mm (green) and 242 mm (brown) AWHC that are determined by cover depths of 35 cm, 100 cm, 120 cm and 150 cm respectively.

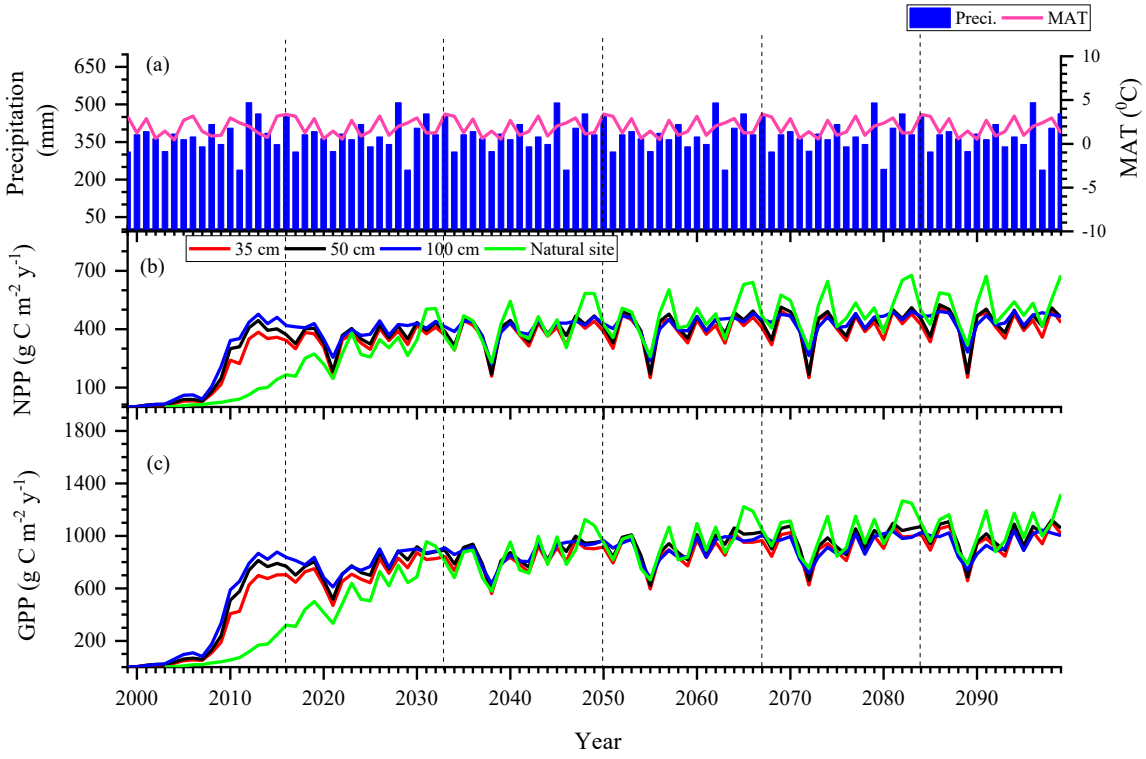

Figure 5.4. (a) Annual precipitation and mean annual air temperature (MAT) modelled from repeated sequences of 1999 - 2016 weather data over 100 years and modelled long-term tree (b) NPP and (c) GPP in regenerating natural site (green) (2003 - 2099) and averaged over slope positions in 35 cm (red), 50 cm (black), 100 cm (blue) covers (1999 – 2099) under current climate. Verticle dash lines represent the repeated sequences of weather data.

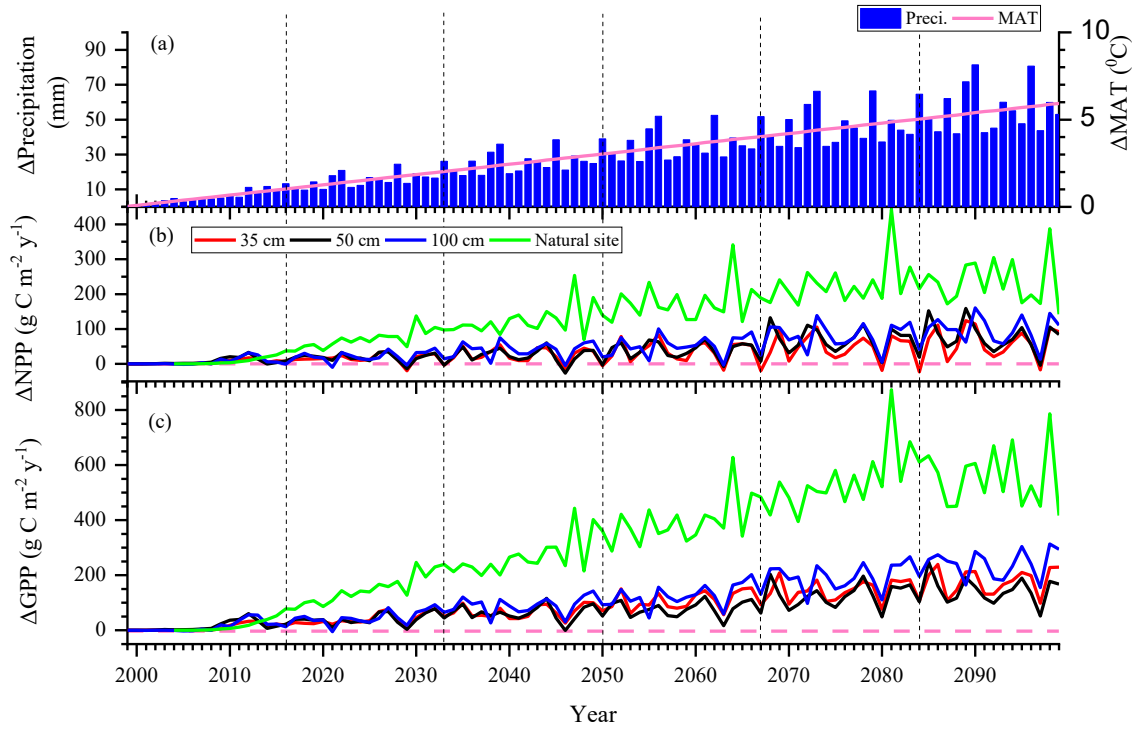

Figure 5.5. (a) Changes in mean annual air temperature (MAT) and changes in annual precipitation from those in Fig. 5.4a modelled from repeated sequences of 1999-2016 weather data with RCP 8.5 climate scenario ensemble projections over 100 years and modelled long-term changes in planted tree (b) NPP and (c) GPP in regenerating natural site (green) (2003 - 2099) and averaged over slope positions in 35 cm (red), 50 cm (black), 100 cm (blue) covers (1999 - 2099) under warming. Verticle dash lines represent the repeated sequences of weather data and horizontal pink dash line represent zero change of productivity.

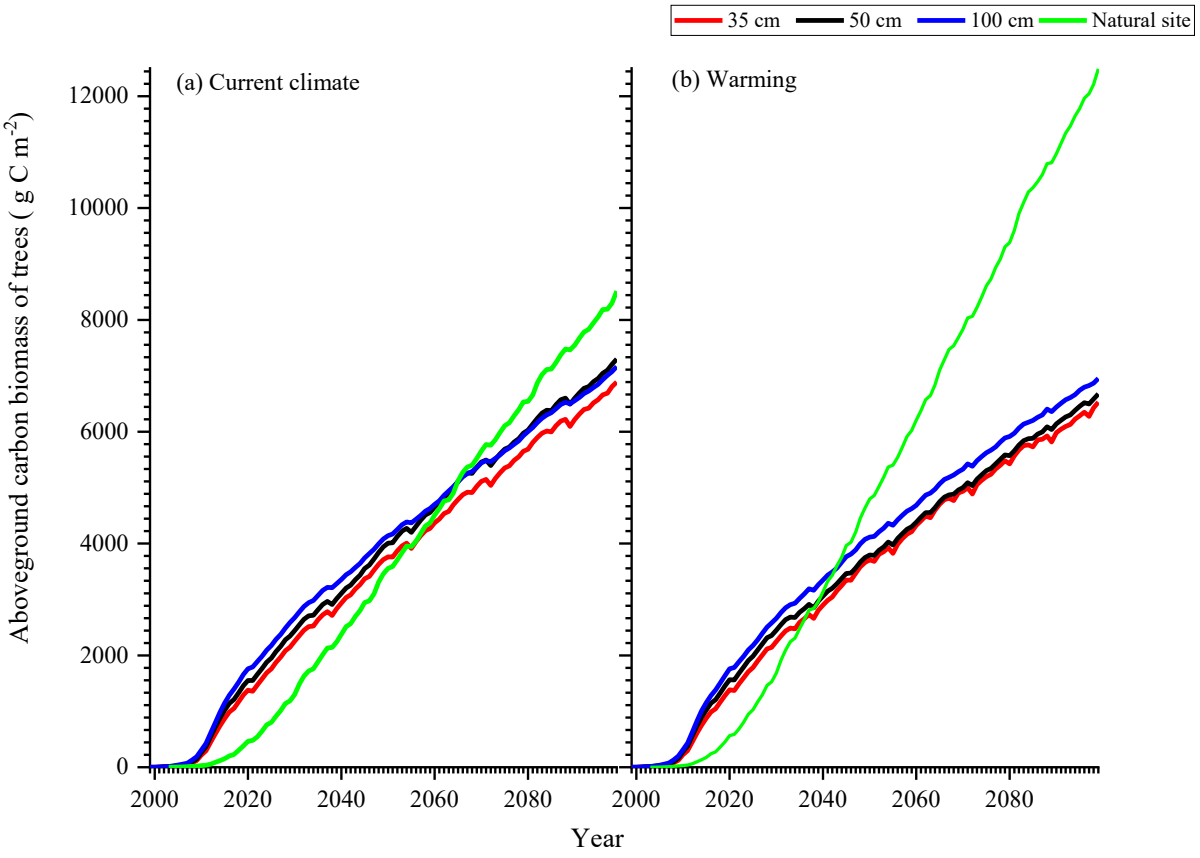

Figure 5.6. Modelled cumulative aboveground carbon biomass in regenerating natural site (green) and averaged over slope positions in 35 cm (red), 50 cm (black) and 100 cm (blue) covers (a) under current and (b) gradual warming climate.

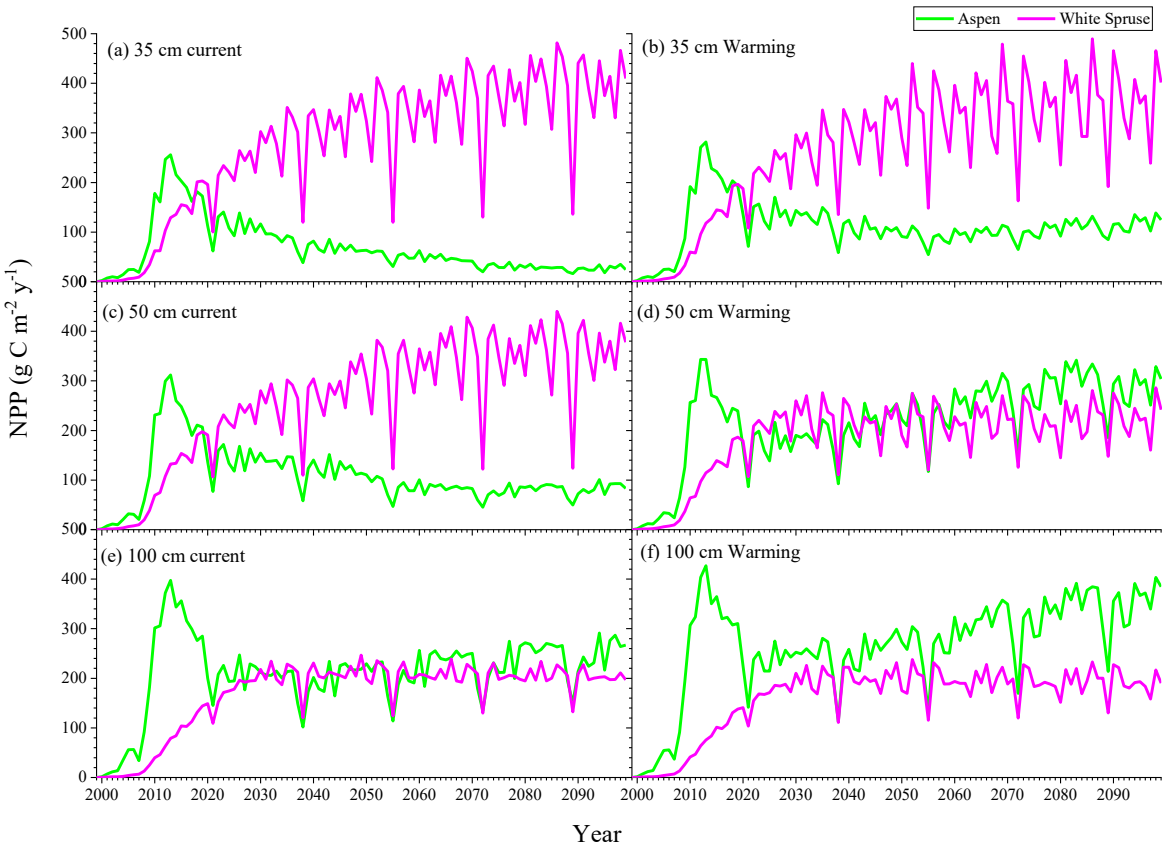

Figure 5.7. Modelled NPP of aspen (green) and white spruce (pink) averaged over slope positions in 35 cm, 50 cm and 100 cm covers under current and gradual warming climate.

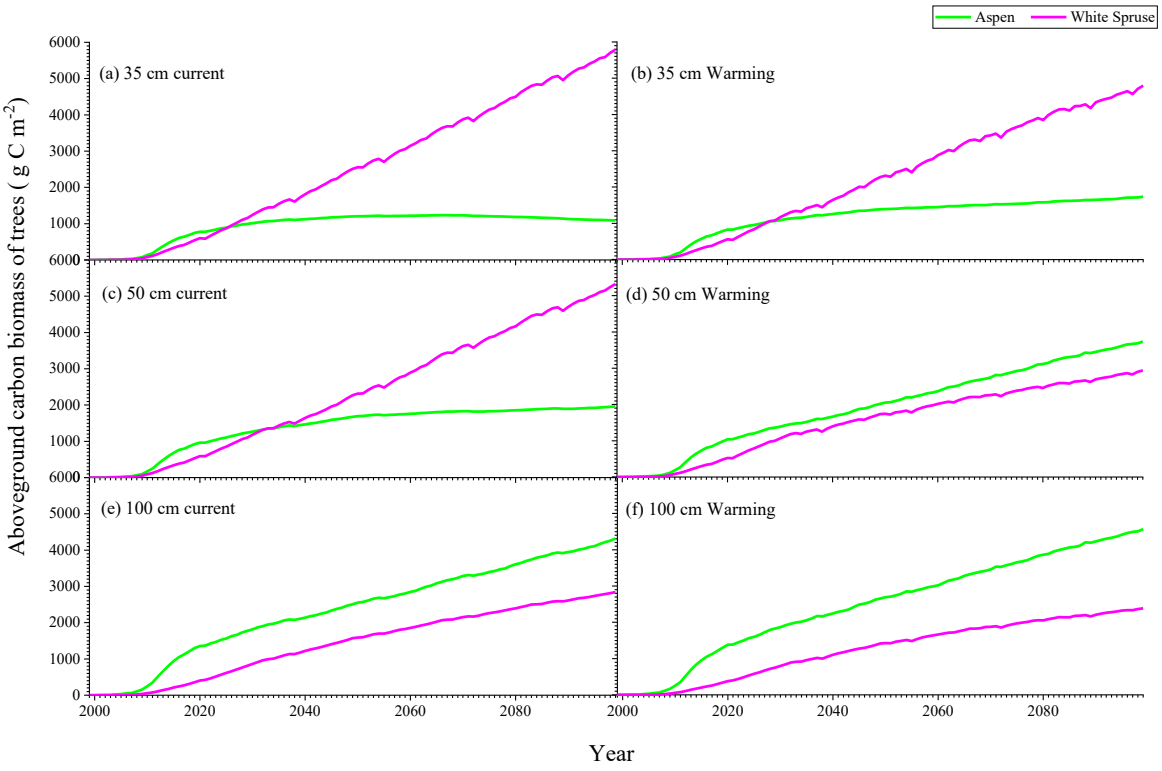

Figure 5.8. Modelled cumulative aboveground carbon biomass of aspen (green) and white spruce (pink) averaged over slope positions in 35 cm, 50 cm and 100 cm covers under current and gradual warming climate.

Chapter 6

Chapter Summaries and Conclusions

6.1. Chapter summaries

In the current study**,** a process based ecosystem model, *ecosys* was used to forecast short and long-term effects of reclamation cover depth on soil moisture, salinity, nitrogen (N) availability and thereby plant productivity in different reclamation covers. Model hypotheses for depth effects on plant water uptake, solute concentration in root zones, N mineralization and hence plant productivity were tested with three different reclamation covers (35 cm, 50 cm and 100 cm) at a 17-year-old forest reclamation site on an overburden dump constructed with saline sodic overburden material, capped with a cover soil, and planted with trembling aspen and white spruce at the Syncrude Mildred Lake mine site in northern Alberta (Canada). The changes in soil moisture, rooting depth, tree water-use, salt concentrations, soil and foliar N concentrations and aboveground tree biomass modelled with soil cover depth followed the same trends as those of independent measurements. The key findings of each study are summarized below. However, the relationships developed during each study are specific to the PMM and mineral subsoil materials used in this study, and would change with a different capping material (*e.g.*, LFH). Also the suitable cover depth for reclamation is site specific and mainly depends on end land use and other factors such as quality of mining waste and reclamation materials, climatic conditions, topography, and PFTs.

Chapter 2: Modelling hydrological characteristics and plant water-use efficiency as affected by soil cover depth in reclaimed forestlands of Northern Alberta

(i) Increases in θ, tree water uptake and hence CO_2 fixation, and tree growth from 35 cm and 50 cm covers to 100 cm cover were attributed to increases in available soil water holding capacity (AWHC) with cover depth. Greater tree water uptake in 100 cm *vs.* other two covers was further enabled by the modelled deeper root system that was corroborated by deeper measurements of root mass density.

(ii) The cover depth effect on transpiration was tested against the field measured aspen and white spruce sap flow in 35 cm and 100 cm covers, which showed a significant ($p < 0.001$) relationship ($R^2 > 0.5$) with modelled tree water uptake/transpiration.

(iii) The model clearly simulated less plant water uptake and productivity particularly in upper slope positions during drier years which were consistent with the field observations.

(iv) Since transpiration increased non-linearly with AWHC, increases in cover depth and hence in AWHC will have little effect on transpiration beyond the depth at which the maximum transpiration is approached. Because NPP increased linearly with transpiration, the relation between transpiration and AWHC indicates the importance of optimizing AWHC to achieve target NPP for the reclaimed sites.

Chapter 3: Modelling salt redistribution as affected by cover depths and topography in reclaimed saline-sodic overburden upland forests of Northern Alberta

(i) The modelled results suggested that the upward salt diffusion from overburden to cover soil was influenced by the cover depth and soil water content.

(ii) Some plant growth reduction was modelled with salinity from upward salt diffusion into shallow covers during dry years. However a clear relationship between root zone salt concentrations and biomass growth was not apparent in the model results.

(iii) Upward salt diffusion into the covers equilibrated with salt removal from the covers through convection with downslope water movement over time, maintaining stable salt concentrations in the root zone. This equilibration indicated that long term plant growth in the covers may not be affected by the salinity in the overburden.

(iv) A clear steady topographical effect was not found for salinity in the reclamation covers during the study period. However, salt removal and consequent discharge with downslope water flow from the covers indicated a risk of salinization in downslope areas.

Chapter 4: Modelling nitrogen mineralization and plant nitrogen uptake as affected by soil cover depth in reclaimed upland forestlands of Northern Alberta

(i) Greater profile net N mineralization and N uptake were modelled in the 100 cm cover *vs.* the 35 cm and 50 cm covers particularly during dry and intermediate years.

(ii) The θ greatly influenced the net N mineralization in each cover over the reclamation period. However, modelled net N mineralization rates relative to TN decreased with increasing cover depth and hence TN due to reduced microbial activities from lower temperature and O_2 concentrations in deeper soil.

(iii) Modelled and measured foliar N concentrations did not vary with cover depth. However lower N uptake modelled in shallow covers caused lower NPP, particularly in wet years during which water stress or salinity effects were not apparent.

(iv) Modelled NPP increased linearly with N uptake from the three reclamation covers (Figure 4.4(c)). However a non-linear relationship was modelled between TN and N mineralization that drove tree N uptake from the covers (Figure 4.3(b)). This relationship indicated that increasing cover depth and hence TN beyond that at which maximum N uptake is approached will have little effect on NPP.

(v) Nitrogen deficiency in all the covers for aspen and white spruce growth was evident by the modelled and measured foliar N concentrations.

(vi) The 100 cm cover showed greater foliar production and thereby greater litterfall and N return to soil than in the 35 cm and 50 cm covers ensuring earlier establishment of N cycling in the 100 cm cover similar to that in natural sites recovering after severe fire disturbances.

Chapter 5: Modelling long-term effects of reclamation cover depth on forest regeneration in reclaimed landscapes in Northern Alberta under current and future climates

(i) The non-linear relationship between AWHC as determined by cover depth and modelled NPP indicated that effect of AWHC on NPP was minimal after reaching a threshold AWHC at SBH (162 mm for the current study).

(ii) Even though the 100 cm cover reached full productivity earlier than did the other two covers, long term modelling under current climate projected that all the reclamation covers would achieve productivity similar to thst of a regenerating natural forest after 25 years of reclamation.

(iii) Lower NPP gains modelled in reclaimed sites *vs.* natural site under a warming climate were attributed to long term nutrient limitations, particularly P, in reclaimed covers.

(iv) These projections could be changed with ecosystem disturbances such as drought, fire, insect and disease outbreaks that have been predicted to increase under warming in boreal forests.

6.2. Model uncertainties due to uncertainties in model inputs

The current modelling study included a few assumed model inputs that might have caused uncertainties in modelled results. These sources of potential uncertainties are discussed below.

(1) Rooting depth: Soil resistance equations used in the model for root growth in crops (Da Silva and Kay,1997; Chen and Weil, 2011) did not limit root penetration into modelled overburden as much as was observed in the field due to different soil characteristics in overburden *vs.* natural soil profiles. Following root assessment in the field as conducted in 2013, maximum rooting depth of each cover was forced to be limited to 25 cm below the cover-overburden interface. However, the forced maximum root depth was based on empirical evidence from only one year of study and hence may still be uncertain. Moreover, limiting the maximum root depth also prevented additional root development to be modelled into the overburden with time, which limited the long-term uptake of water and nutrient from overburden. The greater modelled *vs.* measured soil moisture content at 42 cm depth (Figure 2.2a in Chapter 2) and consequent underestimation of water uptake in Figure 2.6b,d suggest that there may have been more plant water uptake from the overburden in 35 cm cover than was modelled particularly during dry period. However, water uptake modelled in the 100 cm cover was not underestimated (Figure 2.6c,e) particularly during dry period, even with the same limitation to water uptake from the overburden. Therefore vegetation in the 100 cm cover indicated minimal or no water use from the overburden. This further suggests

that plants in shallow covers have ability to draw more water from the overburden than was modelled, particularly during dry years.

(2) Soil properties: Measured soil properties such as bulk density, volumetric water contents at field capacity (θ_{FC}) and permanent wilting point (θ_{PWP}), and organic C and N concentrations in the PMM and subsoil varied among the three covers. However average values were used for each material in all reclamation covers so that modelled differences in soil and plant water, nutrient status and in plant growth could be attributed only to the capping depth. The use of average θ_{FC} and θ_{PWP} for each material in all reclamation covers may have contributed to RMSD in soil moisture as described in section 2.3.1 in Chapter 2.

The average θ_{FC} and θ_{PWP} of PMM and subsoil derived from field measurements with TDR probes were lower than those measured in the lab (Huang et al., 2015, Figure 2). This caused a lower AWHC in the field than was estimated from measured values in the lab. This difference was described by Huang et al. (2015a) using the dual-porosity characteristics of the reclamation materials and van Genuchten model (VGM) considering water flow in micropores (immobile) and macropores (mobile). However the use of the modified Campbell method in *ecosys* to model soil moisture retention with this lower AWHC may also have contributed to the variation between modelled and measured θ as indicated in Figures 2.2 and 2.3 in Chapter 2 and hence RMSD in soil moisture of each reclamation cover.

(3) Nutrient availability: Detailed in-situ nutrient assessments were not conducted in the different reclamation covers, particularly for P. Thus, the N:P ratio in subsoil and overburden was assumed as 10:1. This ratio affected the relative limitations to plant

growth imposed by N and P in the model. Lack of measured soil and vegetation N and P data also limited the validation of modelled nutrient outputs.

6.3. Implications for land reclamation

In *ecosys*, the effect of cover depth on short and long-term water availability and movement, plant water relations, salinity in the rooting zone, net N mineralization, N uptake and hence biomass production were modelled from basic soil-plant-atmosphere hydrological processes, the parameters of which were derived from basic research conducted independently from the current study and so remained unchanged from those used in earlier studies as stated in the supplement. Model findings should therefore be robust. Also the results of this study demonstrated the ability of *ecosys* to predict the cover depth required to achieve target NPP in reclaimed upland areas as determined by site conditions, cover compositionand end land use without calibrating to a specific site. Therefore *ecosys* would be useful for further studies in reclaimed areas with a wide range of reclamation materials and depths, compositions, PFTs, weather and management conditions. Model findings established the requirements for reclamation success in recovering target NPP according to the end land-use or ecosite by quantifying:

(i) Sufficient cover depth to achieve threshold AWHC to avoid water stress and salt stress during dry years, and to facilitate N mineralization and N cycling, thereby reducing N limitation for plant growth.

(ii) How cover depth influences the growth of different plant functional types.

(iii) How water movement down artificial slopes affects NPP.

(iv) Long term salinity effects on forestland productivity.

(v) How to ensure appropriate reclamation cover depth over steep SSOB lands to prevent salinization of surrounding lands and to prevent osmotic stress particularly in early reclamation period.

(vi) Contribution of legumes to N mineralization in reclaimed sites. Also how P fertilization might avoid P limitation to plant growth, particularly under warming climate.

6.4. Concluding remarks

The model outputs in the current study were closely aligned with results from other independent modelling and field studies conducted at SBH, providing more confidence for the findings of these studies. Also this study demonstrated the potential of *ecosys* for assessing short and long-term plant productivity in oil sands reclamation covers. In addition, the study has provided detailed descriptions for processes and field measurements in reclaimed covers using basic fundamental theories, and an integrated assessment of water, salinity, nutrient and carbon cycling, and their interactions, for different reclamation cover depths constructed on a reclaimed landform. Long-term modelling with a RCP 8.5 climate change scenario indicated that nutrients particularly phosphorous would limit the plant growth in reclaimed areas compared to that in regenerating natural sites, which has not been examined through previous modelling or field studies. Therefore this study indicated that *ecosys* is a useful tool for oil sands operators and regulators in conducting integrated assessments of water, salinity, nutrients and their interactions, and thereby forecasting land capability for reclamation soil covers of different depths under different climatic conditions particularly under climate change. Collectively, findings of this study and *ecosys* are helpful to assess long-term reclamation cover designs and strategies in the future.

References

Alberta Energy, 2018. 'Facts and Statistics'. https://www.energy.alberta.ca/OS/AOS/Pages/FAS.aspx. Accessed 20/05/ 2018.

Alberta Energy Regulator, 2015. 'Environmental Protection and Enhancement Act', Approval No. 26-02-09. Approval to Syncrude Canada Limited for construction, operation, and reclamation.

Alberta Environment, 2007. 'Specified gas emitters regulation – Quantification protocol for afforestation projects'. Environmental monitoring and evaluation, Alberta Environment. Edmonton, Alberta.

Alberta Environment, 2010. 'Guidelines for Reclamation to Forest Vegetation in the Athabasca Oil Sands Region', 2nd Edition. Prepared by the Terrestrial Subgroup of the Reclamation Working Group of the Cumulative Environmental Management Association, Fort McMurray, AB.

Alberta Environment, 2014. Alberta's oil sands [online]. Available by Alberta Government, http://oilsands.alberta.ca/resource.html. Accessed 20/05/ 2014.

Alberta Environment and Parks, 2014. 'Airdata'. http://airdata.alberta.ca/aepContent/Reports/DataReports.aspx. Accessed 14/01/ 2015.

Alberta Environment and Water. 2012. 'Best management practices for conservation of reclamation materials in the mineable oil Sands region of Alberta'. Prepared by MacKenzie, D. for the Terrestrial Subgroup, Best Management Practices Task Group of the Reclamation Working Group of the Cumulative Environmental Management Association, Fort McMurray, AB. March 9, 2011.

Amiro, B.D., Chen, J.M., Liu, J., 2000. Net primary productivity following forest fire for Canadian ecoregions. Can. J. For. Res. 30, 939-947.

Amos, R.T., Blowes, D.W., Bailey, B.L., Sego, D.C., Smith, L., Ritchie, A.I.M., 2015. Waste-rock hydrogeology and geochemistry. Appl. Geochem. 57,140–156.

Anghinoni, I., Barber, S.A., 1980. Phosphorus influx and growth characteristics of corn roots as influenced by phosphorus supply. Agron. J. 72, 685–688.

Angstmann, J.L., Ewers, B.E., Barber, J., Kwon, H., 2013. Testing transpiration controls by quantifying spatial variability along a boreal black spruce forest drainage gradient. Ecohydrol. 6, 783–793.

Appels, W.M., Wall, S.N., Barbour, S.L., Hendry, M.J., Nichol, C.F., Chowdhury, S.R., 2017. Pyrite weathering in reclaimed shale overburden at an oil sands mine near Fort McMurray, Canada. Mine Water Environ. 36 (4), 479-494.

Ballard, T.M., Carter, R.E., 1986. Evaluating forest stand nutrient status. Land Manage. Rep. No. 20, Ministry of Forests, Victoria, British Columbia, 60 pp.

Barbour, S.L., Chanasyk, D., Hendry, J., Leskiw, L., Macyk, T., Mendoza, C., Naeth, A., Nichol, C., OKane, M., Purdy, B., Qualizza, C., Quideau, S. and Welham, C. 2007. Soil capping research in the Athabasca oil sands region volume 1: Technology synthesis. Syncrude Canada Ltd., Fort McMurray, AB.

Beckingham, J.D., Archibald, J.H., 1996. Field guide to ecosites of northern Alberta. Nat. Resour. Canada., Can. For. Serv., North. For. Centre, Edmonton, Alberta.

Bernacchi, C., Pimentel, C., Long, S. 2003. In vivo temperature response functions of parameters required to model RuBP-limited photosynthesis Plant. Cell Environ. 26, 1419-1430.

Bernacchi, C., Singsaas, E., Pimentel, C., Portis, A., Jr., Long, S., 2001. Improved temperature response functions for models of Rubisco-limited photosynthesis. Plant Cell Environ. 24, 253–259.

Bleby, T.M., Burgess, S.S.O., Adams, M.A., 2004. A validation, comparison and error analysis of two heat-pulse methods for measuring sap flow in *Eucalyptus marginata* saplings. Funct. Plant Biol. 31, 645–658.

Bockstette, S.W., Pinno, B.D., Dyck, M.F., Landhäusser, S.M., 2017. Root competition, not soil compaction, restricts access to soil resources for aspen on a reclaimed mine soil. Botany. 95, 685-695.

Boese, C. D., 2003. The design and installation of a field instrumentation program for the evaluation of soil-atmosphere water fluxes in a vegetated cover over saline/sodic shale overburden. M.Sc. Thesis. University of Saskatchewan, Saskatoon, SK.

Bonan, G. 2015. Atmospheric Radiation. In Ecological Climatology: Concepts and Applications.3rd ed. Cambridge University Press. Cambridge, UK . pp. 61-73.

Boone, R.D. 1992. Influence of sampling date and substrate on nitrogen mineralization: comparison of laboratory-incubation and buried-bag methods for two Massachusetts forest soils. Can. J. For. Res. 22: 1895–1900.

Bradshaw, A., 1997. Restoration of mine lands – using natural processes. Ecol. Eng. 8, 255-269.

Bresler, E., 1973. Simultaneous transport of solutes and water under transient unsaturated flow conditions. Water Resour. Res. 9, 975-986.

Burgess, S.S.O., Adams, M.A., Turner, N.C., Beverly, C.R., Ong, C.K., Khan, A.A.H., Bleby, T.M., 2001. An improved heat pulse method to measure low and reverse rates of sap flow in woody plants. Tree Physiol. 21, 589–598.

Burton, P.J., 1993. Some limitations inherent to static indices of plant competition. Can. J. For. Res. 23, 2141–2152.

Buttle, J.M., Creed, I.F., Moore, R.D., 2005. Advances in Canadian forest hydrology, 1999-2003. Hydrol. Process. 19, 169-200.

Campbell, G. S., 1974. A simple method for determining unsaturated conductivity from moisture retention data. Soil Sci. 117, 311–314.

Cannell, M.G.R., 1982. World forest biomass and primary production data, Academic Press. London. 391 pp.

Carey, S.K., 2008. Growing season energy and water exchange from an oil sands overburden reclamation soil cover, Fort McMurray, Alberta, Canada. Hydrol. Process. 22:2847-2857.

Carmosini, N., Devito, K.J., Prepas, E.E., 2003. Net nitrogen mineralization and nitrification in trembling aspen forest soil on the Boreal Plain. Can. J. For. Res. 33, 2262-2268.

CEMA., 2006. Land Capability Classification System for Forest Ecosystems in the Oil Sands, 3rdEdition, A document prepared for Alberta Environment by the Cumulative Environmental Management Association. Edmonton, Alberta.

Chaikowsky, C.L.A, 2003. Soil moisture regime and salinity on a tailings sand storage facility. M.Sc. Thesis. University of Alberta, Edmonton, AB.

Chang, S., Yan, E., Hu, Y., 2010. Soil nitrogen indicators for land reclamation policy development for forest ecosystems in the oil sands region of Alberta. Report submitted to the Cumulative Environmental Management Association, Fort McMurray, AB.

Chen, G., Weil, R.R., 2011. Root growth and yield of maize as affected by soil compaction and cover crops. Soil Tillage Res. 117, 17–27.

Chen, H.Y.H., Klinka, K., Kabzems, R.D., 1998. Site index, site quality, and foliar nutrients of trembling aspen: relationships and predictions. Can. J. For. Res. 28, 1743-1755.

Chen, H.Y.H., Popadiouk, R.V., 2002. Dynamics of North American boreal mixedwoods. Environ. Rev. 10, 137-166.

Chen, J., Chen,W.J., Liu, J., Cihlar, J. and Gray, S., 2000 Annual carbon balance of Canada's forests during 1895–1996. Global Biogeochem.Cy. 14, 839–849.

Ciais, P., Tans, P.P., Trolier, M., White, J.W.C., Francey, R.J., 1995. A large northern hemisphere terrestrial CO_2 sink indicated by the $^{13}C/^{12}C$ Ratio of Atmospheric CO_2. Science. 269(5227), 1098-1102.

Cole, D.W., Rapp, M., 1981. Elemental cycling in forest ecosystem. In: D.E. Reichle (Editor), Dynamic properties of forest ecosystems. Cambridge University Press, London, pp. 341-409.

Cortini, F., Comeau, P.G., Bokalo, M., 2012. Trembling aspen competition and climate effects on white spruce growth in boreal mixtures of Western Canada. Forest Ecol. Magt. 277, 67-73.

Crown, P.H., Twardy, A.G,. 1970. Soils of the Fort McMurray region, Alberta, and their relation to agricultural and urban development, Contribution M70-2, Alberta Institute of Pedology, University of Alberta, 52 pp.

Da Silva, A.P., Kay, B.D., 1997. Estimating the least limiting waterrange of soil from properties and management. Soil Sci. Soc. Am. J. 61, 877–883.

Das Gupta, S., 2015. Spatial variability in disturbed boreal ecosystems: Aboveground and belowground controls. Ph.D. Thesis. University of Alberta, Edmonton, AB.

De Vries, W., Solberg, S., Dobbertin, M., Sterba, H., Laubhann, D., van Oijen, M., Evans, C., Gundersen, P., Kros, J., Wamelink, G.W.W., Reinds, G.J., Sutton, M.A. 2009. The impact of nitrogen deposition on carbon sequestration by European forests and heathlands. Forest Ecol. Manag. 258, 1814-1823.

Devito, K.J., Creed, I.F., Fraser, C.J.D., 2005. Controls on runoff from a partially harvested aspen-forested headwater catchment, Boreal Plain, Canada. Hydrol. Process. 19, 3–25.

Devito, K.J., Westbrook, C.J., Schiff, S.L., 1999. Nitrogen mineralization and nitrification in upland and peatland forest soils in two Canadian Shield catchments. Can. J. For. Res. 29, 1793-1804.

Dietrich, S.T., 2018. Characterization of soil spatial heterogeneity and improvement of capping materials for oil sands mine reclamation. Ph.D. Thesis. University of Alberta, Edmonton, AB.

Dimitrov, D.D., Grant, R.F., LaFleur, P.M., Humphreys, E.R., 2010. Modelling subsurface hydrology of Mer Bleue bog. Soil Sci. Soc. Am. J. 74,680-694.

D'Orangeville, L., Duchesne, L., Houle, D., Kneeshaw, D., Côté, B., Pederson, N., 2016. Northeastern North America as a potential refugium for boreal forests in a warming climate. Sci. 352 (6292), 1452-1455.

Drozdowksi, B., Bauman, L., Underwood, A., Faught, B., 2014. Carbon dynamics in reclaimed and natural landscapes at the operations of Syncrude Canada Ltd. Report prepared for Syncrude Canada Ltd. Alberta Innovates - Technology Futures, Edmonton, AB.

Drozdowksi, B., Faught, R.L., Underwood, A., 2011. Carbon dynamics in reclaimed and natural landscapes at the operations of Syncrude Canada Ltd. Report prepared for Syncrude Canada Ltd. Alberta Research Council Inc. Edmonton, AB.

Drozdowksi, B., Faught, R.L., Underwood, A., Degenhardt, D., 2012. Carbon dynamics in reclaimed and natural landscapes at the operations of Syncrude Canada Ltd. Report prepared for Syncrude Canada Ltd. Alberta Innovates - Technology Futures, Edmonton, AB.

Duan, M., Chang, S.X., 2015. Responses of lodgepole pine (*Pinus contorta*) and white spruce (*Picea glauca*) to fertilization in some reconstructed boreal forest soils in the oil sands region. Ecol. Eng. 84, 354-361.

Duan, M., House, J., Chang, S.X., 2015. Limiting factors for lodgepole pine (*Pinus contorta*) and white spruce (*Picea glauca*) growth differ in some reconstructed sites in the Athabasca oil sands region. Ecol. Eng. 75, 323–331.

Duveneck, M.J., Thompson, J.R. 2017. Climate change imposes phenological trade-offs on forest net primary productivity. J. Geophys. Res. Biogeosci. 122.

Edwards, I.K., 1985. Salt effects on vegetation. In Gel and Saline Drilling Wastes in Alberta: Workshop Proceedings. D. A. Lloyd (ed.). Edmonton, AB. pp.168-178.

Eggers, J., Lindner, M., Zudin, S., Zaehle, S., Liski. J., 2008. Impact of changing wood demand, climate and land use on European forest resources and carbon stocks during the 21st century. Glob. Chang. Biol. 14, 2288-2303.

Elshorbagy, A., Barbour, S.L., 2007. A probabilistic approach for design and hydrologic performance assessment of reconstructed watersheds. J. Geotech. Geoenv. Eng. 133, 1110-1118.

Elshorbagy, A., Barbour, S. L., Qualizza, C., 2006. Chapter 14: Multi-criterion decision making approach to assess the performance of reconstructed watersheds. In: Topics on System

Analysis and Integrated Water Resource Management (ed. by A. Castelletti & R. S. Sessa), 257–269. Elsevier, Amsterdam, The Netherlands.

Elshorbagy, A., Jutla, A., Barbour, S.L., Kells, J., 2005. System dynamics approach to assess the sustainability of reclamation of disturbed watersheds. Can. J. Civ. Eng. 32, 144–158.

Elshorbagy, A., Jutla, A., Kells, J., 2007. Simulation of the hydrological processes on reconstructed watersheds using system dynamics. Hydrol. Sci. J. 52(3), 538–561.

Environment Canada., 2014. Canadian Climate Normals 1981-2010. http://climate.weather.gc.ca/climate_normals/results_1981_2010_e.html?stnID=2519&lang=e&StationName=fortmcmurray&SearchType=Contains&stnNameSubmit=go&dCode=1&dispBack=1. (Accessed 10/08/ 2014).

Environment and Parks, 2017. Oil Sands Mine Reclamation and Disturbance Tracking by Year. http://osip.alberta.ca/library/Dataset/Details/27. Accessed 05/12/2017.

Farquhar, G., Caemmerer, S., Berry, J., 1980. A biochemical model of photosynthetic CO_2 assimilation in leaves of C 3 species. Planta. 149 (1), 78–90.

Filipescu, C., Comeau, P.G., 2007a. Aspen competition affects light and white spruce growth across several boreal sites in western Canada. Can. J. For. Res. 37, 1701-1713.

Filipescu, C., Comeau, P.G., 2007b. Competitive interactions between aspen and white spruce vary with stand age in boreal mixedwoods. For. Ecol. Manage. 247, 175–184.

Finzi, A. C., Norby, R. J., Calfapietra, C., Gallet-Budynek, A., Gielen, B., Holmes,W. E., Hoosbeek, M. R., Iversen, C. M., Jackson, R. B., Kubiske, M. E., Ledford, J., Liberloo, M., Oren, R., Polle, A., Pritchard, S., Zak, D. R., Schlesinger, W. H., and Ceulemans, R., 2007. Increases in nitrogen uptake rather than nitrogen-use efficiency support higher rates of temperate forest productivity under elevated CO_2. PNAS. 104, 14014-14019.

Fung, M.Y.P., Macyk, T.M., 2000. Reclamation of oil sands mining areas, in: Barnhisel, R.I., Darmody, R.G., Daniels, W.L. (Eds.), Reclamation of Drastically Disturbed lands. ASA, CSSA and SSSA, Agronomy Monograph 41, Madison. pp. 755-774.

Gao, Q., Zhao, P., Zeng, X., Cai, X., Shen, W., 2002. A model of stomatal conductance to quantify the relationship between leaf transpiration, microclimate and soil water stress. Plant CellEnviron. 25, 1373–1381.

Garrah, K., Gulyas, G., Straker, J., Thrower, J., 2013. South Bison Hill research synthesis – vegetation overstory response to reclamation cover depth. Report prepared for Syncrude Canada Ltd. Integral Ecology Group Ltd. Victoria, B.C. Canada.

Gower, S.T., Krankina, O.N., Olson, R.J., Apps, M.J., Linder, S., Wang, C., 2001. Net primary production and carbon allocation patterns of boreal forest ecosystems. Ecol. Appl.11, 1395-1411.

Grant, R.F., 1991. The distribution of water and nitrogen in the soil-crop system: A simulation study with validation from a winter wheat field trial. Fert. Res. 27, 199-214.

Grant, R.F., 1993. Simulation model of soil compaction and root growth. I. Model development. Plant Soil. 150, 1-14.

Grant, R.F., 1995. Salinity, water use and yield of maize: Testing of the mathematical model *ecosys*. Plant Soil. 172, 309-322.

Grant, R.F., 1998. Simulation in *ecosys* of root growth response to contrasting soil water and nitrogen. Ecol. Model. 107(2), 237-264.

Grant, R.F., 2001. A review of the Canadian ecosystem model *ecosys*. in modeling carbon and nitrogen dynamics for soil management: pp. 173-264, CRC Press, Boca Raton, FL.

Grant, R.F., 2004. Modeling topographic effects on net ecosystem productivity of boreal black spruce forests. Tree Physiol. 24(1), 1-18.

Grant, R. F., 2013. Modelling changes in nitrogen cycling to sustain increases in forest productivity under elevated atmospheric CO2 and contrasting site conditions. Biogeosciences. 10, 7703-7721.

Grant, R.F., 2014. Nitrogen mineralization drives the response of forest productivity to soil warming: Modelling in *ecosys vs.* measurements from the Harvard soil heating experiment. Ecol. Model. 288, 38-46.

Grant, R. F., 2015. Ecosystem CO_2 and CH_4 exchange in a mixed tundra and a fen within a hydrologically diverse Arctic landscape: 2. Modeled impacts of climate change. J. Geophys. Res. Biogeosci. 120, 1388-1406.

Grant, R.F., Amrani, M., Heaney, D.J., Wright, R., Zhang, M., 2004. Mathematical modelling of phosphorus losses from land application of hog and cattle manure. J. Environ. Qual. 33, 210-233.

Grant, R.F., Arain, A., Arora, V., Barr A., Black, T.A., Chen, J., Wang, S., Yuan, F., Zhang, Y., 2005. Intercomparison of techniques to model high temperature effects on CO_2 and energy exchange in temperate and boreal coniferous forests. Ecol. Model. 188, 217-252.

Grant, R.F., Arkebauer, T.J., Dobermann, A., Hubbard, K.G., Schimelfenig, T.T., Suyker, A.E., Verma, S.B., Walters, D.T., 2007a. Net Biome Productivity of Irrigated and Rainfed Maize–Soybean Rotations: Modeling vs. Measurements. Agron. J. 99:1404-1423.

Grant, R.F., Baldocchi, D.D., Ma, S., 2012. Ecological controls on net ecosystem productivity of a seasonally dry annual grassland under current and future climates: Modelling with *ecosys*. Agric. For. Meteorol. 152, 189-200.

Grant, R.F., Barr, A.G., Black, T.A., Margolis, H.A., Dunn, A.L., Metsaranta, J., Wang, S., McCaughey, J. H., Bourque, C. A., 2009a. Interannual variation in net ecosystem productivity of Canadian forests as affected by regional weather patterns – A Fluxnet-Canada synthesis. Agric. For. Meteorol. 149(11), 2022-2039.

Grant, R.F., Barr, A.G., Black, T.A., Iwashita, I., Kidson, J., McCaughey, H., Morgenstern, K., Murayama, S., Nesic, Z., Saigusa, N., Shashkov, A., Zha, T., 2007b. Net ecosystem productivity of boreal jack pine stands regenerating from clearcutting under current and future climates. Global Change Biol. 13(7), 1423-1440.

Grant, R. F., Barr, A. G., Black, T. A., Margolis, H. A., McCaughey, J. H., and Trofymow, J. A. 2010. Net ecosystem productivity of temperate and boreal forests after clearcutting – a Fluxnet-Canada synthesis. Tellus B. 62, 475–496.

Grant, R.F., Black, T.A., Gaumont-Guay, D., Klujn, N., Barr, A.G., Morgenstern, K., Nesic, Z., 2006a. Net ecosystem productivity of boreal aspen forests under drought and climate change: Mathematical modelling with *Ecosys*. Agric. For. Meteorol. 140(1-4), 152-170.

Grant, R.F., Black, T.A., Humphreys, E., Morgenstern, K., 2007c. Changes in net ecosystem productivity with forest age following clearcutting of a coastal Douglas-fir forest: testing a mathematical model with eddy covariance measurements along a forest chronosequence. Tree Physiol. 27(1), 115-131.

Grant, R.F., Flanagan, L.B., 2007. Modeling stomatal and nonstomatal effects of water deficits on CO_2 fixation in a semiarid grassland. J. Geophys. Res. 112, G03011.

Grant, R.F., Goulden, M.L., Wofsy, S.C., Berry, J.A., 2001. Carbon and energy exchange by a black spruce–moss ecosystem under changing climate: testing the mathematical model ecosys with data from the BOREAS experiment. J. Geophys. Res.106, 33,605-33,621.

Grant, R.F., Humphreys, E.R., Lafleur, P.M., 2015. Ecosystem CO_2 and CH_4 exchange in a mixed tundra and a fen within a hydrologically diverse Arctic landscape: 1. Modeling versus measurements. J. Geophys. Res. Biogeosci. 120, 1366-1387.

Grant, R. F., Humphreys, E.R., Lafleur, P.M., Dimitrov, D.D., 2011. Ecological controls on net ecosystem productivity of a mesic arctic tundra under current and future climates J. Geophys. Res. Biogeosci. 116 G01031.

Grant, R.F., Margolis, H.A., Barr, A.G., Black, T.A., Dunn, A.L., Bernier, P.Y., Bergeron, O., 2008. Changes in net ecosystem productivity of boreal black spruce stands in response to changes in temperature at diurnal and seasonal time scales. Tree Physiol. 29(1), 1–17.

Grant, R.F., Mekonnen, Z.A., Riley, W.J., Wainwright, H.M., Graham, D., Torn, M.S., 2017. I: microtopography determines how active layer depths respond to changes in temperature and precipitation at an Arctic polygonal tundra site: mathematical modelling with ecosys J. Geophys. Res. Biogeosci. 122, 3161-73.

Grant, R.F., Nyborg, M., Laidlaw, J., 1993. Evolution of nitrous oxide from soil: II. Experimental results and model testing. Soil Sci. 156, 266-277.

Grant, R. F., Oechel, W.C., Ping, C.L., 2003. Modelling carbon balances of coastal arctic tundra under changing climate Glob. Change Biol. 9, 16-36.

Grant, R.F., Robertson, J.A., 1997. Phosphorus uptake by root systems: mathematical modelling in *ecosys*. Plant Soil. 188, 279-297.

Grant R.F., Wall, G.W., Frumau, K.F.A., Pinter, P.J. Jr., Hunsaker, D., Kimball, B.A., LaMorte, R.L., 1999. Crop water relations under different CO_2 and irrigation: testing of *ecosys* with the free air CO_2 enrichment (FACE) experiment. Agric. For. Meteorol. 95(1), 27-51.

Grant, R.F., Zhang, Y., Yuan, F., Wang, S., Hanson, P.J., Gaumont-Guay, D., Chen, J., Black, T.A., Barr, A., Baldocchi, D.D., Arain, A., 2006b. Intercomparison of techniques to model water stress effects on CO_2 and energy exchange in temperate and boreal deciduous forests. Ecol. Model. 196(3-4), 289-312.

Gray, L.K., Hamann, A., 2011. Strategies for reforestation under uncertain future climates: guidelines for Alberta, Canada. PLoS ONE. 6 (8), e22977.

Green, R.E., Corey, R.B., 1971. Calculation of hydraulic conductivity: A further evaluation of some predictive methods. Soil Sci. Soc. Am. Proc. 35, 3-8.

Grossnickle, S.C., 2005. Importance of root growth in overcoming planting stress. New For. 30, 273-294.

Hansen, E. A., 1994. A guide for determining when to fertilize hybrid poplar plantations. Res. Pap. NC-319. St. Paul, MN: U.S. Department of Agriculture, Forest Service, North Central Forest ExperimentStation. 7 pp.

Hart, S.C., 2006. Potential impacts of climate change on nitrogen transformations and greenhouse gas fluxes in forests: a soil transfer study. Glob. Change Biol. 12, 1032–1046.

Hemstock, S.S., 2008. Plant productivity, soil microorganisms, and soil nitrogen cycling in peat amendments used for oil sands reclamation. M.Sc.Thesis. University of Alberta, Edmonton, AB.

Hemstock, S.S., Quideau, S.A., Chanasyk, D.S., 2010. Nitrogen availability from peat amendments used in boreal oil sands reclamation. Can. J. Soil Sci. 90, 165-175.

Hickler, T., Smith, B., Prentice, I.C., Mjöfors, K., Miller, P., Arneth, A., Sykes, M.T., 2008. CO_2 fertilization in temperate FACE experiments not representative of boreal and tropical forests. Global Change Biol. 14(7): 1531–1542.

Hilderman, J.N., 2011. Net percolation as a function of topographic variation in a reclamation cover over a saline-sodic overburden dump. M.Sc. Thesis, University of Saskatchewan, Saskatoon, SK.

Hogg, E.H., Hurdle, P.A., 1997. Sap flow in trembling aspen: implications for stomatal responses to vapor pressure deficit. Tree Physiol. 17, 501–509.

Horton, J.L., Hart, S.C., 1998. Hydraulic lift: A potentially important ecosystem process. Trends Ecol. Evol. 13, 232–235.

Howat, D.R., 2000. Acceptable salinity, sodicity and pH values for boreal forest reclamation., Alberta Environment, Environmental Sciences Division, Edmonton Alberta. Report no. ESD/LM/00-2. 191 pp.

Howell, D.M., Das Gupta, S., Pinno, B.D., MacKenzie, M.D., 2017. Reclaimed soils, fertilizer, and bioavailable nutrients: Determining similarity with natural benchmarks over time. Can. J. Soil Sci. 97, 149-158.

Huang, M., Barbour, S.L., Carey, S.K., 2015a. The impact of reclamation cover depth on the performance of reclaimed shale overburden at an oil sands mine in northern Alberta, Canada. Hydrol. Process. 29(12), 2840–2854.

Huang, M., Barbour, S.L., Elshorbagy, A., Zettl, J.D., Si, B.C., 2011. Water availability and forest growth in coarse textured soils. Can. J. Soil Sci. 91, 199–210.

Huang, M., Hilderman, J.N., and Barbour, L., 2015b. Transport of stable isotopes of water and sulphate within reclaimed oil sands saline–sodic mine overburden. J. Hydrol. 529, 1550-1561.

Huang, M., Zettl, J.D., Barbour, S.L., Elshorbagy, A., Si, B.C., 2013. The impact of soil moisture availability on forest growth indices for variably layered coarse-textured soils. Ecohydrol. 6, 214-227.

Hudson, J.M.G., Henry, G.H.R., 2009. Increased plant biomass in a High Arctic heath community from 1981 to 2008. Ecology. 90, 2657-2663.

Hunt, E.R,Jr., Running, S.W., 1992. Simulated dry matter yields for aspen and spruce stands in the North American boreal forest. Can. J. Remote Sensing. 18, 126-133.

ICT International., 2017. Available at: http://au.ictinternational.com/products/plants/sap-flow/ . Accessed 05/04/ 2017.

Ineson, P., Benham, D.G., Poskitt, J., Harrison, A.F., Taylor, K., Woods, C., 1998. Effects of climate change on nitrogen dynamics in upland soils. 2. A soil warming study. Glob. Change Biol. 4, 153–161.

IPCC, 2013. Climate change 2013: The Physical Science Basis. Contribution of Working Group I to the fifth assessment report of the Intergovernmental Panel on Climate Change [Stocker TF, Qin D, Plattner G-K, Tignor M, Allen SK, Boschung J, Nauels A, Xia Y, Bex V, Midgley PM, eds]. Cambridge, UK & New York, NY, USA: Cambridge University Press.

Jackson, R.B., Canadell, J., Ehleringer, J.R., Mooney, H.A., Sala, O.E., Schulze, E.D., 1996. A global analysis of root distributions for terrestrial biomes. Oecologia. 108(3), 389–411.

Jerabkova, L., Prescott, C.E., Kishchuk, B.E. 2006. Nitrogen availability in soil and forest floor of contrasting types of boreal mixedwood forests. Can. J. For. Res. 36, 112-122.

Jones, D.L., Magthab, E.A., Gleeson, D.B., Hill, P.W., Sánchez-Rodríguez, A.R., Roberts, P., Ge, T., Murphy, D.V., 2018. Microbial competition for nitrogen and carbon is as intense in the subsoil as in the topsoil. Soil Biol. Biochem. 117, 72-82.

Karst, J., Landhäusser, S., 2014.Identification of roots in South Bison Hill capping study and selected natural soils.Report prepared for Syncrude Canada Ltd. University of Alberta. Edmonton, AB.

Kasischke, E.S., Christensen, Jr. N. L., Stocks, B.J., 1995. Fire, global warming, and the carbon balance of boreal forests. Ecol. Appl. 5, 437-451.

Kaye, J.P., Hart S.C., 1997. Competition for nitrogen between plants and soil microorganisms. Trends Ecol. Evol. 12, 139-143.

Kelln, C.J., 2008. The effects of meso-scale topography on the performance of engineered soil covers. Ph.D. Thesis, University of Saskatchewan, Saskatoon, SK.

Kelln, C.J., Barbour, S.L., Purdy, B., Qualizza, C., 2009. A multidisciplinary approach to reclamation research in the oil sands region of Canada, volume appropriate technologies for environmental protection in the developing world. Springer-Verlag, Berlin, Germany. pp. 205–215.

Kelln, C., Barbour, L., Qualizza, C., 2007. Preferential flow in a reclamation cover: Hydrological and geochemical response. Can. J. Soil Sci. 133(10), 1277–1289.

Kelln, C., Barbour, S.L., Qualizza, C., 2008. Controls on the spatial distribution of soil moisture and solute transport in a sloping reclamation cover. Can. Geotech. J. 45(3), 351-366.

Keshta, N., Elshorbagy, A., Barbour, S.L., 2010. Comparative probabilistic assessment of the hydrological performance of reconstructed and natural watersheds. Hydrol. Process. 24, 1333–1342.

Kessler, S., 2007. Salinity profiles in reconstructed soils over saline-sodic waste from the oil sands industry. M.Sc. Thesis, University of Saskatchewan, Saskatoon, SK.

Kessler, S., Barbour, S.L., van Rees, K.C., Dobchuk, B.S., 2010. Salinization of soil over saline-sodic overburden from the oil sands in Alberta. Can. J. Soil Sci. 90, 637–647.

Ketcheson, S., Price, J., 2016. A comparison of the hydrological role of two reclaimed slopes of different age in the Athabasca oil sands region, Alberta, Canada. Can. Geotech. J. 53, 1533–1546.

Khasa, P.D., Hambling, B., Kernaghan, G., Fung, M., Ngimbi, E, 2002. Genetic variability in salt tolerance of selected boreal woody seedlings. For. Ecol. Manage. 165, 257-269.

Kimball, J.S., Zhao, M., McDonald, K.C., Running, S.W., 2006. Satellite remote sensing of terrestrial net primary production for the pan-arctic basin and Alaska. Miti. Adapt. Strat. Global Change, 11(4), 783-804.

King, J.S., Kubiske, M.E., Pregizer, K.S., Hendrey, G.R., McDonald, E.P., Giardina, C.P., Quinn,V.S., Karnosky, D.F., 2005. Tropospheric O_3 compromises net primary production in young stands of trembling aspen, paper birch and sugar maple in response to elevated atmospheric CO_2. New Phytologist 168, 623-636.

Kirkby, E., 2012. Introduction, Definition and Classification of Nutrients, in Marschner, P. (ed): Marschner's Mineral Nutrition of Higher Plants, 3rd Edition, Elsevier Science. pp. 3-5.

Klohn Crippen Berger Ltd. 2013. South Bison Hill research synthesis - 2012 south Bison Hill salinity study. Report prepared for Syncrude Canada Ltd. Edmonton, AB.

Koenig, R.T., Pan, W.L., 1996. Calcium Effects on Quantity-Intensity Relationships and Plant Availability of Ammonium. Soil Sci. Soc. Am. J. 60,492-497.

Kronzucker, H.J., Siddiqi, M.Y., Glass, A.D.M., 1997. Conifer root discrimination against soil nitrate and the ecology of forest succession. Nature. 385, 59-61.

Kurz, W.A., Apps, M.J., Stocks, B.J., Volney, W.J.A., 1995. Global climate change: Disturbance regimes and biospheric feedbacks of temperate and boreal forests. In Biotic feedbacks in the global climatic system: Will the warming feed the warming? Edited by G.M. Woodwell and F.T. MacKenzie. Oxford University Press, New York, Oxford. pp. 119–133.

Kurz, W.A., Shaw, C.H., Boisvenue, C., Stinson, G., Metsaranta, J., Leckie, D., Dyk, A., Smyth, C., Neilson, E.T., 2013. Carbon in Canada's boreal forest - A synthesis. Environ. Rev. 21, 260-292.

Kurz, W.A., Stinson, G., and Rampley, G. 2008. Could increased boreal forest ecosystem productivity offset carbon losses from increased disturbances? Phil. Trans. R. Soc. B, 363, 2261–2269.

Kwak, J-H, Chang, S.X., Naeth, M.A., Schaaf, W., 2015. Coarse woody debris extract decreases nitrogen availability in two reclaimed oil sands soils in Canada. Ecol. Eng. 84, 13-21.

Lambers, H., Poorter, H., 1992. Inherent variation in growth rate between higher plants: a search for physiological causes and ecological consequences. Adv. Ecol. Res. 23, 187-261.

Lanoue, A.V.L., 2003. Phosphorus content and accumulation of carbon and nitrogen in boreal forest soils. M.Sc. Thesis. University of Alberta, Edmonton, AB.

Larcher, W., 2003. Physiological Plant Ecology 4th ed. Springer-Verlag. Berlin.

Lazorko, H.M., Van Rees, K.C.J., 2012. Root distributions of planted boreal mixedwood species on reclaimed saline–sodic overburden. Water Air and Soil Pollut. 223, 215-231.

Leskiw, L.A., 1998. Land capability classification for forest ecosystems in the Oil sand region (Revised edition). Tailings sand reclamation practices working group. Edmonton, AB. 73 pp.

Lilles, E.C., Purdy, B.G., Chang, S.X., Macdonald, S.E., 2010. Soil and ground water characteristics of saline sites supporting boreal mixedwood forests in northern Alberta. Can. J. Soil Sci. 90, 1-14.

Lilles, E.B., Purdy, B.G., Macdonald, S.E., Chang, S.X., 2012. Growth of aspen and white spruce on naturally saline sites in northern Alberta: Implications for development of boreal forest vegetation on reclaimed saline soils. Can. J. of Soil Sci. 92, 213-227.

Liu, S., Wei, Y., Post, W.M., Cook, R.B., Schaefer, K., Thornton, M.M., 2013. The Unified North American Soil Map and its implication on the soil organic carbon stock in North America. Biogeosci. 10, 2915-2930.

Logan, J.A., Régnière, J., Powell, J.A., 2003. Assessing the impacts of global warming on forest pest dynamics. Front Ecol. Environ. 1, 130-137.

Macdonald, S.E., Landhäusser, S.M., Skousen, J., Franklin, J., Frouz, J., Hall, S., Jacobs, D.F., Quideau, S., 2015. Forest restoration following surface mining disturbance: challenges and solutions. New For. 46, 703-732.

MacKenzie, D.D., 2013. Oil sands mine reclamation using boreal forest surface soil (LFH) in northern Alberta. Ph.D. Thesis. University of Alberta, Edmonton AB.

MacKenzie, D.D., Naeth, M.A., 2010. The role of the forest soil propagule bank in assisted natural recovery after oil sands mining. J. Rest. Eco. 18, 418-427.

MacKenzie, M.D., Quideau, S.A., 2010. Microbial community structure and nutrient availability in oil sands reclaimed boreal soils. Appl. Soil Ecol. 44, 32-41.

MacKenzie, M. D., Quideau, S. A., 2012. Laboratory-based nitrogen mineralization and biogeochemistry of two soils used in oil sands reclamation. Can. J. Soil Sci. 92, 131-142.

Macpherson, D.N., 2000. 1s growth of trembling aspen affected by white spruce understories in Alberta's boreal mixedwood forests? M.Sc. Thesis. University of Alberta, Edmonton, AB.

Macyk, T.M., 1999. Soil monitoring at the 30 dump overburden area. Report prepared for Syncrude Canada Ltd. Alberta Research Council Inc. Edmonton, AB.

Macyk, T.M., Faught, R.L., Drozdowski, B., Underwood, A., 2009. Carbon storage in reclaimed and natural landscapes at the operations of Syncrude Canada Ltd. Annual report prepared for Syncrude Canada Ltd. Alberta Research Council Inc. Edmonton, AB.

Mahendrappa, M.K., Salonius, P.O., 1982. Nutrient dynamics and growth response in a fertilized black spruce stand. Soil Sci. Soc. Am. J. 46, 127–133.

Man, R., Lieffers, V.J. 1999 Are mixtures of aspen and white spruce more productive than single species stands? The Forestry Chronicle. 75, 505-513.

Maynard, D.G., Mallett, K.I., Myrholm, C. L. 1996. Sodium carbonate inhibits emergence and growth of greenhouse-grown white spruce. Can. J. Soil Sci. 77, 99-105.

McKeague, J.A., 1978. Manual on Soil Sampling and Methods of Analysis. 2nd ed. Can. Soc. Soil Sci. 212 pp.

McKenzie, R. C., Mathers, H. M., Robertson, M. J., Woods, S. A. 1993. Salinity and cold tolerance of ornamental trees and shrubs, Alberta Agriculture, Edmonton, AB. Rep. 920050.

McMillian, R., Quideau, S. A., MacKenzie, M. D., Biryukova, O., 2007. Nitrogen mineralization and microbial activity in oil sands reclaimed boreal forest soils. J. Environ. Qual. 36, 1470-1478.

Meiers, G., 2002. The use of field measurements of hydraulic conductivity to characterize the performance of reclamation covers with time. M. Eng. Thesis. University of Saskatchewan, Saskatoon, SK.

Meiers, G., Barbour, S.L., Qualizza, C., Dobchuk, B., 2011. Evolution of the hydraulic conductivity of reclamation covers over sodic/saline mining overburden. J. Geotech. Geoenviron. Eng. 137(1), 968–976.

Meinshausen, M., Smith, S.J., Calvin, K., Daniel, J.S., Kainuma, M., Lamarque, J., Matsumoto, K., Montzka, S., Raper, S., Riahi, K., 2011. The RCP greenhouse gas concentrations and their extensions from 1765–2300. Clim. Change. 109, 213-41.

Mekonnen, Z.A., Grant, R.F., Schwalm, C., 2016. Contrasting changes in gross primary productivity of different regions of North America as affected by warming in recent decades. Agric. For. Meteorol. 218–219: 50–64.

Mekonnen, Z.A., Grant, R.F., Schwalm, C. 2018a. Modelling impacts of recent warming on seasonal carbon exchange in higher latitudes of North America. Arctic Science . 1–14.

Mekonnen, Z.A., William Riley, J., Grant, R.F. 2018b. Accelerated nutrient cycling and increased light competition will lead to 21st century shrub expansion in North American Arctic tundra. J. Geophys. Res. Biogeosci.

Mencuccini, M., Grace, J., 1996. Hydraulic conductance, light interception and needle nutrient concentration in Scots pine stands and their relations with net primary productivity. Tree Physiol. 16, 459-468.

Mezbahuddin, M., Grant, R.F., Flanagan, L.B., 2016. Modeling hydrological controls on variations in peat water content, water table depth, and surface energy exchange of a boreal western Canadian fen peatland. J. Geophys. Res. Biogeosci. 121, 2216-2242.

Mezbahuddin, M., Grant, R.F., Flanagan, L.B., 2017. Coupled eco-hydrology and biogeochemistry algorithms enable the simulation of water table depth effects on boreal peatland net CO2 exchange. Biogeosci. 14, 5507-5531.

Mezbahuddin, M., Grant, R.F., Hirano, T., 2014. Modelling effects of seasonal variation in water table depth on net ecosystem CO_2 exchange of a tropical peatland. Biogeosci. 11, 577-599.

Mezbahuddin, M., Grant, R.F., Hirano, T., 2015. How hydrology determines seasonal and interannual variations in water table depth, surface energy exchange, and water stress in a tropical peatland: Modeling versus measurements. J. Geophys. Res. Biogeosci. 120, 2132-2157.

Min, X., Siddiqi, M.Y., Guy, R.D., Glass, A.D.M., Kronzucker, H.J., 2000. A comparative kinetic analysis of nitrate and ammonium influx in two early-successional tree species of temperate and boreal forest ecosystems. Plant Cell Environ. 23, 321-328.

Myneni, R.B., Keeling, C., Tucker, C., Asrar, G., Nemani, R., 1997. Increased plant growth in the northern high latitudes from 1981 to 1991. Nature. 386 (6626), 698–702.

Nadelhoffer, K.J., Aber, J.D., Melillo, J.M., 1985. Fine roots, net primary production, and soil nitrogen availability: A new hypothesis. Ecology. 66(4), 1377-1390.

Naeth, M.A., Archibald, H.A., Nemirsky, C.L., Leskiw, L.A., Brierley, J.A., Bock, M.D., VandenBygaart, A.J., Chanasyk, D.S., 2012. Proposed classification for human modified soils in Canada: anthroposolic order. Can. J. Soil Sci. 92, 7-18.

Naeth, M.A., Wilkinson, S.R., Mackenzie, D.D., Archibald, H.A., Powter, C.B., 2013. Potential of LFH Mineral Soil Mixes for Land Reclamation in Alberta. Oil Sands Research and Information Network, University of Alberta, School of Energy and the Environment, Edmonton, Alberta. OSRIN Report No. TR-35. 64 pp.

National Research Council, 1993. Soil and water quality: an agenda for agriculture. Committee on long-range soil and water conservation, Board on agriculture, National Research council. National Academies press. Washington, D.C. 516 pp.

Nelson, D.W., Sommers, L.E., 1996. Total carbon, organic carbon, and organic matter. In Sparks, D.L., et al., Eds., Methods of Soil Analysis. Part 3, SSSA Book Series. Madison. 961-1010.

Nichol, C., Kessler, S., Wall, S.N., Barbour, S.L., Hendry, J., 2006. 30 Dump instrumented watersheds geochemical analysis: A report prepared for Syncrude Canada Ltd., University of Saskatchewan, Saskatoon.

Nienstaedt, H., Zasada, J.C., 1990. *Picea glauca* (Moench) Voss: white spruce. In: Burns, R.M., Honkala, B.H. (Eds.), Silvics of North America: vol. 1. Conifers. USDA Forest Service, Washington, DC, pp. 204–226.

Nitschke, C.R., Waeber, P.O., Klaassen, J.W., Dordel, J., Innes, J.L., Aponte, C., 2017. Nutrient uptake and use efficiency in co-occurring plants along a disturbance and nutrient availability gradient in the boreal forests of the southwest Yukon, Canada. J. Veg.Sci. 28, 69-81.

Norby, R.J., DeLuca, E.H., Gielen, B., Calfapietra, C., Giardina, C.P., King, J.S., Redford, J., McCarthy, H.R., Moore, D.J.P., Ceulemans, R., De Angelis, P., Finzi, A.C., Karnosky, D.F., Kubiske, M.E., Lukac, M., Pregitzer, K.S., Scarascia-Mugnozza, G.E., Schlesinger, W.H., Oren, R. 2005. Forest Response to elevated CO_2 is conserved across a broad range of productivity. PNAS 102(50), 18052-18056.

Norby, R.J., Warren, J.M., Iversen, C.M., Medlyn, B.E., McMurtrie, R.E., 2010.CO_2 enhancement of forest productivity constrained by limited nitrogen availability. Proc. Natl.Acad. Sci.U.S.A. 107(45), 19368–19373.

Northwind Land Resources Inc., 2014. South Bison Hill capping study and selected natural sites – 2013 root and soil sampling field program – methodology and results. Report prepared for Syncrude Canada Ltd. Edmonton, AB.

O'Kane Consultants Inc., 2012a. Temperature correction for matric suction at D1A monitoring station. Report prepared for Syncrude Canada Ltd.

O'Kane Consultants Inc., 2012b. Spring melt monitoring program monitoring data summary report for the period March 2012 to April 2012. Report No. 690/01-40 prepared for Syncrude Canada Ltd.

O'Kane Consultants Inc., 2013. Instrumented watershed monitoring program monitoring data summary report for the period January 2012 to December 2012. Report No. 690/01-46 prepared for Syncrude Canada Ltd.

O'Kane Consultants Inc., 2014. Instrumented watershed monitoring program monitoring data summary report for the period January 2013 to December 2013. Report No. 690/01-53 prepared for Syncrude Canada Ltd.

Pastor, J., 1987. Successional changes in nitrogen availability as a potential factor contributing to spruce declines in boreal North America. Can. J. For. Res. 17, 1394-1400.

Peng, C.H. and Apps, M.J., 1999. Modelling the response of net primary productivity (NPP) of boreal forest ecosystems to changes in climate and fire disturbance regimes. Ecol.Model. 122, 175–193.

Persson, T., Wiren, A., 1995. Nitrogen mineralization and potential nitrification at different depths in acidic forest soils. Plant Soil. 168, 55–65.

Peterson, E.B., Peterson, N.M., 1995. Aspen managers' handbook for British Columbia. FRDA Report No. 230, Canada–British Columbia Partnership Agreement on Forest Resource Development FRDA II and BC Ministry of Forests, Victoria, BC.

Pieper, S.J., Loewen, V., Gill, M., Johnstone, J.F., 2011. Plant responses to natural and experimental variations in temperature in Alpine Tundra, Southern Yukon, Canada. Arct. Antarct. Alpine Res. 43 (3), 442–456.

Pinno, B.D., Hawkes, V.C., 2015. Temporal trends of ecosystem development on different site types in reclaimed boreal forests. Forests. 6, 2109-2124.

Pinno, B.D., Landhausser, S.M., MacKenzie, M.D., Quideau, S.A., Chow, P.S., 2012. Trembling aspen seedling establishment, growth, and response to fertilization on contrasting soils used in oil sands reclamation. Can. J. Soil Sci. 92, 143-151.

Power, J.F., Sandoval, M., Ria, R.E., 1979. Topsoil-subsoil requirements to restore North Dakota mined land to original productivity. Mining Engi. 31, 708-1712.

Prepas, E.E., Pinel-Alloul, B., Planas, D., M´ethot, G., Paquet, S., Reedyk, S., 2001. Forest harvest impacts on water quality and aquatic biota on the Boreal Plain: introduction to the TROLS lake program. Can. J. Fish. Aquat. Sci. 58, 421-436.

Prescott, C., Maynard, D., Laiho, R., 2000. Humus in northern forests: friend or foe? For. Ecol. Manage.133, 23–36.

Purdy, B.G., Macdonald, S.E., Lieffers, V.J., 2005. Naturally saline boreal communities as models for reclamation of saline oil Sand tailings. Restoration. Ecol. 13(4), 667-677.

Quideau, S.A., Norris, C.E., Rees, F., Dyck, M., Samadi, N., Oh, S-W., 2017. Carbon, nitrogen, and phosphorus release from peat and forest floor-based cover soils used during oil sands reclamation. Can. J. Soil Sci. 97, 757-768.

Randerson, J.T., Chapin, F.S.I., Harden, J.W., Neff, J.W., Harmon, M.E., 2002. Net ecosystem production: a comprehensive measure of net carbon accumulation by ecosystems. Ecol. Appl. 12, 937-947.

Redding, T.E., Devito, K.J., 2008. Lateral flow thresholds for aspen forested hillslopes on the Western Boreal Plain, Alberta, Canada. Hydrol. Process. 22, 4287-4300.

Renault, S., Paton, E., Nilsson, G., Zwiazek, J.J., MacKinnon, M.D., 1999. Responses of Boreal Plants to High Salinity Oil Sands Tailings Water. J. Environ. Qual. 28, 1957-1962.

Richards, L.A., 1954. Diagnosis and Improvement of Saline and Alkali Soils. Handbook No. 60. United States Department of Agriculture, Washington, DC. 160 pp.

Rowland, S., Prescott, C. E., Grayston, S. J., Quideau, S. A., Bradfield, G. E., 2009. Recreating a functioning forest soil in reclaimed oil sands in northern Alberta: An approach for measuring success in ecological restoration. J. Environ. Qual. 38, 1580-1590.

Sandoval, F.M., Gould, W.L., 1978. Improvement of saline- and sodium-affected disturbed lands. 485–504. In F.W. Schaller, and P. Sutton (ed.) Reclamation of drastically disturbed lands. ASA, Madison, WI.

Shaver, G. R., Canadell, J., Chapin, F.S., Gurevitch, J., Harte, J., Henry, G., Ineson, P., Jonasson, S., Melillo, J., Pitelka, L., Rustad, L., 2000. Global warming and terrestrial ecosystems: a conceptual framework for analysis. BioSci. 50, 871-882.

Shenoy, A., Kielland, K., Johnstone, J.F., 2013. Effects of fire severity on plant nutrient uptake reinforce alternate pathways of succession in boreal forests. Plant Ecol. 214, 587–596.

Shurniak, R.E., 2003. Predictive modeling of moisture movement within soil cover systems for saline/sodic overburden piles. M.Sc. Thesis. University of Saskatchewan, Saskatoon, SK.

Shurniak, R.E., Barbour, S.L., 2002. Modeling of water movement within reclamation covers on oilsands mining overburden piles. pp 622-644 in Proceedings of the National Meeting of the American Society of Mining and Reclamation. Lexington, KY.

Smith, J.L., Doran, J.W., 1996. Measurement and use of pH and electrical conductivity for soil quality analysis. In Methods for assessing soil quality. Soil Sci. Soc. of Am. J. Special Publication. 49, 169-185.

Sobek, A.A., Skousen, J.G., Fisher, S.E., 2000. Chemical and physical properties of overburdens and minesoils. In: Barnhisel RI (ed) Reclamation of drastically disturbed lands, 2nd ed. Agron. Monogr. 41. ASA, CSSA, and SSSA, Madison, WI, pp 77–104.

Stinson, G., Kurz, W.A., Smyth, C.E., Neilson, E.T., Dymond, C.C., Metsaranta, J.M., Boisvenue, C., Rampley, G.J., Li, Q., White, T.M., Blain, D., 2011. An inventory-based analysis of Canada's managed forest carbon dynamics, 1990 to 2008. Global Change Biol. 17(6), 2227-2244.

Stottlemeyer, R., Toczydlowski, D., 1999. Nitrogen mineralization in a mature boreal forest, Isle Royale, Michigan. J. Environ. Qual. 28, 709-720.

Stoy, P.C., Katul, G.G., Siquera, M.B.S., Juang, J.-Y., Novick, K.A., McCarthy, J.R., Oishi,A.C., Oren, R., 2008. Role of vegetation in determining carbon sequestration alongecological succession in the southeastern United States. Global Change Biol. 14,1–19,

Strilesky, S.L., Humphreys, E.R., Carey, S.K., 2017. Forest water use in the initial stages of reclamation in the Athabasca Oil Sands Region. Hydrol. Process. 31, 2781-2792.

Strong, W.L., La Roi, G. H., 1983. Root-system morphology of common boreal forest trees in Alberta, Canada. Can. J. For. Res. 13(6), 1164-1173.

Struecker, J., Joergensen, R.G., 2015. Microorganisms and their substrate utilization patterns in topsoil and subsoil layers of two silt loams, differing in soil organic C accumulation due to colluvial processes. Soil Biol. Biochem. 91, 310-317.

Sulman, B.N., Desai, A.R., Schroeder, N.M., Ricciuto, D., Barr, A., Richardson, A.D., Flanagan, L.B., Lafleur, P.M., Tian, H., Chen, G., Grant, R.F., Poulter, B., Verbeeck, H., Ciais, P., Ringeval, B., Baker, I., Schaefer, K., Luo, Y., Weng, E., 2012. Impact of hydrological variations on modeling of peatland CO_2 fluxes: results from the North American Carbon Program site synthesis. J. Geophys. Res. 117(G1), G01031.

Tani, M., 1997. Runoff generation processes estimated from hydrological observations on a steep forested hillslope with a thin soil layer. J. Hydrol. 200(1– 4), 84-109.

Todd, M.C.L., Adams, M. A., Grierson, P.F., 2000. Mineralisation of nitrogen in a chronosequence of rehabilitated bauxite mines. Aust. J. Soil Res. 38, 435-451.

Van Cleve, K., Oliver, L., Schlentner, R., Viereck , L.A., Dyrness, C.T., 1983. Productivity and nutrient cycling in taiga forest ecosystems. Can. J. For. Res. 13, 747-766.

Van den Driessche, R. 2000. Phosphorus, copper and zinc supply levels influence growth and nutrition of a young *Populus trichocarpa* (Torr. & Gray) *X P. deltoides* (Bartr. Ex Marsh) hybrid. New For. 19, 143-157.

Van Rees, K., 2014. Comparison of rooting distributions for vegetation growing on a reclaimed saline-sodic overburden and natural undisturbed landscapes. Report prepared for Syncrude Canada Ltd. University of Saskatchewan, Saskatoon, SK.

Wall, S. N., 2005. Characterizing geochemical reactions in an overburden waste pile: South Bison Hill, Syncrude, Canada. M.Sc. Thesis, University of Saskatchewan, Saskatoon, SK.

Wang, G.G., Klinka, K., 1997. White spruce foliar nutrient concentrations in relation to tree growth and soil nutrient amounts. For. Ecol. Mgmt. 98. 89-99.

Wang, T., Hamann, A., Spittlehouse, D., Carroll, C., 2016. Locally downscaled and spatially customizable climate data for historical and future periods for North America. PLoS ONE. 11(6), e0156720.

Yarmuch, M., 2003. Measurement of soil physical parameters to evaluate soil structure quality in reclaimed oil sands soils, Alberta, Canada. M.Sc. thesis. University of Alberta, Edmonton, AB.

Yuan, Z.Y., Chen, H.Y.H., 2010. Fine root biomass, production, turnover rates, and nutrient contents in boreal forest ecosystems in relation to species, climate, fertility, and stand age: literature review and meta-analyses. CRC Crit. Rev. Plant Sci. 29(4), 204-221.

Supplementary Material

Appendix A: Microbial C, N and P Transformations

Decomposition

$D_{Si,j,l,C} = D'_{Si,j,l,C}\ M_{i,d,l,C}\ f_{tgl}\ (S_{i,l,C} / G_{i,l,C})$	decomposition of litter, POC, humus	[A1a]
$D_{Zi,j,l,C} = D'_{Zi,j,l,C}\ M_{i,d,l,C}\ f_{tgl}\ (Z_{i,l,C} / G_{i,l,C})$	decomposition of microbial residues	[A1b]
$D_{Ai,l,C} = D'_{Ai,l,C}\ M_{i,d,l,C}\ f_{tgl}\ (A_{i,l,C} / G_{i,l,C})$	decomposition of adsorbed SOC	[A1c]
$S_{i,l,C} = \Sigma_j\ S_{i,j,l,C}$	total C in all kinetic components of litter, POC, humus	[A2a]
$Z_{i,l,C} = \Sigma_j\ Z_{i,j,l,C}$		[A2b]
$G_{i,l,C} = S_{i,l,C} + Z_{i,l,C} + A_{i,l,C}$	total C in all kinetic components of microbial residues	[A2c]
$M_{i,d,l,C} = M_{i,a,l,C} + \boldsymbol{q_m}\ (M_{i,a,l,C}\ G_{ix,l,C} - M_{ix,a,l,C}\ G_{i,l,C}) / (G_{ix,l,C} + G_{i,l,C})$	total C in substrate-microbe complexes redistribution of active microbial biomass	[A3a]
$M_{i,a,l,C} = \Sigma_n\ M_{i,n,a,l,C}$	populations from each substrate-microbe complex *i* to other substrate-microbe complexes *ix* according to concentration differences (priming)	[A3b]
$D'_{Si,j,l,C} = \{\boldsymbol{D}_{Sj,C}\ [S_{i,j,l,C}]\} / \{[S_{i,j,l,C}] + \boldsymbol{K_{mD}}\ (1.0 + [\Sigma M_{i,d,l,C}] / \boldsymbol{K_{iD}})\}$	substrate and water constraint on *D* from	[A4a]
$D'_{Zi,j,l,C} = \{\boldsymbol{D}_{Zj,C}\ [Z_{i,j,l,C}]\} / \{[Z_{i,j,l,C}] + \boldsymbol{K_{mD}}\ (1.0 + [M_{i,d,l,C}] / \boldsymbol{K_{iD}})\}$	colonized litter, POC and humus, microbial	[A4b]
$D'_{Ai,l,C} = \{\boldsymbol{D}_{A,C}\ [A_{i,l,C}]\} / \{[A_{i,l,C}] + \boldsymbol{K_{mD}}\ (1.0 + [M_{i,d,l,C}] / \boldsymbol{K_{iD}})\}$	residues and adsorbed SOC	[A4c]
$\delta S_{i,j,k,l,C} / \delta t = \boldsymbol{\beta}\ \Sigma_n\ (U_{i,n,l C} - R_{hi,n,l})\ (S'_{i,j,k,l,C} / S'_{i,j,l,C})\ \{(S'_{i,j,l,C} / S_{i,j,l,C}) / (S'_{i,j,l,C} / S_{i,j,l,C} + \boldsymbol{K_{iS}})\}$	colonized litter increases with microbial growth into uncolonized litter	[A5]
$f_{tgl} = T_{sl}\ \{e^{[B - \boldsymbol{H_a} / (\boldsymbol{R}\ T_{sl})]}\} / \{1 + e^{[(\boldsymbol{H_{dl}} - \boldsymbol{S}T_{sl}) / (\boldsymbol{R}\ T_{sl})]} + e^{[(\boldsymbol{S}T_{sl} - \boldsymbol{H_{dh}}) / (\boldsymbol{R}\ T_{sl})]}\}$	Arrhenius function for *D* and R_h	[A6]
$D_{Si,j,l,N,P} = D_{Si,j,l,C}\ (S_{i,j,l,N,P} / S_{i,j,l,C})$	decomposition of N and P are driven by that of C in litter, POC, humus, microbial residues and adsorbed SOC	[A7a]
$D_{Zi,j,l,N,P} = D_{Zi,j,l,C}\ (Z_{i,j,l,N,P} / Z_{i,j,l,C})$		[A7b]
$D_{Ai,l,N,P} = D_{Ai,l,C}\ (A_{i,l,N,P} / A_{i,l,C})$		[A7c]
$Y_{i,l,C} = \boldsymbol{k_{ts}}\ (G_{i,l,C}\ F_s\ [Q_{i,l,C}]^{\boldsymbol{b}} - V_{i,l,C})$	Freundlich sorption of DOC	[A8]
$Y_{i,l,N,P} = Y_{i,l,C}\ (Q_{i,l,N,P} / Q_{i,l,C})$	($Y_{i,l,C} > 0$) adsorption of DON, DOP	[A9]

$Y_{i,l,\mathrm{N,P}} = Y_{i,l,\mathrm{C}} \, (V_{i,l,\mathrm{N,P}} / V_{i,l,\mathrm{C}})$	$(Y_{i,l,\mathrm{C}} < 0)$ desorption of DON, DOP	[A10]

Microbial Growth

$R_{\mathrm{h}} = \Sigma_i \Sigma_n \Sigma_l R_{\mathrm{h}i,n,l}$	total heterotrophic respiration	[A11]
$\boldsymbol{R}_{\mathrm{h}i,n,l} = \boldsymbol{R}'_{\mathrm{h}n} \min\{C_{\mathrm{N}i,n,l,a} / \boldsymbol{C}_{\mathrm{N}j}, C_{\mathrm{P}i,n,l,a} / \boldsymbol{C}_{\mathrm{P}j}\}$	R_{h} constrained by microbial N, P	[A12]
$R_{\mathrm{h}}{}'_{i,n,l} = M_{i,n,a,l,\mathrm{C}} \, \{\boldsymbol{R}_{\mathrm{h}i,n,l} \, [Q_{i,l,\mathrm{C}}]\} / \{(\boldsymbol{K}_{\mathbf{m}\boldsymbol{Q}\mathbf{C}} + [Q_{i,l,\mathrm{C}}])\} \, f_{\mathrm{tg}l} \, f_{\psi \mathrm{g}l}$	R_{h} constrained by substrate DOC, T_{s} and ψ	[A13]
$R_{\mathrm{h}i,n,l} = R_{\mathrm{h}}{}'_{i,n,l} \, (U_{\mathrm{O2}i,n,l} / U'_{\mathrm{O2}i,n,l})$	R_{h} constrained by O_2	[A14]
$f_{\psi \mathrm{g}l} = e^{(\sigma \psi_{\mathrm{s}} l)}$	ψ_{s} constraints on microbial growth	[A15]
$U'_{\mathrm{O2}i,n,l} = 2.67 \, R_{\mathrm{h}}{}'_{i,n,l}$	O_2 demand driven by potential R_{h}	[A16]
$U_{\mathrm{O2}i,n,l} = U'_{\mathrm{O2}i,n,l} [\mathrm{O}_{2\mathrm{m}i,n,l}] / ([\mathrm{O}_{2\mathrm{m}i,n,l}] + \boldsymbol{K}_{\mathbf{O_2}})$	active uptake coupled with radial diffusion of O_2	[A17a]
$= 4 \, \pi \, n \, M_{i,n,a,l,\mathrm{C}} \, D_{\mathrm{sO2}l} \, [\boldsymbol{r}_{\mathbf{m}} \, r_{\mathrm{w}l} / (r_{\mathrm{w}l} - \boldsymbol{r}_{\mathbf{m}})]([\mathrm{O}_{2\mathrm{s}l}] - [\mathrm{O}_{2\mathrm{m}i,n,l}]$		[A17b]
$R_{\mathrm{m}i,n,j,l} = \boldsymbol{R}_{\mathrm{m}} \, M_{i,n,j,l,\mathrm{N}} \, f_{\mathrm{tm}l}$	maintenanace respiration	[A18]
$f_{\mathrm{tm}l} = e^{[y \, (T_{\mathrm{s}l} - 298.16)]}$	temperature sensitivity of R_{m}	[A19]
$R_{\mathrm{g}i,n,l} = R_{\mathrm{h}i,n,l} - \Sigma_j \, R_{\mathrm{m}i,n,j,l}$	growth respiration	[A20]
$U_{i,n,l\mathrm{C}} = \min (R_{\mathrm{h}i,n,l}, \Sigma_j \, R_{\mathrm{m}i,n,j,l}) + R_{\mathrm{g}i,n,l} (1 + \boldsymbol{\Delta G}_{\boldsymbol{x}} / \boldsymbol{E}_{\mathbf{m}})$	DOC uptake driven by R_{g}	[A21]
$U_{i,n,l\mathrm{N,P}} = U_{i,n,l} \, Q_{i,l,\mathrm{N,P}} / Q_{i,l,\mathrm{C}}$	DON, DOP uptake driven by $U_{i,n,l\mathrm{C}}$	[A22]
$D_{Mi,n,j,l,\mathrm{C}} = \boldsymbol{D}_{Mi,j} \, M_{i,n,j,\mathrm{C}} \, (1.0 - (\boldsymbol{X}_{\mathbf{C}mn} + (\boldsymbol{X}_{\mathbf{C}mx} - \boldsymbol{X}_{\mathbf{C}mn}) \, f_{\lambda \mathrm{C}i,n,j,l}))$	decay of microbial C less internal recycling	[A23a]
$D_{Mi,n,j,\mathrm{N,P}} = \boldsymbol{D}_{Mi,j} \, M_{i,n,j,l,\mathrm{N,P}} \, (1.0 - \boldsymbol{X}_{\mathbf{N,P}} \, f_{\lambda \mathrm{N,P}i,n,j,l})$	decay of microbial N, P less internal recycling	[A23b]
$f_{\lambda \mathrm{C}i,n,j,l} = \min\{M_{i,n,n,l,\mathrm{N}} / (M_{i,n,n,l,\mathrm{N}} + M_{i,n,n,l,\mathrm{C}} \, \boldsymbol{K}_{\boldsymbol{\lambda}\mathbf{N}}), M_{i,n,n,l,\mathrm{P}} + M_{i,n,n,l,\mathrm{C}} \, \boldsymbol{K}_{\boldsymbol{\lambda}\mathbf{P}}\}$ $(1.0 - [Q_{i,l,\mathrm{C}}]/(\boldsymbol{K}_{\mathbf{m}\boldsymbol{Q}\mathbf{C}} + [Q_{i,l,\mathrm{C}}])$	internal C,N,P recycling determined by nonstructural C,N,P ratios and by substrate concentration	[A24a] [A24b]
$f_{\lambda \mathrm{N,P}i,n,j,l} = M_{i,n,n,l,\mathrm{C}} / (M_{i,n,n,l,\mathrm{C}} + M_{i,n,n,l,\mathrm{N,P}} / \boldsymbol{K}_{\boldsymbol{\lambda}\mathbf{N,P}})$		
$\delta M_{i,n,j,l,\mathrm{C}} / \delta t = F_j \, U_{i,n,l\mathrm{C}} - F_j \, R_{\mathrm{h}i,n,l} - D_{Mi,n,j,l,\mathrm{C}}$	$[R_{\mathrm{h}i,n,l} > R_{\mathrm{m}i,n,j,l}]$ microbial growth	[A25a]
$\delta M_{i,n,j,l,\mathrm{C}} / \delta t = F_j \, U_{i,n,l\mathrm{C}} - R_{\mathrm{m}i,n,j,l} - D_{Mi,n,j,l,\mathrm{C}}$	$[R_{\mathrm{h}i,n,l} < R_{\mathrm{m}i,n,j,l}]$ microbial senescence	[A25b]

Microbial Nutrient Exchange

$U_{NH4i,n,j,l} = (M_{i,n,j,l,C}\ \boldsymbol{C_{Nj}} - M_{i,n,j,l,N})$	$U_{NH_4} < 0$	net mineralization	[A26a]
$U_{NH_4i,n,j,l} = \min\ \{(M_{i,n,j,l,C}\ \boldsymbol{C_{Nj}} - M_{i,n,j,l,N}),$ $\boldsymbol{U'_{NH_4}}\ a_{i,n,j,l}\ ([NH_4^+{}_{i,n,j,l}] - [\boldsymbol{NH_4^+{}_{mn}}]) / ([NH_4^+{}_{i,n,j,l}] - [\boldsymbol{NH_4^+{}_{mn}}] + \boldsymbol{K_{NH_4}})\}$	$U_{NH_4} > 0$	net immobilization	[A26b]
$U_{NO_3i,n,j,l} = \min\ \{(M_{i,n,j,l,C}\ \boldsymbol{C_{Nj}} - (M_{i,n,j,l,N}\ + U_{NH_4i,n,j,l}))\ ,$ $\boldsymbol{U'_{NO_3}}\ a_{i,n,j,l}\ ([NO_3^-{}_{i,n,j,l}] - [\boldsymbol{NO_3^-{}_{mn}}]) / ([NO_3^-{}_{i,n,j,l}] - [\boldsymbol{NO_3^-{}_{mn}}] + \boldsymbol{K_{NO_3}})\}$	$U_{NO_3} > 0$	net immobilization	[A26c]
$U_{PO4i,n,j,l} = (M_{i,n,j,l,C}\ \boldsymbol{C_{Pj}} - M_{i,n,j,l,P})$	$U_{PO_4} < 0$	net mineralization	[A26d]
$U_{PO4i,n,j,l} = \min\ \{(M_{i,n,j,l,C}\ \boldsymbol{C_{Pj}} - M_{i,n,j,l,P}),$ $\boldsymbol{U'_{PO_4}}\ A_{i,n,j,l}\ (\boldsymbol{[H_2PO_4^-{}_{i,n,j,l}] - [H_2PO_4^-{}_{mn}])\ /\ ([H_2PO_4^-{}_{i,n,j,l}] - [H_2PO_4^-{}_{mn}] + K_{PO_4})\}$	$U_{PO_4} > 0$	net immobilization	[A26e]
$\Phi_{i,n=f,j,l} = max\ \{0, M_{i,n=f,j,l,C}\ \boldsymbol{C_{Nj}} - M_{i,n=f,j,l,N} - max\{0, U_{i,n=f,j,l,N}\}\}$	N_2 fixation driven by N deficit of diazotrophic population		[A27]
$R_{\Phi i,n=f,j,l} = \boldsymbol{E_\Phi}\ \Phi_{i,n=f,j,l}$	respiration needed to drive N_2 fixation		[A28]
$\delta M_{i,n,j,l,N} / \delta t = F_j\ U_{i,n,l,N} + U_{NH_4i,n,j,l} + U_{NO_3i,n,j,l} + \Phi_{i,n=f,j,l} - D_{Mi,n,j,l,N}$	growth *vs*. losses of microbial N, P		[A29a]
$\delta M_{i,n,j,l,P} / \delta t = F_j U_{i,n,l,P} + U_{PO_4i,n,j,l} - D_{Mi,n,j,l,P}$			[A29b]
$M_{i,n,a,l,C} = M_{i,n,j=labile,l,C} + M_{i,n,j=resistant,l,C}\ F_r / F_l$	active microbial biomass calculated from labile fraction		[A30a]

Humification

$H_{Si,j=lignin,l,C} = D_{Si,j=lignin,l,C}$	decomposition products of litter substrate added to POC depending on lignin		[A31]
$H_{Si,j=lignin,l,N,P} = D_{Si,j=lignin,l,N,P}$			[A32]
$H_{Si,j\neq lignin,l,C} = H_{Si,j=lignin,l,C}\ \boldsymbol{L_{hj}}$			[A33]
$H_{Si,j\neq lignin,l,N,P} = H_{Si,j\neq lignin,l,C}\ S_{i,l,N,P} / S_{i,l,C}$			[A34]
$H_{Mi,n,j,l,C} = D_{Mi,n,j,l,C}\ \boldsymbol{F_h}$	fraction of microbial decay products added to humus		[A35]
$H_{Mi,n,j,l,N,P} = H_{Mi,n,j,l,C}\ M_{i,n,j,l,N,P} / M_{i,n,j,l,C}$			[A36]
$\boldsymbol{F_h} = 0.167 + 0.167\ F_{clay} + 0.167 \times 10^{-6}\ G_{i,l,C}$	fraction of D_M added to humus depends on clay and SOC		[A37]
$H_{Zi,n,j,l,C} = D_{Mi,n,j,l,C} - H_{Mi,n,j,l,C}$	remainder of microbial decay products added to microbial residues		[A38]
$H_{Zi,n,j,l,N,P} = D_{Mi,n,j,l,N,P} - H_{Mi,n,j,l,N,P}$			[A39]

Definition of Variables in Appendix A

Variable	Definition	Unit	Equation	Value	Reference
		subscripts			
i	substrate-microbe complex: coarse woody litter, fine non-woody litter, POC, humus				
j	kinetic component: labile l, resistant r, active a, nonstructural n				
l	soil or litter layer				
n	microbial functional type: heterotrophic (bacteria, fungi), autotrophic (nitrifiers, methanotrophs), diazotrophic, obligate aerobe, facultative anaerobes (denitrifiers), obligate anaerobes (methanogens)				
		variables			
$A_{i,l,\mathrm{C}}$	mass of adsorbed SOC	g C m^{-2}	[A1c,A2c]		
$[A_{i,l,\mathrm{C}}]$	concentration of adsorbed SOC in soil	g C Mg^{-1}	[A4c]		
a	microbial surface area	m^2 m^{-2}	[A26]		
$\boldsymbol{B}$	parameter such that $f_{\mathrm{tg}} = 1.0$ at $T_l = 298.15$ K		[A6]	26.235	
$\boldsymbol{b}$	Freundlich exponent for sorption isotherm		[A8]	0.85	Grant et al. (1993a,b)
$\boldsymbol{\beta}$	specific colonization rate of uncolonized substrate	-	[A5]	2.5	Grant et al. (2010)
$C_{\mathrm{N,P}i,n,a,l}$	ratio of $M_{i,n,a,\mathrm{N,P}}$ to $M_{i,n,a,\mathrm{C}}$	g N or P g C^{-1}	[A12]		
$\boldsymbol{C}_{\mathbf{N,P}j}$	maximum ratio of $M_{i,n,j,\mathrm{N,P}}$ to $M_{i,n,j,\mathrm{C}}$ maintained by $M_{i,n,j,\mathrm{C}}$	g N or P g C^{-1}	[A12,A26,A27]	0.22 and 0.13 (N), 0.022 and 0.013 (P) for j = labile and resistant, respectively	Grant et al. (1993a,b)
$D_{Ai,l,\mathrm{C}}$	decomposition rate of $A_{i,l,\mathrm{C}}$ by $M_{\boldsymbol{i,d,l},\mathrm{C}}$ producing Q in [A13]	g C m^{-2} h^{-1}	[A1c,A7c,A31c]		
$\boldsymbol{D}_{Aj,\mathrm{C}}$	specific decomposition rate of $A_{i,l,\mathrm{C}}$ by $M_{\boldsymbol{i,d,l},\mathrm{C}}$ at 25°C and saturating$[A_{i,l,\mathrm{C}}]$	g C g C^{-1} h^{-1}	[A4c]	0.025	Grant et al. (1993a,b)
$D_{Ai,j,\,l,\mathrm{N,P}}$	decomposition rate of $A_{i,l,\mathrm{N,P}}$ by $M_{\boldsymbol{i,d,l},\mathrm{C}}$	g N or P m^{-2} h^{-1}	[A7c]		
$D'_{Ai,j,\,l,\mathrm{C}}$	specific decomposition rate of $S_{i,j,l,\mathrm{C}}$ by $\Sigma_n M_{i,n,a,l}$ at 25°C	g C g C^{-1} h^{-1}	[A1a,A4c]		

$\boldsymbol{D}_{Mi,j}$	specific decomposition rate of $M_{i,n,j}$ at 30°C	g C g C^{-1} h^{-1}	[A23a,b]	2.0 x 10^{-3} and 1.0 x 10^{-4} for j = labile and resistant, respectively	Grant et al. (1993a,b)
$D_{Mi,n,j,l,\mathrm{C}}$	decomposition rate of $M_{i,n,j,l,\mathrm{C}}$	g C m^{-2} h^{-1}	[A23a,A25, A35,A38]		
$D_{Mi,n,j,l,\mathrm{N,P}}$	decomposition rate of $M_{i,n,j,l,\mathrm{N,P}}$	g N or P m^{-2} h^{-1}	[A23b,A29, A39]		
$D_{Si,j,l,\mathrm{C}}$	decomposition rate of $S_{i,j,l,\mathrm{C}}$ by $\Sigma_n M_{i,n,a,l}$ producing Q in [A13]	g C m^{-2} h^{-1}	[A1a,A7a,A 31a]		
$\boldsymbol{D}_{Sj,\mathrm{C}}$	specific decomposition rate of $S_{i,j,l,\mathrm{C}}$ by $\Sigma_n M_{i,n,a,l}$ at 25°C and saturating [$S_{i,l,\mathrm{C}}$]	g C g C^{-1} h^{-1}	[A4a]	1.0, 1.0, 0.15, and 0.025 for j = protein, carbohydrat e, cellulose, and lignin, 0.009 for POC, and 0.009 and 0.003 for active and passive humus.	Grant et al. (1993a,b)
$D_{Si,j,\ l,\mathrm{N,P}}$	decomposition rate of $S_{i,j,l,\mathrm{N,P}}$ by $\Sigma_n M_{i,n,a,l}$	g N or P m^{-2} h^{-1}	[A7a, A32]		
$D'_{Si,j,\ l,\mathrm{C}}$	specific decomposition rate of $S_{i,j,l,\mathrm{C}}$ by $\Sigma_n M_{i,n,a,l}$ at 25°C	g C g C^{-1} h^{-1}	[A1a,A4a]		
D_{sO2l}	aqueous dispersivity–diffusivity of O2 during microbial uptake in soil	m^2 h^{-1}	[A17]		
$D_{Zi,j,l,\mathrm{C}}$	decomposition rate of $Z_{i,j,l,\mathrm{C}}$ by $\Sigma_n M_{i,n,a,l}$ producing Q in [A13]	g C m^{-2} h^{-1}	[A1b,A7b]		
$D_{Zi,j,\mathrm{N,P}}$	decomposition rate of $Z_{i,j,l,\mathrm{N,P}}$ by $\Sigma_n M_{i,n,a,l}$	g N or P m^{-2} h^{-1}	[A7b]		
$\boldsymbol{D}_{Zj,\mathrm{C}}$	specific decomposition rate of $Z_{i,j,l,\mathrm{C}}$ by $\Sigma_n M_{i,n,a,l}$ at 25°C and saturating[$Z_{i,l,\mathrm{C}}$]	g C g C^{-1} h^{-1}	[A4b]	0.25 and 0.05 for j = labile and resistant biomass	Grant et al. (1993a,b)
$D'_{Zi,j,l,\mathrm{C}}$	specific decomposition rate of $Z_{i,j,l,\mathrm{C}}$ by $\Sigma_n M_{i,n,a,l}$ at 25°C	g C g C^{-1} h^{-1}	[A1b,A4b]		
$\boldsymbol{\Delta G_x}$	energy yield of C oxidation with different reductants x	kJ g C^{-1}	[A21]	37.5 (x = O_2), 4.43 (x = DOC)	
$\boldsymbol{E}_{\mathbf{m}}$	energy requirement for growth of $M_{i,n,a,l}$	kJ g C^{-1}	[A21]	25	
$\boldsymbol{E_\Phi}$	energy requirement for non-symbiotic N_2 fixation by heterotrophic diazotrophs ($n = f$)	g C g N^{-1}	[A28]	5	Waring and Running (1998)
F_{clay}	fraction of mineral soil as clay	Mg Mg^{-1}	[A37]		

$\boldsymbol{F_h}$	fraction of products from microbial decomposition that are humified (function of clay content)		[A35, A37]		Sørenson (1981)
$\boldsymbol{F_l}$	fraction of microbial growth allocated to labile component $M_{i,n,l}$		[A25,A29,A30]	0.55	Grant et al. (1993a,b)
$\boldsymbol{F_r}$	fraction of microbial growth allocated to resistant component $M_{i,n,r}$		[A25,A29,A30]	0.45	Grant et al. (1993a,b)
F_s	equilibrium ratio between $Q_{i,l,C}$ and $H_{i,l,C}$		[A8]		
$f_{\lambda C i,n,j,l}$	fraction of C recycled to nonstructural pool during decomposition	-	[A23a,A24a]		
$f_{\lambda N,P i,n,j,l}$	fraction of N or P recycled to nonstructural pool during decomposition	-	[A23b,A24b]		
$f_{tg l}$	temperature function for microbial growth respiration	dimensionless	[A1,A6,A13]		
$f_{tm l}$	temperature function for maintenance respiration	dimensionless	[A18,A19]		
$f_{\psi g l}$	soil water potential function for microbial, root or mycorrhizal growth respiration	dimensionless	[A13,A15]		Pirt (1975)
$\Phi_{i,n=f,j,l}$	non-symbiotic N_2 fixation by heterotrophic diazotrophs ($n = f$)	g N m^{-2} h^{-1}	[A27,A28,A29]		
$G_{i,l,C}$	total C in substrate-microbe complex	g C Mg^{-1}	[A1,A2c,A3a,A8,A37]		
$[H_2PO_4^-]$	concentration of $H_2PO_4^-$ in soil solution	g P m^{-3}	[A26]		
$\boldsymbol{H_a}$	energy of activation	J mol^{-1}	[A6,C10]	65 x 10^3	Addiscott (1983)
$\boldsymbol{H_{dh}}$	energy of high temperature deactivation	J mol^{-1}	[A6,C10]	225 x 10^3	
$\boldsymbol{H_{dl}}$	energy of low temperature deactivation	J mol^{-1}	[A6,C10]	195 x 10^3	
$H_{Mi,n,j,l,C}$	transfer of microbial C decomposition products to humus	g C m m^{-2} h^{-1}	[A35,A36,A38]		
$H_{Mi,n,j,l,N,P}$	transfer of microbial N or P decomposition products to humus	g N or P m^{-2} h^{-1}	[A36,A39]		
$H_{Si,j,l,C}$	transfer of C hydrolysis products to particulate OM	g C m^{-2} h^{-1}	[A31,A32,A33, A34]		
$H_{Si,j,l,N,P}$	transfer of N or P hydrolysis products to particulate OM	g N or P m^{-2} h^{-1}	[A32,A34]		
$H_{Zi,n,j,l,C}$	transfer of microbial C decomposition products to microbial residue	g C m m^{-2} h^{-1}	[A38]		
$H_{Zi,n,j,l,N,P}$	transfer of microbial N or P decomposition products to microbial residue	g N or P m^{-2} h^{-1}	[A39]		
$\boldsymbol{K_{\lambda N}}$	C:N ratio used to calculate internal recycling of C, N	-	[A24a,b]	0.1	
$\boldsymbol{K_{\lambda P}}$	C:P ratio used to calculate internal recycling of C, P	-	[A24a,b]	0.01	
$\boldsymbol{K_{iS}}$	inhibition constant for microbial colonization of substrate	-	[A5]	0.5	Grant et al. (2010)
$\boldsymbol{K_{NH_4}}$	M-M constant for NH_4^+ uptake at microbial surfaces	g N m^{-3}	[A26]	0.40	

K_{NO_3}	M-M constant for NO_3^- uptake at microbial surfaces	g N m^{-3}	[A26]	0.35	
K_{PO_4}	M-M constant for $H_2PO_4^-$ uptake at microbial surfaces	g P m^{-3}	[A26]	0.125	
K_{iD}	inhibition constant for $[M_{i,n,a}]$ on $S_{i,C}$, $Z_{i,C}$	g C m^{-3}	[A4]	25	Grant et al. (1993a,b); Lizama and Suzuki (1990)
K_{mD}	Michaelis–Menten constant for $D_{Si,j,C}$	g C Mg^{-1}	[A4]	75	
K_{mQ_C}	Michaelis–Menten constant for $R'_{hi,n}$ on $[Q_{i,C}]$	g C m^{-3}	[A13,A24a]	12	
K_{O_2}	Michaelis–Menten constant for reduction of O_{2s} by microbes, roots and mycorrhizae	g O_2 m^{-3}	[A17]	0.064	Griffin (1972); Longmuir (1954_
k_{ts}	equilibrium rate constant for sorption	h^{-1}	[A8]	0.01	Grant et al. (1993a,b)
L_{hj}	ratio of nonlignin to lignin components in humified hydrolysis products		[A33]	0.10, 0.05, and 0.05 for j = protein, carbohydrate, and cellulose, respectively	Shulten and Schnitzer (1997)
M	molecular mass of water	g mol^{-1}	[A15]	18	
$M_{i,d,l,C}$	heterotrophic microbial C used for decomposition	g C m^{-2}	[A1,A3a,A4]		
$M_{i,n,j,l,C}$	microbial C	g C m^{-2}	[A13,A17A23,A24,A25,A26, A30,A36]		
$M_{i,n,j,l,N}$	microbial N	g N m^{-2}	[A18,A23,A24A27,A29]		
$M_{i,n,j,l,P}$	microbial P	g P m^{-2}	[A23,A24,A29,A26, A36]		
$M_{i,n,a,l,C}$	active microbial C from heterotrophic population n associated with $G_{i,l,C}$	g C m^{-2}	[A3,A13,A17, A30]		
$[M_{i,n,a,l,C}]$	concentration of $M_{i,n,a}$ in soil water = $M_{i,n,a,l,C}/\theta_l$	g C m^{-3}	[A3, A5]		
n	number of microbial microsites	m^{-2}	[A17b]		
$[NH_4^+{}_{i,n,j,l}]$	concentration of NH_4^+ at microbial surfaces	g N m^{-3}	[A26]		
$[NH_4^+{}_{mn}]$	concentration of NH_4^+ at microbial surfaces below which $U_{NH_4} = 0$	g N m^{-3}	[A26]	0.0125	
$[NO_3^-{}_{i,n,j,l}]$	concentration of NH_4^+ at microbial surfaces	g N m^{-3}	[A26]		
$[NO_3^-{}_{mn}]$	concentration of NO_3^- at microbial surfaces below which $U_{NO_3} = 0$	g N m^{-3}	[A26]	0.03	
$[H_2PO_4^-{}_{i,n,j,l}]$	concentration of $H_2PO_4^-$ at microbial surfaces	g N m^{-3}	[A26]		
$[H_2PO_4^-{}_{mn}]$	concentration of $H_2PO_4^-$ at microbial surfaces below which $U_{PO_4} = 0$	g N m^{-3}	[A26]	0.002	

$[O_{2mi,n,l}]$	O_2 concentration at heterotrophic microsites	g O_2 m^{-3}	[A17]		
$[O_{2sl}]$	O_2 concentration in soil solution	g O_2 m^{-3}	[A17]		
$Q_{i,l,C}$	*DOC* from products of $D_{Si,j,l,C}$ [A3] and $D_{Zi,j,l,C}$) [A5]	g C m^{-2}	[A8,A13,A22]		
$[Q_{i,l,C}]$	solution concentration of $Q_{i,l,C}$	g C Mg^{-1}	[A8,A13,A24a]		
$Q_{i,l,N,P}$	*DON* and DOP from products of ($D_{Si,j,l,N,P}$ + $D_{Zi,j,l,N,P}$)	g N or P m^{-2}	[A9,A22]		
q_m	rate constant for reallocating $M_{i,a,l,C}$ to $M_{i,d,l,C}$	h^{-1}	[A3a]	0.5	
R	gas constant	J mol^{-1} K^{-1}	[A6,A15,C10]	8.3143	
$R_{\Phi i,n=f,j,l}$	respiration for non-symbiotic N_2 fixation by heterotrophic diazotrophs ($n = f$)	g C m^{-2} h^{-1}	[A28]		
$R_{gi,n,l}$	growth respiration of $M_{i,n,a,l}$ on $Q_{i,l,C}$ under nonlimiting O_2 and nutrients	g C g C^{-1} h^{-1}	[A20]		
R_h	total heterotrophic respiration of all $M_{i,n,a,l}$ under ambient DOC, O_2, nutrients, θ and temperature	g C m^{-2} h^{-1}	[A11]		
$R_{hi,n,l}$	heterotrophic respiration of $M_{i,n,a,l}$ under ambient DOC, O_2, nutrients, θ and temperature	g C m^{-2} h^{-1}	[A5,A11,A14,A20, A21,A25]		
$R_{hi,n,l}$	specific heterotrophic respiration of $M_{i,n,a,l}$ under nonlimiting O_2, DOC, θ and 25°C	g C g C^{-1} h^{-1}	[A12,A13]		
$R_{h'n}$	specific heterotrophic respiration of $M_{i,n,a,l}$ under nonlimiting DOC, O_2, nutrients, θ and 25°C	g C g C^{-1} h^{-1}	[A12]	0.125	Shields et al. (1973)
$R_{h'i,n,l}$	heterotrophic respiration of $M_{i,n,a,l}$ under nonlimiting O_2 and ambient DOC, nutrients, θ and temperature	g C m^{-2} h^{-1}	[A13,A14,A16]		
R_m	specific maintenance respiration at 25°C	g C g N^{-1} h^{-1}	[A18]	0.0115	Barnes et al. (1998)
$R_{mi,n,j,l}$	maintenance respiration by $M_{i,n,j,l}$	g C m^{-2} h^{-1}	[A18,A20,A21,A25]		
σ	shape parameter in $f_{\psi g}$	-	[A15]	0.2	Choudhury et al., (2011)
r_{wl}	radius of r_m + water film at current water content	m	[A17]		
r_m	radius of heterotrophic microsite	m	[A17]	2.5×10^{-6}	
r_{wl}	thickness of water films	m	[A17]		
S	change in entropy	J mol^{-1} K^{-1}	[A6,C10]	710	Sharpe and DeMichelle (1977)
$[S_{i,j,l,C}]$	concentration of $S_{i,j,l,C}$ in soil	g C Mg^{-1}	[A4a]		
$S_{i,j,l,C}$	mass of colonized litter, POC or humus C	g C m^{-2}	[A2a,A5,A7a,A33]		
$S'_{i,j,l,C}$	mass of uncolonized litter, POC or humus C	g C m^{-2}	[A5]		

$S_{i,j,l,\mathrm{N,P}}$	mass of litter, POC or humus N or P	g N or P m^{-2}	[A7a,A33]	
T_{sl}	soil temperature	K	[A6,A15.A19]	
$U_{i,n,l\mathrm{C}}$	uptake of $Q_{i,l,\mathrm{C}}$ by $\Sigma_n M_{i,n,a,l}$ under limiting nutrient availability	g C m^{-2} h^{-1}	[A5,A21,A22,A25]	
$U_{i,n,\mathrm{N,P}}$	uptake of $Q_{i,l,\mathrm{N,P}}$ by $\Sigma_n M_{i,n,a,l}$ under limiting nutrient availability	g N or P m^{-2} h^{-1}	[A22,A29]	
$U_{\mathrm{NH4}i,n,j,l}$	NH_4^+ uptake by microbes	g N m^{-2} h^{-1}	[A26, A27,A29]	
$\boldsymbol{U'_{NH_4}}$	maximum U_{NH_4} at 25 ºC and non-limiting NH_4^+	g N m^{-2} h^{-1}	[A26]	5.0 x 10^{-3}
$U_{\mathrm{NO3}i,n,j,l}$	NO_3^- uptake by microbes	g N m^{-2} h^{-1}	[A26,A27,A29]	
$\boldsymbol{U'_{NO_3}}$	maximum U_{NO_3} at 25 ºC and non-limiting NO_3^-	g N m^{-2} h^{-1}	[A26]	5.0 x 10^{-3}
$U_{\mathrm{O2}i,n}$	O_2 uptake by $M_{i,n,a,l}$ under ambient O_2	g m^{-2} h^{-1}	[A14,A17]	
$U'_{\mathrm{O2}i,n}$	O_2 uptake by $M_{i,n,a,l}$ under nonlimiting O_2	g m^{-2} h^{-1}	[A14,A16,A17]	
$U_{\mathrm{PO4}i,n,j,l}$	$H_2PO_4^-$ uptake by microbes	g N m^{-2} h^{-1}	[A26,A27,A29]	
$\boldsymbol{U'_{PO_4}}$	maximum U_{PO_4} at 25 ºC and non-limiting $H_2PO_4^-$	g N m^{-2} h^{-1}	[A26]	5.0 x 10^{-3}
$V_{i,l,\mathrm{C}}$	adsorbed C hydrolysis products	g C Mg^{-1}	[A8,A10]	
$V_{i,l,\mathrm{N,P}}$	adsorbed N or P hydrolysis products	g P Mg^{-1}	[A10]	
$\boldsymbol{X_{Cmn}}$	minimum C internal recycling fraction	-	[A23a]	0.167
$\boldsymbol{X_{Cmx}}$	maximum C internal recycling fraction	-	[A23a]	0.833
$\boldsymbol{X_{N,P}}$	maximum N,P internal recycling fraction	-	[A23b]	0.80
$\boldsymbol{y}$	selected to give a Q_{10} for f_{tm} of 2.25		[A19]	0.081
ψ_s	soil or residue water potential	MPa	[A15]	
$Y_{i,l,\mathrm{C}}$	sorption of C hydrolysis products	g C m^{-2} h^{-1}	[A8,A9,A10]	
$Y_{i,l,\mathrm{N,P}}$	sorption of N or P hydrolysis products	g P m^{-2} h^{-1}	[A9,A10]	
$[Z_{i,j,l,\mathrm{C}}]$	concentration of $Z_{i,j,l,\mathrm{C}}$ in soil	g C Mg^{-1}	[A4b]	
$Z_{i,j,l,\mathrm{C}}$	mass of microbial residue C in soil	g C m^{-2}	[A2b,A7b]	
$Z_{i,j,l,\mathrm{N,P}}$	mass of microbial residue N or P in soil	g P m^{-2}	[A7b]	

Appendix B: Soil-Plant Water Relations

Canopy Transpiration

$Rn_{ci} + LE_{ci} + H_{ci} + G_{ci} = 0$ — canopy energy balance [B1a]

$\boldsymbol{L}E_{ci} = L\,(e_a - e_{ci(T_{ci},\psi_{ci})}) / r_{ai}$ — *LE* from canopy evaporation [B1b]

$\boldsymbol{L}E_{ci} = L\,(e_a - e_{ci(T_{ci},\psi_{ci})}) / (r_{ai} + r_{ci})$ - $\boldsymbol{L}E_{ci}$ from [B1b] [B1c]

$H_{ci} = \rho C_p\,(T_a - T_{ci}) / r_{ai}$ — *LE* from canopy transpiration [B1d]

H from canopy energy balance

$r_{cmini} = 0.64\,(C_b - \boldsymbol{C}_i'_i) / V_c'_i$ — r_c driven by rates of carboxylation *vs.* diffusion [B2a]

$r_{ci} = r_{cmini} + (\boldsymbol{r_{cmaxi}} - r_{cmini})\, e^{(-\boldsymbol{\beta}\,\psi_{ti})}$ — r_c constrained by water status [B2b]

$r_{ai} = \{(\ln((z_u - z_{di}) / z_{ri})^2 / (\boldsymbol{K}^2 u_a)\} / (1 - 10\,Ri)$ — r_a driven by windspeed, surface roughness [B3a]

$Ri = \{g\,(z_u - z_{ri}) / (u_a^2\,T_a)\}\,(T_a - T_c)$ — r_a adjusted for stability vs. buoyancy [B3b]

$\psi_{ti} = \psi_{ci}$ - $\psi_{\pi i}$ [B4]

Root and Mycorrhizal Water Uptake

$U_{wi} = \Sigma_l \Sigma_r U_{wi,r,l}$ [B5]

$U_{wi,r,l} = (\psi_c'_i - \psi_s'_l) / (\Omega_{si,r,l} + \Omega_{ri,r,l} + \Sigma_x \Omega_{ai,r,l,x})$ — U_w along hydraulic gradient [B6]

$\psi_c'_i = \psi_{ci} + 0.01\,z_{bi}$ [B7]

$\psi_s'_l = \psi_{sl} - 0.01\,z_l$ [B8]

$\Omega_{si,r,l} = \ln\{(d_{i,r,l} / r_{i,r,l}) / (2\pi L_{i,r,l}\,\kappa_{ri,r,l})\}\;\theta_{wl} / \theta_{pl}$ [B9]

$\Omega_{ri,r,l} = \boldsymbol{\Omega'_{ri,r}} / L_{i,r,l}$ [B10]

$\Omega_{ai,r,l,x=1} = \boldsymbol{\Omega}_{\boldsymbol{ai,r}}\,z_l / \{n_{i,r,l,1}\,(r_{i,r,l,1} / \boldsymbol{r'}_{i,r})^4\} + \boldsymbol{\gamma\,\Omega}_{\boldsymbol{ai,r}}\,z_{bi} / \{n_{i,r,l,1}\,(r_{bi} / r_b'_i)^4\}\,\Sigma_{i,r,l}\,(M_{i,r,l}) / M_{i,r,l}$ [B11]

$\Omega_{ai,r,l,x=2} = \boldsymbol{\Omega}_{\boldsymbol{ai,r}}\,(L_{i,r,l,2} / n_{i,r,l,2}) / \{n_{i,r,l,2}\,(r_{i,r,l,2} / r'_{i,r})^4\}$ [B12]

$\delta L_{i,r,l,1} / \delta t = \delta M_{i,r,l,1} / \delta t\;\nu_r / \{\rho_r\,(1 - \theta_{Pi,r})\,(\pi\,r_{i,r,l,1}^2)\}$ [B13]

Canopy Water Potential

$(e_a - e_{i(T_{ci})}) / (r_{ai} + r_{ci})$ [B1] $= \Sigma_l\;\Sigma_r (\psi_c'_i - \psi_s'_l) / (\Omega_{si,r,l} + \Omega_{ri,r,l} + \Sigma_x \Omega_{ai,r,l,x}) + X_{ci}\delta\psi_{ci} / \delta t$ — ψ_c solved when transpiration from [B1-B4] (LHS) equals uptake from [B5-B13] + change in storage (RHS) [B14]

Definition of Variables in Appendix B

Variable	Definition	Unit	Equation	Value
	subscripts			
i	plant species or functional type: coniferous, deciduous, annual, perennial, C_3, C_4, monocot, dicot etc.			
j	branch or tiller			
k	node			
l	soil or canopy layer			
m	leaf azimuth			
n	leaf inclination			
o	leaf exposure (sunlit *vs*. shaded)			
r	root or mycorrhizae			
	variables			
$\boldsymbol{\beta}$	stomatal resistance shape parameter	MPa^{-1}	[B2b,C4,C9]	-5.0	Grant and Flanagan (2007)
C_b	$[CO_2]$ in canopy air	$\mu mol\ mol^{-1}$	[B2,C2,C5]		
$\boldsymbol{C_i'_i}$	$[CO_2]$ in canopy leaves at $\psi_{c_i} = 0$ MPa	$\mu mol\ mol^{-1}$	[B2]	0.70 C_b	Larcher (2001)
$d_{i,r,l}$	half distance between adjacent roots	m	[B9]		
E_{ci}	canopy transpiration	$m^3\ m^{-2}\ h^{-1}$	[B1,B14]		
e_a	atmospheric vapor density at T_a and ambient humidity	$g\ m^{-3}$	[B1]		
$e_{ci(T_{ci}, \psi_{ci})}$	canopy vapor density at T_{c_i} and ψ_{c_i}	$g\ m^{-3}$	[B1]		
G_{ci}	canopy storage heat flux	$W\ m^{-2}$	[B1]		
H_{ci}	canopy sensible heat flux	$W\ m^{-2}$	[B1]		
K	von Karman's constant		[B3a]	0.41	
$\kappa_{ri,r,l}$	hydraulic conductivity between soil and root surface	$m^2\ MPa^{-1}\ h^{-1}$	[B9]		
$\boldsymbol{\gamma}$	scaling factor for bole axial resistance from primary root axial resistance	-	[B11]	1.6×10^4	Grant et al. (2007)
$\boldsymbol{L}$	latent heat of evaporation	$J\ g^{-1}$	[B1]	2460	
$\boldsymbol{L}E_{ci}$	latent heat flux between canopy and atmosphere	$W\ m^{-2}$	[B1]		

$L_{i,r,l}$	length of roots or mycorrhizae	m m^{-2}	[B9,B10,B12,B13]		
$M_{i,r,l}$	mass of roots or mycorrhizae	g m^{-2}	[B11,B13]		
$n_{i,r,l,x}$	number of primary (x = 1) or secondary (x = 2) axes	m^{-2}	[B11,B12]		
$\Omega_{ai,r}$	axial resistivity to water transport along root or mycorrhizal axes	MPa h m^{-4}	[B11,B12]	4.0 x 10^{9} deciduous 1.0 x 10^{10} coniferous	Larcher (2001)
$\Omega_{ai,r,l,x}$	axial resistance to water transport along axes of primary (x = 1) or secondary (x = 2) roots or mycorrhizae	MPa h m^{-1}	[B6,B11,B12]		
$\Omega_{ri,r}$	radial resistivity to water transport from surface to axis of roots or mycorrhizae	MPa h m^{-2}	[B10]	1.0 x 10^{4}	Doussan et al. (1998)
$\Omega_{ri,r,l}$	radial resistance to water transport from surface to axis of roots or mycorrhizae	MPa h m^{-1}	[B6,B10]		
$\Omega_{si,r,l}$	radial resistance to water transport from soil to surface of roots or mycorrhizae	MPa h m^{-1}	[B6,B9]		
θ_{wl}	soil water content	m^3 m^{-3}	[B9]		
θ_{pl}	soil porosity	m^3 m^{-3}	[B9]		
$\theta_{Pi,r}$	root porosity	m^3 m^{-3}	[B13]		
Ri	Richarson number		[B3a,B3b]		van Bavel and Hillel (1976)
Rn_{ci}	canopy net radiation	W m^{-2}	[B1]		
r_{ai}	aerodynamic resistance to vapor flux from canopy	s m^{-1}	[B1,B3a]		
r_{bi}	radius of bole at ambient ψ_{ci}	m	[B11]		
$r_{b}'_{i}$	radius of bole at ψ_{ci} = 0 MPa	m	[B11]		
r_{ci}	canopy stomatal resistance to vapor flux	s m^{-1}	[B1,B2b]		
r_{cmaxi}	canopy cuticular resistance to vapor flux	s m^{-1}	[B2b]	5.0 x 10^{3}	Larcher (2001)
r_{cmini}	minimum r_{ci} at ψ_{ci} = 0 MPa	s m^{-1}	[B2,B2b]		
$r_{i,r,l,x}$	radius of primary (x=1) or secondary (x=2) roots or mycorrhizae at ambient $\psi_{ri\,l,z}$	m	[B9,B11,B12,B13]		
$r'_{i,r}$	radius of secondary roots or mycorrhizae at $\psi_{ri\,l,z}$ = 0 MPa	m	[B11,B12]	2.0 x 10^{-4} tree 1.0 x 10^{-4} bush 0.05 x 10^{-4} mycorrhizae	
ρ_r	root specific density	g C g FW^{-1}	[B13]	0.05	Grant (1998)
T_a	air temperature	K	[B3b]		
T_c	canopy temperature	K	[B3b]		

U_{wi}	total water uptake from all rooted soil layers	$m^3\ m^{-2}\ h^{-1}$	[B5,B14]		
$U_{wi,r,l}$	water uptake by root and mycorrhizal surfaces in each soil layer	$m^3\ m^{-2}\ h^{-1}$	[B5,B6]		
u_a	wind speed measured at z_u	$m\ s^{-1}$	[B3a,B3b]		
$V_c'_i$	potential canopy CO_2 fixation rate at ψ_{c_i} = 0 MPa	$\mu mol\ m^{-2}\ s^{-1}$	[B2]		
ν_r	root specific volume	$m^3\ g\ FW^{-1}$	[B13]	10^{-6}	Grant (1998)
X_{ci}	canopy capacitance	$m^3\ m^{-2}\ MPa^{-1}$	[B14]		
ψ_{ci}	canopy water potential	MPa	[B4,B7,B14]		
$\psi_c'_i$	ψ_{ci} + canopy gravitational potential	MPa	[B6,B7]		
$\psi_{\pi i}$	canopy osmotic potential	MPa	[B4]		
ψ_{sl}	soil water potential	MPa	[B8]		
$\psi_s'_l$	ψ_{sl} + soil gravitational potential	MPa	[B6,B8]		
ψ_{ti}	canopy turgor potential	MPa	[B2b,B4]	1.25 at ψ_c = 0	
z_{bi}	length of bole from soil surface to top of canopy	m	[B7,B11]		
z_{di}	canopy zero-plane displacement height	m	[B3a]		Perrier (1982)
z_l	depth of soil layer below surface	m	[B8,B11]		
z_r	canopy surface roughness	m	[B3a,B3b]		Perrier (1982)
z_u	height of wind speed measurement	m	[B3a,B3b]		

Appendix C: Gross Primary Productivity, Autotrophic Respiration, Growth and Litterfall

C_3 Gross Primary Productivity

$$GPP = \Sigma_{i,j,k,l,m,n,o} \left(V_{ci,j,k,l,m,n,o} = V_{gi,j,k,l,m,n,o}\right) A_{i,j,k,l,m,n,o}\, \boldsymbol{CF_i}$$ solve for $C_{ii,j,k,l,m,n,o}$ at which $V_{ci,j,k,l,m,n,o} = V_{gi,j,k,l,m,n,o}$ [C1]

$$V_{gi,j,k,l,m,n,o} = (C_b - C_{ii,j,k,l,m,n,o}) / r_{li,j,k,l,m,n,o}$$ diffusion [C2]

$$V_{ci,j,k,l,m,n,o} = min\{V_{bi,j,k,l,m,n,o},\ V_{ji,j,k,l,m,n,o}\}$$ carboxylation [C3]

$$r_{li,j,k,l,m,n,o} = r_{lmini,j,k,l,m,n,o} + (r_{lmaxi} - r_{lmini,j,k,l,m,n,o})\, e^{(-\boldsymbol{\beta}\, \psi_{ti})}$$ r_l is leaf-level equivalent of r_c [C4]

$$r_{lmini,j,k,l,m,n,o} = (C_b - \boldsymbol{C_i'_i}) / V_{c}'_{i,j,k,l,m,n,o}$$ minimum r_l is driven by carboxylation [C5]

$$V_{bi,j,k,l,m,n,o} = V_{bmaxi,j,k} (C_{ci,j,k,l,m,n,o} - \Gamma_{i,j,k}) / (C_{ci,j,k,l,m,n,o)} + K_{c_i})\ f_{\psi\ i,j,k,l,m,n,o}$$ CO_2 and water f_ψ constraints on V_b [C6a]

$$V_{bmax_{i,j,k}} = \boldsymbol{V_b'}_i \boldsymbol{F_{rubisco}}_i M_{\boldsymbol{L_{i,j,k,prot}}} / A_{i,j,k}\, f_{tbi}\, f_{iCi}$$ [C6b]

$$\Gamma_{i,j,k} = 0.5\, O_c\, V_{omax_{i,j,k}}\ \boldsymbol{K_{c}}_i / (V_{bmax_{i,j,k}}\ \boldsymbol{K_{o}}_i)$$ temperature f_{tb} and nutrient f_{iC} constraints on V_{bmax} [C6c]

$$V_{omax_{i,j,k}} = \boldsymbol{V_o'}_i \boldsymbol{F_{rubisco}}_i M_{\boldsymbol{L_{i,j,k,prot}}} / A_{i,j,k}\, f_{toi}$$ CO_2 compensation point [C6d]

$$K_{c_i} = \boldsymbol{K_{c}}_i\, f_{tkci}\, (1 + O_c / (\boldsymbol{K_{o}}_i\, f_{tkoi}))$$ oxygenation [C6e]

$$V_{ji,j,k,l,m,n,o} = J_{i,j,k,l,m,n,o}\ Y_{i,j,k,l,m,n,o} f_{\psi\ i,j,k,l,m,n,o}$$ M-M constant for V_b water constraints on V_j [C7a]

$$Y_{i,j,k,l,m,n,o} = (C_{ci,j,k,l,m,n,o} - \Gamma_{i,j,k,l}) / (4.5\ C_{ci,j,k,l,m,n,o} + 10.5\ \Gamma_{i,j,k,l})$$ carboxylation efficiency of V_j [C7b]

$$J_{i,j,k,l,m,n,o} = (\boldsymbol{\varepsilon}\, I_{i,l,m,n,o} + J_{maxi,j,k} - ((\boldsymbol{\varepsilon}\, I_{i,l,m,n,o} + J_{maxi,j,k})^2 - 4\boldsymbol{\alpha\varepsilon}\, I_{i,l,m,n,o}\, J_{maxi,j,k})^{0.5}) / (2\boldsymbol{\alpha})$$ irradiance constraints on J [C8a]

$$J_{maxi,j,k} = \boldsymbol{V_j'}_i \boldsymbol{F_{chlorophyll}}_i M_{L_{i,j,k,prot}} / A_{i,j,k}\, f_{tji}\ f_{iCi}$$ [C8b]

$$f_{\psi\ i,j,k,l,m,n,o} = (r_{lmin_{i,j,k,l,m,n,o}} / r_{l_{i,j,k,l,m,n,o}})^{0.5}$$ temperature and nutrient constraints on J_{max} [C9]

$$f_{tbi} = \exp[\boldsymbol{B_v} - \boldsymbol{H_{av}} / (\boldsymbol{R} T_{ci})] / \{1 + \exp[(\boldsymbol{H_{dl}} - \boldsymbol{S} T_{ci}) / (\boldsymbol{R} T_{ci})] + \exp[(\boldsymbol{S} T_{ci} - \boldsymbol{H_{dh}}) / (\boldsymbol{R} T_{ci})]\}$$ non-stomatal effect related to stomatal effect [C10a]

$$f_{toi} = \exp[\boldsymbol{B_o} - \boldsymbol{H_{ao}} / (\boldsymbol{R} T_{ci})] / \{1 + \exp[(\boldsymbol{H_{dl}} - \boldsymbol{S} T_{ci}) / (\boldsymbol{R} T_{ci})] + \exp[(\boldsymbol{S} T_{ci} - \boldsymbol{H_{dh}}) / (\boldsymbol{R} T_{ci})]]$$ Arrhenius functions for carboxylation, oxygenation and electron transport [C10b]

$$f_{tji} = \exp[\boldsymbol{B_j} - \boldsymbol{H_{aj}} / (\boldsymbol{R} T_{ci})] / \{1 + \exp[(\boldsymbol{H_{dl}} - \boldsymbol{S} T_{ci}) / (\boldsymbol{R} T_{ci})] + \exp[(\boldsymbol{S} T_{ci} - \boldsymbol{H_{dh}}) / (\boldsymbol{R} T_{ci})]\}$$ temperature sensitivity of $\boldsymbol{K_{c}}_i$, $\boldsymbol{K_{o}}_i$ [C10c]

$$f_{tkci} = \exp[\boldsymbol{B_{kc}} - \boldsymbol{H_{akc}} / (\boldsymbol{R} T_{ci})]$$ [C10d]

$$f_{tkoi} = \exp[\boldsymbol{B_{ko}} - \boldsymbol{H_{ako}} / (\boldsymbol{R} T_{ci})]$$ [C10e]

$f_{iCi} = min\{\sigma_{Ni,j} / (\sigma_{Ni,j} + \sigma_{Ci,j} / \boldsymbol{K}_{iC_N}),\ \sigma_{Pi,j} / (\sigma_{Pi,j} + \sigma_{Ci,j} / \boldsymbol{K}_{iC_P})\}$ — control of σ_N and σ_P *vs.* σ_C in shoots on V_b, V_j through product inhibition and on leaf protein growth through leaf structural C:N:P ratios [C11]

$\delta M_{L_R i,j,k} / \delta t = \delta M_{L_{i,j,k}} / \delta t \min\{[\boldsymbol{N'}_{leaf} + (\boldsymbol{N}_{leaf} - \boldsymbol{N'}_{leaf}) f_{iCi}] / \mathbf{N}_{prot}, [\boldsymbol{P'}_{leaf} + (\boldsymbol{P}_{leaf} - \boldsymbol{P'}_{leaf}) f_{iCi}] / \mathrm{P}_{prot}\}$ — growth of remobilizable leaf protein C [C12]

Autotrophic Respiration

$R_a = \Sigma_i \Sigma_j (R_{ci,j} + R_{si,j}) + \Sigma_i \Sigma_l \Sigma_z (R_{ci,r,l} + R_{si,r,l}) + \boldsymbol{E}_{N,P} (U_{NH4i,r,l} + U_{NO3i,r,l} + U_{PO4i,r,l})$ — total autotrophic respiration [C13]

$R_{ci,j} = \boldsymbol{R}_c' \sigma_{Ci,j} f_{tai}$ — O_2 constraint on root respiration from active uptake coupled with diffusion of O_2 from soil [C14a]

$R_{ci,r,l} = \boldsymbol{R}_c' \sigma_{C\,i,r,l} f_{ta\,i,l} (U_{O2i,r,l} / U'_{O2i,r,l})$ [C14b]

$U_{O2i,r,l} = U'_{O2\,i,r,l} [O_{2ri,r,l}] / ([O_{2ri,r,l}] + \boldsymbol{K}_{O_2})$ as for heterotrophic respiration in [A17], and [C14c]

$= U_{w_{i,r,l}} [O_{2sl}] + 2\pi L_{i,r,l} D_{sO2} ([O_{2sl}] - [O_{2ri,r,l}]) \ln\{(r_{sl} + r_{ri,r,l}) / r_{ri,r,l}\}$
$+ 2\pi L_{i,r,l} D_{rO2} ([O_{2qi,r,l}] - [O_{2\,ri,r,l}]) \ln(r_{qi,r,l}) / r_{ri,r,l})$ from active uptake coupled with diffusion of O_2 from roots [C14d]

$U'_{O2\,i,r,l} = 2.67\, R_a'_{i,r,l}$ [C14e]

$R_{si,j} = -\, min\{0.0, R_{ci,j} - R_{mi,j}\}$ — remobilization in branchs, roots and mycorrhizae when $R_m > R_c$ [C15]

$R_{si,r,l} = -\, min\{0.0, R_{ci,r,l} - R_{mi,r,l}\}$

$R_{mi,j} = \Sigma_z (N_{i,j,z} \boldsymbol{R}_m' f_{tmi})$ — maintenance respiration of branchs, roots and mycorrhizae [C16]

$R_{mi,r,l} = \Sigma_z (N_{i,r,l,z} \boldsymbol{R}_m' f_{tmi})$

$R_{gi,j} = max\{0.0, min\{(R_{ci,j} - R_{mi,j}) min\{1.0, max\{0.0, \psi_{ti} - \psi_t'\}\}$ — growth respiration of branchs, roots and mycorrhizae when $R_m < R_c$ [C17]

$R_{gi,r,l} = max\{0.0, min\{(R_{ci,r,l} - R_{mi,r,l}) min\{1.0, max\{0.0, \psi_{ti,l} - \psi_t'\}\}$

Growth and Litterfall

$l_{i,j,z,C} = R_{si,j} M_{L_N i,j} / M_{L_R i,j} (1.0 - (\boldsymbol{X}_{Cmn} + (\boldsymbol{X}_{Cmx} - \boldsymbol{X}_{Cmn}) f_{\lambda Ci,j}))$ — senescence drives litterfall of non-remobilizable C less C recycling [C18a]

$l_{i,j,z,\mathrm{N}} = l_{i,j,z,\mathrm{C}}\, \mathbf{N_{prot}}\, (1.0 - \boldsymbol{X_{\mathbf{N}}} f_{\lambda \mathrm{N}i,j})$

litterfall of N and P is driven by that of C less N and P recycling [C18b]

$l_{i,j,z,\mathrm{P}} = l_{i,j,z,\mathrm{C}}\, \mathbf{P_{prot}}\, (1.0 - \boldsymbol{X_{\mathbf{P}}} f_{\lambda \mathrm{P}i,j})$

root and mycorrhizal litterfall calculated as for branch litterfall [C18c]

$f_{\lambda \mathrm{C}i,j} = \min\{\sigma_{\mathrm{N}i,j} / (\sigma_{\mathrm{N}i,j} + \sigma_{\mathrm{C}i,j}\ \boldsymbol{K_{\lambda \mathbf{N}}}),\ \sigma_{\mathrm{P}i,j} / (\sigma_{\mathrm{P}i,j} + \sigma_{\mathrm{C}i,j}\ \boldsymbol{K_{\lambda \mathbf{P}}})\}$ [C19a]

$f_{\lambda \mathrm{N}i,j} = \sigma_{\mathrm{C}i,j} / (\sigma_{\mathrm{C}i,j} + \sigma_{\mathrm{N}i,j} / \boldsymbol{K_{\lambda \mathbf{N}}})$

C, N and P recycling calculated from nonstructural C,N,P ratios [C19b]

$f_{\lambda \mathrm{P}i,j} = \sigma_{\mathrm{C}i,j} / (\sigma_{\mathrm{C}i,j} + \sigma_{\mathrm{P}i,j} / \boldsymbol{K_{\lambda \mathbf{P}}})$ [C19c]

$x_{i,r,l,\mathrm{C}} = r_x\ \sigma_{\mathrm{C}i,r,l}$ [C19d]

$x_{i,r,l,\mathrm{N}} = r_x\ \sigma_{\mathrm{N}i,r,l} f_{\mathrm{x}i,r,l,\mathrm{N}}$ [C19e]

$x_{i,r,l,\mathrm{P}} = r_x\ \sigma_{\mathrm{P}i,r,l} f_{\mathrm{x}i,r,l,\mathrm{P}}$

root and mycorrhizal exudation driven by σ_{C}, σ_{N} and σ_{P}, and by $\sigma_{\mathrm{C}}{:}\sigma_{\mathrm{N}}$ and $\sigma_{\mathrm{C}}{:}\sigma_{\mathrm{P}}$. [C19f]

$f_{\mathrm{x}i,r,l,\mathrm{N}} = \sigma_{\mathrm{N}i,j} / (\sigma_{\mathrm{N}i,j} + \sigma_{\mathrm{C}i,j} / \boldsymbol{K_{\mathbf{xN}}})$ [C19g]

$f_{\mathrm{x}i,r,l,\mathrm{P}} = \sigma_{\mathrm{P}i,j} / (\sigma_{\mathrm{P}i,j} + \sigma_{\mathrm{C}i,j} / \boldsymbol{K_{\mathbf{xP}}})$ [C19h]

$\delta M_{\mathrm{B}i,j} / \delta t = \Sigma_z\, [R_{\mathrm{g}i,j}\, (1 - \boldsymbol{Y_{\mathbf{g}i,z}})\, / \boldsymbol{Y_{\mathbf{g}i,z}}] - R_{\mathrm{s}i,j} - l_{i,j,\mathrm{C}}$

branch growth driven by R_{g} [C20a]

$\delta M_{\mathrm{R}i,r,l} / \delta t = [R_{\mathrm{g}i,r,l}\, (1 - \boldsymbol{Y_{\mathbf{g}i,r}})\, / \boldsymbol{Y_{\mathbf{g}i,r}}] - R_{\mathrm{s}i,r,l} - l_{i,r,l,\mathrm{C}}$ [C20b]

root growth driven by R_{g}

$\delta A_{\mathrm{L}i,j,k,l} / \delta t = \boldsymbol{\chi}\, (M_{\mathrm{L}i,j,k,l} / y_i)^{-0.33}\ \delta M_{\mathrm{L}i,j,k,l} / \delta t \min\{1,\ \max\{0, \psi_{\mathrm{t}i} - \psi_{\mathrm{t}}'\}$

leaf expansion driven by leaf mass growth [C21a]

$\delta L_{i,r,l,1} / \delta \mathrm{t} = (\delta M_{\mathrm{R}i,r,l,1} / \delta \mathrm{t}) / y_i\ \nu_r / \{\rho_r\, (1 - \boldsymbol{\theta_{\mathbf{P}i,r}})\, (\pi\, r_{\mathrm{r}i,r,l,1}{}^2)\}$

root extension of primary and secondary axes driven by root mass growth [C21b]

$\delta L_{i,r,l,2} / \delta \mathrm{t} = (\delta M_{\mathrm{R}i,r,l,2} / \delta \mathrm{t})\ \nu_r / \{\rho_r\, (1 - \boldsymbol{\theta_{\mathbf{P}i,r}})\, (\pi\, r_{\mathrm{r}i,r,l,2}{}^2)\}$ [C21c]

$f_{\mathrm{t}ai} = T_{ci}\{\exp[\boldsymbol{B_{\mathbf{v}}} - \boldsymbol{H_{\mathbf{av}}} / (\boldsymbol{R} T_{ci})]\} / \{1 + \exp[(\boldsymbol{H_{\mathbf{dl}}} - \boldsymbol{S} T_{ci}) / (\boldsymbol{R} T_{ci})] + \exp[(\boldsymbol{S} T_{ci} - \boldsymbol{H_{\mathbf{dh}}}) / (\boldsymbol{R} T_{ci})]\}$

Arrhenius function for R_{a} [C22a]

$f_{\mathrm{tm}i} = e^{(0.0811\ (T_{ci} - 298.15))}$

temperature function for R_{m} [C22b]

Root and Mycorrhizal Nutrient Uptake

$U_{NH4i,r,l} = \{U_{wi,r,l}[NH_4^+{}_l] + 2\pi L_{i,r,l} D_{eNH_4 l}([NH_4^+{}_l] - [NH_4^+{}_{i,r,l}]) / \ln(d_{i,r,l}/r_{ri,r,l})\}$ root N and P uptake [C23a]

$= \boldsymbol{U'_{NH_4}}(U_{O2i,r,l}/U'_{O2i,r,l})\, A_{i,r,l}([NH_4^+{}_{i,r,l}] - \mathbf{[NH_4^+{}_{mn}]})/([NH_4^+{}_{i,r,l}] - \mathbf{[NH_4^+{}_{mn}]} + \boldsymbol{K_{NH_4}})\, f_{tai,l}\, f_{iNi,r,l}$ from mass flow + diffusion coupled with active uptake of NH_4^+, [C23b]

$U_{NO3i,r,l} = \{U_{wi,r,l}[NO_3^-{}_l] + 2\pi L_{i,r,l} D_{eNO_3 l}([NO_3^-{}_l] - [NO_3^-{}_{i,r,l}]) / \ln(d_{i,r,l}/r_{ri,r,l})\}$ [C23c]

$= \boldsymbol{U'_{NO_3}}(U_{O2i,r,l}/U'_{O2i,r,l})\, A_{i,r,l}([NO_3^-{}_{i,r,l}] - \mathbf{[NO_3^-{}_{mn}]})/([NO_3^-{}_{i,r,l}] - \mathbf{[NO_3^-{}_{mn}]} + \boldsymbol{K_{NO_3}})\, f_{tai,l}\, f_{iNi,r,l}$ NO_3^- and $H_2PO_4^-$ constrained by O_2 uptake, as modelled for microbial N and P uptake in [A26] [C23d]

[C23e]

[C23f]

$U_{PO4i,r,l} = \{U_{wi,r,l}[H_2PO_4^-{}_l] + 2\pi L_{i,r,l} D_{ePO_4 l}([H_2PO_4^-{}_l] - [H_2PO_4^-{}_{i,r,l}]) / \ln(d_{i,r,l}/r_{ri,r,l})\}$ [C23g]

$= \boldsymbol{U'_{PO_4}}(U_{O2i,r,l}/U'_{O2i,r,l})\, A_{i,r,l}([H_2PO_4^-{}_{i,r,l}] - \mathbf{[H_2PO_4^-{}_{mn}]})/([H_2PO_4^-{}_{i,r,l}] - \mathbf{[H_2PO_4^-{}_{mn}]} + \boldsymbol{K_{PO_4}})\, f_{tai,l}\, f_{iPi,r,l}$ [C23h]

$f_{iNi,r,l} = \sigma_{Ci,r,l}/(\sigma_{Ci,r,l} + \sigma_{Ni,r,l}/\boldsymbol{K_{iN_C}})$ product inhibition of U_{NH4}, U_{NO3} and U_{PO4} determined by σ_N and σ_P *vs.* σ_C in roots

$f_{iPi,r,l} = \sigma_{Ci,r,l}/(\sigma_{Ci,r,l} + \sigma_{Pi,r,l}/\boldsymbol{K_{iP_C}})$

C₄ Gross Primary Productivity

C₄ Mesophyll

$GPP = \Sigma_{i,j,k,l,m,n,o}(V_{g(m4)i,j,k,l,m,n,o} = V_{c(m4)i,j,k,l,m,n,o})$ [C24]

$V_{g(m4)i,j,k,l,m,n,o} = (C_b - C_{i(m4)i,j,k,l,m,n,o}) / r_{lfi,j,k,l,m,n,o}$ gaseous diffusion [C25]

$V_{c(m4)i,j,k,l,m,n,o} = min\{V_{b(m4)i,j,k,l,m,n,o}, V_{j(m4)i,j,k,l,m,n,o}\}$ mesophyll carboxylation [C26]

$r_{lfi,j,k,l,m,n,o} = r_{lfmini,j,k,l,m,n,o} + (r_{lfmaxi} - r_{lfmini,j,k,l,m,n,o})\, e^{(-\beta\, \psi_{ti})}$ [C27]

$r_{lfmini,j,k,l,m,n,o} = (C_b - C_{i(m4)'i}) / V_{c_0(m4)i,j,k,l,m,n,o}$ [C28]

$V_{b(m4)i,j,k,l,m,n,o} = V_{bmax(m4)i,j,k}(C_{c(m4)i,j,k,l,m,n,o} - \Gamma_{(m4)i,j,k}) / (C_{c(m4)i,j,k,l,m,n,o)} + K_{c(m4)_i})$ CO_2-limited carboxylation [C29]

$V_{j(m4)i,j,k,l,m,n,o} = J_{(m4)i,j,k,l,m,n,o}\, Y_{(m4)i,j,k,l,m,n,o}$ light-limited carboxylation [C30a]

$Y_{(m4)i,j,k} = (C_{c(m4)i,j,k,l,m,n,o} - \Gamma_{(m4)i,j,k}) / (3.0\, C_{c(m4)i,j,k,l,m,n,o)} + 10.5\, \Gamma_{(m4)i,j,k})$ [C30b]

$J_{(m4)i,j,k,l,m,n,o} = (\varepsilon I_{i,l,m,n,o} + J_{max(m4)i,j,k} - ((\varepsilon I_{i,l,m,n,o} + J_{max(m4)i,j,k})^2 - 4\alpha\varepsilon I_{i,l,m,n,o} J_{ma}$ / (2α) irradiance response function [C31]

$V_{bmax(m4)i,j,k} = V_{bmax(m4)}'[N_{pep(m4)i,j,k}]'\, N_{lfi,j,k}\, A_{lfi,j,k}\, f_{C(m4)i,j,k} f_{\psi i}\, f_{tbi}$ PEPc activity [C32]

$J_{max(m4)i,j,k} = J_{max}'[N_{chl(m4)i,j,k}]'\, N_{lfi,j,k}\, A_{lfi,j,k}\, f_{C(m4)i,j,k}, f_{\psi i}\, f_{tji}$ chlorophyll activity [C33]

$f_{C(m4)i,j,k} = 1.0 / (1.0 + [\chi_{C4(m4)i,j,k}] / K_{I\chi_{C4(m4)}})$ C_4 product inhibition [C34]

$f_{\psi\, i,j,k,l,m,n,o} = (r_{lfmin_{i,j,k,l,m,n,o}} / r_{lf_{i,j,k,l,m,n,o}})^{0.5}$ non-stomatal water limitation [C35]

C₄ Mesophyll-Bundle Sheath Exchange

$V_{\chi C4(m4)i,j,k} = \kappa_{\chi C4(m4)}(\chi_{C4(m4)i,j,k}\, W_{lf(b4)i,j,k} - \chi_{C4(b4)i,j,k}\, W_{lf(m4)i,j,k}) / (W_{lf(b4)i,j,k} + W_{lf(n}$ mesophyll-bundle sheath transfer [C37]

$V_{\chi C4(b4)i,j,k} = \kappa_{\chi C4(b4)}\, \chi_{C4(b4)i,j,k} / (1.0 + C_{c(b4)i,j,k} / K_{I\chi_{C4(b4)}})$ bundle sheath decarboxylation [C38]

$V_{\phi(b4)i,j,k} = \kappa_{Cc(b4)} (C_{c(b4)i,j,k} - C_{c(m4)i,j,k}) (12 \times 10^{-9}) W_{lf(b4)i,j,k}$	bundle sheath-mesophyll leakage	[C39]
$\delta\chi_{C4(m4)i,j,k}/\delta t = \Sigma_{l,m,n,o} V_{c(m4)i,j,k,l,m,n,o} - V_{\chi C4(m4)i,j,k}$	mesophyll carboxylation products	[C40]
$\delta\chi_{C4(b4)i,j,k}/\delta t = V_{\chi C4(m4)i,j,k} - V_{\chi C4(b4)i,j,k}$	bundle sheath carboxylation products	[C41]
$\delta C_{c(b4)i,j,k}/\delta t = V_{\chi C4(b4)i,j,k} - V_{\phi(b4)i,j,k} - \Sigma_{l,m,n,o} V_{c(b4)i,j,k,l,m,n,o}$	bundle sheath CO_2 concentration	[C42]

C_4 Bundle Sheath

$V_{c(b4)i,j,k,l,m,n,o} = min\{V_{b(b4)i,j,k}, V_{j(b4)i,j,k,l,m,n,o}\}$	bundle sheath carboxylation	[C43]
$V_{b(b4)i,j,k} = V_{bmax(b4)i,j,k} (C_{c(b4)i,j,k} - \Gamma_{(b4)i,j,k}) / (C_{c(b4)i,j,k} + K_{c(b4)i})$	CO_2-limited carboxylation	[C44]
$V_{j(b4)i,j,k,l,m,n,o} = J_{(b4)i,j,k,l,m,n,o} Y_{(b4)i,j,k}$	light- limited carboxylation	[C45a]
$Y_{(b4)i,j,k} = (C_{c(b4)i,j,k} - \Gamma_{(b4)i,j,k}) / (4.5 C_{c(b4)i,j,k} + 10.5 \Gamma_{(b4)i,j,k})$	carboxylation efficiency of $V_{j(b4)}$	[C45b]
$J_{(b4)i,j,k,l,m,n,o} = (\varepsilon I_{i,l,m,n,o} + J_{max(b4)i,j,k} - ((\varepsilon I_{i,l,m,n,o} + J_{max(b4)i,j,k})^2 - 4\alpha\varepsilon I_{i,l,m,n,o} J_{max(b}$ (2α)	irradiance response function	[C46]
$V_{bmax(b4)i,j,k} = V_{bmax(b4)}' [N_{rub(b4)i,j,k}]' N_{lfi,j,k} A_{lfi,j,k} f_{C(c3)i,j,k} f_{\psi i} f_{tvi}$	RuBPc activity	[C47]
$J_{max(b4)i,j,k} = J_{max}' [N_{chl(b4)i,j,k}]' N_{lfi,j,k} A_{lfi,j,k} f_{C(c3)i,j,k} f_{\psi i} f_{tvi}$	chlorophyll activity	[C48]
$f_{C(c3)i,j,k} = \min\{[\nu_{lfi,j}] / ([\nu_{lfi,j}] + [\chi_{c3(b4)i,j}] / K_{I\nu_{lf}}), [\pi_{lfi,j}] / ([\pi_{lfi,j}] + [\chi_{c3(b4)i,j}] / K_{I\pi_{lf}})\}$	C_3 product inhibition	[C49]

Shoot – Root - Mycorrhizal C, N, P Transfer

$Z_{sCi,j-i,r,l} = g_{sCi,j-i,r,l} (\sigma_{Ci,j} M_{Ri,r,l} - \sigma_{Ci,r,l} M_{Bi,j}) / (M_{Ri,r,l} + M_{Bi,j})$	shoot – root C transfer driven by σ_C concentration gradients	[C50]
$Z_{sN,Pi,j-i,r,l} = \boldsymbol{g}_{\boldsymbol{sN,P}i,j-i,r,l} (\sigma_{N,Pi,j} \sigma_{Ci,r,l} - \sigma_{N,Pi,r,l} \sigma_{Ci,j}) / (\sigma_{Ci,r,l} + \sigma_{Ci,j})$	shoot – root N,P transfer driven by $\sigma_{N,P}$ concentration gradients	[C51]
$Z_{rCi,j-i,r,l} = \boldsymbol{g}_{\boldsymbol{rC}i,j-i,r,l} (\sigma_{Ci,r,l} M_{Mi,r,l} - \sigma_{Ci,m,l} M_{Ri,r,l}) / (M_{Mi,r,l} + M_{Ri,r,l})$	root – mycorrhizal C transfer driven by σ_C conc'n gradients	[C52]
$Z_{rN,Pi,j-i,r,l} = \boldsymbol{g}_{\boldsymbol{rN,P}i,j-i,r,l} (\sigma_{N,Pi,r,l} \sigma_{Ci,m,l} - \sigma_{N,Pi,m,l} \sigma_{Ci,r,l}) / (\sigma_{Ci,m,l} + \sigma_{Ci,r,l})$	root – mycorrhizal N,P transfer driven by $\sigma_{N,P}$ conc'n gradients	[C53]

Definition of Variables in Appendix C

Variable	Definition	Unit	Equation	Value
	subscripts			
i	species or functional type: evergreen, coniferous, deciduous, annual, perennial, C_3, C_4, monocot, dicot, legume etc.			
j	branch or tiller			
k	node			

l	soil or canopy layer
m	leaf azimuth
n	leaf inclination
o	leaf exposure (sunlit *vs*. shaded)
z	organ including leaf, stem, root *r*, mycorrhizae *m*

variables

A	Leaf (irradiated), root or mycorrhizalsurface area	$m^2\ m^{-2}$	[C1,C6b,C6 d,C8b,C21,C 23,C32,C33, C47]		
$\boldsymbol{\beta}$	shape parameter for stomatal effects on CO_2 diffusion and non-stomatal effects on carboxylation	MPa^{-1}	[C4 C27,C35,]	-5.0	Grant and Flanagan (2007)
$\boldsymbol{B_j}$	parameter such that $f_{tji} = 1.0$ at $T_c = 298.15$ K		[C10c]	17.354	
$\boldsymbol{B_{kc}}$	parameter such that $f_{tkci} = 1.0$ at $T_c = 298.15$ K		[C10d]	22.187	
$\boldsymbol{B_{ko}}$	parameter such that $f_{tkoi} = 1.0$ at $T_c = 298.15$ K		[C10e]	8.067	
$\boldsymbol{B_o}$	parameter such that $f_{toi} = 1.0$ at $T_c = 298.15$ K		[C10b]	24.212	
$\boldsymbol{B_v}$	parameter such that $f_{tvi} = 1.0$ at $T_c = 298.15$ K		[C10a, C22]	26.229	
C_b	$[CO_2]$ in canopy air	$\mu mol\ mol^{-1}$	[C2,C5 C25,C28]		
C_c	$[CO_2]$ in canopy chloroplasts in equilibrium with $C_{ii,j,k,l,m,n,o}$	μM	[C6a,C7b]		
$C_{c(b4)}$	$[CO_2]$ in C_4 bundle sheath	μM	[C38,C39,C 42,C44,C45 b]		
$C_{c(m4)}$	$[CO_2]$ in C_4 mesophyll in equilibrium with $C_{ii,j,k,l,m,n,o}$	μM	[C29,C30b, C39]		
$\boldsymbol{CF_i}$	Clumping factor	-	[C1]	0.45 (needleleaf) 0.675 (broadleaf	He (2016)
$\boldsymbol{C_i'}$	$[CO_2]$ in canopy leaves when $\psi_{ci} = 0$	$\mu mol\ mol^{-1}$	[C5]	0.70 x C_b	Larcher (2001)
C_i	$[CO_2]$ in canopy leaves	$\mu mol\ mol^{-1}$	[C2]		
$C_{i(m4)}'$	$[CO_2]$ in C_4 mesophyll air when $\psi_{ci} = 0$	$\mu mol\ mol^{-1}$	[C28]	0.45 x C_b	
$C_{i(m4)}$	$[CO_2]$ in C_4 mesophyll air	$\mu mol\ mol^{-1}$	[C25]		
$C_{i,j,z=l}$	C content of leaf ($z = l$)	$g\ C\ m^{-2}$	[C18a]		
$D_{e\ NH4l}$	effective dispersivity-diffusivity of NH_4^+ during root uptake	$m^2\ h^{-1}$	[C23]		
$D_{e\ NO3l}$	effective dispersivity-diffusivity of NO_3^- during root uptake	$m^2\ h^{-1}$	[C23]		

$D_{e\ PO4l}$	effective dispersivity-diffusivity of $H_2PO_4^-$ during root uptake	$m^2\ h^{-1}$	[C23]		
D_{rO2}	aqueous diffusivity of O_2 from root aerenchyma to root or mycorrhizal surfaces	$m^2\ h^{-1}$	[C14d]		
D_{sO2}	aqueous diffusivity of O_2 from soil to root or mycorrhizal surfaces	$m^2\ h^{-1}$	[C14d]		
$d_{i,r,l}$	half distance between adjacent roots assumed equal to uptake path length	m	[C23]	$(\pi\ L_{s,z}\ /\Delta z)^{-1/2}$	Grant (1998)
$\boldsymbol{E_{N,P}}$	energy cost of nutrient uptake	g C g N^{-1} or P^{-1}	[C13]	2.15	Veen (1981)
$f_{C(c3)}$	C_3 product inhibition of RuBP carboxylation activity in C_4 bundle sheath or C_3 mesophyll	–	[C47,C48,C49]		
$f_{C(m4)}$	C_4 product inhibition of PEP carboxylation activity in C_4 mesophyll	–	[C32,C33,C34]		
$\boldsymbol{F_{chl}}$	fraction of leaf protein in chlorophyll	-	[C8b]	0.025	
f_{iC}	N,P inhibition on carboxylation, leaf structural N,P growth	–	[C6a,C7,C11,C12]		
f_{iN}	N inhibition on root N uptake	–	[C23g]		
f_{iP}	P inhibition on root P uptake	–	[C23h]		
$f_{\lambda C}$	fraction of $\boldsymbol{X_{Cmx}}$ translocated out of leaf or root before litterfall	–	[C18a,C19a]		
$f_{\lambda N}$	fraction of $\boldsymbol{X_N}$ translocated out of leaf or root before litterfall	–	[C18b,C19b]		
$f_{\lambda P}$	fraction of $\boldsymbol{X_P}$ translocated out of leaf or root before litterfall	–	[C18c,C19c]		
$\boldsymbol{F_{rubisco}}$	fraction of leaf protein in rubisco	-	[C6b,d]	0.125	
f_{ta}	temperature effect on $R_{ai,j}$ and U	–	[C14,C22,C23]		
f_{tb}	temperature effect on carboxylation	–	[C6b,C10a]		
f_{tj}	temperature effect on electron transport		[C8b,C10c]		
f_{tkc}	temperature effect on $\boldsymbol{K_{c}}_i$		[C6e,C10d]		Bernacchi et al. (2001,2003)
f_{tko}	temperature effect on $\boldsymbol{K_{o}}_i$		[C6e,C10e]		Bernacchi et al. (2001,2003)
f_{tm}	temperature effect on $R_{mi,j}$	–	[C16, C22b]	$Q_{10} = 2.25$	
f_{to}	temperature effect on oxygenation		[C6d,C10b]		
f_{tv}	temperature effect on carboxylation	–	[C32,C33,C36,C47,C48]		

f_{xN}	inhibition of root or mycorrhizal N exudation	–	[C19e,g]		
f_{xP}	inhibition of root or mycorrhizal P exudation	–	[C19f,h]		
$f_{\psi i}$	non-stomatal water effect on carboxylation	–	[C6a,C7a,C9]		Medrano et al. (2002)
$f_{\psi i}$	non-stomatal water effect on carboxylation	–	[C32,C33,C35C47,C48]		
g_{sC}	conductance for shoot-root C transfer	h^{-1}	[C50]	calculated from root depth, axis number	Grant (1998)
$\boldsymbol{g_{sN,P}}$	rate constant for shoot-root N,P transfer	h^{-1}	[C51]	0.1	Grant (1998)
$\boldsymbol{g_{rC}}$	rate constant for root-mycorrhizal C transfer	h^{-1}	[C52]	0.1	Grant (1998)
$\boldsymbol{g_{rN,P}}$	rate constant for root-mycorrhizal N,P transfer	h^{-1}	[C53]	0.1	Grant (1998)
$\boldsymbol{H_{aj}}$	energy of activation for electron transport	J mol^{-1}	[C10c]	43 x 10^3	Bernacchi et al. (2001,2003)
$\boldsymbol{H_{akc}}$	parameter for temperature sensitivity of $\boldsymbol{K_{c_i}}$	J mol^{-1}	[C10d]	55 x 10^3	Bernacchi et al. (2001,2003)
$\boldsymbol{H_{ako}}$	parameter for temperature sensitivity of $\boldsymbol{K_{o_i}}$	J mol^{-1}	[C10e]	20 x 10^3	Bernacchi et al. (2001,2003)
$\boldsymbol{H_{ao}}$	energy of activation for oxygenation	J mol^{-1}	[C10b, C22]	60 x 10^3	Bernacchi et al. (2001,2003)
$\boldsymbol{H_{av}}$	energy of activation for carboxylation	J mol^{-1}	[C10a, C22]	65 x 10^3	Bernacchi et al. (2001,2003)
$\boldsymbol{H_{dh}}$	energy of high temperature deactivation	J mol^{-1}	[C10, C22]	222.5 x 10^3	
$\boldsymbol{H_{dl}}$	energy of low temperature deactivation	J mol^{-1}	[C10, C22]	197.5 x 10^3	
$[H_2PO_4^-{}_{i,r,l}]$	concentration of $H_2PO_4^-$ root or mycorrizal surfaces	g N m^{-3}	[C23]		
$[\boldsymbol{H_2PO_4^-{}_{mn}}]$	concentration of $H_2PO_4^-$ at root or mycorrizal surfaces below which U_{PO_4} = 0	g N m^{-3}	[C23]	0.002	Barber and Silberbush, 1984
I	irradiance	µmol m^{-2} s^{-1}	[C8a,]		
J	electron transport rate in C_3 mesophyll	µmol m^{-2} s^{-1}	[C7a,C8a]		
$J_{(b4)}$	electron transport rate in C_4 bundle sheath	µmol m^{-2} s^{-1}	[C45a,C46]		
$J_{(m4)}$	electron transport rate in C_4 mesophyll	µmol m^{-2} s^{-1}	[C30a,C31]		

J_{max}'	specific electron transport rate at non-limiting I and 25ºC when $\psi_{ci} = 0$ and nutrients are nonlimiting	μmol g^{-1} s^{-1}	[C33,C48]	400	
$J_{max(b4)}$	electron transport rate in C_4 bundle sheath at non-limiting I	μmol m^{-2} s^{-1}	[C46,C48]		
$J_{max(m4)}$	electron transport rate in C_4 mesophyll at non-limiting I	μmol m^{-2} s^{-1}	[C31,C33]		
J_{max}	electron transport rate at non-limiting I, ψ_{ci}, temperature and N,P	μmol m^{-2} s^{-1}	[C8a,C8b]		
$K_{c(b4)}$	Michaelis-Menten constant for carboxylation in C_4 bundle sheath	μM	[C44]	30.0 at 25ºC and zero O_2	Lawlor (1993)
$K_{c(m4)}$	Michaelis-Menten constant for carboxylation in C_4 mesophyll	μM	[C29]	3.0 at 25ºC	Lawlor (1993)
$\boldsymbol{K_c}$	Michaelis-Menten constant for carboxylation at zero O_2	μM	[C6c,C6e]	12.5 at 25 ºC	Farquhar et al. (1980)
K_c	Michaelis-Menten constant for carboxylation at ambient O_2	μM	[C6e]		
$\boldsymbol{K_{iC_N}}$	inhibition constant for growth in shoots from σ_C *vs.* σ_N	g C g N^{-1}	[C11]	100	Grant (1998)
$\boldsymbol{K_{iC_P}}$	inhibition constant for growth in shoots from σ_C *vs.* σ_P	g C g P^{-1}	[C11]	1000	Grant (1998)
$K_{I\chi_{C4(b4)}}$	constant for CO_2 product inhibition of C_4 decarboxylation in C_4 bundle sheath	μM	[C38]	1000.0	
$K_{I\chi_{C4(m4)}}$	constant for C_4 product inhibition of PEP carboxylation activity in C_4 mesophyll	μM	[C34]	5 x 10^6	
$K_{I\nu_{lf}}$	constant for C_3 product inhibition of RuBP carboxylation activity in C_4 bundle sheath or C_3 mesophyll caused by [$\nu_{lfi,j}$]	g C g N^{-1}	[C49]	100	
$K_{I\pi_{lf}}$	constant for C_3 product inhibition of RuBP carboxylation activity in C_4 bundle sheath or C_3 mesophyll caused by [$\pi_{lfi,j}$]	g C g P^{-1}	[C49]	1000	
$\boldsymbol{K_{iN_C}}$	inhibition constant for N uptake in roots from $\sigma_{Ci,j}$ *vs.* σ_{Nj}	g N g C^{-1}	[C23]	0.1	Grant (1998)
$\boldsymbol{K_{iP_C}}$	inhibition constant for P uptake in roots from $\sigma_{Ci,j}$ *vs.* $\sigma_{Pi,j}$ roots	g P g C^{-1}	[C23]	0.01	Grant (1998)
$\boldsymbol{K_{\lambda N}}$	constant used to calculate remobilization of leaf or root C and N during senescence	g N g C^{-1}	[C19a,C19b]	0.1	
$\boldsymbol{K_{\lambda P}}$	constant used to calculate remobilization of leaf or root C and P during senescence	g P g C^{-1}	[C19a,C19c]	0.01	
$\boldsymbol{K_{NH_4}}$	M-M constant for NH_4^+ uptake at root or mycorrhizal surfaces	g N m^{-3}	[C23]	0.40	Barber and Silberbush, 1984
$\boldsymbol{K_{NO_3}}$	M-M constant for NO_3^- uptake at root or mycorrhizal surfaces	g N m^{-3}	[C23]	0.35	Barber and Silberbush, 1984

$\boldsymbol{K_{PO_4}}$	M-M constant for $H_2PO_4^-$ uptake root or mycorrhizal surfaces	g P m^{-3}	[C23]	0.125	Barber and Silberbush, 1984
$\boldsymbol{K_{O_2}}$	Michaelis-Menten constant for root or mycorrhizal O_2 uptake	g m^{-3}	[C14c]	0.32	Griffin (1972)
$\boldsymbol{K_o}$	inhibition constant for O_2 in carboxylation	μM	[C6c,C6e]	500 at 25 °C	Farquhar et al. (1980)
$\boldsymbol{K_{xN}}$	inhibition constant for exudation of root or mycorrhizal N	g C g N^{-1}	[C19g]	1.0	
$\boldsymbol{K_{xP}}$	inhibition constant for exudation of root or mycorrhizal P	g C g N^{-1}	[C19h]	10.0	
L	root length	m m^{-2}	[C14d,C21b, C23]		
l_C	C litterfall from leaf or root	g C m^{-2} h^{-1}	[C18a,C18b, C18c,C20]		
l_N	N litterfall from leaf or root	g C m^{-2} h^{-1}	[C18b]		
l_P	P litterfall from leaf or root	g C m^{-2} h^{-1}	[C18c]		
M_L	leaf C phytomass	g C m^{-2}	[C12,C21]		
M_{L_N}, M_{L_R}	non-remobilizable, remobilizable (protein) leaf C phytomass	g C m^{-2}	[C12,C18a]		
M_M	mycorrhizal C phytomass	g C m^{-2}	[C52]		
M_R	root C phytomass	g C m^{-2}	[C20,C21,C 50,C52]		
$M_{L_{iprot}}$	leaf protein phytomass calculated from leaf N, P contents	g N m^{-2}	[C6b,C6d,C 8b]		
N,P	N or P content of organ z	g N m^{-2}	[C16, C19]		
$\boldsymbol{N_{leaf}}$	maximum leaf structural N content	g N g C^{-1}	[C12]	0.10	
$\boldsymbol{N'_{leaf}}$	minimum leaf structural N content	g N g C^{-1}	[C12]	0.33 x $\boldsymbol{N_{leaf}}$	
N_{lf}	total leaf N	g N m^{-2} leaf	[C32,C33,C 47,C48]		
$\mathbf{N_{prot}}$	N content of protein remobilized from leaf or root	g N C^{-1}	[C12,C18b]	0.4	
$[N_{chl(b4)}]'$	ratio of chlorophyll N in C_4 bundle sheath to total leaf N	g N g N^{-1}	[C48]	0.05	
$[N_{chl(m4)}]'$	ratio of chlorophyll N in C_4 mesophyll to total leaf N	g N g N^{-1}	[C33]	0.05	
$[NH_4^+{}_{i,r,l}]$	concentration of NH_4^+ at root or mycorrizal surfaces	g N m^{-3}	[C23]		
$[\mathbf{NH_4^+{}_{mn}}]$	concentration of NH_4^+ at root or mycorrizal surfaces below which U_{NH_4} = 0	g N m^{-3}	[C23]	0.0125	Barber and Silberbush, 1984
$[NO_3^-{}_{i,r,l}]$	concentration of NH_4^+ at root or mycorrizal surfaces	g N m^{-3}	[C23]		
$[\mathbf{NO_3^-{}_{mn}}]$	concentration of NO_3^- at root or mycorrizal surfaces below which U_{NO_3} = 0	g N m^{-3}	[C23]	0.03	Barber and Silberbush, 1984

$[N_{pep(m4)}]'$	ratio of PEP carboxylase N in C_4 mesophyll to total leaf N	g N g N^{-1}	[C32]	0.025	
$[N_{rub(b4)}]'$	ratio of RuBP carboxylase N in C_4 bundle sheath to total leaf N	g N g N^{-1}	[C47]	0.025	
O_{2q}	aqueous O_2 concentration in root or mycorrhizal aerenchyma	g m^{-3}	[C14c,d]		
O_{2r}	aqueous O_2 concentration at root or mycorrhizal surfaces	g m^{-3}	[C14c,d]		
O_{2s}	aqueous O_2 concentration in soil solution	g m^{-3}	[C14c,d]		
O_c	$[O_2]$ in canopy chloroplasts in equilibrium with $O_{2\ in}$ atm.	μM	[C6c,C6e]		
$\boldsymbol{P_{leaf}}$	maximum leaf structural P content	g P g C^{-1}	[C12]	0.10	
$\boldsymbol{P'_{leaf}}$	minimum leaf structural P content	g P g C^{-1}	[C12]	0.33 x $\boldsymbol{P_{leaf}}$	
$\mathbf{P_{prot}}$	P content of protein remobilized from leaf or root	g P C^{-1}	[C12,C18c]	0.04	
$[\pi_{lf}]$	concentration of nonstructural root P uptake product in leaf	g P g C^{-1}	[C49]		
$\boldsymbol{\theta_P}$	root or mycorrhizal porosity	$m^3\ m^{-3}$	[C21b]	0.1 – 0.5	
$\boldsymbol{R}$	gas constant	J mol^{-1} K^{-1}	[C10, C22]	8.3143	
R_a	total autotrophic respiration	g C m^{-2} h^{-1}	[C13]		
R_a'	R_a under nonlimiting O_2	g C m^{-2} h^{-1}	[C14]		
$\boldsymbol{R_c'}$	specific autotrophic respiration of $\sigma_{Ci,j}$ at T_{ci} = 25 °C	g C g C^{-1} h^{-1}	[C14]	0.015	
R_c	autotrophic respiration of $\sigma_{Ci,j}$ or $\sigma_{Ci,r,l}$	g C m^{-2} h^{-1}	[C13,C14,C17, C15]		
R_g	growth respiration	g C m^{-2} h^{-1}	[C17,C20]		
r_{lf}	leaf stomatal resistance	s m^{-1}	[C25,C27,C39]		
r_{lfmaxi}	leaf cuticular resistance	s m^{-1}	[C27]		
$r_{lfmini,j,k,l,m,n,o}$	leaf stomatal resistance when ψ_{ci} = 0	s m^{-1}	[C27,C28,C35		
$r_{li,j,k,l,m,n,o}$	leaf stomatal resistance	s m^{-1}	[C2,C4,C9]		
r_{lmaxi}	leaf cuticular resistance	s m^{-1}	[C4]		
$r_{lmini,j,k,l,m,n,o}$	leaf stomatal resistance when ψ_{ci} = 0	s m^{-1}	[C4,C5,C9]		
$\boldsymbol{R_m'}$	specific maintenance respiration of $\sigma_{Ci,j}$ at T_{ci} = 25 °C	g C g N^{-1} h^{-1}	[C16]	0.0115	Barnes et al. (1998)
$R_{mi,j}$	above-ground maintenance respiration	g C m^{-2} h^{-1}	[C16,C17,C15]		
$r_{qi,r,l}$	radius of root aerenchyma	m	[C14d]		

$r_{ri,r,l}$	root or mycorrhizal radius	m	[C14d,C21b, c,C23a,c,e]	1.0×10^{-4} or 5.0×10^{-6}	
$R_{si,j}$	respiration from remobilization of leaf C	g C m^{-2} h^{-1}	[C13,C15,C 18a, C20]		
r_{sl}	thickness of soil water films	m	[C14d]		
r_x	rate constant for root or mycorrhizal exudation	h^{-1}	[C19d,e,f]	0.001	
ρ_r	dry matter content of root biomass	g g-1	[C21b]	0.125	
S	change in entropy	J mol^{-1} K^{-1}	[C10, C22]	710	Sharpe and DeMichelle (1977)
σ_C	nonstructural C product of CO_2 fixation	g C g C^{-1}	[C11,C19,C 23g,h,C50-53]		
σ_N	nonstructural N product of root uptake	g N g C^{-1}	[C11,C19.C 23g,h,C51,C 53]		
σ_P	nonstructural P product of root uptake	g P g C^{-1}	[C11,C19,C 23g,h,C51,C 53]		
T_c	canopy temperature	K	[C10, C22]		
$U_{NH4i,r,l}$	NH_4^+ uptake by roots or mycorrhizae	g N m^{-2} h^{-1}	[C23]		
U'_{NH_4}	maximum U_{NH_4} at 25 ºC and non-limiting NH_4^+	g N m^{-2} h^{-1}	[C23]	5.0 x 10^{-3}	Barber and Silberbush, 1984
$U_{NO3i,r,l}$	NO_3^- uptake by roots or mycorrhizae	g N m^{-2} h^{-1}	[C23]		
U'_{NO_3}	maximum U_{NO_3} at 25 ºC and non-limiting NO_3^-	g N m^{-2} h^{-1}	[C23]	5.0 x 10^{-3}	Barber and Silberbush, 1984
$U_{PO4i,r,l}$	$H_2PO_4^-$ uptake by roots or mycorrhizae	g N m^{-2} h^{-1}	[C23]		
U'_{PO_4}	maximum U_{PO_4} at 25 ºC and non-limiting $H_2PO_4^-$	g N m^{-2} h^{-1}	[C23]	5.0 x 10^{-3}	Barber and Silberbush, 1984
$U_{O2i,r,l}$	O_2 uptake by roots and mycorrhizae under ambient O_2	g O m^{-2} h^{-1}	[C14b,c,C23 b,d,f]		
$U'_{O2i,l.r}$	O_2 uptake by roots and mycorrhizae under nonlimiting O_2	g O m^{-2} h^{-1}	[C14b,c,C23 b,d,f]		
$U_{wi,r,l}$	root water uptake	m^3 m^{-2} h^{-1}	[C14d,C23]		
$V_{\phi(b4)i,j,k}$	CO_2 leakage from C_4 bundle sheath to C_4 mesophyll	g C m^{-2} h^{-1}	[C39,C42]		
V_b'	specific rubisco carboxylation at 25 ºC	µmol g $^{-1}$ rubisco s^{-1}	[C6b]	45	Farquhar et al. (1980)
$V_{b(b4)i,j,k}$	CO_2-limited carboxylation rate in C_4 bundle sheath	µmol m^{-2} s^{-1}	[C43,C44]		

$V_{b(m4)i,j,k,l,m,n,o}$	CO_2-limited carboxylation rate in C_4 mesophyll	µmol m^{-2} s^{-1}	[C26]		
$V_{bi,j,k,l,m,n,o}$	CO_2-limited leaf carboxylation rate	µmol m^{-2} s^{-1}	[C3,C6]		
$V_{bmax(b4)}'$	RuBP carboxylase specific activity in C_4 bundle sheath at 25ºC when $\psi_{ci} = 0$ and nutrients are nonlimiting	µmol g^{-1} s^{-1}	[C47]	75	
$V_{bmax(b4)i,j,k}$	CO_2-nonlimited carboxylation rate in C_4 bundle sheath	µmol m^{-2} s^{-1}	[C44,C47]		
$V_{bmax(m4)}'$	PEP carboxylase specific activity in C_4 mesophyll at 25ºC when $\psi_{ci} = 0$ and nutrients are nonlimiting	µmol g^{-1} s^{-1}	[C32]	150	
$V_{bmax(m4)i,j,k}$	CO_2-nonlimited carboxylation rate in C_4 mesophyll	µmol m^{-2} s^{-1}	[C29,C32]		
$V_{bmaxi,j,k}$	leaf carboxylation rate at non-limiting CO_2, ψ_{ci}, T_c and N,P	µmol m^{-2} s^{-1}	[C6a,C6b,C6c]		
$V_{c(b4)i,j,k,l,m,n,o}$	CO_2 fixation rate in C_4 bundle sheath	µmol m^{-2} s^{-1}	[C43]		
$V_{c(m4)i,j,k,l,m,n,o}$	CO_2 fixation rate in C_4 mesophyll	µmol m^{-2} s^{-1}	[C24,C26,C40,C41]		
$V_{c_0(m4)i,j,k,l,m,n,o}$	CO_2 fixation rate in C_4 mesophyll when $\psi_{ci} = 0$ MPa	µmol m^{-2} s^{-1}	[C28]		
$V_{ci,j,k,l,m,n,o}$	leaf CO_2 fixation rate	µmol m^{-2} s^{-1}	[C1,C3]		
$V_c'{}_{i,j,k,l,m,n,o}$	leaf CO_2 fixation rate when $\psi_{ci} = 0$	µmol m^{-2} s^{-1}	[C5]		
$V_{g(m4)i,j,k,l,m,n,o}$	CO_2 diffusion rate into C_4 mesophyll	µmol m^{-2} s^{-1}	[C24,C25]		
$V_{gi,j,k,l,m,n,o}$	leaf CO_2 diffusion rate	µmol m^{-2} s^{-1}	[C1,C2]		
$\boldsymbol{V_j'}$	specific chlorophyll e^- transfer at 25 ºC	µmol g^{-1} chlorophyll s^{-1}	[C8b]	450	Farquhar et al. (1980)
$V_{j(b4)i,j,k,l,m,n,o}$	irradiance-limited carboxylation rate in C_4 bundle sheath	µmol m^{-2} s^{-1}	[C43,C45a]		
$V_{j(m4)i,j,k,l,m,n,o}$	irradiance-limited carboxylation rate in C_4 mesophyll	µmol m^{-2} s^{-1}	[C26,C30a]		
$V_{ji,j,k,l,m,n,o}$	irradiance-limited leaf carboxylation rate	µmol m^{-2} s^{-1}	[C3,C7a]		
$\boldsymbol{V_o'}$	specific rubisco oxygenation at 25 ºC	µmol g^{-1} rubisco s^{-1}	[C6d]	9.5	Farquhar et al. (1980)
$V_{omaxi,j,k}$	leaf oxygenation rate at non-limiting O_2, ψ_{ci}, T_c and N,P	µmol m^{-2} s^{-1}	[C6c,d]		
$V_{\chi C4(b4)i,j,k}$	decarboxylation of C_4 fixation product in C_4 bundle sheath	g C m^{-2} h^{-1}	[C38,C41,C42]		
$V_{\chi C4(m4)}$	transfer of C_4 fixation product between C_4 mesophyll and bundle sheath	g C m^{-2} h^{-1}	[C37]		

$[\nu_{lf}]$	concentration of nonstructural root N uptake product in leaf	g N g C^{-1}	[C49]		
ν_r	specific volume of root biomass	m^3 g^{-1}	[C21b]		
$W_{lf(b4)}$	C_4 bundle sheath water content	g m^{-2}	[C37,C39]		
$W_{lf(m4)}$	C_4 mesophyll water content	g m^{-2}	[C37]		
$\boldsymbol{X_{Cmn}}$	minimum fraction of remobilizable C translocated out of leaf or root during senescence	-	[C18a]	0.167	Kimmins (2004)
$\boldsymbol{X_{Cmx}}$	maximum fraction of remobilizable C translocated out of leaf or root during senescence	-	[C18a]	0.50	Kimmins (2004)
$\boldsymbol{X_{N,P}}$	maximum fraction of remobilizable N or P translocated out of leaf or root during senescence	-	[C18b,C18c]	0.8	Kimmins (2004)
$x_{i,r,l,C}$	root and mycorrhizal C exudation	g C m^{-2} h^{-1}	[C19d]		
$x_{i,r,l,N}$	root and mycorrhizal C exudation	g N m^{-2} h^{-1}	[C19e]		
$x_{i,r,l,P}$	root and mycorrhizal C exudation	g P m^{-2} h^{-1}	[C19f]		
Y	carboxylation yield from electron transport in C_3 mesophyll	µmol CO_2 µmol e^{-} $^{-1}$	[C7a,b]		
$Y_{(b4)}$	carboxylation yield from electron transport in C_4 bundle sheath	µmol CO_2 µmol e^{-} $^{-1}$	[C45a,b]		
$Y_{(m4)}$	carboxylation yield from electron transport in C_4 mesophyll	µmol CO_2 µmol e^{-} $^{-1}$	[C30a,b]		
$\boldsymbol{Y_g}$	fraction of $\sigma_{Ci,j}$ used for growth expended as $R_{gi,j,z}$ by organ z	g C g C^{-1}	[C20]	0.28 (z = leaf), 0.24 (z = root and other non-foliar), 0.20 (z = wood)	Waring and Running (1998)
y	plant population	m^{-2}	[C21]		
$Z_{s}C$	shoot-root C transfer	g C m^{-2} h^{-1}	[C50]		
$Z_{s}N,P$	shoot-root N,P transfer	g N,P m^{-2} h^{-1}	[C51]		
$Z_{r}C$	root-mycorrhizal C transfer	g C m^{-2} h^{-1}	[C52]		
$Z_{r}N,P$	root-mycorrhizal N,P transfer	g N,P m^{-2} h^{-1}	[C53]		
Γ	CO_2 compensation point in C_3 mesophyll	µM	[C6a,C6c,C7b]		
$\Gamma_{(b4)}$	CO_2 compensation point in C_4 bundle sheath	µM	[C44,C45b]		
$\Gamma_{(m4)}$	CO_2 compensation point in C_4 mesophyll	µM	[C29,C30b]		

$\boldsymbol{\alpha}$	shape parameter for response of J to I	-	[C8a]	0.7	
α	shape parameter for response of J to I	-	[C31,C46]	0.75	
$\boldsymbol{\chi}$	area:mass ratio of leaf growth	m g^{-3}	[C21]	0.0125	Grant and Hesketh (1992)
$\chi_{C4(b4)}$	non-structural C_4 fixation product in C_4 bundle sheath	g C m^{-2}	[C37,C38,C41]		
$\chi_{C4(m4)}$	non-structural C_4 fixation product in C_4 mesophyll	g C m^{-2}	[C37,C40]		
$[\chi_{c3(b4)}]$	concentration of non-structural C_3 fixation product in C_4 bundle sheath	g g^{-1}	[C49]		
$[\chi_{C4(m4)}]$	concentration of non-structural C_4 fixation product in C_4 mesophyll	µM	[C34]		
$\boldsymbol{\varepsilon}$	quantum yield	µmol e^- µmol $quanta^{-1}$	[C8a]	0.45	Farquhar et al. (1980)
ε	quantum yield	µmol e^- µmol $quanta^{-1}$	[C31,C46]	0.45	Farquhar et al., (1980)
$\kappa_{Cc(b4)}$	conductance to CO_2 leakage from C_4 bundle sheath	h^{-1}	[C39]	20	
ψ_t	canopy turgor potential	MPa	[C4]	1.25 at ψ_c = 0	

Appendix D: Soil Water, Heat, Gas and Solute Fluxes

Surface Water Flux

$Q_{rx(x,y)} = v_{x(x,y)}\, d_{mx,y}\, L_{y(x,y)}$ — lateral water transfer from 2D Manning equation in x (EW) and y (NS) directions [D1a]

$Q_{(s,w,i)x(x,y)} = (2\, \boldsymbol{F}\, [(Z_{x,y} + z_{sx,y}) - (Z_{x+1,y} + z_{sx+1,y})]/\, (L_{x(x,y)} + L_{x(x+1,y)}))\, V_{(s,w,i)}$
$Q_{(s,w,i)y(x,y)} = (2\, \boldsymbol{F}\, [(Z_{x,y} + z_{sx,y}) - (Z_{x,y+1} + z_{sx,y+1})]/\, (L_{x(x,y)} + L_{x(x,y+1)}))\, V_{(s,w,i)}$ — topographically-driven snowpack snow s, water w and ice i transfer in x (EW) and y (NS) directions [D1b]

$d_{x,y} = \max(0,\, d_{w(x,y)} + d_{i(x,y)} - d_{s(x,y)})\, d_{w(x,y)} / (d_{w(x,y)} + d_{i(x,y)})$ — surface water depth [D2]

$v_{x(x,y)} = R^{0.67}\, s_{x(x,y)}{}^{0.5} / z_{r(x,y)}$ — runoff velocity over E slope [D3]

$v_{y(x,y)} = R^{0.67}\, s_{y(x,y)}{}^{0.5} / z_{r(x,y)}$ — runoff velocity over S slope

$v_{x(x,y)} = -R^{0.67}\, s_{x(x,y)}{}^{0.5} / z_{r(x,y)}$ — runoff velocity over W slope

$v_{y(x,y)} = -R^{0.67}\, s_{y(x,y)}{}^{0.5} / z_{r(x,y)}$ — runoff velocity over N slope

$\Delta(d_{w(x,y)} A_{x,y}) / \Delta t = Q_{r,x(x,y)} - Q_{r,x+1(x,y)} + Q_{r,y(x,y)} - Q_{r,y+1(x,y)} + P - E_{x,y} - Q_{wz(x,y,1)}$ — 2D kinematic wave theory for overland flow [D4]

$R = s_r\, d_m / [2\, (s_r^2 + 1)\, 0.5]$ — wetted perimeter [D5a]

$s_{x(x,y)} = 2\, abs[(Z_{x,y} + d_{sx,y} + d_{mx,y}) - (Z_{x+1,y} + d_{sx+1,y} + d_{mx+1,y})] / (L_{x(x,y)} + L_{x(x+1,y)})$

$s_{y(x,y)} = 2\, abs[(Z_{x,y} + d_{sx,y} + d_{mx,y}) - (Z_{x,y+1} + d_{sx,y+1} + d_{mx,y+1})] / (L_{y(x,y)} + L_{y(x,y+1)})$ — 2D slope from topography and pooled surface water in x (EW) and y (NS) directions [D5b]

$\boldsymbol{L}E_l = L\, (e_a - e_{l(T_l, \psi_l)}) / r_{al}$ — evaporation from surface litter [D6a]

$\boldsymbol{L}E_s = L\, (e_a - e_{s(T_s, \psi_s)}) / r_{as}$ — evaporation from soil surface [D6b]

Subsurface Water Flux

$Q_{wx(x,y,z)} = K'_x\, (\psi_{sx,y,z} - \psi_{sx+1,y,z})$

$Q_{wy(x,y,z)} = K'_y\, (\psi_{sx,y,z} - \psi_{sx,y+1,z})$

$Q_{wz(x,y,z)} = K'_z\, (\psi_{sx,y,z} - \psi_{sx,y,z+1})$ — 3D Richard's or Green-Ampt equation depending on saturation of source or target cell in x (EW), y (NS) and z (vertical) directions [D7]

$\Delta\theta_{w\,x,y,z} / \Delta t = (Q_{wx(x,y)} - Q_{wx+1(x,y)} + Q_{wy(x,y)} - Q_{wy+1(x,y)} + Q_{wz(x,y)} - Q_{wz+1(x,y)} + Q_{f(x,y,z)}) / L_{z(x,y,z)}$ — 3D water transfer plus freeze-thaw [D8]

$K'_x = 2\, K_{x,y,z}\, K_{x+1,y,z} / (K_{x,y,z}\, L_{x,(x+1,y,z)} + K_{x+1,y,z}\, L_{x,(x,y,z)})$ — in direction x if source and destination cells are unsaturated [D9a]

$= 2\, K_{x,y,z} / (L_{x(x+1,y,z)} + L_{x(x,y,z)})$ — in direction x if source cell is saturated [D9b]

$= 2\ K_{x+1,y,z} / (L_{x(x+1,y,z)} + L_{x(x,y,z)})$	in direction x if destination cell is saturated	
$K'_y = 2\ K_{x,y,z}\, K_{x,y+1,z} / (K_{x,y,z}\, L_{y(x,y+1,z)} + K_{x,y+1,z}\, L_{y(x,y,z)})$	in direction y if source and destination cells are unsaturated	[D9a]
$= 2\ K_{x,y,z} / (L_{y(x,y+1,z)} + L_{y(x,y,z)})$	in direction y if source cell is saturated	[D9b]
$= 2\ K_{x,y+1,z} / (L_{y(x,y+1,z)} + L_{y(x,y,z)})$	in direction y if destination cell is saturated	
$K'_z = 2\ K_{x,y,z}\, K_{x,y,z+1} / (K_{x,y,z}\, L_{z(x,y,z+1)} + K_{x,y,z+1}\, L_{z(x,y,z)})$	in direction z if source and destination cells are unsaturated	[D9a]
$= 2\ K_{x,y,z} / (L_{z(x,y,z+1)} + L_{z(x,y,z)})$	in direction z if source cell is saturated	[D9b]
$= 2\ K_{x,y,z+1} / (L_{z(x,y,z+1)} + L_{z(x,y,z)})$	in direction z if destination cell is saturated	

Exchange with Water Table

$Q_{tx(x,y,z)} = K_{x,y,z}\ [\psi' - \psi_{sx,y,z} + 0.01\ (d_{zx,y,z} - d_t)] / (L_{tx} + 0.5\ L_{x,(x,y,z)})$ $Q_{ty(x,y,z)} = K_{x,y,z}\ [\psi' - \psi_{sx,y,z} + 0.01\ (d_{zx,y,z} - d_t)] / (L_{ty} + 0.5\ L_{y,(x,y,z)})$	if $\psi_{sx,y,z} > \psi' + 0.01(d_{zx,y,z} - d_t)$ in x (EW) and y (NS) directions for all depths z from $d_{zx,y,z}$ to d_t or if $d_{zx,y,z} > d_t$	[D10]

Heat Flux

$R_n + \boldsymbol{L}E + H + G = 0$	for eachcanopy, snow, residue and soil surface, depending on exposure	[D11]
$G_{x(x,y,z)} = 2\ \kappa_{(x,y,z),(x+1,y,z)} (T_{(x,y,z)} - T_{(x+1,y,z)}) / (L_{x\,(x,y,z)} + L_{x\,(x+1,y,z)}) + c_w\, T_{(x,y,z)}\, Q_{wx(x,y,z)}$	3D conductive – convective heat flux	[D12a]
$G_{y(x,y,z)} = 2\ \kappa_{(x,y,z),(x,y+1,z)} (T_{(x,y,z)} - T_{(x,y+1,z)}) / (L_{y\,(x,y,z)} + L_{y\,(x,y+1,z)}) + c_w\, T_{(x,y,z)}\, Q_{wy(x,y,z)}$	among snowpack, surface residue and soil layers in x (EW), y (NS) and z (vertical) directions	[D12b]
$G_{z(x,y,z)} = 2\ \kappa_{(x,y,z),(x,y,z+1)} (T_{(x,y,z)} - T_{(x,y,z+1)}) / (L_{z\,(x,y,z)} + L_{z\,(x,y,z+1)}) + c_w\, T_{(x,y,z)}\, Q_{wz(x,y,z)}$		[D12c]
$\kappa_{(x,y,z)} = (\boldsymbol{W}_{\mathbf{o}(x,y,z)}\, V_{o(x,y,z)}\, \boldsymbol{\kappa}'_{\mathbf{o}(x,y,z)} + \boldsymbol{W}_{\mathbf{m}(x,y,z)}\, V_{m(x,y,z)}\, \boldsymbol{\kappa}'_{\mathbf{m}(x,y,z)} + \boldsymbol{W}_{\mathbf{w}(x,y,z)}\, V_{w(x,y,z)}\, \boldsymbol{\kappa}'_{\mathbf{w}(x,y,z)} + \boldsymbol{W}_{\mathbf{i}(x,y,z)}\, V_{i(x,y,z)}\, \boldsymbol{\kappa}'_{\mathbf{i}(x,y,z)} + \boldsymbol{W}_{\mathbf{a}(x,y,z)}\, V_{a(x,y,z)}\, \boldsymbol{\kappa}'_{\mathbf{a}(x,y,z)}) / (\boldsymbol{W}_{\mathbf{o}(x,y,z)}\, V_{o(x,y,z)} + \boldsymbol{W}_{\mathbf{m}(x,y,z)}\, V_{m(x,y,z)} + \boldsymbol{W}_{\mathbf{w}(x,y,z)}\, V_{w(x,y,z)} + \boldsymbol{W}_{\mathbf{i}(x,y,z)}\, V_{i(x,y,z)} + \boldsymbol{W}_{\mathbf{a}(x,y,z)}\, V_{a(x,y,z)})$	thermal conductivity of soil and surface litter	[D12d]
$\kappa_{s(x,y)} = 8.28 \times 10^{-5} + 8.42 \times 10^{-4}\ \rho_s$	($\rho_s <$ 0.156) thermal conductivity of snow	[D12e]
$\kappa_{s(x,y)} = 4.97 \times 10^{-4} - 3.64 \times 10^{-3}\ \rho_s + 1.16 \times 10^{-2}\ \rho_s^2$	($\rho_s >$ 0.156) thermal conductivity of snow	

$G_{x(x-1,y,z)} - G_{x(x,y,z)} + G_{y(x,y-1,z)} - G_{y(x,y,z)} + G_{z(x,y,z-1)} - G_{z(x,y,z)} + \boldsymbol{L}Q_{f(x,y,z)} + c_{(x,y,z)} (T_{(x,y,z)} - T'_{(x,y,z)}) / \Delta t = 0$	3D general heat flux equation driving freezing-thawing in snowpack, surface residue and soil layers	[D13]

Gas Flux

$Q_{ds\gamma x,y,z} = a_{gsx,y,z}\, D_{d\gamma}\, (\boldsymbol{S}'_{\gamma} ft_{d_\gamma x,y,z}\, [\gamma_{gs}]_{x,y,z} - [\gamma_{ss}]_{x,y,z})$	volatilization – dissolution between aqueous and gaseous phases in soil and root	[D14a]
$Q_{dr\gamma x,y,z} = a_{grx,y,z}\, D_{d\gamma}\, (\boldsymbol{S}'_{\gamma} ft_{d_\gamma x,y,z}\, [\gamma_{gr}]_{x,y,z} - [\gamma_{sr}]_{x,y,z})$		[D14b]
$Q_{gs\gamma z x,y,1} = g_{ax,y}\, \{[\gamma_a] - \{2\, [\gamma_{gs}]_{x,y,1} D_{gs\gamma z(x,y,1)} / L_{z(x,y,1)} + g_{ax,y}\, [\gamma_a]\} / \{2\, D_{gs\gamma z(x,y,1)} / L_{z(x,y,1)} + g_{ax,y}\}\}$	volatilization – dissolution between gaseous and aqueous phases at the soil surface ($z = 1$) and the atmosphere	[D15a]
$Q_{ds\gamma x,y,1} = a_{gsx,y,1}\, D_{d\gamma}\, (\boldsymbol{S}'_{\gamma} ft_{d_\gamma x,y,1}\, [\gamma_a] - [\gamma_{ss}]_{x,y,1})$		[D15b]
$Q_{gs\gamma x(x,y,z)} = - Q_{wx(x,y,z)}\, [\gamma_{gs}]_{x,y,z} + 2\, D_{gs\gamma x(x,y,z)} ([\gamma_{gs}]_{x,y,z} - [\gamma_{gs}]_{x+1,y,z}) / (L_{x\,(x,y,z)} + L_{x\,(x+1,y,z)})$	3D convective - conductive gas flux among soil layers in x (EW), y (NS) and z (vertical) directions,	[D16a]
$Q_{gs\gamma y(x,y,z)} = - Q_{wy(x,y,z)}\, [\gamma_{gs}]_{x,y,z} + 2\, D_{gs\gamma y(x,y,z)} ([\gamma_{gs}]_{x,y,z} - [\gamma_{gs}]_{x,y+1,z}) / (L_{y\,(x,y,z)} + L_{y\,(x,y+1,z)})$		[D16b]
$Q_{gs\gamma z(x,y,z)} = - Q_{wz(x,y,z)}\, [\gamma_{gs}]_{x,y,z} + 2\, D_{g\gamma z(x,y,z)} ([\gamma_{gs}]_{x,y,z} - [\gamma_{gs}]_{x,y,z+1}) / (L_{z\,(x,y,z)} + L_{z\,(x,y,z+1)})$		[D16c]
$Q_{gr\gamma z(x,y,z)} = D_{gr\gamma z(x,y,z)}\, ([\gamma_{gr}]_{x,y,z} - [\gamma_a]) / \Sigma_{1,z} L_{z\,(x,y,z)}$	convective - conductive gas flux between roots and the atmosphere	[D16d]
$D_{gs\gamma x(x,y,z)} = \boldsymbol{D}'_{g\gamma}\, ft_{gx,y,z}\, [0.5\, (\theta_{gx,y,z} + \theta_{gx+1,y,z})]^2 / \theta_{psx,y,z}^{0.67}$	gasous diffusivity as a function of air-filled porosity in soil	[D17a]
$D_{gs\gamma y(x,y,z)} = \boldsymbol{D}'_{g\gamma}\, ft_{gx,y,z}\, [0.5\, (\theta_{gx,y,z} + \theta_{gx,y+1,z})]^2 / \theta_{psx,y,z}^{0.67}$		[D17b]
$D_{gs\gamma z(x,y,z)} = \boldsymbol{D}'_{g\gamma}\, ft_{gx,y,z}\, [0.5\, (\theta_{gx,y,z} + \theta_{gx,y,z+1})]^2 / \theta_{psx,y,z}^{0.67}$		[D17c]
$D_{gr\gamma z(x,y,z)} = \boldsymbol{D}'_{g\gamma}\, ft_{gx,y,z}\, \boldsymbol{\theta}_{prx,y,z}^{1.33}\, A_{r\,(x,y,z)} / A_{x,y}$	gasous diffusivity as a function of air-filled porosity in roots	[D17d]
$Q_{b\gamma z} = \min[0.0, \{(44.64\, \theta_{wx,y,z}\, 273.16 / T_{(x,y,z)}) - \Sigma_\gamma ([\gamma_s]_{x,y,z} / (\boldsymbol{S}'_{\gamma} ft_{d_\gamma x,y,z} M_\gamma))\}]$ $([\gamma_s]_{x,y,z} / (\boldsymbol{S}'_{\gamma} ft_{d_\gamma x,y,z} M_\gamma)) / \Sigma_\gamma ([\gamma_s]_{x,y,z} / (\boldsymbol{S}'_{\gamma} ft_{d_\gamma x,y,z} M_\gamma))\, \boldsymbol{S}'_{\gamma} ft_{d_\gamma x,y,z} M_\gamma\, V_{x,y,z}$	bubbling (-ve flux) when total of all partial gas pressures exceeds atmospheric pressure	[D18]

Solute Flux

$$Q_{a\gamma x(x,y,z)} = - Q_{wx(x,y,z)} [\gamma_{ss}]_{x,y,z} + 2 D_{s\gamma x(x,y,z)} ([\gamma_s]_{x,y,z} - [\gamma_s]_{x+1,y,z}) / (L_{x\,(x,y,z)} + L_{x\,(x+1,y,z)})$$ [D19a]

$$Q_{a\gamma y(x,y,z)} = - Q_{wy(x,y,z)} [\gamma_{ss}]_{x,y,z} + 2 D_{s\gamma y(x,y,z)} ([\gamma_s]_{x,y,z} - [\gamma_s]_{x,y+1,z}) / (L_{y\,(x,y,z)} + L_{y\,(x,y+1,z)})$$ [D19b]

$$Q_{a\gamma z(x,y,z)} = - Q_{wz(x,y,z)} [\gamma_{ss}]_{x,y,z} + 2 D_{s\gamma z(x,y,z)} ([\gamma_s]_{x,y,z} - [\gamma_s]_{x,y,z+1}) / (L_{z\,(x,y,z)} + L_{z\,(x,y,z+1)})$$ [D19c]

3D convective - dispersive solute flux among soil layers in x (EW), y (NS) and z (vertical) directions

$$Q_{r\gamma(x,y,z)} = - Q_{wr(x,y,z)} [\gamma_{ss}]_{x,y,z} + 2\pi L_{i,r} D_{s\gamma}([\gamma_{ss}] - [\gamma_{rri,r}]) \ln\{(r_s + r_{ri,r}) / r_{ri,r}\} + 2\pi L_{i,r} D_{r\gamma}([\gamma_{sri,r}] - [\gamma_{rri,r}]) \ln(r_{qi,r}) / r_{ri,r})$$ [D19d]

convective - dispersive solute flux between soil and root aqueous phases

$$D_{s\gamma x(x,y,z)} = D_{qx(x,y,z)} \left| Q_{wx(x,y,z)} \right| + \boldsymbol{D'_{s\gamma}} f t_{sx,y,z} [0.5(\theta_{wx,y,z} + \theta_{wx+1,y,z})] \tau$$ [D20a]

$$D_{s\gamma y(x,y,z)} = D_{qy(x,y,z)} \left| Q_{wy(x,y,z)} \right| + \boldsymbol{D'_{s\gamma}} f t_{sx,y,z} [0.5(\theta_{wx,y,z} + \theta_{wx+1,y,z})] \tau$$ [D20b]

$$D_{s\gamma z(x,y,z)} = D_{qz(x,y,z)} \left| Q_{wz(x,y,z)} \right| + \boldsymbol{D'_{s\gamma}} f t_{sx,y,z} [0.5(\theta_{wx,y,z} + \theta_{wx+1,y,z})] \tau$$ [D20c]

$$D_{r\gamma(x,y,z)} = \boldsymbol{D'_{qr}} \left| Q_{wr(x,y,z)} \right| + \boldsymbol{D'_{s\gamma}} f t_{sx,y,z} \theta_{wx,y,z} \tau$$ [D20d]

aqueous dispersivity in soil as functions of water flux and water-filled porosity in x, y and z directions

aqueous dispersivity to roots as functions of water flux and water-filled porosity

$$D_{qx(x,y,z)} = 0.5\, \boldsymbol{\alpha} (L_{x\,(x,y,z)} + L_{x\,(x+1,y,z)})^{\boldsymbol{\beta}}$$ [D21a]

$$D_{qy(x,y,z)} = 0.5\, \boldsymbol{\alpha} (L_{y\,(x,y,z)} + L_{y\,(x,y+1,z)})^{\boldsymbol{\beta}}$$ [D21b]

$$D_{qz(x,y,z)} = 0.5\, \boldsymbol{\alpha} (L_{z\,(x,y,z)} + L_{z\,(x,y,z+1)})^{\boldsymbol{\beta}}$$ [D21c]

dispersivity as a function of water flow length

Definition of Variables in Appendix D

Variable	Definition	Unit	Equation	Value	Reference
		subscripts			
x	grid cell position in west to east direction				
y	grid cell position in north to south direction				
z	grid cell position in vertical direction			$z = 0$: surface residue, z = 1 to n: soil layers	
		variables			
A	area of landscape position	m^2	[D17c]		
A_r	root cross-sectional area of landscape position	m^2	[D17c]		
a_{gr}	air-water interfacial area in roots	$m^2\ m^{-2}$	[D14b]		

a_{gs}	air-water interfacial area in soil	$m^2\ m^{-2}$	[D14a,D15b]		Skopp (1985)
$\boldsymbol{\alpha}$	dependence of D_q on L	-	[D21]	0.20	
$\boldsymbol{\beta}$	dependence of D_q on L	-	[D21]	1.07	
c	heat capacity of soil	MJ m^{-3} $^oC^{-1}$	[D13]		
c_w	heat capacity of water	MJ m^{-3} $^oC^{-1}$	[D12]	4.19	
$D_{d\gamma}$	volatilization - dissolution transfer coefficient for gas γ	$m^2\ h^{-1}$	[D14,D15a]		
$D_{gr\gamma}$	gaseous diffusivity of gas γ in roots	$m^2\ h^{-1}$	[D16d,D17d]		Luxmoore et al. (1970a,b)
$D_{gs\gamma}$	gaseous diffusivity of gas γ in soil	$m^2\ h^{-1}$	[D15a,D16a,b,c,D17a,b,c]		Millington and Quirk (1960)
$\boldsymbol{D'_{g\gamma}}$	diffusivity of gas γ in air at 0 ^{o}C	$m^2\ h^{-1}$	[D17]	6.43 x 10^{-2} for $\gamma = O_2$	Campbell (1985)
$\boldsymbol{D'_{qr}}$	dispersivity in roots	m	[D20d]	0.004	
D_q	dispersivity in soil	m	[D20,D21]		
$D_{r\gamma}$	aqueous diffusivity of gas or solute γ in roots	$m^2\ h^{-1}$	[D19d,D20d]		
$D_{s\gamma}$	aqueous diffusivity of gas or solute γ in soil	$m^2\ h^{-1}$	[D19,D20]		
$\boldsymbol{D'_{s\gamma}}$	diffusivity of gas γ in water at 0 ^{o}C	$m^2\ h^{-1}$	[D20]	8.57 x 10^{-6} for $\gamma = O_2$	Campbell (1985)
d_m	depth of mobile surface water	m	[D1a,D2,D5a,D6]		
d_i	depth of surface ice	m	[D2]		
d_s	maximum depth of surface water storage	m	[D2,D5b]		
d_t	depth of external water table	m	[D10]		
d_w	depth of surface water	m	[D1,D2]		
d_z	depth to mid-point of soil layer	m	[D10]		
E	evaporation or transpiration flux	$m^3\ m^{-2}\ h^{-1}$	[D4,D11]		
e_a	atmospheric vapor density	$m^3\ m^{-3}$	[D6]		
$e_{l(T_l,\psi_l)}$	surface litter vapor density at current T_l and ψ_l	g m^{-3}	[D6a]		
$e_{s(T_s,\psi_s)}$	soil surface vapor density at current T_s and ψ_s	g m^{-3}	[D6b]		
$\boldsymbol{F}$	rate constant for lateral transfer of $V_{(s,w,i)}$	h^{-1}	[D1b]	0.005	
ft_{d_γ}	temperature dependence of $\boldsymbol{S'_\gamma}$	-	[D14,D15b,D18]		Wilhelm et al. (1977)
ft_g	temperature dependence of $\boldsymbol{D'_{g\gamma}}$	-	[D17]		Campbell (1985)

ft_s	temperature dependence of $\boldsymbol{D'}_{s\gamma}$	-	[D20]		Campbell (1985)
G	soil surface heat flux	$m^3\ m^{-2}\ h^{-1}$	[D11]		
G_x , G_y , G_z	soil heat flux in x, y or z directions	MJ $m^{-2}\ h^{-1}$	[D12,D13]		
g_a	boundary layer conductance	m h^{-1}	[D15a]		
γ	gas (H_2O, CO_2, O_2, CH_4, NH_3, N_2O, N_2, H_2) or solute (from appendix E)		[D14,D15]		
$[\gamma_a]$	atmospheric concentration of gas γ	g m^{-3}	[D15,D16d]		
$[\gamma_{gr}]$	gasous concentration of gas γ in roots	g m^{-3}	[D14b,D16d]		
$[\gamma_{gs}]$	gasous concentration of gas γ in soil	g m^{-3}	[D14a,D15a,D16a,D16b,D16c]		
$[\gamma_{sr}]$	aqueous concentration of gas γ in roots	g m^{-3}	[D14b, D19d]		
$[\gamma_{rr}]$	aqueous concentration of gas γ at root surface	g m-3	[D19b]		
$[\gamma_{ss}]$	aqueous concentration of gas γ in soil	g m^{-3}	[D14a,D15b,D18,D19]		
H	sensible heat flux	MJ $m^{-2}\ h^{-1}$	[D11]		
K	hydraulic conductivity	$m^2\ MPa^{-1}\ h^{-1}$	[D9,D10]		Green and Corey (1971)
K'_x , K'_y ,K'_z	hydraulic conductance in x, y or z directions	m $MPa^{-1}\ h^{-1}$	[D7,D9]		
κ	bulk thermal conductivity of soil or surface litter	MJ $m^{-1}\ h^{-1}\ {}^oC^{-1}$	[D12a,b,c,d, e]		de Vries (1963)
κ_s	bulk thermal conductivity of snowpack	MJ $m^{-1}\ h^{-1}\ {}^oC^{-1}$	[D12e]		Sturm et al. (1997)
$\boldsymbol{\kappa'}_{o,\ m,\ w,\ i,\ a}$	thermal conductivity of organic matter, mineral water, ice and air	MJ $m^{-1}\ h^{-1}\ {}^oC^{-1}$	[D12d]	9.05 x 10^{-4}, 1.06 x 10^{-2}, 2.07 x 10^{-3}, 7.84 x 10^{-3}, 9.05 x 10^{-5}	
L_i	root length	m m^{-2}	[D19d]		
L_t	distance from boundary to external water table in x or y directions	m	[D10]		
L_x , L_y , L_z	length of landscape element in x, y or z directions	m	[D1a,D1b,D5b,D8,D9,D10,D12,D15a,D16,D19]		
$\boldsymbol{L}E_l$	latent heat flux from surface litter	[D6a]	MJ $m^{-2}\ h^{-1}$		
$\boldsymbol{L}E_s$	latent heat flux from soil surface	[D6b]	MJ $m^{-2}\ h^{-1}$		
$\boldsymbol{L}$	latent heat of evaporation	MJ m^{-3}	[D6,D11,D13]	2460	
M_γ	atomic mass of gas γ	g mol^{-1}	[D18]		

P	precipitation flux	$m^3\ m^{-2}\ h^{-1}$	[D4]		
$Q_{a\gamma}$	aqueous flux of gas or solute γ in soil	g m^{-2}	[D19a,]		
$Q_{b\gamma z}$	bubbling flux	g $m^{-2}\ h^{-1}$	[D18]		
$Q_{dr\gamma}$	volatilization – dissolution of gas γ between aqueous and gaseous phases in roots	g $m^{-2}\ h^{-1}$	[D14b]		
$Q_{ds\gamma}$	volatilization – dissolution of gas γ between aqueous and gaseous phases in soil	g $m^{-2}\ h^{-1}$	[D14a,D15b]		
Q_f	freeze-thaw flux (thaw +ve)	$m^3\ m^{-2}\ h^{-1}$	[D8,D13]		
$Q_{gr\gamma}$	gaseous flux of gas γ between roots and the atmosphere	g $m^{-2}\ h^{-1}$	[D16d]		
$Q_{gs\gamma}$	gaseous flux of gas γ in soil	g $m^{-2}\ h^{-1}$	[D15a,D16a ,b,c]		
Q_{rx}, Q_{ry}	surface water flow in x or y directions	$m^3\ m^{-2}\ h^{-1}$	[D1a,D4]		
$Q_{r\gamma}$	aqueous flux of gas or solute γ from soil and root aqueous phases to root surface	g $m^{-2}\ h^{-1}$	[D19d]		
$Q_{(s,w,i)}$	lateral redistribution of snowpack snow s, water w and ice i in x or y directions	$m^3\ m^{-2}\ h^{-1}$	[D1b]		
Q_t	water flux between boundary grid cell and external water table in x or y directions	$m^3\ m^{-2}\ h^{-1}$	[D10]		
Q_{wr}	root water uptake	$m^3\ m^{-2}\ h^{-1}$	[D19d, D20d]		
Q_{wx},Q_{wy}, Q_{wz}	subsurface water flow in x, y or z directions	$m^3\ m^{-2}\ h^{-1}$	[D4,D7,D8, D12,D16,D 19,D20]		
θ_g	air-filled porosity	$m^3\ m^{-3}$	[D17a,b,c]		
$\boldsymbol{\theta_{pr}}$	root porosity	$m^3\ m^{-3}$	[D17d]	dryland spp. 0.10 wetland spp. 0.20	Luxmoore et al. (1970a,b)
θ_{ps}	soil porosity	$m^3\ m^{-3}$	[D17a,b,c]		
θ_w	water-filled porosity	$m^3\ m^{-3}$	[D8,D18,D2 0]		
R	ratio of cross-sectional area to perimeter of surface flow	m	[D3,D5a]		
R_n	net radiation	MJ $m^{-2}\ h^{-1}$	[D11]		
r_{al}	surface litter boundary layer resistance	m h^{-1}	[D6a]		
r_{as}	Soil surface boundary layer resistance	m h^{-1}	[D6b]		
$r_{qi,r}$	radius of root or mycorrhizal aerenchyma	m	[D19d]		
$r_{ri,r}$	root or mycorrhizal radius	m	[D19d]	1.0×10^{-4} or 5.0×10^{-6}	

r_s	thickness of soil water films	m	[D19d, D21d]		
ρ_s	density of snowpack	Mg m^{-3}	[D12e]		
S'_γ	Ostwald solubility coefficient of gas γ at 30 ^{o}C	-	[D14,D15b, D18]	0.0293 for γ = O_2	Wilhelm et al. (1977)
s_r	slope of channel sides during surface flow	m m^{-1}	[D5a]		
s_x , s_y	slope in x or y directions	m m^{-1}	[D3,D5b]		
T	soil temperature	^{o}C	[D12,D18]		
τ	tortuosity	-	[D20]		
$V_{o, m, w, i, a}$	volumetric ratios of organic matter, mineral water, ice and air	-	[D12d]		
$V_{(s,w,i)}$	Volume of snow s, water w and ice i in snowpack	m^3 m^{-2}	[D1b]		
v_x , v_y	velocity of surface flow in x or y directions	m h^{-1}	[D1a,D3]		
$W_{o, m, w, i, a}$	weighting factors for organic matter, mineral water, ice and air	-	[D12d]	1.253, 0.514, 1.00 0.611, 1.609	de Vries (1963)
ψ'	soil water potential at saturation	MPa	[D10]	5.0 x 10^{-3}	
ψ_s	soil water potential	MPa	[D7,D10]		
Z	surface elevation	m	[D1b,D5b]		
z_s	snowpack depth	m	[D1b]		
z_r	Manning's roughness coefficient	m$^{-1/3}$ h	[D3]	0.01	

Appendix E: Solute Transformations

Precipitation - Dissolution Equilibria

$Al(OH)_{3(s)} \Leftrightarrow (Al^{3+}) + 3\,(OH^-)$	(amorphous $Al(OH)_3$)	*-33.0*	[E1] [1]
$Fe(OH)_{3(s)} \Leftrightarrow (Fe^{3+}) + 3\,(OH^-)$	(soil Fe)	*-39.3*	[E2]
$CaCO_{3(s)} \Leftrightarrow (Ca^{2+}) + (CO_3^{2-})$	(calcite)	-9.28	[E3]
$CaSO_{4(s)} \Leftrightarrow (Ca^{2+}) + (SO_4^{2-})$	(gypsum)	*-4.64*	[E4]
$AlPO_{4(s)} \Leftrightarrow (Al^{3+}) + (PO_4^{3-})$	(variscite)	*-22.1*	[E5] [2]
$FePO_{4(s)} \Leftrightarrow (Fe^{3+}) + (PO_4^{3-})$	(strengite)	*-26.4*	[E6]
$Ca(H_2PO_4)_{2(s)} \Leftrightarrow (Ca^{2+}) + 2\,(H_2PO_4^-)$	(monocalcium phosphate)	*-1.15*	[E7] [3]
$CaHPO_{4(s)} \Leftrightarrow (Ca^{2+}) + (HPO_4^{2-})$	(monetite)	*-6.92*	[E8]
$Ca_5(PO_4)_3OH_{(s)} \Leftrightarrow 5\,(Ca^{2+}) + 3\,(PO_4^{3-}) + (OH^-)$	(hydroxyapatite)	*-58.2*	[E9]

Cation Exchange Equilibria [4]

$X\text{-}Ca + 2\,(NH_4^+) \Leftrightarrow 2\,X\text{-}NH_4 + (Ca^{2+})$	*1.00*	[E10]
$3\,X\text{-}Ca + 2\,(Al^{3+}) \Leftrightarrow 2\,X\text{-}Al + 3\,(Ca^{2+})$	*1.00*	[E11]
$X\text{-}Ca + (Mg^{2+}) \Leftrightarrow X\text{-}Mg + (Ca^{2+})$	*0.60*	[E12]
$X\text{-}Ca + 2\,(Na^+) \Leftrightarrow 2\,X\text{-}Na + (Ca^{2+})$	*0.16*	[E13]
$X\text{-}Ca + 2\,(K^+) \Leftrightarrow 2\,X\text{-}K + (Ca^{2+})$	*3.00*	[E14]
$X\text{-}Ca + 2\,(H^+) \Leftrightarrow 2\,X\text{-}H + (Ca^{2+})$	*1.00*	[E15]
$3\,X\text{-}Al + 2\,(X\text{-}Ca + X\text{-}Mg) + X\text{-}NH_4 + X\text{-}K + X\text{-}Na + X\text{-}H = CEC$		[E16]

Anion Adsorption Equilibria

$X\text{-}OH_2^+ \Leftrightarrow X\text{-}OH + (H^+)$	*-7.35*	[E17]
$X\text{-}OH \Leftrightarrow X\text{-}O^- + (H^+)$	*-8.95*	[E18]
$X\text{-}H_2PO_4 + H_2O \Leftrightarrow X\text{-}OH_2^+ + (H_2PO_4^-)$	*-2.80*	[E19]
$X\text{-}H_2PO_4 + (OH^-) \Leftrightarrow X\text{-}OH + (H_2PO_4^-)$	*4.20*	[E20]
$X\text{-}HPO_4^- + (OH^-) \Leftrightarrow X\text{-}OH + (HPO_4^{2-})$	*2.60*	[E21]
$X\text{-}OH_2^+ + X\text{-}OH + X\text{-}O^- + X\text{-}H_2PO_4 + X\text{-}HPO_4^- + X\text{–}COO^- = AEC$		[E22]

Organic Acid Equilibria

$X\text{-}COOH \Leftrightarrow X\text{–}COO^- + (H^+)$	*-5.00*	[E23]

[1] Round brackets denote solute activity. Numbers in italics denote log *K* (precipitation-dissolution, ion pairs), Gapon coefficient (cation exchange) or log *c* (anion exchange).
[2] All equlilibrium reactions involving N and P are calculated for both band and non-band volumes if a banded fertilizer application has been made. These volumes are calculated dynamically from diffusive transport of soluble N and P.
[3] May only be entered as fertilizer, not considered to be naturally present in soils.
[4] X- denotes surface exchange site for cation or anion adsorption.

Ion Pair Equilibria

$(NH_4^+) \Leftrightarrow (NH_3)_{(g)} + (H^+)$	*-9.24*	[E24]
$H_2O \Leftrightarrow (H^+) + (OH^-)$	*-14.3*	[E25]
$(CO_2)_{(g)} + H_2O \Leftrightarrow (H^+) + (HCO_3^-)$	*-6.42*	[E26]
$(HCO_3^-) \Leftrightarrow (H^+) + (CO_3^{2-})$	*-10.4*	[E27]
$(AlOH^{2+}) \Leftrightarrow (Al^{3+}) + (OH^-)$	*-9.06*	[E28]
$(Al(OH)_2^+) \Leftrightarrow (AlOH^{2+}) + (OH^-)$	*-10.7*	[E29]
$(Al(OH)_3^0) \Leftrightarrow (Al(OH)_2^+) + (OH^-)$	*-5.70*	[E30]
$(Al(OH)_4^-) \Leftrightarrow (Al(OH)_3^0) + (OH^-)$	*-5.10*	[E31]
$(AlSO_4^+) \Leftrightarrow (Al^{3+}) + (SO_4^{2-})$	*-3.80*	[E32]
$(FeOH^{2+}) \Leftrightarrow (Fe^{3+}) + (OH^-)$	*-12.1*	[E33]
$(Fe(OH)_2^+) \Leftrightarrow (FeOH^{2+}) + (OH^-)$	*-10.8*	[E34]
$(Fe(OH)_3^0) \Leftrightarrow (Fe(OH)_2^+) + (OH^-)$	*-6.94*	[E35]
$(Fe(OH)_4^-) \Leftrightarrow (Fe(OH)_3^0) + (OH^-)$	*-5.84*	[E36]
$(FeSO_4^+) \Leftrightarrow (Fe^{3+}) + (SO_4^{2-})$	*-4.15*	[E37]
$(CaOH^+) \Leftrightarrow (Ca^{2+}) + (OH^-)$	*-1.90*	[E38]
$(CaCO_3^0) \Leftrightarrow (Ca^{2+}) + (CO_3^{2-})$	*-4.38*	[E39]
$(CaHCO_3^+) \Leftrightarrow (Ca^{2+}) + (HCO_3^-)$	*-1.87*	[E40]
$(CaSO_4^0) \Leftrightarrow (Ca^{2+}) + (SO_4^{2-})$	*-2.92*	[E41]
$(MgOH^+) \Leftrightarrow (Mg^{2+}) + (OH^-)$	*-3.15*	[E42]
$(MgCO_3^0) \Leftrightarrow (Mg^{2+}) + (CO_3^{2-})$	*-3.52*	[E43]
$(MgHCO_3^+) \Leftrightarrow (Mg^{2+}) + (HCO_3^-)$	*-1.17*	[E44]
$(MgSO_4^0) \Leftrightarrow (Mg^{2+}) + (SO_4^{2-})$	*-2.68*	[E45]
$(NaCO_3^-) \Leftrightarrow (Na^+) + (CO_3^{2-})$	*-3.35*	[E46]
$(NaSO_4^-) \Leftrightarrow (Na^+) + (SO_4^{2-})$	*-0.48*	[E47]
$(KSO_4^-) \Leftrightarrow (K^+) + (SO_4^{2-})$	*-1.30*	[E48]
$(H_3PO_4) \Leftrightarrow (H^+) + (H_2PO_4^-)$	*-2.15*	[E49]
$(H_2PO_4^-) \Leftrightarrow (H^+) + (HPO_4^{2-})$	*-7.20*	[E50]
$(HPO_4^{2-}) \Leftrightarrow (H^+) + (PO_4^{3-})$	*-12.4*	[E51]
$(FeH_2PO_4^{2+}) \Leftrightarrow (Fe^{3+}) + (H_2PO_4^-)$	*-5.43*	[E52]
$(FeHPO_4^+) \Leftrightarrow (Fe^{3+}) + (HPO_4^{2-})$	*-10.9*	[E53]
$(CaH_2PO_4^+) \Leftrightarrow (Ca^{2+}) + (H_2PO_4^-)$	*-1.40*	[E54]
$(CaHPO_4^0) \Leftrightarrow (Ca^{2+}) + (HPO_4^{2-})$	*-2.74*	[E55]
$(CaPO_4^-) \Leftrightarrow (Ca^{2+}) + (PO_4^{3-})$	*-6.46*	[E56]
$(MgHPO_4^0) \Leftrightarrow (Mg^{2+}) + (HPO_4^{2-})$	*-2.91*	[E57]

Appendix F: Symbiotic N_2 Fixation

Microbial Growth

$R_{maxi,l} = M_{ni,l}\, R'\, [\chi_{ni,l}] / ([\chi_{ni,l}] + K_{\chi n})\, f_t\, f_{NP}$	respiration demand		[F1]
$f_t = T_l \{\exp[B - H_a / (R\, T_l)]\} / \{1 + \exp[(H_{dl} - ST_l) / (RT_l)] + \exp[(ST_l - H_{dh}) / (R\, T_l)]\}$	Arrhenius function		[F2]
$f_{NP} = \min\{[N_{ni,l}] / [N_n'], [P_{ni,l}] / [P_n']\}$	N or P limitation		[F3]
$R_{i,l} = R_{maxi,l}\, (V_{O_2 i,l} / V_{O_2 maxi,l})$	O_2 limitation		[F4]
$V_{O_2 maxi,l} = 2.67\, R_{maxi,l}$	O_2 demand		[F5]
$V_{O_2 i,l} = V_{O_2 maxi,l}\, [O_{2ri,l}] / ([O_{2ri,l}] + K_{O_2 r})$	equilibrate O_2 uptake with supply		[F6a]
$= 2\pi\, L_{ri,l}\, D_{sO_2}\, ([O_{2l}] - [O_{2ri,l}]) / \ln((r_{ri,l} + r_{wl})) / r_{ri,l})$			[F6b]
$R_{mi,l} = \boldsymbol{R}_m\, N_{ni,l}\, f_{tm}$	maintenance respiration		[F7]
$f_{tm} = e^{[y\,(T_l - 298.16)]}$	temperature function		[F8]
$R_{gi,l} = \max\{0.0, R_{i,l} - R_{mi,l}\}$	growth + fixation respiration		[F9]
$R_{si,l} = \max\{0.0, R_{mi,l} - R_{i,l}\}$	microbial senescence		[F10]
$L_{Ci,l} = R_{si,l}\ \min\{M_{ni,l} / (2.5\, N_{ni,l}), M_{ni,l} / (25.0\, P_{ni,l})\}$	microbial C litterfall		[F11]

N_2 Fixation

$V_{N_2 i,l} = \min\{R_{gi,l}\, E_{N_2}'\, f_{CP}, M_{ni,l}\, [N_n'] - N_{ni,l}\}\, [N_{2ri,l}] / ([N_{2ri,l}] + K_{N_2 r})$	rate of N_2 fixation		[F12]
$f_{CP} = \min\{[\chi_{ni,l}] / (1.0 + [\nu_{ni,l}] / K_{I\chi_n}), [\pi_{ni,l}] / (1.0 + [\nu_{ni,l}] / K_{I\pi_n})\}$	product inhibition of N_2 fixation		[F13]
$R_{N_2 i,l} = V_{N_2 i,l} / E_{N_2}'$	fixation respiration		[F14]
$U_{\chi i,l} = (R_{gi,l} - R_{N_2 i,l}) / (1 - Y_n')$	growth respiration		[F15]
$\delta M_{ni,l} / \delta t = U_{i,l}\, Y_n' - L_{Ci,l}$	microbial C growth		[F16]
$\delta N_{ni,l} / \delta t = \delta M_{ni,l} / \delta t\, \min\{\nu_{ni,l} / \chi_{ni,l}, [N_n']\}$	microbial N growth	$\delta M_{ndi,l} / \delta t > 0$	[F17a]
$\delta N_{ni,l} / \delta t = N_{ni,l} / M_{ni,l}\, \delta M_{ni,l} / \delta t$	microbial N growth	$\delta M_{ndi,l} / \delta t < 0$	[F17b]
$\delta P_{ni,l} / \delta t = \delta M_{ni,l} / \delta t\, \min\{\pi_{ni,l} / \chi_{ni,l}, [P_n']\}$	microbial P growth	$\delta M_{ndi,l} / \delta t > 0$	[F18a]
$\delta P_{ni,l} / \delta t = P_{ni,l} / M_{ni,l}\, \delta M_{ni,l} / \delta t$	microbial P growth	$\delta M_{ndi,l} / \delta t < 0$	[F18b]
$L_{Ni,l} = \text{abs}(\delta N_{ni,l} / \delta t)$	microbial N litterfall	$\delta N_{ndi,l} / \delta t < 0$	[F19]
$L_{Pi,l} = \text{abs}(\delta P_{ni,l} / \delta t)$	microbial P litterfall	$\delta P_{ndi,l} / \delta t < 0$	[F20]

Nodule – Root Exchange

$$V_{\chi i,l} = \kappa\,(\chi_{ri,l}\,M_{ni,l} - \chi_{ni,l}\,M_{ri,l}) \,/\, (M_{ni,l} + M_{ri,l})$$ nodule–root C exchange [F21]

$$V_{vi,l} = \kappa\,(v_{ri,l}\,\chi_{ni,l} - v_{ni,l}\,\chi_{ri,l}) \,/\, (\chi_{ni,l} + \chi_{ri,l})$$ nodule–root N exchange [F22]

$$V_{\pi i,l} = \kappa\,(\pi_{ri,l}\,\chi_{ni,l} - \pi_{ni,l}\,\chi_{ri,l}) \,/\, (\chi_{ni,l} + \chi_{ri,l})$$ nodule–root P exchange [F23]

$$\delta\chi_{ni,l}/\delta t = V_{\chi i,l} - \min\{R_{mi,l}, R_{i,l}\} - R_{N_2 i,l} - U_{\chi i,l} + F_{LC\,l}\,L_{Ci,l}$$ nodule nonstructural C [F24]

$$\delta v_{ni,l}/\delta t = V_{vi,l} - \delta N_{ni,l}/\delta t + V_{N_2 i,l} + F_{LN\,l}\,L_{Ni,l}$$ nodule nonstructural N [F25]

$$\delta\pi_{ni,l}/\delta t = V_{\pi i,l} - \delta P_{ni,l}/\delta t + F_{LP\,l}\,L_{Pi,l}$$ nodule nonstructural P [F26]

Definition of Variables in Appendix F

Variable	Definition	Units	Equations	Input Values	Reference
B	parameter such that $f_t = 1.0$ at $T_l = 298.15$ K		F2	17.533	
$\chi_{ni,l}$	nodule nonstructural C	g m^{-2}	F17a,F18a,F21,F22,B23,B24		
$[\chi_{ni,l}]$	nodule nonstructural C concentration	g g^{-1}	F1,F13		
$\chi_{ri,l}$	root nonstructural C	g m^{-2}	F21,F22,F23		
D_{sO_2}	diffusivity of aqueous O_2	m^2 h^{-1}	F6b		
E_{N_2}'	direct energy cost of N_2 fixation	g N g C^{-1}	F12,F14	0.25	Gutschick, (1981), Voisin et al., (2003)
$F_{LC\,l}$	fraction of nodule C litterfall remobilized as nonstructural C	-	F24		
$F_{LN\,l}$	fraction of nodule N litterfall remobilized as nonstructural N	-	F25		
$F_{LP\,l}$	fraction of nodule P litterfall remobilized as nonstructural P	-	F26		
f_{CP}	effect of nodule nonstructural C or P content on N_2 fixation	-	F12,F13		
f_{NP}	effect of nodule N or P content on respiration	-	F1,F3		
f_t	temperature function for nodule respiration	-	F1,F2		
f_{tm}	temperature function for nodule maintenance respiration	-	F7,F8		

H_a	energy of activation	J mol^{-1}	F2	57.5 x 10^3
H_{dh}	energy of high temperature deactivation	J mol^{-1}	F2	220 x 10^3
H_{dl}	energy of low temperature deactivation	J mol^{-1}	F2	190 x 10^3
$K_{\chi n}$	Michaelis-Menten constant for nodule respiration of $\chi_{ndi,l}$	g g^{-1}	F1	0.01
$K_{I\chi_n}$	inhibition constant for nonstructural N:C on N_2 fixation	g g^{-1}	F13	10
$K_{I\pi_n}$	inhibition constant for nonstructural N:P on N_2 fixation	g g^{-1}	F13	1000
K_{N_2r}	Michaelis-Menten constant for nodule N_2 uptake	g N m^{-3}	F12	0.14
K_{O_2r}	Michaelis-Menten constant for nodule O_2 uptake	g O m^{-3}	F6a	0.32
κ	rate constant for nonstructural C,N,P exchange between root and nodule	h^{-1}	F21,F22,F23	
$L_{ri,l}$	root length	m m^{-2}	F6b	
$L_{Ci,l}$	nodule C litterfall	g C m^{-2} h^{-1}	F11,F16,F24	
$L_{Ni,l}$	nodule N litterfall	g N m^{-2} h^{-1}	F19,F25	
$L_{Pi,l}$	nodule P litterfall	g P m^{-2} h^{-1}	F20,F26	
$M_{ni,l}$	nodule structural C	g C m^{-2}	F1,F11,F12,F16 ,F17,F18,F21	
$M_{ri,l}$	root structural C	g C m^{-2}	F21	
$[N_n']$	maximum nodule structural N concentration	g N g C^{-1}	F3,F12	0.1
$N_{ni,l}$	nodule structural N	g N m^{-2}	F7,F11,F12,F17,F19,F25	
$[N_{ni,l}]$	nodule structural N concentration	g N g C^{-1}	F3,F17a	
$[N_{2ri,l}]$	rhizosphere aqueous N_2 concentration	g N m^{-3}	F12	
$\nu_{ni,l}$	nodule nonstructural N	g N m^{-2}	F17a,F22,F25	
$\nu_{ri,l}$	root nonstructural N	g N m^{-2}	F22	
$[\nu_{ni,l}]$	nodule concentration of nonstructural N	g g^{-1}	F13,F17a	
$[O_{2ri,l}]$	rhizosphere aqueous O_2 concentration	g O m^{-3}	F6a,b	

$[O_{2l}]$	soil aqueous O_2 concentration	g O m^{-3}	F6b	
$[P_n']$	maximum nodule structural P concentration	g P g C^{-1}	F3,F18a	0.01
$P_{ni,l}$	nodule structural P	g P m^{-2}	F18a,F20,F26	
$[P_{ni,l}]$	nodule structural P concentration	g P g C^{-1}	F3,F11	
$\pi_{ni,l}$	nodule nonstructural P	g P m^{-2}	F18a,F23,F26	
$\pi_{ri,l}$	root nonstructural P	g P m^{-2}	F23	
$[\pi_{ni,l}]$	nodule concentration of nonstructural P	g g^{-1}	F13	
R	gas constant	J mol^{-1} K^{-1}	F2	8.3143
$R_{gi,l}$	nodule growth respiration	g C m^{-2} h^{-1}	F9,F12,F15	
R'	specific nodule respiration at 25°C, and non-limiting O_2, $\chi_{ndi,l}$, $\nu_{ndi,l}$ and $\pi_{ndi,l}$	h^{-1}	F1	0.125
$R_{i,l}$	nodule respiration under ambient O_2	g C m^{-2} h^{-1}	F4,F9,F10,F24	
$\boldsymbol{R}_m$	specific nodule maintenance respiration at 25°C	g C g C^{-1} h^{-1}	F7	
$R_{maxi,l}$	nodule respiration under non-limiting O_2	g C m^{-2} h^{-1}	F1,F4,F5	
$R_{mi,l}$	nodule maintenance respiration	g C m^{-2} h^{-1}	F7,F9,F10,F24	
$R_{N_2i,l}$	nodule respiration for N_2 fixation	g C m^{-2} h^{-1}	F14,F15,F24	
$R_{si,l}$	nodule senescence respiration	g C m^{-2} h^{-1}	F9,F11	
$r_{ri,l}$	root radius	m	F6b	
r_{wl}	radius of soil water films	m	F6b	
S	change in entropy	J mol^{-1} K^{-1}	F2	710
T_l	soil temperature	K	F2,F8	
$U_{\chi i,l}$	uptake of nodule nonstructural C for growth	g C m^{-2} h^{-1}	F15,F16,F24	
$V_{\chi i,l}$	nonstructural C transfer between root and nodule	g C m^{-2} h^{-1}	F21,F24	
$V_{vi,l}$	nonstructural N transfer between root and nodule	g N m^{-2} h^{-1}	F22,F25	
$V_{N_2i,l}$	N_2 fixation	g N m^{-2} h^{-1}	F12,F14,F25	

$V_{O_2max i,l}$	O_2 uptake by nodules under non-limiting O_2	g O m^{-2} h^{-1}	F4,F5,F6a	
$V_{O2i,l}$	O_2 uptake by nodules under ambient O_2	g O m^{-2} h^{-1}	F4,F6	
$V_{\pi i,l}$	nonstructural P transfer between root and nodule	g P m^{-2} h^{-1}	F23,F26	
Y_n'	nodule growth yield	g C g C^{-1}	F15,F16	0.67
y	shape parameter for f_{tm}	-	F8	0.081

Appendix G: CH_4 Production and Consumption

Anaerobic Fermenters and H_2 Producing Acetogens

$R_{i,f} = \{\boldsymbol{R'_f}\ M_{i,f,a}[Q_{i,c}] / ([Q_{i,c}] + \mathbf{K_f}(1+ [O_2] / \mathbf{K_i}))\}\ f_t$	respiration by fermenters		[G1]
$Q_{i,c} \rightarrow 0.67\ A_{i,c} + 0.33\ CO_2\text{-}C + 0.11\ H_2$	partition respiration products		[G2]
$U_{i,f,c} = Rm_{i,f} + (R_{i,f} - Rm_{i,f})\ (1.0 + Y_f)$	uptake of DOC by fermenters	$[R_{i,f} > Rm_{i,f}]$	[G3a]
$U_{i,f,c} = R_{i,f}$		$[R_{i,f} < Rm_{i,f}]$	[G3b]
$Y_f = -\Delta G_f / \mathbf{E_M}$	growth yield of fermentation		[G4]
$\Delta G_f = \mathbf{\Delta G'_f} + \{\boldsymbol{R}\ T\ \ln([H_2] / \mathbf{[H_2']})^4\}$	free energy change of fermentation		[G5]
$\delta M_{i,f,j,c} / \delta t = F_j\ U_{i,f,c} - F_j\ R_{i,f} - D_{i,f,j,c}$	growth of fermenters	$[R_{i,f} > Rm_{i,f}]$	[G6a]
$\delta M_{i,f,j,c} / \delta t = F_j\ U_{i,f,c} - R_{mi,f,j} - D_{i,f,j,c}$		$[R_{i,f} < Rm_{i,f}]$	[G6b]

Acetotrophic Methanogens

$R_{i,m} = \{\boldsymbol{R'_m}\ M_{i,m,a}[A_{i,c}] / (\mathbf{K_m} + [A_{i,c}])\}\ f_t$	respiration by acetotrophic methanogens		[G7]
$A_{i,c} \rightarrow 0.50\ CH_4\text{-}C + 0.50\ CO_2\text{-}C$	partition respiration products		[G8]
$U_{i,m,c} = R_{mi,m} + (R_{i,m} - R_{mi,m})\ (1.0 + Y_m)$	uptake by acetotrophic methanogens	$[R_{i,m} > R_{mi,m}]$	[G9a]
$U_{i,m,c} = R_{i,m}$		$[R_{i,m} < R_{mi,m}]$	[G9b]
$-Y_m = \mathbf{-\Delta G'_m} / \mathbf{E_M}$	growth yield of acetotrophic methanogenesis		[G10]
$\delta M_{i,m,j,c} / \delta t = F_j\ U_{i,m,c} - F_j\ R_{i,m} - D_{i,m,j,c}$	growth of acetotrophic methanogens	$[R_{i,m} > R_{mi,m}]$	[G11a]
$\delta M_{i,m,j,c} / \delta t = F_j\ U_{i,m,c} - R_{mi,m,j} - D_{i,m,j,c}$		$[R_{i,m} < R_{mi,m}]$	[G11b]

Hydrogenotrophic Methanogens

$R_h = \{\boldsymbol{R'_h}\ M_{h,a}[H_2] / (\mathbf{K_h} + [H_2])\ [CO_2] / (\mathbf{K_c} + [CO_2])\}\ f_t$	respiration by hydrogenotrophic methanogens		[G12]
$CO_2\text{-}C + 0.67\ H_2 \rightarrow CH_4\text{-}C$	transform respiration products		[G13]
$U_{h,c} = R_{mh} + (R_h - R_{mh})\ (1.0 + Y_h)$	uptake by hydrogenotrophic methanogens	$[R_h > R_{mh}]$	[G14a]
$U_{h,c} = R_h$		$[R_h < R_{mh}]$	[G14b]

$Y_h = -\Delta G_h / \mathbf{E}_C$	growth yield of hydrogenotrophic methanogenesis		[G15]
$\Delta G_h = \mathbf{\Delta G'_h} - \{\boldsymbol{R}\ T \ln([H_2] / \mathbf{[H_2']})^4\}$	free energy change of hydrogenotrophic methanogenesis		[G16]
$\delta M_{h,j,c} / \delta t = F_j U_{h,c} - F_j R_h - D_{h,j,c}$	growth of hydrogenotrophic methanogens	$[R_h > R_{mh}]$	[G17a]
$\delta M_{h,j,c} / \delta t = F_j U_{h,c} - R_{mh,j} - D_{h,j,c}$		$[R_h < R_{mh}]$	[G17b]

Autotrophic Methanotrophs

$X'_t = \{\boldsymbol{X'_t}\ M_{t,a} [CH_4] / (\mathbf{K_t} + [CH_4])\} f_t$	CH_4 oxidation by methanotrophs under non-limiting O_2		[G18]
$R'_t = X'_t Y_{tR}$	respiration by methanotrophs under non-limiting O_2		[G19]
$Y_{tR} = \mathbf{-\Delta G'_t} / \mathbf{E_G}$	energy yield from CH_4 oxidation		[G20]
$X_t = X'_t f_{O2t}$	CH_4 oxidation by methanotrophs under ambient O_2		[G21a]
$R_t = R'_t f_{O2t}$	respiration by methanotrophs under ambient O_2		[G21b]
$CH_4\text{-}C + 4.0\ O_2 \rightarrow CO_2\text{-}C + 1.5\ H_2O + 0.167\ H^+$	O_2 requirements for CH_4 oxidation by methanotrophs		[G22]
$CH_4\text{-}C + 1.33\ O_2 \rightarrow CH_2O\text{-}C + 0.167\ H^+$	O_2 requirements for growth by methanotrophs		[G23]
$CH_2O\text{-}C + 2.67\ O_2 \rightarrow CO_2\text{-}C + 1.5\ H_2O$	O_2 requirements for respiration by methanotrophs		[G24]
$U_{t,c} = R_{mt} + (R_t - R_{mt})(1.0 + Y_{tG})$	uptake by methanotrophs	$[R_t > R_{mt}]$	[G25a]
$U_{t,c} = R_t$		$[R_t < R_{mt}]$	[G25b]
$Y_{tG} = \mathbf{-\Delta G'_c} / \mathbf{E_M}$	growth yield of methanotrophy		[G26]
$\delta M_{t,j,c} / \delta t = F_j U_{t,c} - F_j R_t - D_{t,j,c}$		$[R_t > R_{mt}]$	[G27a]
$\delta M_{t,j,c} / \delta t = F_j U_{t,c} - R_{mt,j} - D_{t,j,c}$		$[R_t < R_{mt}]$	[G27b]

Definition of Variables in Appendix G

Variable	Definition	Units	Equations	Input	Referenc
A	acetate	g C m^{-2}	[G2]		
[A]	aqueous concentration of acetate	g C m^{-3}	[G7]		

a	descriptor for j = active component of Mi				
$[CH_4]$	aqueous concentration of CH_4	g C m^{-3}	[G18]		
$[CO_2]$	aqueous concentration of CO_2	g C m^{-3}	[G12]		
Dh,j,c	decomposition of hydrogenotrophic methanogens	g C m^{-2} h^{-1}	[G17]		
Di,f,j,c	decomposition of fermenters and acetogens	g C m^{-2} h^{-1}	[G6]		
Di,m,j,c	decomposition of acetotrophic methanogens	g C m^{-2} h^{-1}	[G11]		
Dt,j,c	decomposition of autotrophic methanotrophs	g C m^{-2} h^{-1}	[G27]		
$\mathbf{E_C}$	energy required to construct new M from CO_2	kJ g C^{-1}	[G15]	75	
$\mathbf{E_G}$	energy required to transform CH_4 into organic C	kJ g C^{-1}	[G20]	23.5	Anthony (1982)
$\mathbf{E_M}$	energy required to construct new M from organic C	kJ g C^{-1}	[G4,G10,G26]	25	
Fj	partitioning coefficient for j in Mi,n,j		[G6,G11,G17,G27]		
f	descriptor for fermenters and acetogens in each M_i				
fo_2t	ratio of O_2 uptake to O_2 requirement for CH_4 oxidation		[G21a,b]		
f_t	temperature function for growth-related processes (dimensionless)		[G1,G7,G12]		
$\mathbf{\Delta G'_c}$	free energy change of C oxidation-O_2 reduction	kJ g C^{-1}	[G26]	-37.5	Brock and Madigan (1991)
ΔG_f	free energy change of fermentation plus acetogenesis	kJ g $Q_{i,c}^{-1}$	[G4,G5]		
$\mathbf{\Delta G'_f}$	ΔG_f when $[H_2] = [H_2']$	kJ g $Q_{i,c}^{-1}$	[G5]	-4.43	Brock and Madigan (1991), Schink (1997)
ΔG_h	free energy change of hydrogenotrophic methanogenesis	kJ g CO_2-C^{-1}	[G15,G16]		
$\mathbf{\Delta G'_h}$	free energy change of hydrogenotrophic methanogenesis when $[H_2] = [H_2']$	kJ g CO_2-C^{-1}	[G16]	-0.27	Brock and Madigan (1991)
$\mathbf{\Delta G'_m}$	free energy change of acetotrophic methanogenesis	kJ g $A_{i,c}^{-1}$	[G10]	-1.03	Brock and Madigan (1991), Schink (1997)

$\Delta G'_t$	free energy change of CH_4 oxidation by methanotrophs	kJ g CH_4-C^{-1}	[G20]	-9.45	Brock and Madigan (1991)
$[H_2]$	aqueous concentration of H_2	g H m^{-3}	[G5,G12,G16]		
$[H_2']$	aqueous concentration of H_2 when $\Delta G_h = \Delta G'_h$ and $\Delta G_f = \Delta G'_f$	g H m^{-3}	[G5,G16]	2.0 x 10^{-4}	Brock and Madigan (1991)
h	descriptor for hydrogenotrophic methanogens in each M_i				
i	descriptor for organic matter-microbe complex (i = plant residue, manure, particulate OM, or humus)				
j	descriptor for structural or kinetic components for each functional type within each M_i *(e.g. a = active)*				
K_c	M-M constant for uptake of CO_2 by hydrogenotrophic methanogens	g C m^{-3}	[G12]	0.12	
K_f	M-M constant for uptake of $DOC_{i,c}$ by fermenters and acetogens	g C m^{-3}	[G1]	12	McGill et al. (1981)
K_i	inhibition constant for O_2 on fermentation	g O m^{-3}	[G1]	0.32	
K_h	M-M constant for uptake of H_2 by hydrogenotrophic methanogens	g H m^{-3}	[G12]	0.01	Mosey (1983), Robinson and Tiedje (1982)
K_m	M-M constant for uptake of $A_{i,c}$ by acetotrophic methanogens	g C m^{-3}	[G7]	12	Smith and Mah (1978), Zehnder et al. (1980)
K_t	M-M constant for uptake of CH_4 by methanotrophs	g C m^{-3}	[G18]	3 x 10^{-3}	Conrad (198
k	descriptor for elemental fraction within each j *(j = c, n or p)*				
M	microbial communities	g C m^{-2}			
M_h	hydrogenotrophic methanogen community	g C m^{-2}	[G12,G17]		
$M_{i,f}$	fermenter and acetogenic community	g C m^{-2}	[G1,G6]		
$M_{i,m}$	acetotrophic methanogen community	g C m^{-2}	[G7,G11]		
M_t	autotrophic methanotrophic community	g C m^{-2}	[G18,G27]		
m	descriptor for acetotrophic methanogens in each M_i				

Q	dissolved organic matter (DOC)	g C m^{-2}	[G2]		
[Q]	aqueous concentration of DOC	g C m^{-3}	[G1]		
$\boldsymbol{R}$	gas constant	kJ mol^{-1} K^{-1}	[G5,G16]	8.3143 x 10^{-3}	
$\boldsymbol{R'_f}$	specific respiration by fermenters and acetogens at saturating [$P_{i,c}$], 25 °C and zero water potential	g C g $M_{i,f,a}^{-1}$ h^{-1}	[G1]	0.1	Lawrence (1971), Wofford et al. (1986)
R_h	CO_2 reduction by hydrogenotrophic methanogens	g C m^{-2} h^{-1}	[G12,G13,G14,G17,G18]		
$\boldsymbol{R'_h}$	specific CO_2 reduction by hydrogenotrophic methanogens at saturating [H_2] and [CO_2], and at 25 °C and zero water potential	g C g $M_{h,a}^{-1}$ h^{-1}	[G12]	0.12	Shea et al. (1968), Zehnder and Wuhrman n (1977)
$R_{i,f}$	respiration of hydrolysis products by fermenters and acetogens	g C m^{-2} h^{-1}	[G1,G2,G3,G6]		
$R_{i,m}$	respiration of acetate by acetotrophic methanogens	g C m^{-2} h^{-1}	[G7,G8,G9,G11]		
$\boldsymbol{R'_m}$	specific respiration by acetotrophic methanogens at saturating [$A_{i,c}$], 25 °C and zero water potential	g C g $M_{i,m,a}^{-1}$ h^{-1}	[G7]	0.20	Smith and Mah (1980)
$R_{mh,j}$	maintenance respiration by hydrogenotrophic methanogens	g C m^{-2} h^{-1}	[G14,G17]		
$R_{mi,f,j}$	maintenance respiration by fermenters and acetogens	g C m^{-2} h^{-1}	[G3,G6]		
$R_{mi,m,j}$	maintenance respiration by acetotrophic methanogens	g C m^{-2} h^{-1}	[G9,G11]		
$R_{mt,j}$	maintenance respiration by methanotrophs	g C m^{-2} h^{-1}	[G25,G27]		
R_t	CH_4 oxidation by methanotrophs for respiration	g C m^{-2} h^{-1}	[G21b,G23,G24,G25,G27a]		
R'_t	CH_4 oxidation by methanotrophs for respiration at saturating O_2	g C m^{-2} h^{-1}	[G19,G21b]		
T	soil temperature	K	[G5,G16]		
t	descriptor for autotrophic methanotrophs				
$U_{h,c}$	rate of CO_2 uptake by M_h	g C m^{-2} h^{-1}	[G14,G17,G18]		
$U_{i,f,k}$	rate of $DOC_{i,k}$ uptake by $M_{i,f}$	g C m^{-2} h^{-1}	[G3,G6]		
$U_{i,m,c}$	rate of $A_{i,c}$ uptake by $M_{i,m}$	g C m^{-2} h^{-1}	[G9,G11]		

$U_{t,c}$	rate of CH_4 uptake by M_t	g C m^{-2} h^{-1}	[G25,G27]		
X_t	CH_4 oxidation by methanotrophs	g C m^{-2} h^{-1}	[G21a,G22]		
X'_t	CH_4 oxidation by methanotrophs at saturating O_2	g C m^{-2} h^{-1}	[G1,G2,G4a]		
$\boldsymbol{X'_t}$	specific CH_4 oxidation by methanotrophs at saturating O_2, 30 °C and zero water potential	g C g^{-1} h^{-1}	[G18]	0.5	Conrad (1984)
Y_f	biomass yield from fermentation and acetogenic reactions	g $M_{i,f}$ g $Q_{i,c}^{-1}$	[G3,G4]		
Y_h	biomass yield from hydrogenotrophic methanogenic reaction	g M_h g CO_2-C^{-1}	[G14,G15,G18]		
Y_m	biomass yield from acetotrophic methanogenic reaction	g $M_{i,m}$ g $A_{i,c}^{-1}$	[G9,G10]		
Y_{t_G}	biomass yield from methanotrophic growth respiration	g M_t-C g CH_4-C^{-1}	[G25a,G26]		
Y_{t_R}	ratio of CH_4 respired vs. CH_4 oxidized by methanotrophs	g C g C^{-1}	[G19,G20]		

Appendix H: Inorganic N Transformations

Mineralization and Immobilization of Ammonium by All Microbial Populations

$I_{NH4i,n,j} = (M_{i,m,j,C}\, \boldsymbol{C_{Nj}} - M_{i,m,j,N})$ $(I_{NH4i,n,j} < 0)$ [H1a]

$I_{NH4i,n,j} = (M_{i,m,j,C}\, \boldsymbol{C_{Nj}} - M_{i,m,j,N})\, [NH_4^+] / ([NH_4^+] + \boldsymbol{K_{NH4}}_m)$ $(I_{NH4i,n,j} > 0)$ [H1b]

$I_{NO3i,n,j} = (M_{i,m,j,C}\, \boldsymbol{C_{Nj}} - (M_{i,m,j,N} + I_{NH4i,n,j}))\, [NO_3^-] / ([NO_3^-] + K_{NO3}m)$ $(I_{NO3i,n,j} > 0)$ [H1b]

Oxidation of DOC and Reduction of Oxygen by Heterotrophs

$X'_{DOCi,h} = \{X'_{DOC}\, M_{i,h,a}\, [DOC_i] / ([DOC_i]) + \boldsymbol{K_{Xh}}\}\, f_t$ [H2]

$R'_{O2i,h} = \mathbf{RQ_C}\, X'_{DOCi,h}$ [H3]

$R_{O2i,h} = 4\pi\, n\, M_{i,h,a}\, D_{sO2}\, ([O_{2s}] - [O_{2mi,h}])\, [r_m r_w / (r_w - r_m)]$ [H4a]

$= R'_{O2i,h}\, [O_{2mi,h}] / ([O_{2mi,h}] + \boldsymbol{K_{O2}}_h)$ [H4b]

$X_{DOCi,h} = X'_{DOCi,h}\; R_{O2i,h} / R'_{O2i,h}$ [H5]

Oxidation of DOC and Reduction of Nitrate, Nitrite and Nitrous Oxide by Denitrifiers

$R'_{NO3i,d} = \boldsymbol{E_{No_x}}\, (R'_{O2i,d} - R_{O2i,d})\, (1.0 + \boldsymbol{K_e}\, (R'_{O2i,d} - R_{O2i,d})/V_i)$ [H6]

$R_{NO3i,d} = R'_{NO3i,d}\, [NO_3^-] / ([NO_3^-] + \boldsymbol{K_{NO3}}_d)\, /(1.0+([NO_2^-]\, \boldsymbol{K_{NO3}}_d)/(\, [NO_3^-]\, \boldsymbol{K_{NO2}}_d))$ [H7]

$R_{NO2i,d} = (R'_{NO3i,d} - R_{NO3i,d})\, [NO_2^-] / ([NO_2^-] + \boldsymbol{K_{NO2}}_d)\, /(1.0+([N_2O]\, \boldsymbol{K_{NO2}}_d)/(\, [NO_2^-]\, \boldsymbol{K_{N2O}}_d))$ [H8]

$R_{N2Oi,d} = 2\, (R'_{NO3i,d} - R_{NO3i,d} - R_{NO2i,d})\, [N_2O] / ([N_2O] + \boldsymbol{K_{N2O}}_d)$ [H9]

$X_{DOCi,d} = X_{DOCi,d}$ (from [H5]) $+ \boldsymbol{F_{NO_x}}\, (R_{NO3i,d} + R_{NO2i,d}) + \boldsymbol{F_{N2O}}\, R_{N2Oi,d}$ [H10]

Oxidation of Ammonia and Reduction of Oxygen by Nitrifiers

$X'_{NH3i,n} = X'_{NH3}\, \boldsymbol{M_{i,n,a}}\, \{[NH_{3S}] / ([NH_{3S}] + \boldsymbol{K_{NH3}}_n)\}\, \{[CO_{2S}] / ([CO_{2S}] + \boldsymbol{K_{CO2}})\}\, f_t$ [H11]

$R'_{O2i,n} = \mathbf{RQ_{NH3}}\, X'_{NH3i,n} + \mathbf{RQ_C}\, X'_{Ci,n}$ [H12]

$R_{O2i,n} = 4\pi\, n\, M_{i,n,a}\, D_{sO2}\, (r_m\, r_w / (r_w - r_m))\, ([O_{2S}] - [O_{2mi,n}])$ [H13a]

$= R'_{O2i,n}\, [O_{2mi,n}] / ([O_{2mi,n}] + \boldsymbol{K_{O2}}_n)$ [H13b]

$X_{NH3i,n} = X'_{NH3i,n}\, R_{O2i,n} / R'_{O2i,n}$ [H14]

Oxidation of Nitrite and Reduction of Oxygen by Nitrifiers

$X'_{NO2i,o} = X'_{NO2}\, M_{i,o,a}\, \{[NO_2^-] / ([NO_2^-] + \boldsymbol{K_{NO2}}_o)\}\, \{[CO_{2S}] / ([CO_{2S}] + \boldsymbol{K_{CO2}})\}\, f_t$ [H15]

$R'_{O2i,o} = \mathbf{RQ_{NO2}}\, X'_{NO2i,o} + \mathbf{RQ_C}\, X'_{Ci,o}$ [H16]

$R_{O2i,o} = 4\pi\, n\, M_{i,o,a}\, D_{sO2}\, (r_m\, r_w / (r_w - r_m))\, ([O_{2s}] - [O_{2mi,o}])$ [H17a]

$= R'_{O2i,o}\, [O_{2mi,o}] / ([O_{2mi,o}] + \boldsymbol{K_{O2}}_o)$ [H17b]

$X_{NO2i,o} = X'_{NO2i,o}\, R_{O2i,o} / R'_{O2i,o}$ [H18]

Oxidation of Ammonia and Reduction of Nitrite by Nitrifiers

$R'_{NO2i,n} = \boldsymbol{E_{NO_x}}\, (R'_{O2i,n} - R_{O2i,n})/(1.0 + \boldsymbol{K_e}\, (R'_{O2i,n} - R_{O2i,n})/V_i)$ [H19]

$R_{NO2i,n} = R'_{NO2i,n}\, \{[NO_2^-] / ([NO_2^-] + \boldsymbol{K_{NO2}}_n)\}\, \{[CO_{2S}] / ([CO_{2S}] + \boldsymbol{K_{CO2}})\}$ [H20]

$X_{NH3i,n} = X_{NH3i,n}$ (from [H14]) $+ 0.33\, R_{NO2i,n}$ [H21]

Definition of Variables in Appendix H

Name	Definition	Units	Equations	Input Values	Reference
	Subscripts				
a	active component of $M_{i,m}$				

d	heterotrophic denitrifier population (subset of *h*)
h	heterotrophic community (subset of *m*)
i	substrate-microbe complex
j	kinetic components of $M_{i,m}$
m	all microbial communities
n	autotrophic ammonia oxidizer population (subset of *m*)
o	autotrophic nitrite oxidizer population (subset of *m*)

Variables

C_{Nj}	maximum ratio of $M_{i,m,j,N}$ to $M_{i,m,j,C}$ maintained by $M_{i,m,j}$	g N g C^{-1}	[H1]	0.22 and 0.13 for *j* = labile and resistant	
$[CO_{2S}]$	CO_2 concentration in soil solution	g C m^{-3}	[H11,H15,H20]		
$[DOC_i]$	concentration of dissolved decomposition products	g C m^{-3}	[H2]		
D_{sO_2}	aqueous dispersivity-diffusivity of O_2	m^2 h^{-1}	[H4,H13,H17]		
E_{NO_x}	e^- accepted by NO_x vs. O_2 when oxidizing DOC	g N g O_2^{-1}	[H6,H19]	28/32 = 0.875	
F_{NO_x}	e^- donated by C vs. e^- accepted by NO_x when oxidizing DOC	g C g N^{-1}	[H10]	12/28 = 0.43	
F_{N_2O}	e^- donated by C vs. e^- accepted by N_2O when oxidizing DOC	g C g N^{-1}	[H10]	6/28 = 0.215	
f_t	temperature function for microbial processes	-	[H2,H11,H15]		See AppendixA
$I_{NH_4i,n,j}$	mineralization ($I_{NH_4i,n,j} < 0$) or immobilization ($I_{NH_4i,n,j} > 0$) of NH_4^+ by $M_{i,n,j,C}$	g N m^{-2} h^{-1}	[H1]		
$I_{NO_3i,n,j}$	immobilization ($I_{NO_3i,n,j} > 0$) of NO_3^- by $M_{i,n,j,C}$	g N m^{-2} h^{-1}	[H1]		
K_{CO_2}	Michaelis-Menten constant for reduction of CO_{2S} by $M_{i,n,a}$ and $M_{i,o,a}$	g C m^{-3}	[H11,H15,H20]	0.15	
K_{NH_3n}	M-M constant for oxidation of NH_{3S} by nitrifiers	g N m^{-3}	[H11]	0.0002	Suzuki et al. (1974)
Ke	inhibition constant for electrons not accepted by O_2 and transferred to N oxides	-	[H6,H19]	0.5	from Koike and Hattori (1975)
K_{NH_4m}	M-M constant for microbial NH_4^+ uptake	g N m^{-3}	[H1]	0.35	
K_{NO_2d}	M-M constant for reduction of NO_2^- by denitrifiers	g N m^{-3}	[H7,H8]	1.4	Yoshinari et al. (1977)
K_{NO_2n}	M-M constant for reduction of NO_2^- by nitrifiers	g N m^{-3}	[H20]	1.4	
K_{NO_2o}	M-M constant for oxidation of NO_2^- by nitrifiers	g N m^{-3}	[H15]	3.5	
K_{NO_3d}	M-M constant for reduction of NO_3^- by denitrifiers	g N m^{-3}	[H7,H8]	1.4	Yoshinari et al. (1977);Khalil et al., 2005

$K_{N_2O,d}$	M-M constant for reduction of N_2O by denitrifiers	g N m^{-3}	[H9]	0.028	Yoshinari et al. (1977);Khalil et al., 2005
$K_{O_2,h}$	M-M constant for reduction of O_{2s} by heterotrophs	g O_2 m^{-3}	[H4b]	0.064	Griffin (1972)
$K_{O_2,n}$	M-M constant for reduction of O_{2s} by NH_3 oxidizers	g O_2 m^{-3}	[H13b]	0.064	Focht and Verstraete (1977)
$K_{O_2,o}$	M-M constant for reduction of O_{2s} by NO_2^- oxidizers	g O_2 m^{-3}	[H17b]	0.064	Focht and Verstraete (1977)
$K_{X,h}$	M-M constant for oxidation of DOC by heterotrophs	g C m^{-3}	[H2]	12	(McGill et al., 1981)
$M_{i,h,a}$	active biomass of heterotrophs	g C m^{-2}	[H2,H7]		
$M_{i,n,a}$	active biomass of NH_3 oxidizers	g C m^{-2}	[H11,H13]		
$M_{i,m,j,C}$	C biomass of microbial population $M_{i,m,j}$	g C m^{-2}	[H1]		
$M_{i,m,j,N}$	N biomass of microbial population $M_{i,m,j}$	g N m^{-2}	[H1]		
$M_{i,o,a}$	active biomass of NO_2^- oxidizers	g C m^{-2}	[H15,H17]		
$[NH_{3s}]$	concentration of NH_3 in soil solution	g N m^{-3}	[H11]		
$[NH_4^+]$	concentration of NH_4^+ in soil solution	g N m^{-3}	[H1]		
$[NO_2^-]$	concentration of NO_2^- in soil solution	g N m^{-3}	[H7,H8,H15, H20]		
$[NO_3^-]$	concentration of NO_3^- in soil solution	g N m^{-3}	[H7,H8]		
$[N_2O]$	concentration of N_2O in soil solution	g N m^{-3}	[H9]		
n	number of microbes	g^{-1}	[H13,H17]		
$[O_{2mi,h}]$	O_2 concentration at heterotrophic surfaces	g O_2 m^{-3}	[H7]		
$[O_{2mi,n}]$	O_2 concentration at NH_3 oxidizer surfaces	g O_2 m^{-3}	[H13]		
$[O_{2mi,o}]$	O_2 concentration at NO_2^- oxidizer surfaces	g O_2 m^{-3}	[H17]		
$[O_{2s}]$	O_2 concentration in soil solution	g O_2 m^{-3}	[H7,H13,H17]		
$R_{NO_2i,d}$	NO_2^- reduction by denitrifiers	g N m^{-2} h^{-1}	[H8,H9,H10]		
$R'_{NO_2i,n}$	rate of NO_2^- reduction by NH_3 oxidizers under non-limiting $[NO_2^-]$ and $[CO_{2S}]$	g N m^{-2} h^{-1}	[H19,H20]		
$R_{NO_2i,n}$	rate of NO_2^- reduction by NH_3 oxidizers under ambient $[NO_2^-]$ and $[CO_{2S}]$	g N m^{-2} h^{-1}	[H20,H21]		
$R'_{NO_3i,d}$	NO_3^- reduction by denitrifiers under non-limiting $[NO_3^-]$	g N m^{-2} h^{-1}	[H6,H7,H8,H9]		

$R_{NO_3 i,d}$	NO_3^- reduction by denitrifiers under ambient $[NO_3^-]$	g N m^{-2} h^{-1}	[H7,H8,H9,H10]		
$R_{N_2O i,d}$	N_2O reduction by denitrifiers	g N m^{-2} h^{-1}	[H9,H10]		
$R'_{O_2 i,d}$	rate of O_{2S} reduction by denitrifiers under non-limiting $[O_{2S}]$	g O_2 m^{-2} h^{-1}	[H6]		
$R_{O_2 i,d}$	rate of O_{2S} reduction by denitrifiers under ambient $[O_{2S}]$	g O_2 m^{-2} h^{-1}	[H6]		
$R'_{O_2 i,h}$	rate of O_{2S} reduction by heterotrophs under non-limiting $[O_{2S}]$	g O_2 m^{-2} h^{-1}	[H3,H4,H5]		
$R_{O_2 i,h}$	rate of O_{2S} reduction by heterotrophs under ambient $[O_{2S}]$	g O_2 m^{-2} h^{-1}	[H4,H5]		
$R'_{O_2 i,n}$	rate of O_{2S} reduction by NH_3 oxidizers under non-limiting $[O_{2S}]$	g O_2 m^{-2} h^{-1}	[H12,H13.H14,H19]		
$R_{O_2 i,n}$	rate of O_{2S} reduction by NH_3 oxidizers under ambient $[O_{2S}]$	g O_2 m^{-2} h^{-1}	[H13,H14,H19]		
$R'_{O_2 i,o}$	rate of O_{2S} reduction by NO_2^- oxidizers under non-limiting $[O_{2S}]$	g O_2 m^{-2} h^{-1}	[H16,H17,H18]		
$R_{O_2 i,o}$	rate of O_{2S} reduction by NO_2^- oxidizers under ambient $[O_{2S}]$	g O_2 m^{-2} h^{-1}	[H17,H18]		
$\mathbf{RQ_C}$	respiratory quotient for reduction of O_2 coupled to oxidation of C	g O_2 g C^{-1}	[H3,H12,H16]	2.67	Brock and Madigan (1991)
$\mathbf{RQ_{NH_3}}$	respiratory quotient for reduction of O_2 coupled to oxidation of NH_{3S}	g O_2 g N^{-1}	[H12]	3.43	Brock and Madigan (1991)
$\mathbf{RQ_{NO_2}}$	respiratory quotient for reduction of O_2 coupled to oxidation of NO_2^-	g O_2 g N^{-1}	[H16]	1.14	Brock and Madigan (1991)
r_m	radius of microbial sphere	m	[H4,H13,H17]		
r_w	radius of r_m + water film at current soil water potential	m	[H4,H13,H17]		from ψ_s according to Kemper (1966)
V_i	soil volume occupied by substrate-microbe complex		[H6,H19]		
$X'_{Ci,n}$	rate of C oxidation by NH_3 oxidizers under non-limiting $[O_{2S}]$	g C m^{-2} h^{-1}	[H12]		
$X'_{Ci,o}$	rate of C oxidation by NO_2^- oxidizers under non-limiting $[O_{2S}]$	g C m^{-2} h^{-1}	[H16]		
X'_{DOC}	specific rate of DOC oxidation by heterotrophs at 25 °C under non-limiting [DOC] and $[O_{2S}]$	g C g C^{-1} h^{-1}	[H2]	0.125	Shields et al. (1973)

$X'_{DOCi,h}$	rate of DOC oxidation by heterotrophs under non-limiting $[O_{2S}]$	g N m^{-2} h^{-1}	[H2,H3,H5]		
$X_{DOCi,h}$	rate of DOC oxidation by heterotrophs under ambient $[O_{2S}]$	g N m^{-2} h^{-1}	[H5]		
$X_{DOCi,d}$	rate of DOC oxidation by heterotrophs under ambient $[O_{2S}]$ and $[NO_x]$	g N m^{-2} h^{-1}	[H10]		
X'_{NH_3}	specific rate of NH_3 oxidation by NH_3 oxidizers at 25 °C under non-limiting $[O_{2S}]$	g N g C^{-1} h^{-1}	[H11]]	0.625	Belser and Schmidt (1980)
$X_{NH_3i,n}$	rate of NH_3 oxidation by NH_3 oxidizers coupled with reduction of O_2 + NO_2^- under ambient $[O_{2S}]$	g N m^{-2} h^{-1}	[H14,H21]		
$X'_{NH_3i,n}$	rate of NH_3 oxidation by NH_3 oxidizers under non-limiting $[O_{2S}]$	g N m^{-2} h^{-1}	[H11,H12,H14]		
$X'_{NO_2i,o}$	rate of NO_2^- oxidation by NO_2^- oxidizers under non-limiting $[O_{2S}]$	g N m^{-2} h^{-1}	[H15,H16,H18]		
$X_{NO_2i,o}$	rate of NO_2^- oxidation by NO_2^- oxidizers coupled with reduction of O_2 under ambient $[O_{2S}]$	g N m^{-2} h^{-1}	[H18]		
X'_{NO_2}	specific rate of NO_2^- oxidation by NO_2^- oxidizers at 25 °C under non-limiting $[O_{2S}]$	g N g C^{-1} h^{-1}	[H15]	2.5	Belser (1977)